Epitranscriptomic modification of cellular transcripts regulates KSHV lytic reactivation

Oliver Manners

Submitted in accordance with the requirements for the degree of

Doctor of Philosophy

The University of Leeds

Faculty of Biological Sciences

School of Molecular and Cellular Biology

September 2021

The candidate confirms that the work submitted is his own and that appropriate credit has been given where reference has been made to the work of others.

Acknowledgements

I would firstly like to thank my supervisor Professor Adrian Whitehouse for his wonderful support and guidance throughout my project. His confidence in my abilities and deep discussions of my results always steered me in the correct direction and kept the project advancing. Nevertheless, I still believe salmon pink was the best background colour for that poster.

Many thanks go to all members of the Whitehouse laboratory (even Dr. Samuel Dobson) who made sure I enjoyed every moment of my studies, even when experiments were not working as I'd hoped. It's been a privilege to spend these 4 years working among such a great group of friends.

A special thanks goes to Dr. Belinda Baquero who laid the foundation for my project by kickstarting the Whitehouse lab's investigation into RNA modifications by performing the m^6A-seq experiments.

I would also like to express gratitude towards Dr. Kate Heesom at the University of Bristol Proteomics facility for running the global quantitative proteomics analysis and Dr Ian Carr and Dr Agne Antanaviciute at St James' University Hospital for running the m^6A-seq. Thanks also go to Dr Brian Jackson and Mr Ivaylo Yonchev for their technical support with cloning and CHIP-seq data analysis respectively.

I am very grateful to the MRC and the University of Leeds for jointly funding my PhD research and providing me with a range of training activities to strengthen my core skills.

I would also like to express an enormous appreciation to my family. Making you proud continually keeps me working hard and focused on my studies. My deepest gratitude goes to my grandparents June and Geoffrey Morley who always showed interest in my work and helped me to stay determined. I would like to dedicate this thesis to June who passed away shortly before its submission at the age of 90 years old. Rest in peace Granny.

Lastly, I would like to thank my wonderful girlfriend Maddie who sat next to me in the office on the very first day of my studies. You've shown me how to make the most of things, how to stop worrying and most importantly how to enjoy myself. It's been a wonderful time at university together, I can't wait for our next adventure!

Abstract

Kaposi's Sarcoma Associated Herpesvirus (KSHV) is an oncovirus and the aetiological agent of several malignancies including the endothelial cell tumour Kaposi's Sarcoma (KS). Like all herpesviruses, KSHV undergoes distinct latent and lytic life cycles which are both required for KS pathogenesis. The latent stage is characterised by a state of transcriptional dormancy where viral gene expression is limited; however, the virus may undergo reactivation into the lytic phase where all KSHV proteins are expressed leading to the production of infectious virus particles.

Although modifications of DNA and protein are known to substantially regulate gene expression, the study of RNA modifications which comprise the epitranscriptome is still emerging. m^6A, the most common internal modification of mRNA, is now known to affect all stages of mRNA metabolism and regulate a wide range of biological processes. Importantly, m^6A has been linked with various disease states and is rapidly becoming a key area of interest within viral infections. Notably, the investigation of changes in the cellular m^6A landscape in response to virus infection is lacking and in need of further research.

In this study, cells infected with KSHV were monitored for changes in m^6A content upon cellular transcripts between latent and lytic replication. Fascinatingly, m^6A topology among host transcripts was vastly altered in response to KSHV reactivation. Furthermore, cellular mRNAs with altered m^6A content were enriched in pathways known to be hijacked during KSHV replication such as oncogenic signalling and mRNA dynamics.

Following these findings, two mRNAs were identified with dramatic m^6A-dependent increases in abundance among cells undergoing KSHV lytic replication. The encoded proteins GPRC5A and ZFP36L1 were demonstrated to be crucial for efficient KSHV lytic replication through regulation of plasma membrane dynamics and AU-rich mRNA fate respectively.

In summary, this study provides tantalizing evidence into the remodelling of the host m^6A landscape to affect the expression of mRNAs which regulate KSHV lytic replication.

Contents

List of figures

List of tables

Abbreviations

293T	HEK 293T cells
aa	amino acid
ADP	adenosine diphosphate
AIDS	acquired immune deficiency syndrome
ALKBH5	adenosine-ketoglutarate-dependent dioxygenase alkB homolog 5
AP-1	activator protein 1
APS	ammonium persulfate
ARE	AU-rich element
ART	antiretroviral therapy
ATP	adenosine triphosphate
AU-rich	adenylate/uridylate-rich
BCBL	body cavity based lymphoma
bp	base pair
BSA	bovine serum albumin
CDK	cyclin-dependent kinase
cDNA	complementary DNA
CDS	coding sequence
circRNA	circular RNA
CLIP	cross-linking immunoprecipitation
CT	cycle threshold
C-terminal	carboxy-terminal
DAA	3-deazaadenosine
DAPI	4', 6-diamidino-2-phenylindole
DC1	YTHDC1 protein
DC2	YTHDC2 protein
DE	delayed early
DENV	Dengue virus
DF1	YTHDF1 protein
DF2	YTHDF2 protein
DF3	YTHDF3 protein
dH_2O	distilled water
DMEM	Dulbecco's modified Eagles medium
DMSO	dimethyl sulphoxide
DNA	deoxyribonucleic acid
DNase	deoxyribonuclease
dNTP	deoxyribonucleoside (5'-) triphosphate
dox	doxycycline hyclate
ds	double stranded
DTT	dithiothreitol
E	early
EBV	Epstein-Barr virus
ECL	enhanced chemiluminescence
EDTA	ethylenediaminetetraacetic acid disodium salt

eEF	eukaryotic elongation factor
EGFP	enhanced green fluorescent protein
eIF	eukaryotic initiation factor
EJC	exon junction complex
EphA2	ephrin receptor tyrosine kinase A2
ER	endoplasmic reticulum
eRF	eukaryotic release factor
EV71	enterovirus-71
FBS	foetal bovine serum
FDA	food and drug administration
FDR	false discovery rate
FLIP	FLICE-inhibitory protein
FTO	fat mass obesity protein
GAPDH	glyceraldehyde 3-phosphate dehydrogenase
gB	glycoprotein B
GDP	guanosine diphosphate
GFP	green fluorescent protein
gH	glycoprotein H
gL	glycoprotein L
GO	gene ontology
gRNA	genomic RNA
GTP	guanosine triphosphate
H3K36me3	histone H3 trimethylation at lysine-36
HAART	highly active antiretroviral therapy
HBV	hepatitis B virus
HCl	hydrochloric acid
HCMV	human cytomegalovirus
HCV	hepatitis C virus
HEK	human embryonic kidney
HHV	human herpesvirus
HIV	human immunodeficiency virus
HNRNP	heterogeneous nuclear ribonucleoprotein
HRP	horseradish peroxidase
HSV-1	herpes simplex virus 1
HTLV	human T-cell leukemia virus
hTREX	human transcription/export complex
HVS	herpesvirus saimiri
IAV	Influenza A virus
ICTV	International Committee on Taxonomy of Viruses
IE	immediate early
IF	immunofluorescence
IFN	interferon
IgG	immunoglobulin G
IL-6	interleukin-6
IR	internal repeat

IRF	interferon regulatory factor
Kb	kilobase
KCl	potassium chloride
KD	knockdown
KDE	kernel density estimate
KS	Kaposi's Sarcoma
KSHV	Kaposi's Sarcoma associated herpesvirus
KS-IRIS	KS-associated immune reconstitution inflammatory syndrome
L	late
LANA	latency-associated nuclear antigen
LAT	latency associated transcript
LB	lysogeny broth
LC	liquid chromatography
lncRNA	long non-coding RNA
m^6A-seq	methylated RNA immunoprecipitation-sequencing
MCD	multicentric Castleman's disease
MeRIP-seq	methylated RNA immunoprecipitation-sequencing
METTL14	methyltransferase-like 14
METTL3	methyltransferase-like 3
$MgCl_2$	magnesium chloride
MHV-68	murine gammaherpesvirus 68
miRNA	microRNA
mRNA	messenger RNA
mRNP	messenger ribonucleoprotein particles
MS	mass spectrometry
MTA	mRNA transcript accumulation
MTS	3-(4,5-dimethylthiazol-2-yl)-5-(3-carboxymethoxyphenyl)-2-(4-sulfophenyl)-2H-tetrazolium
N	sample size
Na_2CO_3	sodium carbonate
NaCl	sodium chloride
$NaHCO_3$	sodium hydrogen carbonate
NaOH	sodium hydroxide
ncRNA	non-coding RNA
NEB	New England Biolabs
NF-κB	nuclear factor kappaB
NGS	next generation sequencing
NLS	nuclear localisation signal
NMD	nonsense-mediated decay
NP40	tergitol-type NP-40
NPC	nuclear pore complex
N-terminal	amino-terminal
Nxf1	nuclear RNA export factor 1
Nxt1	nuclear transport factor 2-like export factor 1
OMM	outer mitochondrial membrane
ORF	open reading frame

ori-Lyt	lytic origin of DNA replication
ori-P	latent origin of DNA replication
p	p-value
PABP	polyadenylate binding protein
PAGE	polyacrylamide gel electrophoresis
PAN	polyadenylated nuclear RNA
PBS	phosphate buffered saline
PCR	polymerase chain reaction
PEL	primary effusion lymphoma
pgRNA	pregenomic RNA
PI3K	phosphoinositide 3-kinase
piRNA	Piwi-interacting RNA
poly(A)	polyadenylated
pre-mRNA	precursor-messenger RNA
PTM	post-translational modification
PUS	pseudouridine synthase
qPCR	quantitative PCR
qRT-PCR	quantitative reverse transcriptase PCR
RBP-jκ	recombination signal-binding protein 1 for J-kappa
RFP	red fluorescent protein
RGG	arginine- and glycine-rich
RIPA	radioimmunoprecipitation assay
RIP-seq	RNA-binding protein immunoprecipitation assay coupled with sequencing
RISC	RNA-induced silencing complexes
RNA	ribonucleic acid
RNAPII	RNA polymerase II
RNase	ribonuclease
RNP	ribonucleoprotein particles
ROS	reactive oxygen species
RPMI	Roswell Park memorial institute 1640
RRE	RTA-response element
rRNA	ribosomal RNA
RT	reverse transcriptase
RTA	replication and transcription activator
SAM	S-adenosylmethionine
Scr	scrambled shRNA
SD	standard deviation
SDS	sodium dodecyl sulphate
shRNA	small hairpin RNA
siRNA	small interfering RNA
snRNA	small nuclear RNA
sORF	small open reading frame
SOX	shutoff and exonuclease
SR	serine/arginine rich
SV40	Simian vacuolating virus 40
T	triangulation number

TBS	tris buffered-saline
TBST	tris buffered-saline and tween-20
TEMED	N-N-N’-N’-tetramethylethylenediamine
TF	transcription factor
TLR	toll-like receptors
TMT	tandem mass tagging
TPA	12-*O*-tetradecanoylphorbol-13-acetate
TR	terminal repeat
TREX cells	TREX BCBL-1-Rta cells
Tris	tris(hydroxymethyl)aminoethane
tRNA	transfer RNA
UTR	untranslated region
VEGF	vascular endothelial growth factor
vFLIP	viral FLICE inhibitory protein
vGPCR	viral G protein-coupled receptors
vIL-6	viral interleukin 6
vRNP	viral ribonucleoprotein particles
VZV	varicella-zoster virus
WCL	whole cell lysate
WTAP	Wilms Tumour 1 associated protein
XRN1	5'-3' Exoribonuclease 1
YTH	YT521-B homology
ZIKV	Zika virus
α	alpha
β	beta
γ	gamma
κ	kappa

Units and symbols

Å	angstrom
~	approximately
°C	degrees Celsius
g	gram
g	gravitational force
>	greater than
h	hours
hpi	hours post induction
Kb	kilobase
Kbp	kilobase pair
kDa	kilodalton
<	less than
MDa	megaDalton
µg	microgram

µl	microlitre
µm	micrometre
µM	micromolar
ml	millilitre
mm	millimetre
mM	millimolar
min	minute
M	molar
ng	nanogram
nm	nanometre
nM	nanomolar
%	percentage
pmol	picomole
sec	seconds
3D	three dimensional
V	volts
v/v	volume per volume
w/v	weight per volume

Nucleic acid bases

A	adenine
C	cytosine
G	guanine
T	thymine
U	uracil
5CaC	5-carboxylcytidine
5fC	5-formylcytidine
hm^5C	5-hydroxymethylcytidine
m^1A	N^1-methyladenosine
m^5C	5-methycytidine
m^6A	N^6-methyladenosine
m^6A_m	N^6,2'-O-dimethyladenosine
m^7G	7-methyl-guanine
Nm	2'-*O*-methylation
Ψ	pseudouridine

Chapter 1

~

Introduction

1 Introduction

1.1 Herpesviruses

Herpesviruses comprise a family of viruses which share common structure and life cycles. While the herpesviruses were originally classified into a single family known as *Herpesviridae,* revisions brought about by the International Committee on Taxonomy of Viruses (ICTV) , introduced the new taxonomic order *Herpesvirales* (Arvin et al., 2007; Davison et al., 2009; Sehrawat et al., 2018; Jeffery-Smith and Riddell, 2021). The updated *Herpesviridae* family retained the mammal, reptile and bird viruses. However the two new families, *Alloherpesviridae* and *Malacoherpesviridae*, contained the fish and frog viruses and a single mollusc virus respectively (Davison et al., 2009). In addition to many viruses of animals, at least eight members of the *Herpesviridae* cause diseases in humans, where a lifelong persistent infection is a key feature.

1.1.1 Subclassification of *Herpesviridae*

Herpesviridae are categorised into three subfamilies, *alphaherpesviruses, betaherpesviruses* and *gammaherpesviruses,* all of which share a set of 40 common genes that play key roles in virus replication (Figure 1.1a) (Owen et al., 2015). Initial classification into these three groups was based on biological properties including host range, replication strategies and genetic architecture. Modern molecular phylogenetic analyses estimate that these three subfamilies diverged from a common ancestor approximately 400 million years ago (Matthews, 1979; Owen et al., 2015).

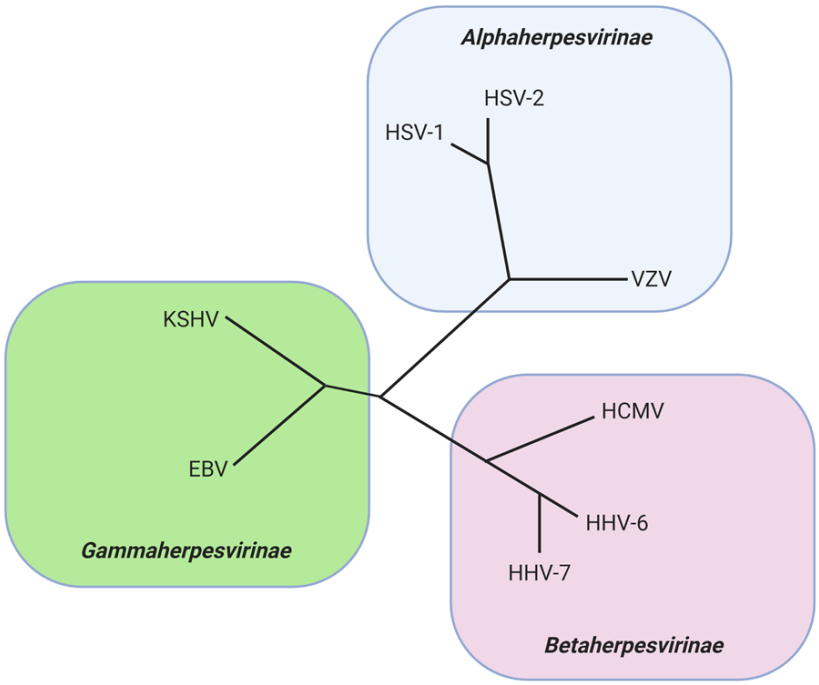

Figure 1.1. *Herpesviridae* subfamilies. Herpesviruses are classified into alpha, beta and gamma subfamilies. Shown within each family are the viruses pathogenic to humans.

1.1.1.1 Alphaherpesvirinae

Alphaherpesvirinae or alphaherpesviruses are widely recognised by their ability to cause latent infection in neuronal cells (Owen et al., 2015). Primary infection usually occurs in epithelial cells; however, the spread of virus to surrounding sensory neurons marks the start of a lifelong persistent infection. Alphaherpesviruses differ from the Betaherpesviruses and Gammaherpesviruses through their short reproductive life cycle, rapid lysis of the host cell and ability to infect a wide range of animal species (Arvin et al., 2007; Jeffery-Smith and Riddell, 2021).

Among the *alphaherpesvirinae*, there are three notable viruses with tropism in humans: Herpes simplex virus type-1 (HSV-1), herpes simplex virus type-1 (HSV-2) and the more distantly related varicella-zoster-virus (Jeffery-Smith and Riddell, 2021). The viruses are also known as human herpesvirus (HHV) 1, 2 and 3 respectively. HSV-1 and HSV-2 infections lead to recurrent oral and genital ulcers whereas varicella-zoster is the causative agent of the highly infectious disease chickenpox (Schiffer and Corey, 2009; Owen et al., 2015).

1.1.1.2 Betaherpesvirinae

Unlike alphaherpesviruses*, betaherpesvirinae* or betaherpesviruses have a restricted host range and undergo an extended life cycle progressing over several days. Generally, these viruses infect cells of the monocyte lineage within the kidneys, the reticuloendothelial system and secretory glands (Arvin et al., 2007). A major feature of betaherpesvirus infection is the formation of cytomegaly without cell lysis. (Jeffery-Smith and Riddell, 2021).

Human pathogens among the betaherpesviruses include human cytomegalovirus (HCMV) or HHV-5, HHV-6 and HHV-7. The latter two viruses belong to the *Roseolovirus* genus and cause a roseola rash in young infants. Additionally, HHV-6 is associated with rejection of kidney transplants (Yoshikawa, 2018; Hanson et al., 2018). HCMV has the largest genome among all human herpesviruses, which causes a range of diseases in immunocompromised individuals and a number of disabilities following congenital infection (Goodrum, 2016).

1.1.1.3 Gammaherpesvirinae

In comparison with the betaherpesviruses, the *gammaherpesvirinae* or gammaherpesviruses have a very restricted host range and display tropism for only a few host cell types (Jeffery-Smith and Riddell, 2021). The preferred host cells of gammaherpesviruses are lymphocytes; however, productive replication in endothelial and epithelial cells may also take place (Stewart et al., 1998; Ackermann, 2006; Mohl et al., 2019).

Unlike the other *herpesviridae* subfamilies, gammaherpesviruses are often associated with cancers, especially lymphoproliferative disorders. Epstein Barr virus (EBV) or HHV-4, the best studied among the gammaherpesviruses, causes infectious mononucleosis and is found in the large majority of cases of Burkitt's lymphoma (Ackermann, 2006; Jha et al., 2016). Kaposi's sarcoma-associated herpesvirus (KSHV) or HHV-8 is the etiological agent of the endothelial cell tumour Kaposi's sarcoma (KS) and two further lymphoproliferative disorders, primary effusion lymphoma (PEL) and Multicentric Castleman's disease (MCD) (Decker et al., 1996; Schumann et al., 2016; Manners et al., 2018).

1.1.2 Virion structure

Herpesviruses have a defining virion structure which separates them from all other viruses (Arvin et al., 2007). All herpesvirus particles share four major architectural features including the genome, capsid, tegument and envelope (Figure 1.2) (Heming et al., 2017).

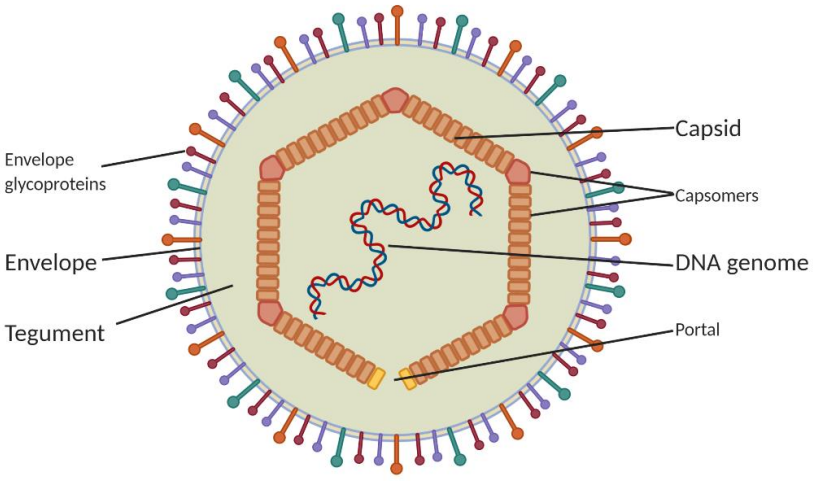

Figure 1.2. Herpesvirus virion structure. The herpesviral dsDNA genome is encapsidated by an icosapentahedral structure of 150 hexon and 11 penton capsomers. The 12th penton is replaced by the portal vertex to allow passage of the dsDNA from the capsid. The nucleocapsid is surrounded by a protein-rich tegument which itself is enveloped by a host-cell derived double membrane littered with glycoproteins.

The large double stranded DNA (dsDNA) genome of herpesviruses varies between 120 and 250 kilobase pairs (kbp) in size, encoding between 70 and 220 open reading frames (ORFs) (Roizmann et al., 1992; Davison et al., 2009). Herpesviral genomes, especially those of gammaherpesviruses, contain additional genes hijacked from their hosts to aid in immune evasion (Holzerlandt et al., 2002; Aswad and Katzourakis, 2018).

The herpesviral genome is encased by an icosahedral capsid with T=16 (triangulation number) symmetry (Furlong et al., 1972; Schrag, 1988). The capsid is comprised of 161 major structural protein subunits termed capsomers and has an approximate diameter of 100-130nm (Bowman et al., 2003). The 162nd capsomer is replaced by a protein 'portal' complex which permits the entry and exit of the dsDNA genome (Schrag, 1988; Bowman et al., 2003; Pageau et al., 2007; Yuan et al., 2018).

Surrounding the nucleocapsid lies a proteinaceous layer unique to herpesviruses, known as the tegument. The tegument contains between 10 and 40 viral proteins depending on herpesvirus subfamily; some of which are essential for virion structure, while others play important roles in infection, immune evasion and viral DNA replication (Kelly et al., 2009). Mass spectrometry of purified virions has also shown the appearance of host proteins, as well as viral and cellular messenger RNA (mRNA) within the tegument (Loret et al., 2008).

Finally, surrounding the entire herpesvirus particle is a host cell-derived lipid bilayer envelope containing approximately 10 different viral glycoproteins essential for binding, fusion and entry into host cells (Eisenberg et al., 2012).

1.1.3 Life cycle

The life cycle of herpesviruses begins with the attachment of the virus particle to its host cell via surface receptors (Eisenberg et al., 2012). In most cases, fusion of the virus with the host cell takes place through interactions with viral envelope glycoproteins, three of which; gH, gB and gL; are conserved among all herpesvirus. However, some herpesviruses, such as EBV can enter the cell by endocytosis after acidification of the endosomal compartment (Nicola et al., 2003; Nicola and Straus, 2004). The insertion of viral glycoproteins into the host cell membrane causes conformational changes leading to pore formation and delivery of the viral tegument proteins and nucleocapsid into the cytoplasm. The nucleocapsid is then propelled along the host cell microtubule network by the dynein/dynactin motor protein complex, allowing viral DNA entry to the nucleus through the nuclear pore complex (Sodeik et al., 1997; Döhner et al., 2002; Pasdeloup et al., 2009). Once inside the host cell nucleoplasm the herpesvirus DNA circularises and enters one of two distinct replication programmes: Latency or lytic replication.

1.1.3.1 Latency

Latency is a period of transcriptional dormancy for herpesviruses where limited viral gene expression occurs and infectious virion production is tightly restricted. Through the action of epigenetic silencing machinery in the host cell, the viral genome becomes maintained as a circular, non-integrated episome packaged by histones into a condensed chromatin state (Deshmane and Fraser, 1989; Amon and Farrell, 2005). Only a small number of genes, known as latency associated transcripts (LATs), are expressed during this replication programme.

In latency, viral DNA is replicated in tandem with host DNA by cellular DNA polymerases during mitosis (Deshmane and Fraser, 1989; Purushothaman et al., 2015).

The latent cycle aids in the evasion of immune signalling pathways and antiviral mechanisms which would otherwise inhibit the production of infectious virions. As a result, this process allows the virus to establish lifelong persistent infections characteristic of herpesviruses. Importantly, in cells infected by alpha- and betaherpesviruses, the majority undergo lytic replication and a small subset of infected cells harbour latent virus (Ackermann, 2006). In contrast, for gammaherpesviruses, latency is the default replication programme with only a few cells undergoing a process of 'reactivation' into the lytic phase (Manners et al., 2018).

1.1.3.2 Lytic replication

Herpesvirus lytic replication is characterised by a highly ordered temporal cascade of gene expression. All viral mRNAs are transcribed by host RNA polymerase II and undergo processing to acquire 5' caps and 3' polyadenylated tails (Costanzo et al., 1977; Lee and Glaunsinger, 2009). After nuclear export, the viral transcripts are translated in the cytoplasm of the host cell. Herpesviral genes are expressed in a temporally regulated manner, starting with the immediate early (IE) genes, followed by the early genes and finally the late genes.

The IE genes do not require prior viral protein synthesis and encode proteins important for transcriptional control of the early genes. The early gene products are required for replication of the viral genome, the initiation of late gene transcription and the accumulation of viral mRNAs in the cytoplasm for incorporation into progeny virus (Gruffat et al., 2016). In contrast with latency, viral DNA replication during the lytic phase is carried out by a viral DNA polymerase rather than that of the host. Finally, late viral proteins play structural roles in newly assembled virions and help with the infection and subversion of a new host cell.

Viral DNA synthesis produces concatemers of head-to-tail genomes that are cleaved to produce standard unit-length genomes (Jacob et al., 1979). Herpesvirus capsids are assembled in the nucleus and package nascently replicated DNA. The nascent nucleocapsids bud through the double nuclear membrane. First, they become enveloped at the inner membrane and enter the perinuclear space; then, they fuse with the outer membrane permitting their release into the cytoplasm (Guo et al., 2009; Johnson and Baines, 2011).

The exported nucleocapsids acquire tegument proteins and bud into vesicles synthesised by the host trans-golgi network. Within these vesicles, the final steps in virion maturation take place and nascent infectious herpesvirus particles bud from the cell after fusion of their surrounding vesicle with the plasma membrane (Lv et al., 2019).

1.2 Kaposi's sarcoma-associated herpesvirus (KSHV)

KSHV is a gammaherpesvirus of the *rhadinovirus* genus. Although the disease KS was described over 100 years earlier by Moritz Kaposi, KSHV was first identified in 1994 after the isolation of herpesvirus DNA from a KS tumour in an AIDS patient (Chang et al., 1994). KSHV has since been confirmed as the aetiological agent of KS and associated with two further lymphoproliferative disorders: Primary effusion lymphoma (PEL) and multicentric Castleman's disease (MCD). As a result, KSHV is classified as a group 1 carcinogenic agent by the International Agency for Research on Cancer (Winther et al., 1997).

KSHV seroprevalence is variable across different regions and populations with the highest rates exist in sub-Saharan Africa (>50%) where KS is endemic (Biryahwaho et al., 2010; Butler et al., 2011). Lower seropositivity is reported in Mediterranean countries (30%) and the rest of Europe, Asia and North America (<10%) (Patrick et al., 1983; N. Regamey et al., 1998; Engels et al., 2007). Outside of endemic regions, seroprevalence is higher among men who have sex with men and African migrants.

The highest levels of KSHV shedding are found in oral epithelial cells, suggesting that saliva is the most common method of transmission for the virus (Koelle et al., 1997). This leads to non-sexual transmission of KSHV between children in endemic areas, accounting for the high level of childhood infections in these regions (Koelle et al., 1997). However, there is also strong evidence that the virus can be transmitted through sexual contact, especially between men who have sex with men, and transplantation of infected organs and blood (Martin et al., 1998; N Regamey et al., 1998; Martin and Osmond, 1999; Martin and Osmond, 2000).

1.2.1 KSHV associated malignancies

1.2.1.1 Kaposi's sarcoma (KS)

KSHV is the aetiological agent of KS and present in all KS tumours whether AIDS-associated or not. The disease is characterised by multifocal angioproliferative neoplasms of the skin, mucosa and sometimes the viscera which present as dark purple lesions. Closer examination of these tumours shows they are polyclonal though the most common cell type among them, the spindle cell, is derived from an endothelial cell origin (Boshoff et al., 1997). Although the disease rarely arises in healthy individuals, those that are immunocompromised, especially HIV-infected, have a drastically elevated risk (Ganem, 1997). In approximately half of patients where immunocompetence is restored, especially through intervention with anti-retrovirals (ARTs) to combat AIDS, KS tumours can be sent into complete remission (Fiorelli et al., 1998). However, in some cases, the initiation of ART therapy in KSHV-infected individuals leads to a paradoxical worsening of disease attributed to KS-associated immune reconstitution inflammatory syndrome (KS-IRIS). Due to increased HIV load and reduced CD4 T cell count at initiation of ART therapy, KS-IRIS is more likely to occur in Africa where it contributes to significant mortality (Murdoch et al., 2008).

KSHV has four clinical sub-types which describe the severity of the disease and extent of immunosuppression: Classic, endemic, iatrogenic and AIDS-related. Classical KS is a slow growing tumour which usually affects older Mediterranean and eastern-European men. Endemic KS is a more aggressive form of the disease prevalent in sub-Saharan Africa (Wabinga et al., 1993). Iatrogenic KS usually occurs after transplantation of infected organs into an immunosuppressed individual (N Regamey et al., 1998). Finally, AIDS-associated KS is the most severe form of the disease with significant morbidity (Gao et al., 1996). Although all these sub-types require infection with KSHV for tumour progression, evidence suggests that the virus alone is insufficient for KS development. For example, not all KSHV-infected AIDS patients develop KS despite extensive immunosuppression, suggesting that certain genetic, immune or environmental cofactors are required (Lanternier et al., 2008).

In contrast to other tumours caused by gammaherpesviruses, both latency and lytic replication are required for KSHV-mediated oncogenesis. On primary infection with KSHV, both latent and lytic replication programmes are active; however, after several replication

cycles, latency predominates. KSHV preferentially targets B-lymphocytes as host cells and establishes a latently-infected B-cell reservoir that persists for life. However, approximately 1-2% of these latently-infected cells undergo activation into the lytic replication state independent of a defined external stimuli, facilitating the production of infectious virions and infection of endothelial cells (Zhong et al., 1996). In KSHV-infected endothelial cell culture systems, viral episomes are rapidly lost unless additional transformational events take place, suggesting the virus places selective pressure on endothelial cells to undergo transformation (Grundhoff and Ganem, 2004). Thus, the persistent infection of endothelial cells by KSHV virions leads to KS tumourigenesis (Figure 1.3). As a result, the study of both latent and lytic replication programmes can help guide the development of novel therapeutics against KS (Cai et al., 2010).

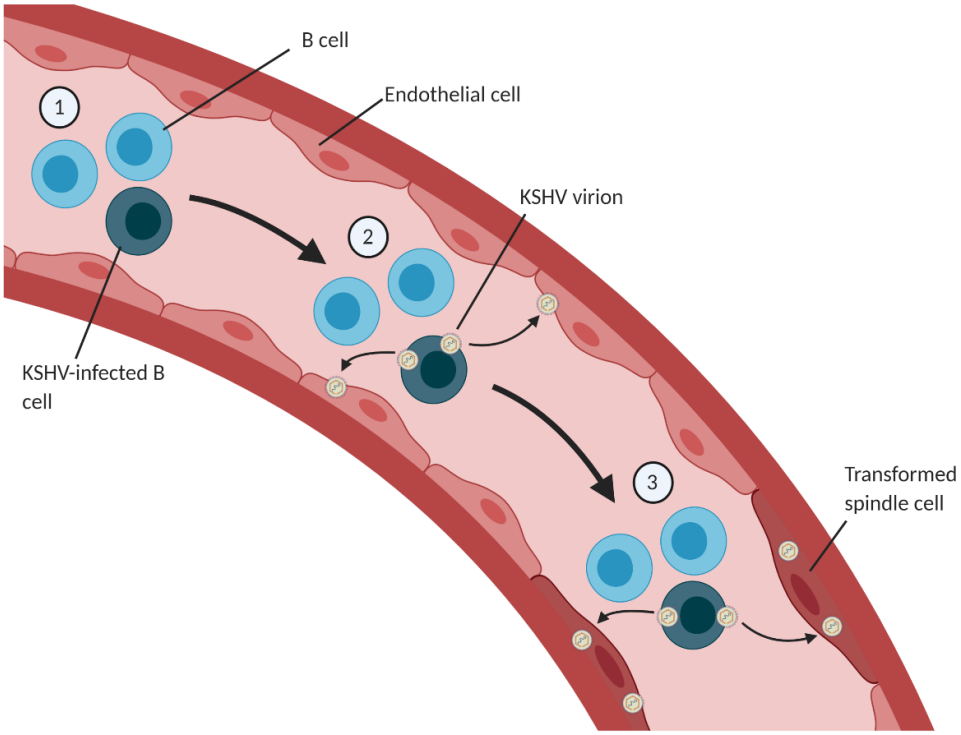

Figure 1.3. KS tumourigenesis. The formation of KS lesions is a multi-step process that requires both KSHV's latent and lytic replication programmes. 1) After initial infection, a latently-infected B-cell reservoir is established in the peripheral blood. 2) Upon stress or immunosuppression, KSHV undergoes reactivation to produce infectious virions. Initial infection of endothelial cells cannot be sustained until the cell has undergone transformation. 3) The constant infection of endothelial cells leads to transformation and spindling phenotypes that over time form highly vascular KS lesions.

1.2.1.2 Primary effusion lymphoma (PEL)

PEL is a rare non-Hodgkin's lymphoma that often affects immunocompromised individuals such as AIDS patients. The malignancy occurs in B cells after persistent infection with KSHV leading to long term expression of viral factors which drive oncogenesis (Nador et al., 1996; Narkhede et al., 2018). PEL-transformed B cells penetrate body cavities lined with serous membranes such as the pleura, peritoneum and pericardium cavities and proliferate rapidly (Kaplan, 2013). Unlike KS, restoration of immunocompetency does not ameliorate the disease and consequently prognosis is very poor (Narkhede et al., 2018). PEL cell lines, latently-infected with KSHV, are commonly used in the laboratory in the study of the virus.

1.2.1.3 Multicentric Castleman's disease (MCD)

MCD is a rare lymphoproliferative disorder with several different clinical forms. KSHV is present in nearly all HIV-positive MCD patients and less common in MCD patients that are HIV-negative (Soulier et al., 1995). Like PEL, the MCD cells derive from a B-cell origin but are polyclonal in nature (Polizzotto et al., 2012). The prognosis for the disease has improved dramatically in patients with KSHV-associated MCD since the introduction of highly active antiretroviral therapy (HAART).

1.2.2 KSHV genome

The KSHV genome is approximately 165kb in length with a 138kb coding region flanked by 801bp terminal repeat sequences which help circularisation (Russo et al., 1996). The KSHV genome encodes 85 ORFs of which 15 (ORFK1-ORFK15) are unique to KSHV (Arias et al., 2014). Moreover, like other herpesviruses, KSHV has acquired a number of ORFs through piracy of host cell genes including vMIPs, vIRFs, vCyclin, vFLIP, vGPCR, vIL-6 and vBCL2 (Sakakibara and Tosato, 2014).

The coding potential of the KSHV genome is greatly enhanced by the use of alternative splicing and alternative translation initiation codons. Furthermore, the virus is proposed to utilise a number of small and upstream open reading frames and encodes a number of non-coding RNAs (ncRNAs) including 12 viral pre-microRNAs (pre-miRNAs) which express 25 mature microRNAs (miRNAs) and long non-coding RNAs (lncRNAs) including circular RNAs

(circRNAs) (Arias et al., 2014; Abere et al., 2020). Of note, is the KSHV lncRNA PAN, which is the most abundant viral transcript in cells undergoing lytic replication.

1.2.3 KSHV life cycle

Like all herpesviruses, KSHV undergoes a complex, multi-step life cycle consisting of latent and lytic replication programmes which act co-operatively to ensure a lifelong infection (Figure 1.4). Upon initial infection, KSHV binds to host cells and enters via the interaction of viral glycoproteins gB, gL and gH to cellular surface receptors such as heparin sulphate, ephrin A2 and integrins (Kumar and Chandran, 2016). The predominant method of entry into target cells is by endocytosis, however KSHV also uses macropinocytosis and clathrin-mediated endocytosis to enter certain cell types (Inoue et al., 2003; Akula et al., 2003; Raghu et al., 2009). Once KSHV has entered the host cell, the nucleocapsid is trafficked to the nuclear pore and the genome injected into the host cell nucleus (Raghu et al., 2009).

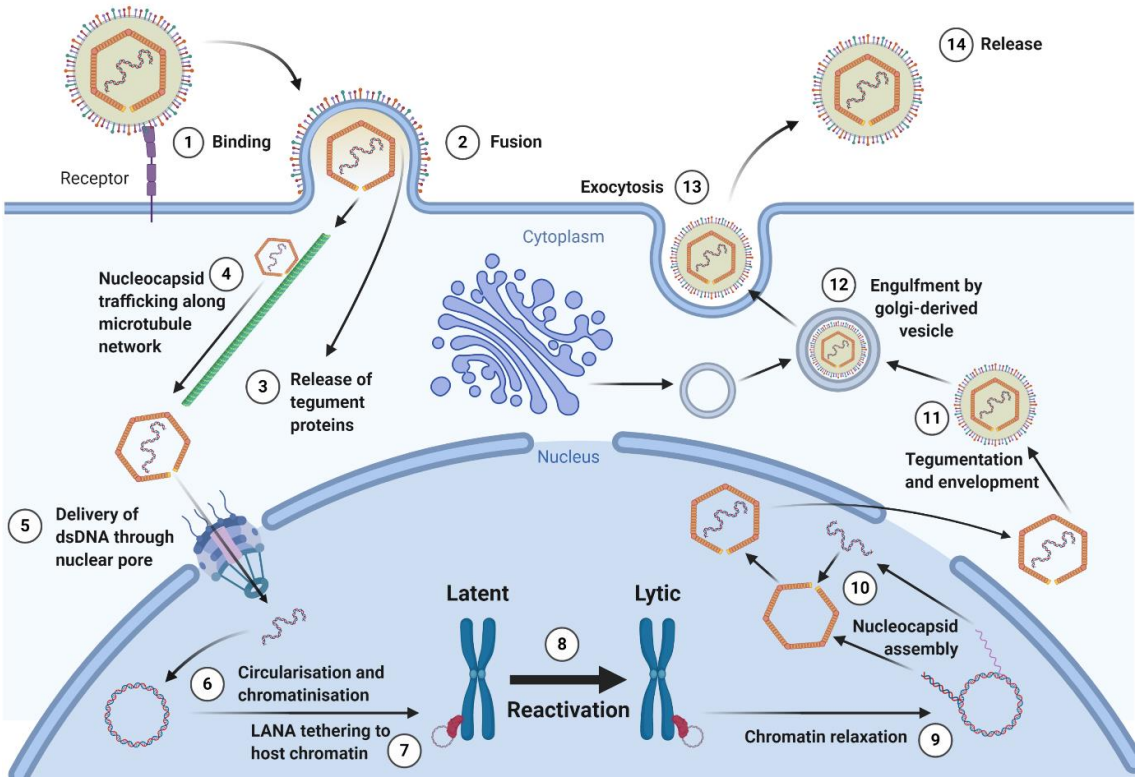

Figure 1.4. KSHV life cycle. KSHV undergoes a complex life cycle consisting of multiple steps. 1) The KSHV virion makes contact with a target cell using its surface glycoproteins. 2) The virus particle enters using cell type-dependent methods of entry. 3) The contents of the KSHV tegument are released into the host cell preparing it for infection. 4) The viral nucleocapsid is trafficked through the cytoplasm by the host cell ESCRT machinery before docking to the nuclear pore. 5) The dsDNA is fired through the nuclear pore into the nucleoplasm. 6) The KSHV genome undergoes circularisation into an episome and becomes chromatinised. 7) The KSHV protein LANA tethers the viral episome to host cell chromatin leading to initiation of the latent KSHV replication programme. 8) Under stress conditions or immunosuppression, KSHV undergoes reactivation into the lytic phase. 9) Chromatin demodifying enzymes are brought to the KSHV episome leading to KSHV gene expression. 10) KSHV gene expression leads to the replication of the viral dsDNA genome by the rolling circle mechanism. Late KSHV gene expression leads to construction of capsids at viral replication centres in the nucleus. Replicated genomes enter capsids through the portal complex. 11) The nucleocapsids bud through the nuclear membrane and reach the cytoplasm where they acquire a tegument and envelope. 12) The mature KSHV virions are engulfed by vesicles derived from the golgi and migrate to the cell membrane. 13) The vesicles containing KSHV virions fuse with the host cell. 14) The KSHV virions are released outside the cell ready to disperse and infect new target cells.

1.2.3.1 Latency

After entry into the target cell nucleus, the KSHV genome is rapidly circularised and tethered to the host chromatin by the latent viral protein latency associated nuclear antigen (LANA) (Uppal et al., 2014). Gene expression is highly restricted in KSHV-infected cells undergoing latency with only a few genes expressed including LANA, vCyclin, vFLIP, kaposin's A, B and C as well as 12 pre-microRNAs (Uppal et al., 2014). The open reading frames (ORFs) of latency

associated genes are located in actively transcribed latency regions lacking both nucleosomes and repressive histone modifications (DeCotiis and Lukac, 2017). In contrast, the expression of lytic genes is tightly restricted by condensed chromatin and no infectious virions are produced. LANA acts as the master regulator of KSHV latency maintaining the chromatinisation, replication and segregation of KSHV episomes and thus is indispensable for long term latent survival of KSHV in infected hosts (Uppal et al., 2014). Importantly however, stable maintenance of KSHV episomes is not observed among any latently-infected cell types, likely due to errors in replication and segregation during cell division (Grundhoff and Ganem, 2004). However, the infection of new cells through virion production in the lytic phase sustains the population of latently infected cells that would otherwise diminish. Thus, KSHV latent and lytic replication programmes complement one another to allow long term persistence of the virus in an infected individual.

1.2.3.2 Lytic replication

Cells infected with latent KSHV can be stimulated to undergo lytic replication in response to external factors such as stress, hypoxia, viral coinfections, immunosuppression or inflammation (Vieira et al., 2001; Gil et al., 2003; Uldrick et al., 2010; Davis et al., 2011; Tang et al., 2012). In addition, latently infected cell culture systems can be induced into lytic replication by the addition of chromatin demodifying chemicals such as sodium butyrate, 12-O-tetradecanoylphorbol-13-acetate (TPA) and valproic acid (Miller et al., 1997). The presence of these environmental or chemical factors leads to reconfiguration of the KSHV episome into an active chromatin state, the expression of all KSHV genes in a temporal cascade and the mass production of infectious virions (Figure 1.5) (Wang et al., 2004).

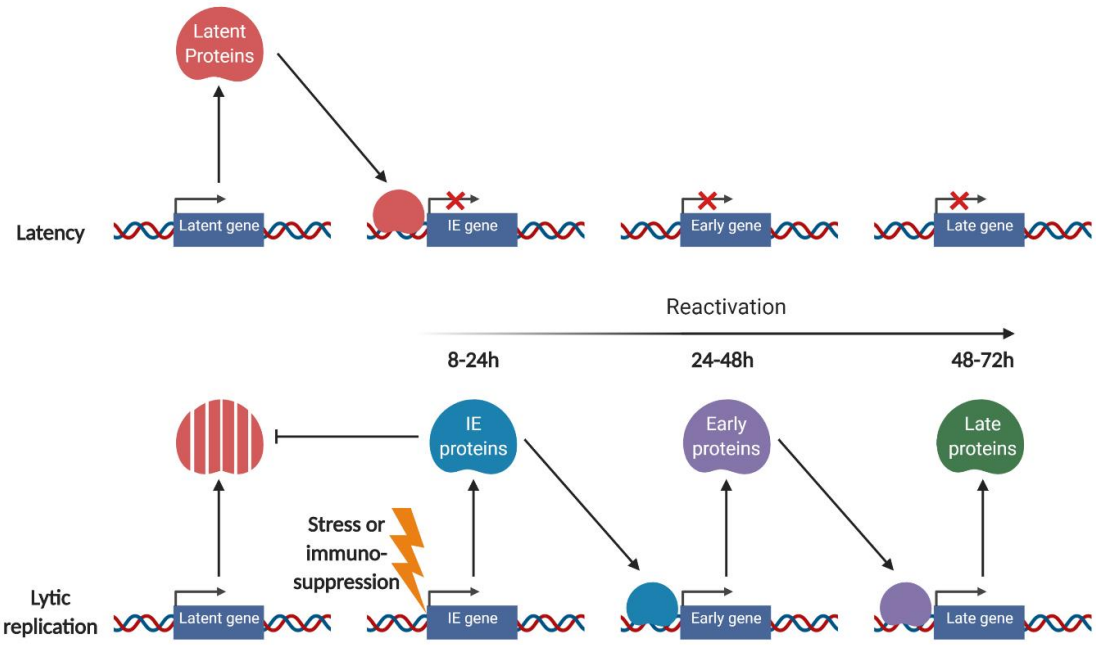

Figure 1.5. KSHV lytic gene expression. KSHV gene expression is a highly ordered temporally regulated process. In latency, latent proteins including LANA bind IE lytic gene promoters and prevent transcription. Under stress or immunosuppression, the virus undergoes reactivation into the lytic phase starting with the expression of IE genes. RTA degrades LANA allowing the active transcription of IE genes encoding proteins which in turn initiate the transcription of the early genes. The early proteins kickstart the replication of the viral genome and commence the transcription of late genes which encode components of the KSHV virion.

Of central importance to the temporal cascade of viral gene expression during lytic reactivation is the lytic master regulator RTA, encoded by the *ORF50* gene. RTA is necessary and sufficient for KSHV reactivation, as ectopic expression of this viral factor leads to completion of lytic replication, through transactivation of a variety of cellular and viral promoters (Lukac et al., 1999; Bu et al., 2008). The N-terminal domain of RTA allows binding to various RTA-response elements (RREs) in the KSHV genome while the transactivation domain induces lytic gene expression (Figure 1.6) (Lukac et al., 2001). In some cases however, RTA interacts with the cellular transcription factor RBP-Jκ, altering the protein's binding specificity and thus relocalising RBP- Jκ to RREs for transactivation (Liang et al., 2002). Similarly, with the aid of several other cellular factors including Oct-1, c-Jun, SP1, STAT3 and c/EBPα, RTA has been found to transactivate the promoters of many additional target genes (Aneja and Yuan, 2017). Finally, RTA has also been found to mediate gene expression through proteosomal degradation of transcriptional repressors, including LANA

and the Notch signalling protein Hey-1, using its E3 ubiquitin ligase domain (Yang et al., 2008; Gould et al., 2009). As the master regulators of KSHV latent and lytic replication programmes, the interplay between LANA and RTA is strictly controlled with both acting antagonistically to each other to ensure efficient persistence in the host (Lan et al., 2004).

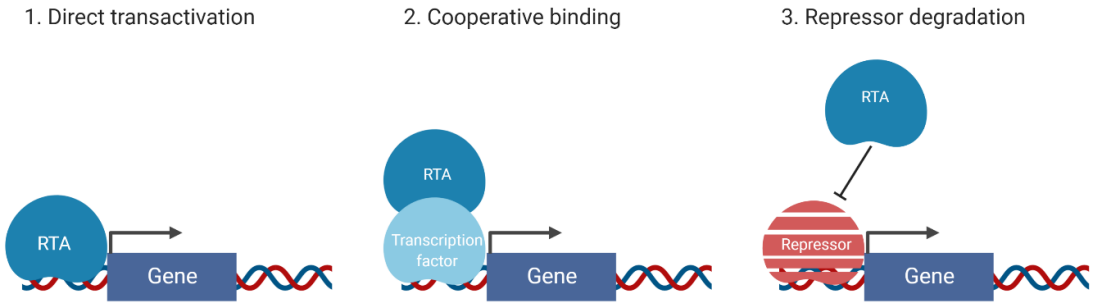

Figure 1.6. RTA mechanisms of controlling gene expression. RTA promotes gene expression through 3 main mechanisms. 1) RTA directly binds to a target gene promoter and activates transcription. 2) RTA recruits transcription factors such as RBP-Jκ to cooperatively activate gene expression. 3) RTA degrades transcriptional repressors such as LANA or HEY1 through use of its E3-ubiquitin ligase domain to target proteins for proteosomal digestion.

1.3 The life cycle of an mRNA

The life cycle of an mRNA is a multistep process starting with transcription and ending with degradation. Importantly, mRNA serves as a critical intermediary between DNA and protein, enabling dynamic control of gene expression. The life cycle of an mRNA starts in the nucleus with the transcription and processing of a pre-mRNA to produce a mature mRNA. The mature mRNA is then exported from the nucleus where it is translated into protein by the ribosome. Finally, the mRNA is degraded and its ribonucleotide components recycled.

1.3.1 The nuclear RNA cycle

1.3.1.1 Transcription

mRNA transcription, using DNA as a template, is carried out by RNA polymerase II (RNAPII) in the nucleus of eukaryotes. This is a three-step process involving initiation, elongation and termination. During initiation, RNAPII associated with general transcription factors binds to the promoter of a gene to form a pre-initiation complex (Figure 1.7). The DNA duplex is

melted to separate the two strands and ribonucleotides are added to start the formation of a nascent RNA strand. Next, RNAPII dissociates from the general transcription factors situated at the promoter and starts elongation. The polymerase progresses along the entire body of the gene with the DNA strands unzipping in front and reannealing behind. The RNA strand continues to elongate until RNAPII recognises the poly(A) signal sequence and transcription terminates. Then, the nascent mRNA is released and RNAPII dissociates from the DNA to be recycled (Lenstra et al., 2016).

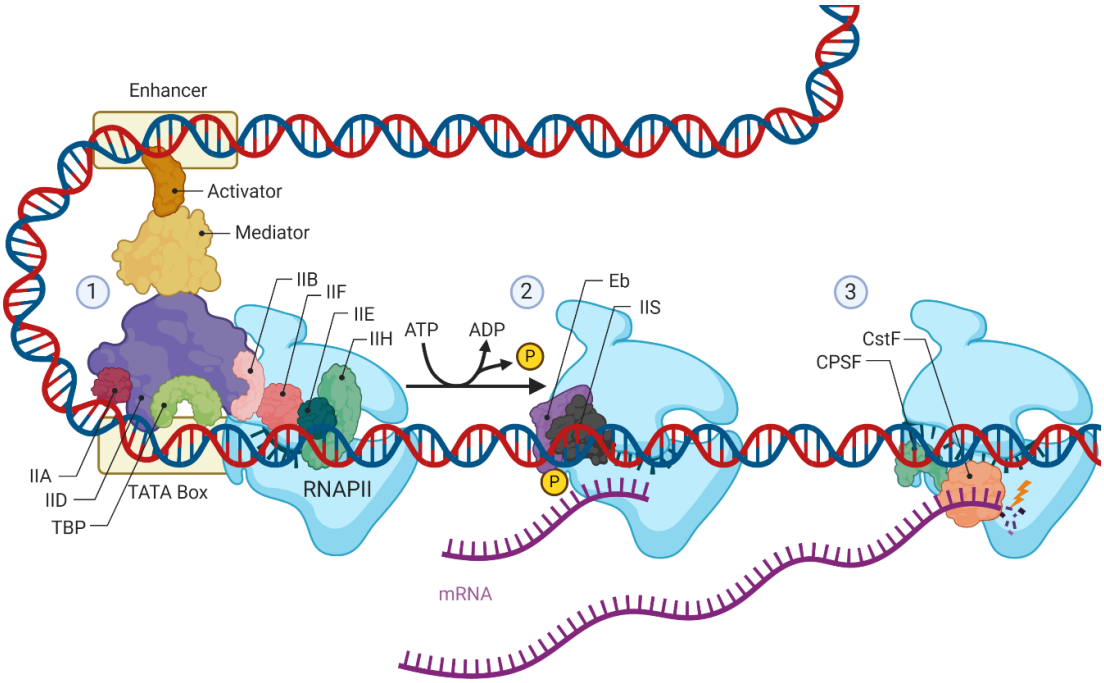

Figure 1.7. Eukaryotic gene transcription by RNA polymerase II. The transcription of eukaryotic genes into mRNA by RNAPII takes place in three distinct phases: (1) Initiation, (2) elongation and (3) termination. 1) Transcription initiation takes place at gene promoters, such as the highly conserved TATA box, slightly upstream of their transcription start site. Other sequence elements, including enhancer and insulator regions, bind transcriptional activators or repressors to alter the rate of transcription for a gene. In promoters that contain a TATA box (~40% of genes), a preinitiation complex assembles starting with the binding of the TATA box binding protein subunit of TFIID. Next, TFIIA and TFIIB stabilise the DNA-transcription factor assembly and recruit RNAPII and TFIIF which bridges TDP and the polymerase. TFIIE binding in turn recruits TFIIH which melts the promoter DNA allowing formation of an RNA-DNA hybrid. Finally, TFIIH's kinase subunits phosphorylate the C-terminal tail domain of RNAPII at every 5th serine residue within a repeated heptapeptide sequence allowing promoter escape and transcription elongation. 2) During elongation, an RNA-DNA hybrid is formed one base at a time with the trailing DNA and RNA exiting from separate tunnels of RNAPII. Unlike initiation, TFEb differentially phosphorylates the C-terminal tail of RNAPII at every 2nd Serine residue to promote elongation. In addition, TFIIS increases the rate of transcription by reducing pause times at certain DNA sequences and helping resolve misincorporated ribonucleotide bases. 3) As RNAPII reaches the end of a gene, CPSF and CstF recognise the poly(A) signal sequence and the latter transcription factor cleaves the mRNA molecule by ATP hydrolysis to achieve transcription termination.

1.3.1.2 Processing and maturation

The pre-mRNA precursor that is generated through transcription undergoes maturation into a mature mRNA through the removal of introns and the addition of two external modifications on each end of the molecule. Importantly, the processing and maturation of a pre-mRNA is a co-transcriptional process that impacts on the later life on an mRNA molecule.

Pre-mRNA splicing is carried out by the spliceosome, a huge dynamic complex of proteins and small nuclear RNAs (snRNAs; Figure 1.8). The spliceosome recognises specific sequences around intron-exon junctions and catalyses a series of reactions that lead to ligation of exons and release of an intron lariat (Shi, 2017). The scars of splicing at exon-exon junctions are marked by the exon junction complex (EJC) which is of critical importance later in the mRNA life cycle.

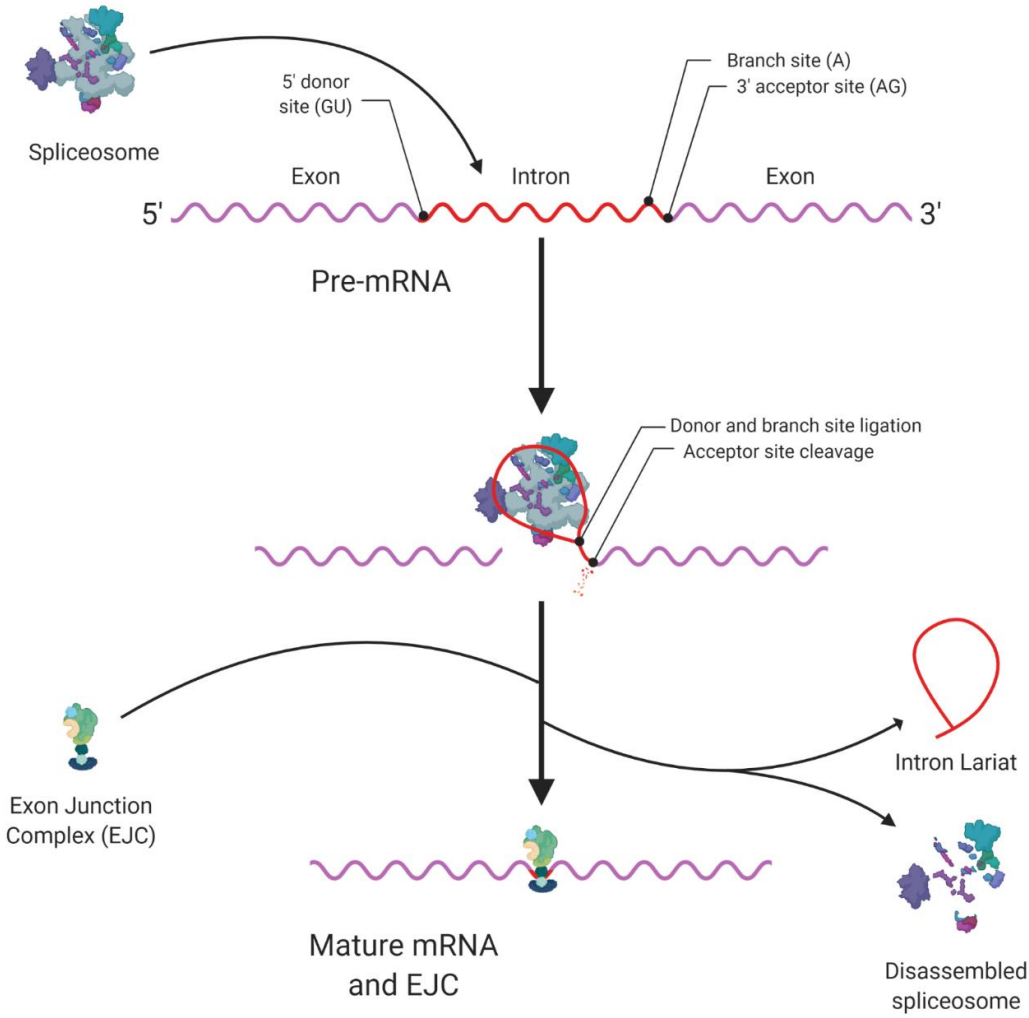

Figure 1.8. Splicing of pre-mRNA. The process of intron removal from pre-mRNA to produce mature mRNA is known as splicing. The process is carried out by a large ribonucleoprotein complex known as the spliceosome which is comprised of 5 snRNAs and approximately 150 proteins. Within an intron, a 5' donor site containing a GU sequence, a near 3' branch site containing an adenine residue and a 3' acceptor site containing an AG dinucleotide are required for splicing. The initiation of splicing involves the binding of the snRNP U1 to the 5' donor site and the protein U2AF to the 3' acceptor site. In turn, U2AF recruits BBP to the branch site which is then displaced by U2 leaving a bulge at this adenine residue. Furthermore, U2AF and U1 dissociate from the intron to be replaced by U4, U5 and U6. The interaction between U6 at the donor site and U2 at the branch site drives a two-step reaction: First, a lariat is formed by ligation of the donor and branch sites and second the acceptor site is cleaved at the AG sequence and the exons are ligated together while the intron lariat is discarded. Finally, the newly formed exon-exon boundaries are marked by the exon junction complex for downstream processes while the spliceosome dissociates and becomes recycled for further splicing events.

Very early in the process of transcription, when the nascent RNA chain is approximately 30bp, a 7-methylguanosine (m^7G) cap is added to the 5' end of the growing molecule (Coppin et al., 2018). Furthermore, once the 3' end of the pre-mRNA is released during transcription termination, a polyadenosine (poly(A)) tail is added (Coppin et al., 2018). Together, these two RNA modifications prevent the degradation of the newly matured mRNA by exoribonucleases.

1.3.1.3 Nuclear export

Only a mature mRNA can undergo export to the cytoplasm as key proteins involved in this process are recruited during the prior processing steps. The transcription and export complex (TREX), a key factor in this process, accumulates at the 5' cap and EJCs along the mRNA during transcription (Sträßer et al., 2002; Katahira, 2015). In turn, TREX components recruit the NXF1-NXT1 heterodimer to these sites and drive a molecular handover event whereby NXF1 undergoes conformational changes that permit RNA binding (Carmody and Wente, 2009; Viphakone et al., 2012). The NXF1-NXT1 heterodimer then exports the mRNA to the cytoplasm through the hydrophobic core of the nuclear pore (Figure 1.9).

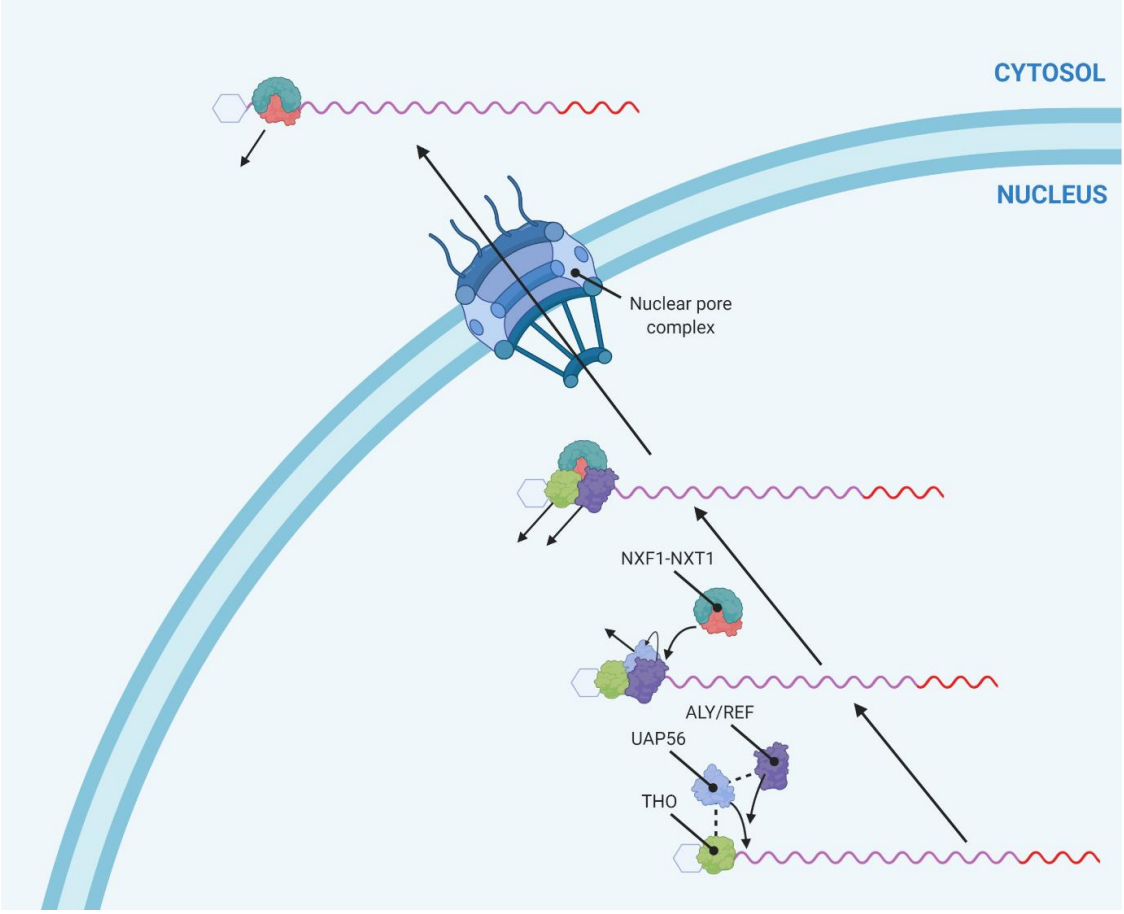

Figure 1.9. Nuclear export of mRNA. The nuclear export of mRNA is essential in shuttling an mRNA from its site of synthesis in the nucleus to where it can be translated in the cytoplasm. During transcription elongation, the phosphorylation of serine residues in the C-terminal domain of RNAPII recruits numerous factors involved in downstream processing and export steps. One of these factors is THO, the first component of the TREX complex to assemble on the mRNA which recruits subsequent members of TREX including UAP56 and ALY/REF. Next, ALY/REF recruits the heterodimeric export receptor NXF1-NXT1 and triggers the ATPase activity of UAP56. The result is a molecular handover event where NXF1-NXT1 displaces UAP56 to bind the mRNA through ALY/REF. Then, NXF1-NXT1 relocates the mRNA to the nuclear pore, a large complex of over 30 nucleoporins with a central channel formed by FG repeat sequences.

Finally, NXF1-NXT1 facilitates the passage of the mRNA through the hydrophobic core of the nuclear pore by interacting with the FG-containing nucleoporins. The exported mRNA may then undergo translation in the cytoplasm.

1.3.2 The cytoplasmic RNA cycle

1.3.2.1 Localisation to RNA granules

Once exported to the cytoplasm, many transcripts localise to RNA granules which permit greater spatiotemporal control of gene expression. Through phase separation, these membraneless compartments become biophysically distinct from the surrounding cytosol. RNA granules enrich a number of RNA-binding proteins which affect the localisation, translation, stability and decay of the mRNA species they contain (Martin and Ephrussi, 2009). For examples, RNA transport granules enable the shuttling of transcripts to certain cellular destinations allowing localised translation. As a result, the localisation of a transcript to a particular RNA granule is a key step in the determination of its fate.

Two types of RNA granule, which arise under cellular stress, are processing-bodies (P-bodies) and stress granules. The former generally contains stalled translation initiation machinery while the latter enriches mRNA decay factors (Decker and Parker, 2012). Importantly, these granules trade mRNAs allowing their degradation or translation once cellular stress is resolved.

1.3.2.2 Translation

Translation is the process of protein synthesis through the decoding of an mRNA by the ribosome. The ribosome is a large complex consisting of ribosomal RNA (rRNA) and multiple ribosome-associated proteins. Like transcription, translation of an mRNA takes place in three phases: Initiation, elongation and termination (Figure 1.10).

During translation initiation, eukaryotic initiation factors (eIFs) play key roles in the recruitment and assembly of a fully formed 80s ribosome to the start codon of an mRNA (Moore and von Lindern, 2018) (Figure 1.11). In elongation, the ribosome advances processively along the mRNA, codon by codon, with a growing polypeptide chain forming in its wake. Charged aminoacyl tRNAs are gradually delivered by eukaryotic elongation factors (eEFs) to add amino acids to the synthesising protein (Dever and Green, 2012; Schuller and

Green, 2018). Finally, when a stop codon is recognised, translation termination is achieved by eukaryotic release factors (eRFs) which release the newly synthesised polypeptide.

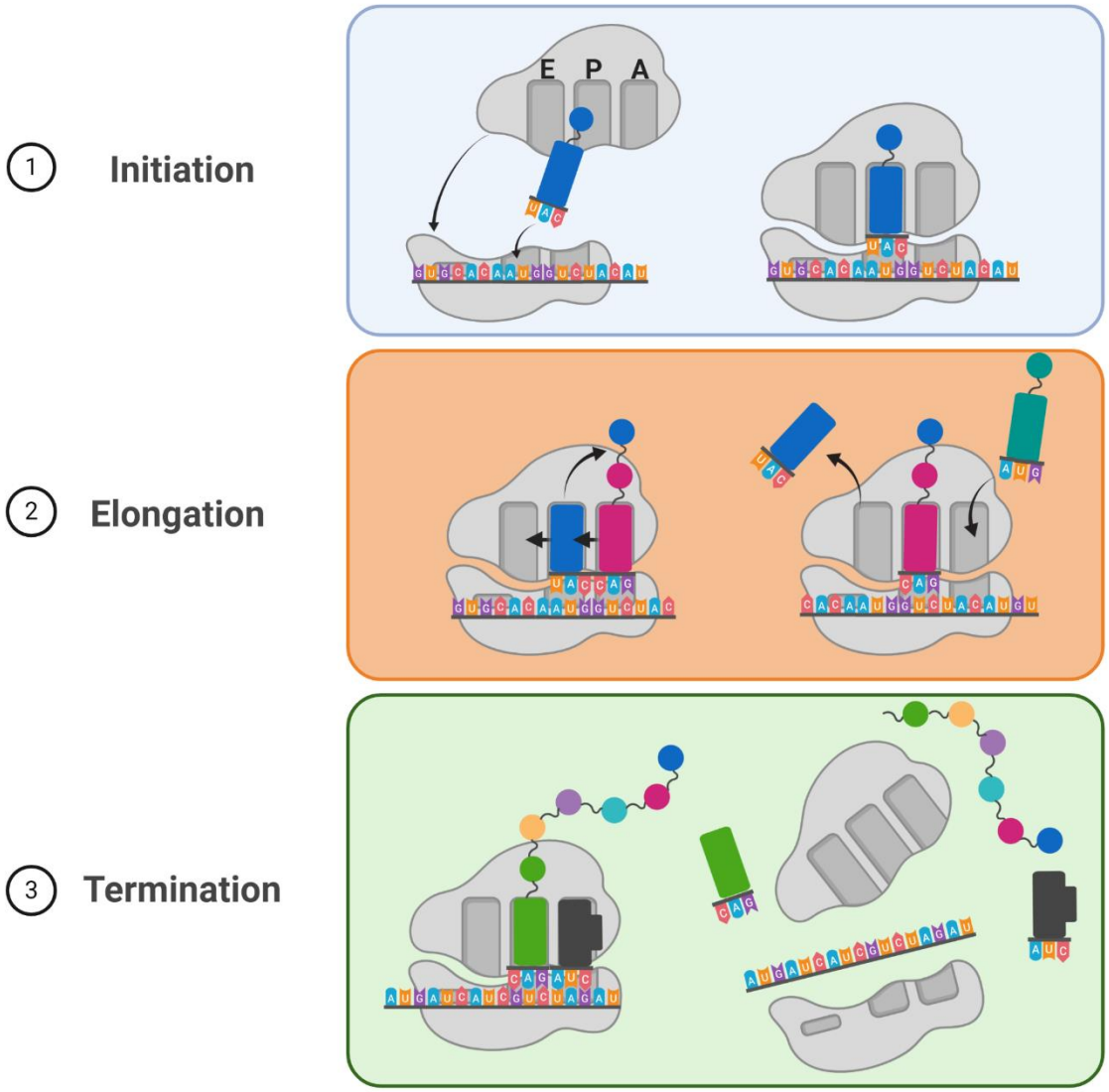

Figure 1.10. Eukaryotic translation. Like transcription, mRNA translation can be separated into 3 steps including initiation, elongation and termination. 1) During initiation, an 80s ribosomal initiation complex is assembled at the start codon of an mRNA. The methionine initiator tRNA occupies the peptidyl (P) site of the ribosome and its anticodon is base paired to the AUG start codon. 2) At the start of elongation, a second tRNA species with an anticodon complementary to the second codon is loaded into the aminoacyl (A) site by EEF1A. Through GTP hydrolysis, a peptide bond is formed between the initiator methionine and the second aminoacyl-tRNA at the A site [106]. The ribosome then shifts by one position on the mRNA so that the empty initiator tRNA enters the E site and leaves the ribosome, while the remaining dipeptidyl-tRNA enters the P site. The process repeats so that a polypeptide chain is formed, one amino acid at a time, by the constant shifting of the ribosome along the mRNA. 3) Finally, when a stop codon enters the P site of the ribosome, translation termination is carried out by eukaryotic release factors [106]. Cooperatively, eRF1 and eRF3 catalyse the hydrolysis of the bond associating the nascent peptide and the tRNA. In addition, the 80s ribosome is disassembled by ABCE1 into 40S and 60S subunits to begin a new round of translation.

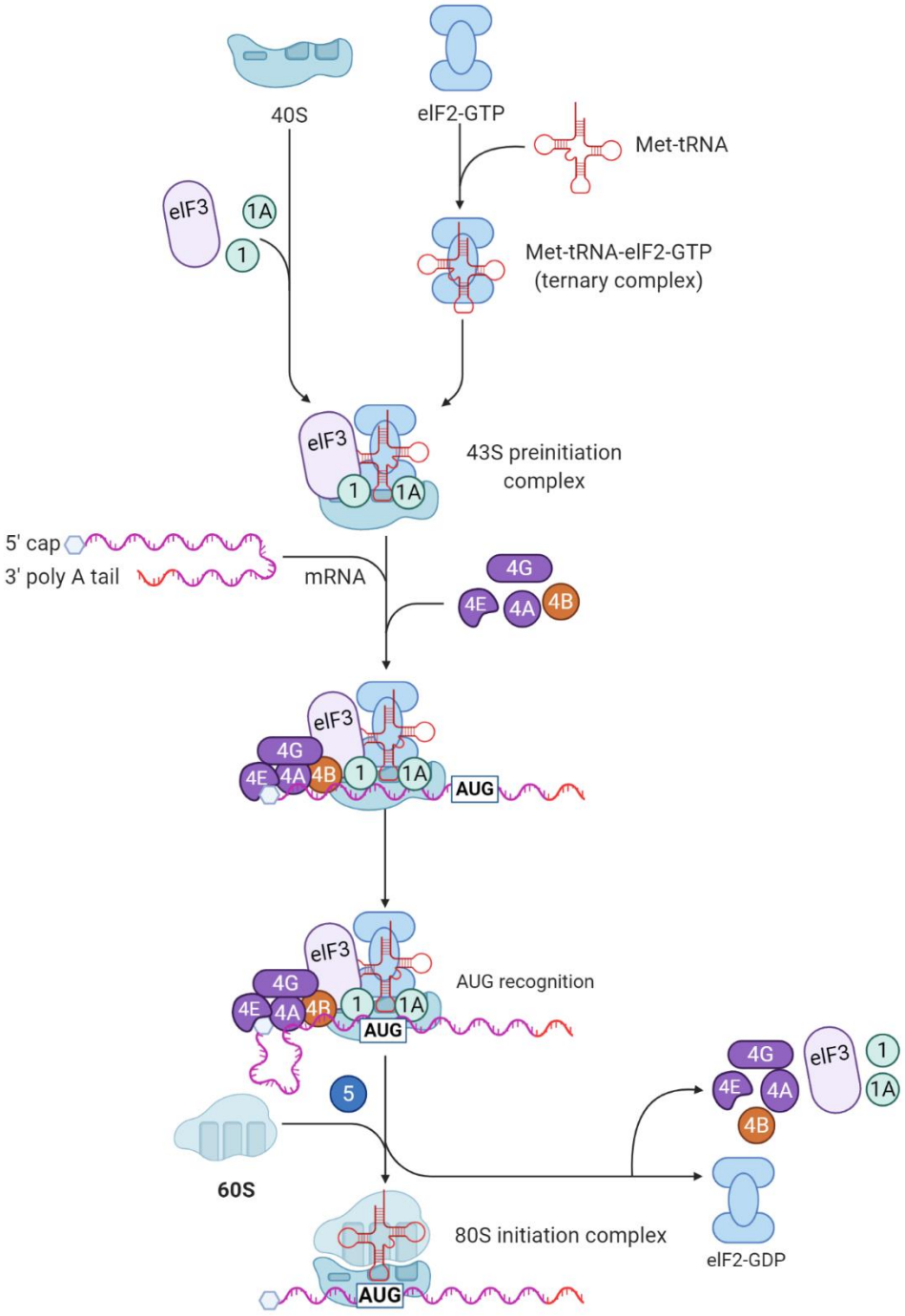

Figure 1.11. Ribosome assembly at start codons. Initiation of translation is carried out by the assembly of initiator tRNA and the 40s and 60s ribosomal subunits into an 80s ribosome by eukaryotic initiation factors. First, eIF1A, eIF1 and eIF3 associate with the small 40s ribosomal unit and are later joined by eIF2 in complex with GTP and an initiator methionine transfer RNA (tRNA) to form the 43S pre-initiation complex [105]. Meanwhile, on the mRNA, eIF4E binds the 5' m^7G cap and eIF4G is associated with the 3' poly(A) tail through poly(A) binding protein. Thus, the interaction of these two proteins from the eIF4 complex with external RNA modifications leads to circularisation of the mRNA (For simplicity, not shown in this diagram). Importantly, eIF4E is the rate limiting factor in canonical cap-dependent translation initiation therefore the translation rate is proportional to eIF4E concentration. Through interactions between eIF4G and eIF3, the 43S preinitiation complex is recruited to the 5' end of the mRNA where it

begins to scan for the initiation codon AUG. Once found, the anticodon of the methionine initiator tRNA base pairs with the AUG codon whereupon eIF5 triggers the hydrolysis of eIF2-GTP, releasing eIF2-GDP and enabling binding of the large 60S subunit. The fully formed 80S ribosome then proceeds with elongation**.**

1.3.2.3 Stability and decay

The functional levels of an mRNA are the result of an equilibrium between synthesis and rate of degradation. Therefore, while transcription is of critical importance, alterations in the decay of a transcript allow rapid changes in gene expression and the healthy functioning of the cell.

Throughout the mRNA life cycle, the 5' cap and 3' poly(A) tail play important roles including the inhibition of transcript degradation by exonucleases (Garneau et al., 2007; Ashworth et al., 2019). In eukaryotes, the predominant method for degradation of mRNAs requires the removal of these external RNA modifications (Figure 1.12). However, the cleavage of an mRNA internally by endonucleases precludes the need for decapping or deadenylation allowing the exonucleases XRN1 and the exosome to degrade the transcript at its nascently exposed termini.

In addition to various RNA decay mechanisms which recycle functional mRNAs, nonsense mediated decay (NMD) is a mechanism through which transcripts containing premature translation termination codons are degraded to prevent the synthesis of truncated proteins with potential toxicity to the cell. The process relies on various UPF proteins which bind to eukaryotic release factors surrounding premature translation termination codons and recruit general mRNA degradation factors.

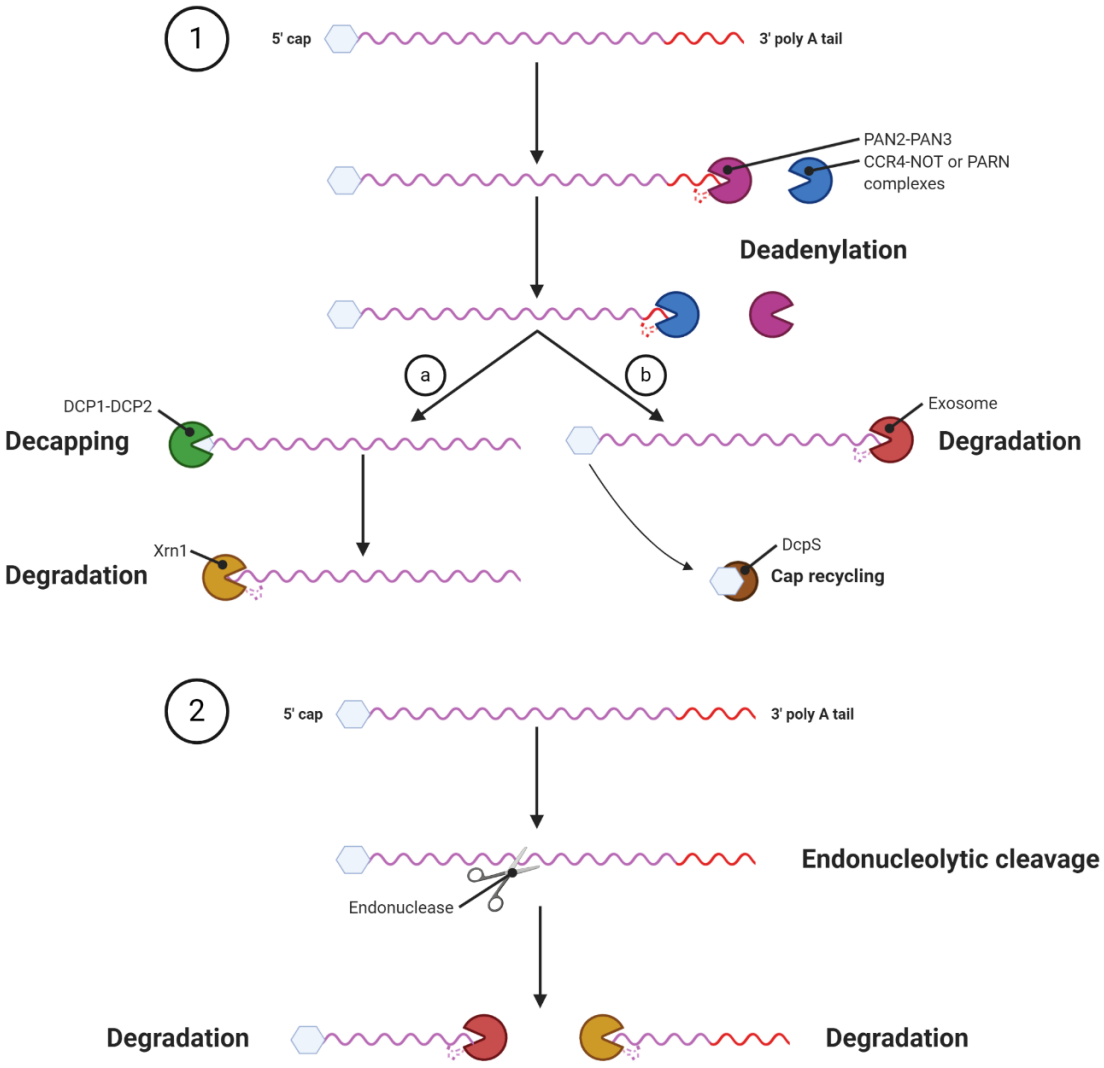

Figure 1.12. mRNA decay. 1) The two most common methods for degradation of an mRNA involve the removal of external RNA modifications, exposing the transcript to exonucleolytic digestion. In both cases, the mRNA is first deadenylated in a two-step process by the PAN2-PAN3 complex, followed by the PARN complex or members of the CCR4-NOT deadenylation machinery. Once the poly(A) tail is removed, the transcript can be either degraded by (a) 5' to 3' or (b) 3' to 5' mechanisms. In the former method, the mRNA must first be decapped by DCP1 and DCP2 and then degraded by the exoribonuclease XRN1. In the latter method, the transcript is degraded by the exosome and the 5' cap scavenged for recycling by DcpS. 2) In the case of mRNA cleavage by an endonuclease, the unprotected ends can be directly degraded by the exonucleases Xrn1 and the exosome.

The stability of mRNAs can be regulated by several additional genetic elements, often situated within the 3' UTR, which determine when the transcript will be degraded (Figure 1.13). AU-rich elements (AREs) are often found in the 3' UTRs of transcripts whose expression must be tightly regulated such as transcription factors and proto-oncogenes (Garneau et al., 2007; Ma and Mayr, 2018). Furthermore, several small RNAs including miRNAs, small interfering RNAs (siRNAs) and Piwi-interacting RNAs (piRNAs) are loaded into RNA-induced silencing complexes (RISCs) in complex with Argonaute proteins permitting

RISC docking at complementary sequences within 3' UTRs (Ghildiyal and Zamore, 2009; Coppin et al., 2018; Ashworth et al., 2019). ARE binding proteins and RISCs recruit deadenylases such as PAN2/PAN3 and CCR4-NOT to cleave the transcript internally allowing the unprotected RNA termini to be swiftly degraded by XRN1 or the exosome. Importantly, many ARE-binding proteins and components of the small RNA-induced silencing pathways are enriched in P-bodies highlighting these molecular compartments as regulatory centres for RNA decay (Garneau et al., 2007).

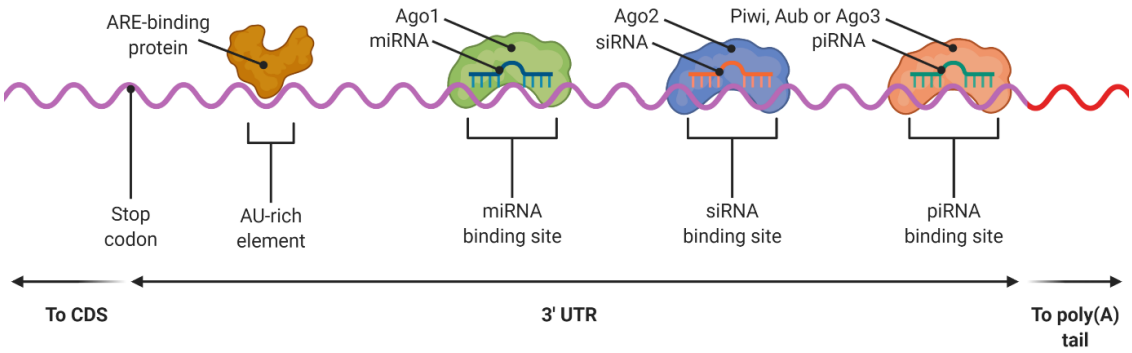

Figure 1.13. Common destabilising genetic elements in 3' UTRs of mRNA. The presence of several genetic elements within an mRNA's 3' UTR may affect the transcript's rate of decay or target the mRNA for degradation. AU-rich elements (AREs) are adenine and uracil-rich sequences often found in mRNAs with rapid turnover. ARE binding proteins may bind these motifs and aid or inhibit the stability of the ARE-mRNA. Furthermore, several small RNAs including miRNAs, siRNAs and piRNAs form RISCs with Ago proteins and base pair with complementary sequences in mRNA 3' UTRs. miRNA RISCs lead to destabilisation or translational repression of their target mRNAs whereas siRNA RISCs harness the endonuclease activity of Ago2 to cleave transcripts internally allowing exonuclease digestion. Finally, piRNAs primarily bind to transposon mRNAs where they are thought to cleave the transcript *in cis.* While the most common 3' UTR genetic elements are shown, additional regulatory elements, RNA binding proteins and RNA interference pathways have been proposed to influence the stability and decay of mRNAs.

1.4 Epitranscriptomics

In parallel with the modifications of DNA which comprise the epigenome and the post-translational modifications of protein which are sometimes referred to as the epiproteome, RNA has its own additional regulatory layer known as the epitranscriptome (Figure 1.14). The existence of these RNA modifications has been recognised for nearly 60 years (DAVIS and ALLEN, 1957; Cohn, 1960). However, recent technological advances are only now beginning to decipher the functional importance of these regulatory marks in widespread physiological processes (Desrosiers et al., 1974; Manners et al., 2019). As a result,

epitranscriptomics is currently a rapidly evolving field with a vast sum of knowledge gathered in recent years. Over 170 different modifications are now known to affect RNA fate and function, with the majority of these existing on noncoding RNA such as tRNAs, rRNAs and snRNAs (Machnicka et al., 2013). However, a number of these RNA modifications also exist on mRNA, exhibiting significant regulatory control over various stages of their biology.

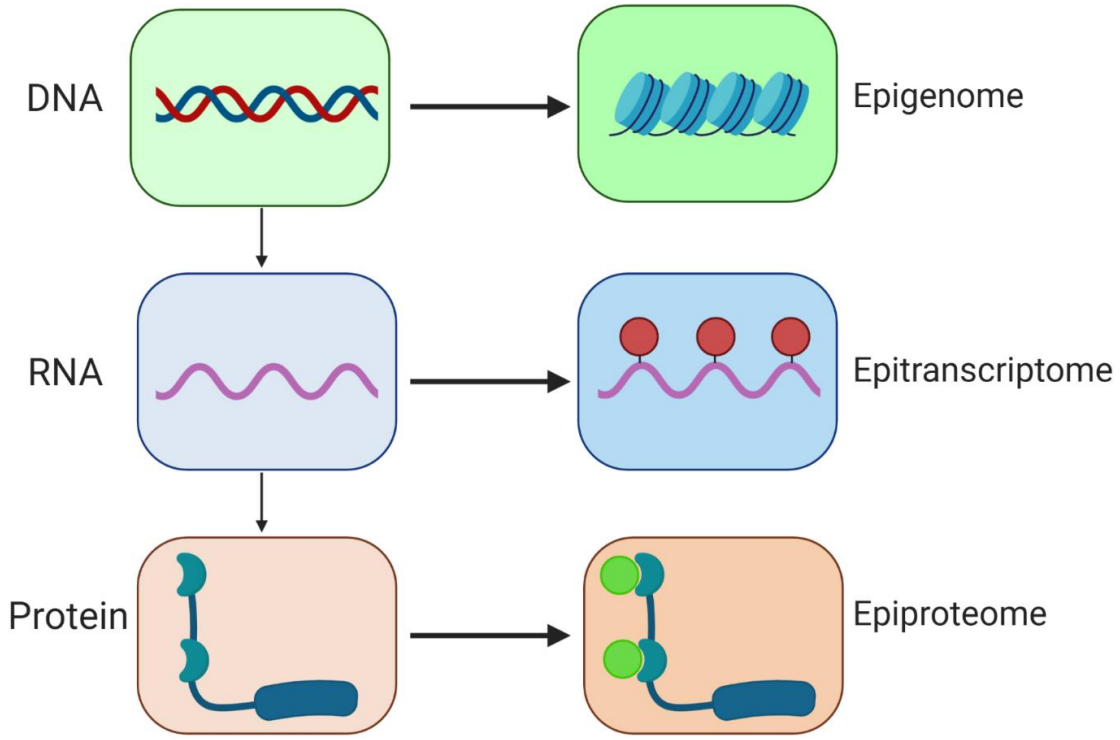

Figure 1.14. Additional regulatory layers of gene expression. The flow of genetic information according to the central dogma of molecular biology is also regulated by additional layers which regulate gene expression. At the DNA level, transcriptional activation is modified by histone modifications and DNA methylation which comprise the epigenome. Somewhat understudied is the epitranscriptome, made up of RNA modifications which regulate the fate and function of RNA. Finally, post-translational modifications of protein, which make up the epiproteome regulate enzymatic activity.

1.4.1 Diversity of internal mRNA modifications

External modifications of mRNA, such as the 5' m^7G cap structure and 3' polyA tail play significant roles in mRNA regulation. These modifications are extensively studied, performing important functions including RNA stability, splicing, nuclear export, translation and recycling. However, recent evidence suggests internal modifications of mRNA also regulate all stages of mRNA life cycle and play key roles in wide-ranging physiological processes and disease pathways. Importantly, some RNA modifications are described as

dynamic in nature with various RNA modifying enzymes identified which install, remove and decode these epitranscriptomic marks. Writers, erasers, and readers, as they are known, help carry out rapid alterations in RNA biology in response to various cellular states such as stress and infection (Esteve-Puig et al., 2020). Considerable diversity exists among the different internal mRNA modifications with common changes occurring on three of the four RNA bases and the ribose sugar (Figure 1.15).

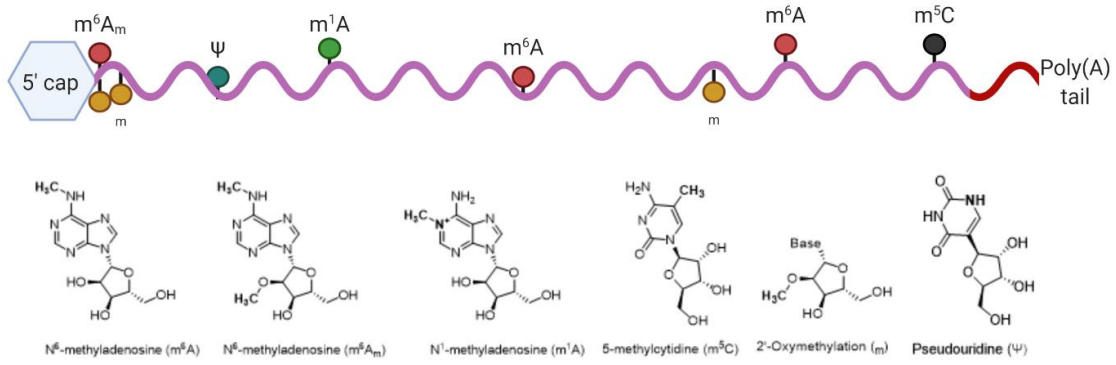

Figure 1.15. Diversity of internal RNA modifications. Numerous chemical modifications of mRNA exist which affect fate and function. Modifications are distributed along the mRNA where they are thought to be most concentrated *in vivo*. Chemical structures of modified residues are shown with changes in bold.

1.4.1.1 Modified adenosines

m^6A is the most common and best studied internal modification of mRNA. This regulatory mark is an ancient modification, conserved between vertebrates, plants, yeast, bacteria, archaea and importantly, viruses (Canaani et al., 1979; Kowalak et al., 1994; Deng et al., 2015; Tirumuru et al., 2016; Kennedy et al., 2016; Lichinchi, Gao, et al., 2016). m^6A is characterised by the addition of a methyl group to the N^6 position of an adenosine residue with approximately 0.1-0.4% of adenosine residues methylated at this position in mammals (Wei et al., 1975). m^6A is dynamically regulated and decoded by several groups of enzymes termed the 'm^6A machinery' which will be discussed in detail later.

Like m^6A, a similar modification known as N^6,2'-O-dimethyladenosine (m^6A_m) is methylated at the N^6 position but also methylated at the 2' hydroxyl of the ribose sugar to produce a methoxy group. m^6A_m uniquely occurs on the first transcribed base of a messenger mRNA, adjacent to the 5' m^7G cap structure (Mauer, Luo, Blanjoie, Jiao, A. V Grozhik, et al., 2017). A recent study has suggested the methyltransferase PCIF1 adds m^6A_m in a m^7G cap-

dependent mechanism and that depletion of this enzyme affects the stability of a pool of mRNAs (Boulias et al., 2019). This reinforces previous evidence that m^6A_m often resides on highly stable mRNAs with enhanced translation efficiency, where it prevents DCP2-mediated decapping (Mauer, Luo, Blanjoie, Jiao, A. V Grozhik, et al., 2017). Thus, it appears this modification is important for the stability of a subset of mRNAs regulated by DCP2.

N^1-methyladenosine (m^1A) differs from m^6A in that its methyl group blocks Watson-Crick base pairing and creates a positive charge under physiological conditions. The modification is enriched in GC-rich sequences and at the 5' UTR where it represents approximately 0.015-0.054% of adenosines in mammalian cells lines and as high as 0.16% in tissues (Dominissini et al., 2016; Li et al., 2016). Various m^1A writers and erasers have been proposed, though these have predominantly been studied in the context of tRNA (Glick and Leboy, 1977; Liu et al., 2016; Woo and Chambers, 2019). As a result, the extent to which they target m^1A-containing mRNAs remains unclear. Currently, little evidence has been gathered as to the effect of m^1A on nucleus-encoded transcripts; however, one study has suggested that m^1A affects the stability of CSF-1 mRNA (Woo and Chambers, 2019). Interestingly, m^1A appears to be enriched in mitochondrial transcripts where it inhibits translation due to the disruption of Watson-Crick based pairing (Zhang and Jia, 2018).

1.4.1.2 Modified cytidines

The most common modification of cytidine ribonucleotides is methylation at the 5' position to produce 5-methycytidine (m^5C) (Desrosiers et al., 1974). m^5C mapping shows that the modification is enriched in 5' and 3' UTRs and especially near transcription start sites; however, estimates on the content of m^5C are variable and further study is required (Squires et al., 2012; Edelheit et al., 2013; Legrand et al., 2017; Yang et al., 2017). The methyltransferases which install m^5C on mRNA have not yet been confirmed but proteins of the NSUN family have been suggested to deposit the modification on ncRNAs (Yang et al., 2017). It has also been suggested that the primary function of m^5C is to influence RNA-protein interactions. This is supported by recent evidence that the nuclear export factor ALY/REF preferentially binds to mRNAs containing m^5C (Yang et al., 2017). Furthermore, depletion of this RNA-binding protein leads to accumulation of m^5C-containing mRNAs in the nucleus.

Recent evidence also suggests that m^5C may, in some contexts, act as an intermediate in the formation of several oxidised derivatives including 5-hydroxymethylcytidine (hm^5C), 5-carboxylcytidine (5caC) and 5-formylcytidine (5fC). In *Drosophila melanogaster* mRNA, over 3000 hm^5C sites were identified with roles in neuronal development, promoting translation (Delatte et al., 2016). Further research is needed to establish whether m^5C and its derivatives affect mRNA function in mammalian cells.

1.4.1.3 Uridine isomerisation

Pseudouridine (Ψ), was the first RNA modification to be discovered and involves a 180° rotation of a uridine base through breakage and reformation of the glycosidic bond (Hamma and Ferré-D'Amaré, 2006). As a result, an extra hydrogen bond is available at the non-Watson-Crick edge of Ψ allowing additional base stacking and improved base pairing which may stabilise RNA secondary structure (Davis, 1995). Given the isomerisation to a more inert state, Ψ is thought to lack the dynamicity observed with other reversible RNA modifications (Zhao and He, 2015). Pseudouridinylation in humans is guided by RNA-dependent and independent mechanisms through the action of dyskerin or pseudouridine synthase (PUS) enzymes respectively (Li et al., 2015). The majority of Ψ exists in tRNA and rRNA, however the development of NGS-based mapping technologies has demonstrated that the modification occurs in many mRNAs, with estimates as high as 2000 Ψ-containing transcripts (Schwartz, Bernstein, et al., 2014; Carlile et al., 2014; Li et al., 2015). Interestingly, Ψ has been suggested to contribute to protein diversity through the conversion of certain non-sense codons to sense, thus preventing translation termination and promoting read-through (Karijolich and Yu, 2011).

1.4.1.4 Ribose modification

Supplementary to modifications of RNA bases, the ribose sugar can itself undergo 2'-*O*-methylation (Nm). In mRNA, Nm often occurs at the two positions downstream of the 5' m^7G cap preventing decapping by the protein DXO. However, the development of Nm mapping has led to the elucidation of thousands of internal Nm sites (Dai et al., 2017). Interestingly, a consensus sequence has been identified and Nm found to be heavily enriched in codons for glutamine, glutamate and lysine. Nm is deposited by the small

nucleolar RNA-guided fibrillarin protein, and has been shown to both increase the stability and inhibit the translation of the mRNA *Pxdn* (Elliott et al., 2019).

1.5 m^{6}A

The most common of all internal mRNA modifications, m^{6}A, is distributed throughout the transcriptome and aids in the fine-tuning of all stages of mRNA processing (Wang et al., 2014; Xiao Wang et al., 2015; Meyer et al., 2015). Originally, m^{6}A was estimated to occupy mRNA with approximately three modifications per transcript (Desrosiers et al., 1974). However, although early studies were able to quantify m^{6}A in RNA lysates, they could not determine the precise location of individual m^{6}A sites within specific transcripts. Thus, the true variability of m^{6}A content across cellular mRNAs remained unclear until the breakthrough of methylated RNA immunoprecipitation-sequencing (MeRIP-seq or m^{6}A-seq) in 2012 (Figure 1.16) (Dominissini et al., 2012). The development of this novel method for mapping the topology of the m^{6}A methylome removed the major limitations preventing the study of the m^{6}A and refocused attention on the field of epitranscriptomics. In the years since, MeRIP-seq and newer, more advanced m^{6}A-sequencing methods have been utilised to uncover vital information into the distribution of m^{6}A (Dominissini et al., 2012; Linder et al., 2015). Tantalizingly, emerging m^{6}A-sequencing methods, such as m^{6}A-seq2, are able to provide additional information as to the exact m^{6}A/A ratio at individual sites (Dierks et al., 2021). It is now clear that m^{6}A is unevenly distributed, with some transcripts, particularly those of housekeeping genes, containing no m^{6}A content, while others have multiple methylation sites. Furthermore, the modification is enriched in long exons greater than 140 bp, 3' UTRs and proximal to stop codons (Meyer et al., 2012). Finally, cross-species studies have shown that m^{6}A sites are highly conserved between tissues and species (Liu et al., 2020). This crucial information into the unequal deposition of m^{6}A at conserved locations within mRNAs suggests fundamental regulatory control over mRNA biology.

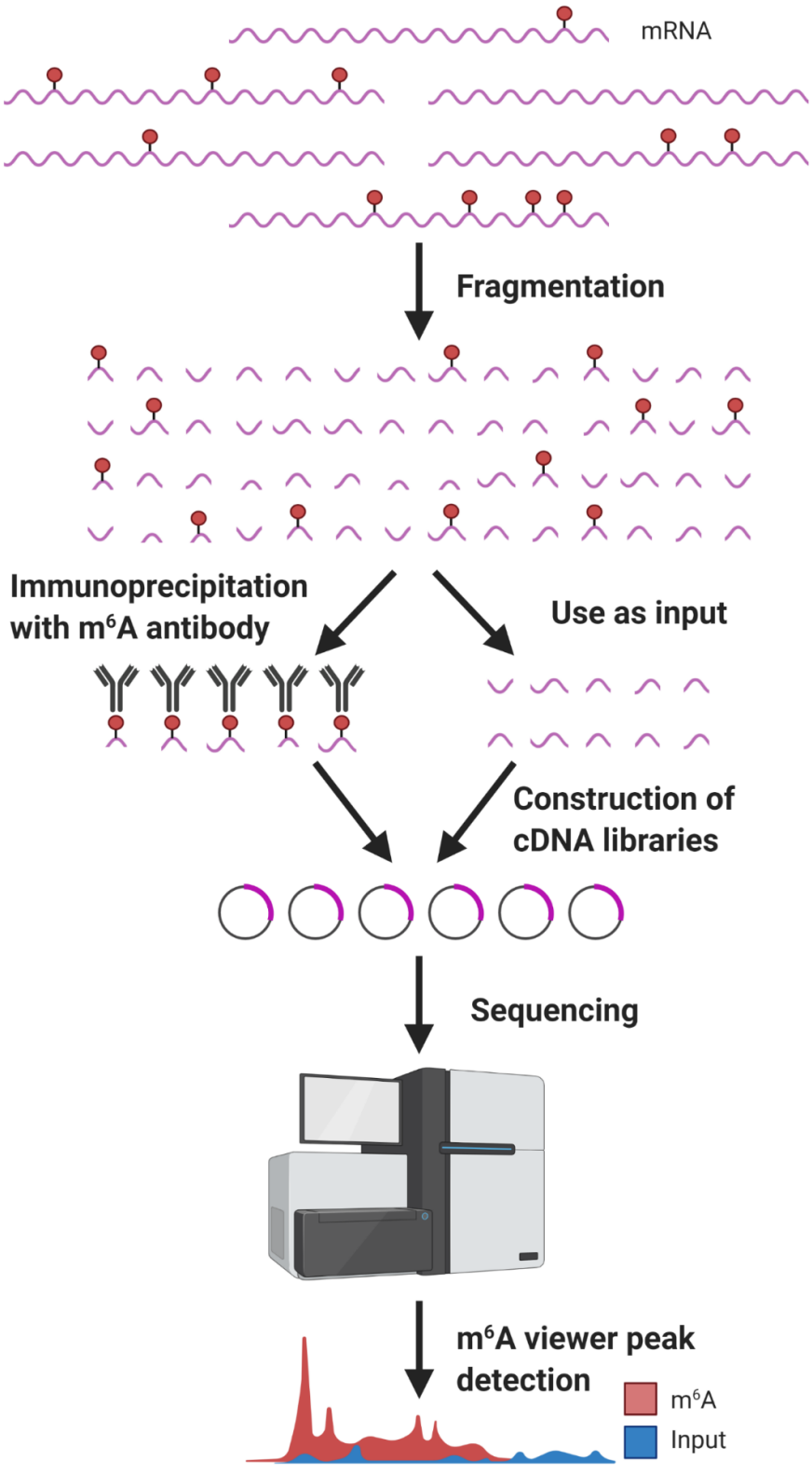

Figure 1.16. m^{6}A-sequencing. m^{6}A-seq was the first technology to allow accurate mapping of internal m^{6}A sites. mRNAs are fragmented in 100-200nt molecules. m^{6}A containing fragments are immunoprecipitated with an m^{6}A-antibody. An input samples is also collected. Fragments are reverse transcribed into cDNA and cloned into libraries for sequencing. Regions enriched in m^{6}A compared to the input sample are identified using a peak calling technology such as MACS2 or m^{6}A viewer.

1.5.1 The m^{6}A machinery: writers, erasers and readers

m^{6}A is a dynamic and reversible modification which permits rapid alterations in mRNA fate and control over widespread physiological processes. The dynamic nature of m^{6}A is achieved by the antagonistic action of proteins that deposit and remove the modification known as writers and erasers, respectively (Figure 1.17). Although most groups agree that co-transcriptional addition of m^{6}A predominates, some studies have shown that m^{6}A writers and erasers are detectable in the cytoplasm of certain cell types (Ke et al., 2017; Louloupi et al., 2018). In addition, m^{6}A is found in the RNA of viruses whose entire life cycle is cytoplasmic; thus, the post-transcriptional addition of m^{6}A to mRNA may occur in certain cellular contexts or disease states (Lichinchi, Zhao, et al., 2016).

m^{6}A base pairs with uracil (U) in a weaker interaction than canonical A:U base pairing and often destabilises RNA secondary structures such as stem loops. However, recent studies have also shown that m^{6}A may stabilise some RNA structures under certain contexts (Roost et al., 2015; B. Liu et al., 2018). In most cases however, to exert its regulatory effects over RNA, this epitranscriptomic cipher must be decoded by RNA binding proteins known as m^{6}A readers. These m^{6}A readers recognise the methyl group and direct the associated RNA towards distinct biological fates.

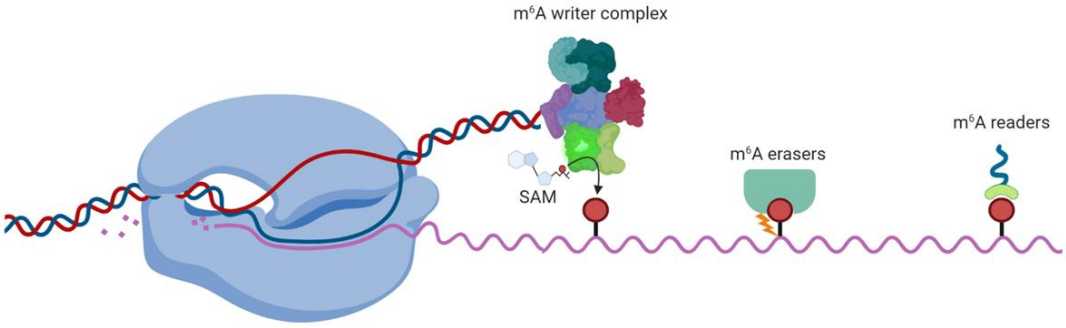

Figure 1.17. Co-transcriptional addition of m^{6}A. In most cases m^{6}A is thought to be added in a co-transcriptional manner upon the nascently transcribing mRNA. m^{6}A is added at its consensus DRACH sequence by METTL3 of the methyltransferase complex using its cofactor SAM which donates the methyl group and becomes hydrolysed to S-adenosylhomocysteine. m^{6}A can be demethylated to adenosine by m^{6}A erasers. Finally, the functions of m^{6}A are decoded by m^{6}A readers in both the nucleus and the cytoplasm.

1.5.1.1 m^6A writers

The addition of m^6A is performed by a large methyltransferase complex consisting of multiple subunits (Figure 1.18). Within this m^6A 'writer' complex, methyltransferase-like 3 (METTL3) is the key methyltransferase required for the transfer of a methyl group from its cofactor S-adenosylmethionine (SAM) to an adenosine ribonucleotide (Bokar et al., 1997; Liu et al., 2014; Patil et al., 2016). The METTL3 cofactor, methyltransferase-like 14 (METTL14), is an adapter protein which positions the RNA substrate in an optimal position for methylation. Despite initial views that METTL14 also possessed methyltransferase activity, it is now clear that the protein is catalytically inactive and merely plays a structural role (Śledź and Jinek, 2016; P. Wang et al., 2016; X. Wang et al., 2016). Complete loss of either METTL3 or METTL14 activity results in a greater than 99% loss of m^6A sites in mRNA, highlighting the importance of these proteins for methylation (Geula et al., 2015). Together, the METTL3-METTL14 heteroduplex deposits m^6A at its consensus DR(m^6A)CH (D=A, G or U; R=A or G; H=A, C or U) sequence (Dominissini et al., 2012). Importantly however, only certain DRACH sequences can be m^6A modified and the stoichiometry of m^6A at a single position is highly variable (Dominissini et al., 2012). Although the selectivity of m^6A distribution is not yet understood, it is hypothesised that additional cofactors and specific sequence or structural contexts help guide mRNA methylation.

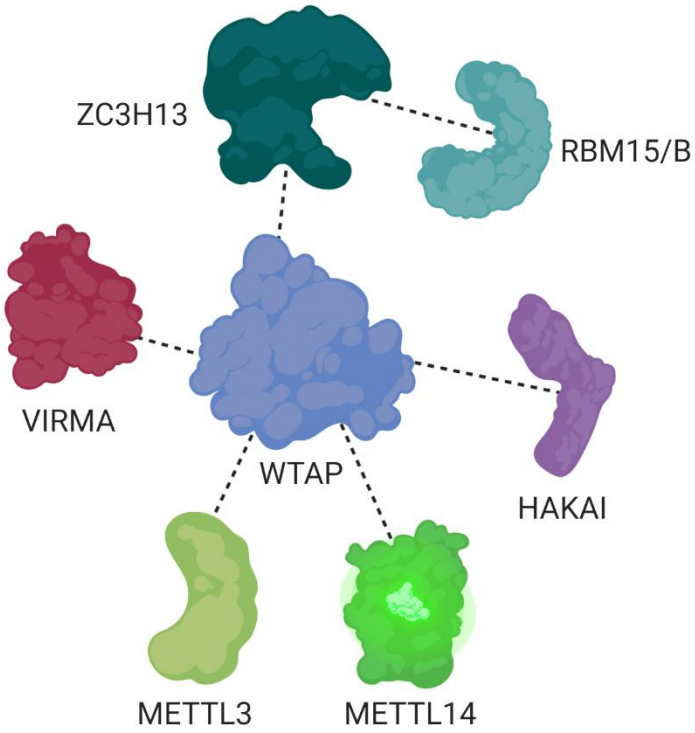

Figure 1.18. The m^{6}A writer complex. The m^{6}A writer complex is a large multi-subunit protein complex. METTL3 is the methyltransferase whereas METTL14 contains a catalytically dead methyltransferase domain. WTAP serves as a scaffold for the binding of additional proteins to the complex which are thought to regulate the activity and selectivity of the complex.

In addition to METTL3 and METTL14, the m^{6}A methyltransferase complex has a number of subunits which play important roles in structure and localisation of the protein complex. Wilms Tumour 1 associated protein (WTAP) helps to locate the entire m^{6}A methyltransferase complex to nuclear speckles and is essential for methylation in yeast and humans (Agarwala et al., 2012; Liu et al., 2014; Ping et al., 2014; X. Wang et al., 2016). KIAA1429 (or VIRMA) acts as a scaffold to maintain the structure of the m^{6}A writer complex and guides the 3' UTR localisation characteristic of the modification. Supporting this hypothesis, depletion of KIAA1429 leads to loss of the preferential enrichment of m^{6}A in 3' UTRs (Schwartz, Mumbach, et al., 2014; Yue et al., 2018).

The newest recognised members of the m^{6}A writer complex are ZC3H13 and HAKAI which both interact with the multi-protein assembly through WTAP. ZC3H13 is important for nuclear localisation of the m^{6}A methyltransferase complex and deletion of this protein leads to an 80% loss of cellular m^{6}A content in mammals (Růžička et al., 2017; Wen et al., 2018; Yue et al., 2018; Knuckles et al., 2018; Guo et al., 2018). Similarly, loss of HAKAI leads to a

reduction in m^{6}A sites though a more precise functional role is not yet known. Finally, adjoining the entire m^{6}A writer complex through ZC3H13, the proteins RBM15 and RBM15B are proposed to mediate the selective distribution of the complex to only a proportion of total DRACH sites for methylation (Horiuchi et al., 2013; Ping et al., 2014; Růžička et al., 2017). Importantly however, the RBM15 proteins only account for a fraction of m^{6}A sites and the wider localisation of the modification to certain DRACH motifs, while not others, remains unclear. The deletion of any subunits of the m^{6}A writer complex cause a substantial reduction in methylation of cellular mRNA, highlighting the importance of each component for efficient regulation of m^{6}A dynamics. Importantly, depletion of a number of additional proteins, including METTL16 and HNRNPU, has also been found to reduce global m^{6}A content, indicating that additional factors may control the activity and localisation of the m^{6}A writer complex (Yue et al., 2018; Nance et al., 2020).

1.5.1.2 m^{6}A erasers

Thus far, two m^{6}A erasers have been identified which demethylate m^{6}A: Fat mass obesity protein (FTO) and adenosine-ketoglutarate-dependent dioxygenase alkB homolog 5 (ALKBH5). However, there is some debate as to whether FTO targets m^{6}A or m^{6}A$_m$ (Jia et al., 2011). *In vitro* studies suggest that FTO has a much higher affinity towards the latter modification (Mauer, Luo, Blanjoie, Jiao, A. V. Grozhik, et al., 2017). Furthermore, the depletion of FTO leads to a substantial increase in m^{6}A$_m$ among snRNAs, suggesting this RNA species is FTO's preferred target (Mauer et al., 2019). However, subtle increases in m^{6}A have been observed in some FTO-depleted cell types (Li et al., 2017). Thus, site-specific evidence of m^{6}A demethylation in mRNA is required to substantiate FTO as an m^{6}A eraser. Despite this, it is widely agreed that ALKBH5 is a true m^{6}A eraser with no activity towards m^{6}A$_m$. m^{6}A demethylation appears to be subtle however and ALKBH5 knockout mice display only impaired fertility (Zheng et al., 2013). Nevertheless, it is likely that the m^{6}A eraser acts on merely a fraction of m^{6}A sites and the current mechanism of selectivity is unknown (Zheng et al., 2013). Although these studies suggest that significant widespread demethylation of m^{6}A residues does not take place in the majority of cell types, the contribution of both FTO and ALKBH5 to the regulation of m^{6}A/$_m$ levels adds an additional layer of fine tuning to the regulation of mRNA biology (Jia et al., 2011; Zheng et al., 2013; Mauer, Luo, Blanjoie, Jiao, A. V Grozhik, et al., 2017; Darnell et al., 2018).

1.5.1.3 m^{6}A readers

The best characterised m^{6}A readers contain a YT521-B homology (YTH) domain for direct and specific binding of m^{6}A (Figure 1.19). Proteins within this group include YTHDF1 (DF1), YTHDF2 (DF2), YTHDF3 (DF3), YTHDC1 (DC1) and finally YTHDC2 (DC2) (Zhang et al., 2010; Xu et al., 2014). DF1, DF2 and DF3 are all cytoplasmic proteins, whereas DC1 is nuclear and DC2 is able to reside in both the nucleus and the cytoplasm. DC1 appears to be the predominant nuclear m^{6}A reader affecting splicing and nuclear export whereas DF1-DF3 regulate translation and mRNA stability in the cytoplasm (Zhang et al., 2010; Du et al., 2016; Xiao et al., 2016; Roundtree et al., 2017). DC2 has an unusual YTH domain that binds weakly to methylated RNAs compared to the other YTH proteins (Xu et al., 2014; Wojtas et al., 2017). In addition, cross-linking immunoprecipitation (CLIP) studies show that DC2 binding sites correlate poorly with m^{6}A sites (Patil et al., 2016). Although some studies demonstrate subtle effects for DC2-depletion on highly methylated mRNAs, it is clear that the protein's role in m^{6}A dynamics is minimal (Wojtas et al., 2017). The YTH domain is an RNA-binding motif comprising three tryptophan residues which make highly specific hydrophobic interactions with m^{6}A (Theler et al., 2014). This aromatic cage encases the methyl group and permits the delivery of modified RNAs towards distinct fates and functions.

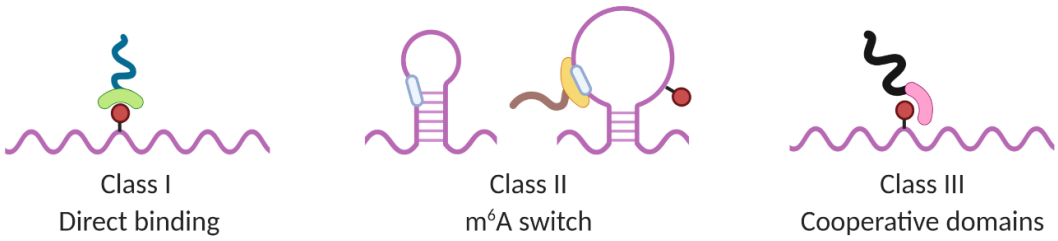

Figure 1.19. Classes of m^{6}A reader proteins. Three classes of m^{6}A reader are categorised by how they bind m^{6}A. Class I bind directly to the methyl group through a YTH domain using hydrophobic interactions. Class II bind their target sequence adjacent to an m^{6}A site as a result of m^{6}A-induced RNA unfolding. Class III bind m^{6}A directly using a common RNA-binding domain as well as flanking peptide sequences.

In addition to the YTH domain-containing proteins, a number of other proteins have been suggested to bind m^{6}A. Transcriptome-wide studies of RNA structure confirm the propensity of m^{6}A to exist in unstructured regions. Some RNA-binding proteins can exploit the increased accessibility to their target RNA motifs when flanked by m^{6}A sites; operating on

an ‘m^{6}A switch’ mechanism. These indirect readers include members of the heterogeneous nuclear ribonucleoprotein (HNRNPs) family: HNRNPC, HNRNPG and HNRNPA2B1 (Liu et al., 2015; Alarcón et al., 2015; N. Liu et al., 2017). A third class of m^{6}A reader has also been described which harnesses the common KH RNA binding motif and adjacent regions to cooperatively bind m^{6}A sites (Huang et al., 2018). Furthermore, a myriad of new readers are described which also contribute to the decryption and implementation of m^{6}A topology (Edupuganti et al., 2017; Baquero-Perez et al., 2019). Importantly, within our own lab, eight new putative m^{6}A readers have been discovered among the Tudor domain ‘royal‘ family of proteins (Baquero-Perez et al., 2019). Previous studies have demonstrated their ability to bind methylated proteins; however, electromobility shift assays show they also bind to m^{6}A in mRNA. Furthermore, CLIP experiments on one of these Tudor domain proteins, SND1, shows binding sites which overlap heavily, but not exclusively, with those of DF1-3. Taken together, the complex multi-layered regulation of m^{6}A reading alludes to an ancient and fundamental role in the regulation of RNA biology.

1.5.2 Functions of m^{6}A

m^{6}A affects all stages of the mRNA life cycle comprising processing, nuclear export, translation and decay (Figure 1.20). It is not entirely clear how different sites of m^{6}A can exert contrasting effects on mRNA fate and recruit alternative reader proteins. Nevertheless, m^{6}A can alter the destiny of an RNA depending on location or physiological context.

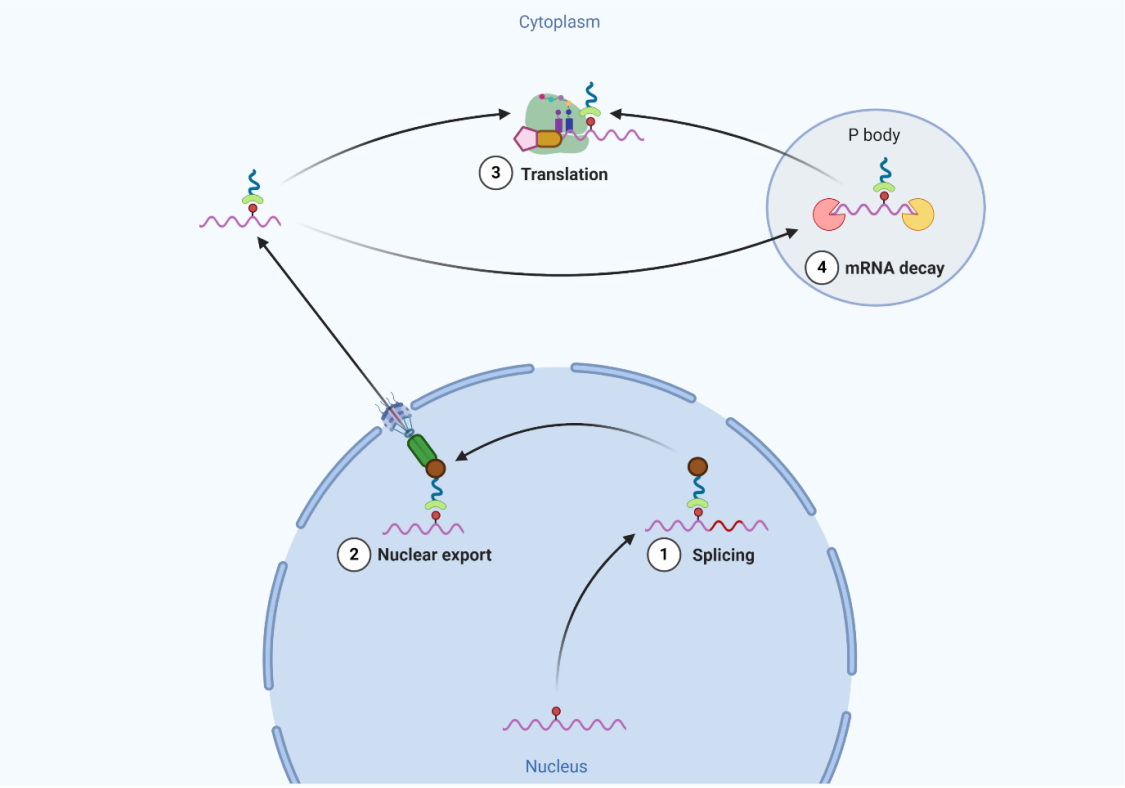

Figure 1.20. Functions of m^{6}A. Depending on the context of an m^{6}A residue within a transcript, the fate of the mRNA may be diverted towards splicing, export, translation or decay.

1.5.2.1 Alternative splicing

After co-transcriptional addition of m^{6}A to pre-mRNA, the molecule undergoes several processing steps including splicing. Several m^{6}A readers that utilise an m^{6}A switch mechanism are thought to regulate this process. Through the binding of their respective target sites in regions with reduced RNA structure, major splicing factors such as HNRNPC and HNRNPG are able to bind U-rich and purine rich target sites and facilitate the alternative splicing of thousands of different mRNAs (Liu et al., 2015; N. Liu et al., 2017). In addition, the depletion of HNRNPA2B1 is suggested to mirror the effect of METTL3 depletion on the alternative splicing of certain primary miRNAs (Alarcón et al., 2015; Wu et al., 2018).

The direct m^{6}A reader DC1 is also known to affect splicing through the recruitment of splicing factors to m^{6}A sites. The DC1-mediated recruitment of SRSF3 to nuclear speckles facilitates the displacement of SRSF10 and promotes exon inclusion (Xiao et al., 2016; Roundtree et al., 2017). Similarly, in *Drosophila*, DC1 prevents the recognition of splicing signals in *Sxl* mRNA, the transcript associated with control of sex determination (Haussmann et al., 2016; Lence et al., 2016; Kan et al., 2017). There is some debate as to the level of

control DC1 has over alternative splicing of mRNA as CLIP studies on the YTH proteins show that nuclear DC1 predominantly binds to ncRNAs, whereas the cytosolic DF1-3 preferentially bind mRNA (Patil et al., 2016). However, further studies have suggested the majority of m^6A sites on nascent pre-mRNAs lie within introns, indicating that m^6A must play a role in mRNA biology before its export to the cytoplasm (Louloupi et al., 2018). Although the extent to which m^6A influences alternative splicing in humans is unknown, it is clear that it exerts some influence which may vary between cell types and physiological contexts.

1.5.2.2 Nuclear Export

Given that the processes of splicing and nuclear export are coupled, it is not surprising that m^6A regulates both processes. Recent evidence suggests that m^6A can serve as a non-canonical nuclear export signal through the recruitment of DC1 and the transcription and export complex (TREX) to modified mRNAs (Lesbirel et al., 2018). After TREX binding, the major mRNA nuclear export factor NFX1 and SRSF3 are recruited to the m^6A site to facilitate export of the methylated transcript (Roundtree et al., 2017). Normally, this process is achieved through the binding of TREX to the exon junction complex (EJC). However, in long internal exons where the EJCs are lacking, m^6A is may act as a surrogate signal for the nuclear export of these transcripts. Supporting this hypothesis, m^6A is enriched in these regions and DC1 depletion leads to increased nuclear residence times (Roundtree et al., 2017).

1.5.2.3 Translation

Upon the export of m^6A-containing mRNAs to the cytoplasm, the decoding of methylated transcripts is primarily performed by DF1-3. Two distinct mechanisms are proposed to regulate the translational efficiency of m^6A modified transcripts, dependent on their requirement for the m^7G cap structure. In the cap-dependent method, DF1 binds m^6A within the 3’ UTR and associates with the 5’ UTR-associated protein eukaryotic initiation factor 3 (eIF3) to enhance translation (Xiao Wang et al., 2015). It is hypothesised that this method stabilises 5’-3’ looping of the mRNP complex to allow rapid recycling of the translation machinery (Xiao Wang et al., 2015). Although this mechanism was originally thought to be unique to DF1, research now suggests that YTH proteins do not perform distinct functions. Importantly, the sequence similarity between these m^6A readers casts doubt on the possibility of distinct roles. Furthermore, numerous studies have shown functional

redundancy among DF1-3 and near identical overlap of m^{6}A-binding sites (Kennedy et al., 2016; Patil et al., 2016; Shi et al., 2017). Nevertheless, it is puzzling how different m^{6}A sites pre-determine distinct mRNA fates and further work is required to establish the extent to which m^{6}A readers account for this discrepancy.

In the second method of m^{6}A-enhanced translation, there is no requirement for binding of eukaryotic initiation factor 4E (eIF4E) to the 5' m^{7}G cap in order to couple the translation machinery to an mRNA. Instead, m^{6}A-crosslinking experiments have demonstrated that eIF3 has the ability to bind directly to 5' UTR m^{6}A sites through a multi-domain interface, recruit the 43S pre-initiation complex and initiate translation (Meyer et al., 2015). This non-canonical, m^{6}A dependent method of translation could be essential where eIF4E activity is inhibited under stress or disease. Supporting this hypothesis, one study shows that m^{6}A becomes redistributed to the 5' UTR during heat shock, suggesting m^{6}A could serve as a surrogate platform for translation initiation (Zhou et al., 2015).

1.5.2.4 mRNA decay

Although m^{6}A modulates all parts of the mRNA life cycle, some have suggested that the predominant role for the modification is the fine-tuning of mRNA half-life (Zaccara et al., 2019). DF2 was the first m^{6}A reader identified to play a role in this process, as upon its depletion m^{6}A-modified transcripts show elevated half-lives (Wang et al., 2014). DF2 is proposed to relocate m^{6}A containing transcripts to P-bodies and recruit members of the CCR4-NOT deadenylase complex through its N-terminal low complexity regions (Wang et al., 2014; Du et al., 2016). As a result, methylated mRNAs are systematically deadenylated and degraded through the action of DF2. Further studies have noted this mechanism is also utilised by DF1 and DF3 suggesting that all of the cytoplasmic YTH proteins act redundantly in RNA decay pathways (Du et al., 2016; Lichinchi, Gao, et al., 2016; Lichinchi, Zhao, et al., 2016; Shi et al., 2017). Supporting this evidence, the depletion of DF2 only partially accounts for the increase in mRNA half-life when METTL3 is depleted, suggesting other m^{6}A readers must be involved (Ke et al., 2017).

1.5.2.5 Phase separation

A major advancement in the understanding of m^{6}A followed the discovery that methylated mRNAs can be regulated through liquid-liquid phase separation (Figure 1.21). In addition to

their YTH domain, DF1-3 all have an approximately 40kDa N-terminal low complexity domain (Ries et al., 2019). In many cases, low complexity regions are known to interact and facilitate phase separation (Lin et al., 2015). As m^{6}A sites tend to cluster, the association of DF proteins in several adjacent positions allows interaction of low complexity domains (Ries et al., 2019). Through phase separation, RNA-protein droplets form allowing the assembly of structures such as P bodies or stress granules. Thus, m^{6}A deposition upon mRNAs in the nucleus may serve as a signal for later compartmentalisation in the cytoplasm, where the transcript can be stored, translated or degraded as required by the cell.

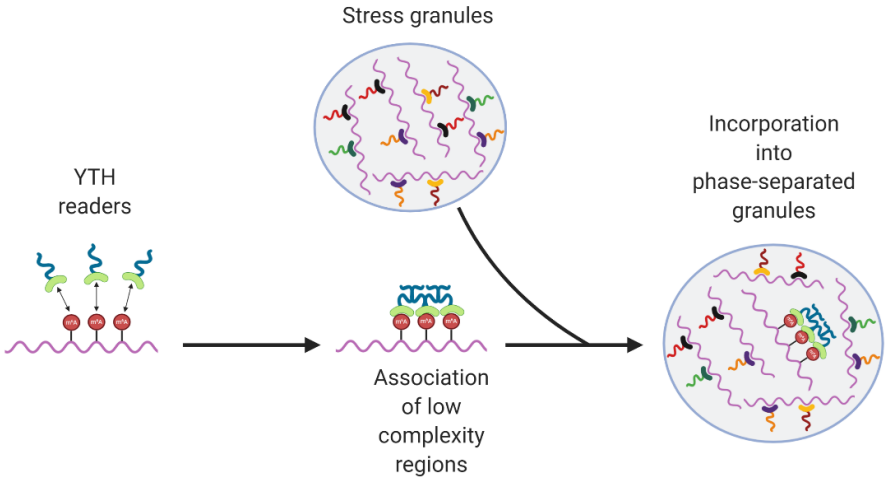

Figure 1.21. m^{6}A-mediated phase separation. The binding of YTH reader proteins to clusters of m^{6}A sites allows the phase separation of modified mRNAs. The association of low complexity domains in the YTH-reader proteins leads to formation of YTH-m^{6}A condensates. These RNA-protein condensates are then recruited to pre-existing RNA granules such as stress granules or P-bodies.

1.5.3 m^{6}A in viral RNAs

The presence of m^{6}A in viral RNA has been known for many years hinting at an extra paradigm of regulatory control over viral infection (Wei et al., 1975; Sommer et al., 1976; Krug et al., 1976; Dimock and Stoltzfus, 1977; Moss et al., 1977; Canaani et al., 1979; Kane and Beemon, 1985; Narayan et al., 1987). Like cellular m^{6}A sites, the study of modified viral RNA was long held back by technological limitations; however, in the last couple of years, several studies have alluded to a potentially fundamental role in the control over virus replication (Table 1.1).

Virus	m^{6}A effect on virus	m^{6}A machinery components depleted	m^{6}A function	Reference
EV71	Proviral	METTL3, FTO, DF1, DF3, DC1	-	H Hao et al., 2019
HBV	Antiviral	METTL3, METTL14, FTO, ALKBH5, DF2, DF3	mRNA abundance, reverse transcription	Imam et al., 2018
HCV	Antiviral	METTL3, METTL14, FTO, DF1-3	Virion packaging	Gokhale et al., 2016
HIV-1	Proviral and antiviral	METTL3, METTL14, FTO, ALKBH5, DF1-3	Nuclear export, mRNA abundance and reverse transcription	Lichinchi et al., 2016,Tirumuru et al., 2016; Kennedy et al., 2016
IAV	Proviral	METTL3, DF2	mRNA abundance	Courtney et al., 2017
KSHV	Proviral and antiviral	METTL3, FTO, DF2	ORF50 mRNA stability	Ye et al., 2017; Tan et al., 2018; Hesser et al., 2018
SV40	Proviral	METTL3, DF2, DF3	Nuclear export, translation	Tsai et al., 2018
ZIKV	Antiviral	METTL3, METTL14, FTO, ALKBH5, DF1-3	-	Lichinchi et al., 2016b

Table 1.1 Role of m^{6}A in virus infections. Summary of existing data for viruses in which m^{6}A has been functionally investigated through depletion or overexpression of components of the m^{6}A machinery.

1.5.3.1 HIV-1

The first virus in which m^{6}A was investigated functionally was HIV-1. In 2016, three studies mapped m^{6}A sites in HIV-1 RNA using meRIP-seq and DF1-3 binding sites using CLIP. The groups consistently identified a number m^{6}A peaks at the 3' end of the HIV-1 genome in

addition to several mechanisms through which the modification exhibits regulatory control over viral replication (Purcell and Martin, 1993; Brasey et al., 2003; Blissenbach et al., 2010). Transfecting cells with luciferase reporter plasmids expressing either wild-type or m^6A deficient HIV-1, one group showed that m^6A increases the abundance of HIV-1 mRNAs (Lichinchi, Gao, et al., 2016). Another study found that m^6A is important for the interaction of HIV-1 Rev protein with its response element; a process critical for the nuclear export of all HIV-1 transcripts, although another study has since cast doubt on this mechanism (Kennedy et al., 2016; Chu et al., 2019). Finally, the third study suggested the m^6A readers DF1-3 bind 5'UTR m^6A sites in HIV-1 genomic RNA (gRNA) to reduce gRNA abundance and inhibit reverse transcription (Tirumuru et al., 2016; Lu et al., 2018). Although the evidence gathered by these three studies was not entirely consistent, it is evident that modifications of viral RNAs play diverse roles in virus life cycles.

1.5.3.2 Flaviviruses

After HIV-1, two studies expanded the functional investigation of m^6A in virus life cycles to the flaviviruses. Although in most cases, m^6A is added in a co-transcriptional manner, the identification of multiple modification sites in flaviviruses, which replicate entirely in the cytoplasm, showed that m^6A deposition may occur outside the nucleus under certain contexts (Gokhale et al., 2016; Lichinchi, Zhao, et al., 2016). In addition, m^6A peaks were concentrated in similar genomic positions among dengue virus, yellow fever virus, west Nile virus and four strains of zika virus (ZIKV), showing that m^6A sites may perform similar biologically functions across related virus life cycles. Through the depletion of members of the m^6A machinery, both studies found that m^6A negatively affects flaviviral life cycles. Furthermore, electroporation of wild type and m^6A deficient HCV E1 RNA into cells showed that m^6A negatively affects the interaction of HCV core protein with E1 RNA and impairs its packaging into nascent virions (Gokhale et al., 2016).

1.5.3.3 Influenza A

Influenza A virus (IAV) was one of the first viruses in which m^6A was discovered (Krug et al., 1976; Narayan et al., 1987). Recently, the topology of m^6A and DF binding sites were mapped within both the negative sense viral RNA segments and the positive sense complementary RNA of IAV (Courtney et al., 2017). Interestingly, m^6A was enriched in the

RNA encoding structural proteins compared with those encoding RNA polymerase subunits. Furthermore, m^{6}A was concentrated in the viral RNA and complementary RNA of haemaglutinin (HA) which encodes a highly expressed IAV envelope glycoprotein. Finally, IAV mutant viruses, deficient in m^{6}A on HA RNAs, showed reduced HA mRNA and protein, as well as attenuated pathogenicity. Given the consistency in changes among mRNA and protein levels, but the lack of effect on splicing ratios or virion assembly, the authors concluded that m^{6}A positively regulates IAV replication by increasing mRNA abundance (Courtney et al., 2017).

1.5.3.4 KSHV

In KSHV infection, multiple studies have mapped the topology of m^{6}A in the viral transcriptome. Unlike other viruses, differential m^{6}A methylation was identified between the two KSHV replication programmes, latent and lytic, in order to identify whether the modification plays a role in the process of reactivation. Numerous m^{6}A peaks were identified in the large KSHV transcriptome on both latent and lytic transcripts (Ye et al., 2017; Tan et al., 2018; Hesser et al., 2018). However, the overall effect of m^{6}A on the viral life cycle differed between the studies, with one group suggesting the modification exerts cell-type specific effects on the viral life cycle (Hesser et al., 2018).

In addition to studying the global effects of m^{6}A, one study identified several intronic m^{6}A sites in ORF50 pre-mRNA, encoding the protein RTA. Further investigation showed these m^{6}A residues were important for DC1 recruitment and efficient splicing of the transcript (Ye et al., 2017). However, in the Whitehouse lab, several sites in ORF50 were identified which are bound by the novel m^{6}A reader SND1 (Baquero-Perez et al., 2019). Depletion experiments showed that SND1 recognition and binding to these sites within *ORF50* promotes the stability of the transcript. Furthermore, in SND1-depleted cells, a dramatic reduction in lytic mRNA and protein was observed suggesting m^{6}A is essential for KSHV reactivation.

1.5.3.5 SV40

Like IAV, transcripts of the prototype polyomavirus simian virus 40 (SV40) have been known to undergo m^{6}A-modification for several decades (Canaani et al., 1979; Finkel and Groner, 1983). Recently, mapping of the m^{6}A methylome and depletion of the m^{6}A machinery in

infected cells showed that the modification is enriched in structural protein mRNAs and positively regulates SV40 infection (K Tsai et al., 2018). Furthermore, the abrogation of m^6A in the viral capsid protein VP1 mRNA led to a 10-fold decrease in VP1 protein levels when both wild type and mutant VP1 constructs were transfected into 293T cells. Further analysis showed that this reduction was caused by a combination of both splicing inhibition and reduced translation (K Tsai et al., 2018).

1.5.3.6 HBV

Although only a single m^6A site could be identified in the dsDNA virus Hepatitis B Virus (HBV) through meRIP-seq, the m^6A site exists in an epsilon stem loop which serves as a template for transcription of all HBV transcripts and is incorporated into the 3' of all HBV mRNAs (Imam et al., 2018). Furthermore, HBV replicates through pregenomic RNA (pgRNA), an RNA intermediate which is reverse transcribed into HBV genomes, which contains the epsilon stem loop at both 5' and 3' ends. Interestingly, m^6A was found to exert dual functions in the HBV life cycle by enhancing pgRNA reverse transcription while restricting RNA stability (Imam et al., 2018). Thus, this study demonstrates the propensity of m^6A to act both as antiviral and proviral depending on the context and highlights the importance of studying m^6A at a site-specific basis.

1.5.3.7 Enterovirus-71

m^6A has also been identified in the RNA genome of enterovirus-71 (EV71), with sites identified in the coding regions of several viral genes (Hao et al., 2019). Abrogation of two of these m^6A sites in the viral genes VP1 and 2C significantly impaired viral replication suggesting m^6A is proviral in EV71 infection. Interestingly, EV71 infection led to relocalisation of several components of the m^6A machinery. The group suggested that movement of METTL3 and METTL14 to the cytoplasm permits the modification of the RNA genome and boosts EV71 replication.

1.5.3.8 EBV

In comparison with KSHV, the presence of m^6A has been mapped on both latent and lytic transcripts in cells infected with EBV. Once again, the modification was shown to affect the stability of viral mRNAs; however, latent transcript stability was increased by m^6A while the

stability of lytic transcripts was diminished (Lang et al., 2019). Interestingly, the viral protein EBNA3C activates the transcription of METTL14 providing direct evidence that the m^{6}A machinery is hijacked by EBV. The upregulation of METTL14 is suggested to drive EBV persistence through the stabilisation of latent transcripts and the decay of lytic transcripts (Lang et al., 2019).

1.5.4 Changes in the host m^{6}A landscape during viral infection

Although the context of m^{6}A in viral infection discussed thus far has been centred around the effect of modifications to viral RNA, several studies have also shown that changes in the host m^{6}A landscape modulate viral infection. Importantly, both proviral and antiviral m^{6}A peaks are nascently deposited on cellular transcripts upon infection; reflecting both the hijacking of the host m^{6}A machinery by the virus and the redistribution of m^{6}A by the cell to combat infection.

Studies to analyse the changes in m^{6}A content upon cellular mRNAs during viral infection initially examined m^{6}A distribution on a transcriptome wide scale. However, further studies have now investigated specific m^{6}A sites to demonstrate their importance in viral life cycles. In HIV-1, ZIKV and KSHV, several groups have reported changes in the m^{6}A methylome during viral infection and identified functional groups of mRNAs with consistently altered m^{6}A profiles (Kennedy et al., 2016; Lichinchi, Gao, et al., 2016; Lichinchi, Zhao, et al., 2016; Tan et al., 2018; Hesser et al., 2018). Interestingly, many of these differentially m^{6}A modified transcripts cluster into pathways including viral replication and immunity, strongly suggesting that cellular m^{6}A sites affect viral infection. There have been suggestions that m^{6}A consensus site preference is altered under viral infection however these changes seem to vary between studies and viruses. Nevertheless, across these different studies, large changes in m^{6}A distribution and stoichiometry during viral infection are a common feature.

Although changes in the distribution of cellular m^{6}A during viral infection hints towards the modulation of virus host interactions, several studies have now show direct examples where m^{6}A exhibits regulatory control of virus life cycles through modification of cellular transcripts. Upon HCMV infection, one group identified that m^{6}A influences the antiviral interferon response by reducing the stability of the *IFNB1* transcript (Rubio et al., 2018). Importantly, the mRNA is dynamically m^{6}A-modified by METTL14 and ALKBH5; both of

which are upregulated by HCMV infection. Additionally, METTL14 depletion impaired HCMV replication, while ALKBH5 knockdown reversed this effect. In another recent study, flaviviruses were revisited in the context of changes in the host m^{6}A landscape during infection. Two transcripts were identified with an m^{6}A peak unique to uninfected cells or consistently present in HCV, ZIKV, WNV or DENV-infected cells while absent from healthy cells (Gokhale et al., 2020). When m^{6}A modified, one of these transcripts, *RIOK3*, displayed enhanced translation while the other, *CIRBP,* was subjected to more robust alternative splicing. Importantly, the methylation of *RIOK3* and *CIRBP* altered cellular pathways including viral activation of immune sensing and endoplasmic reticulum stress, leading to modulation of the viral life cycle. In summary, these studies provide vital information about how single m^{6}A sites can potentiate virus replication.

1.6 Aims of the study

KSHV is an oncogenic herpesvirus which utilises several post-transcriptional regulatory mechanisms to influence gene expression. Previous studies have identified that viral transcripts are m^{6}A-modifed and the modification affects virus replication (Ye, 2017; Tan et al., 2018; Hesser et al., 2018). However, herpesviruses cause large scale remodelling of the host cell to support their replication. Consequently, the interaction between virus and host cell are of crucial importance in understanding herpesvirus infections and antiviral therapeutic targeting. Therefore, the aim of this study was to determine whether changes in m^{6}A topology upon cellular mRNAs regulates KSHV lytic reactivation.

Initially, KSHV lytic replication was found to induce mass remodelling of the host m^{6}A landscape. Cellular transcripts with the largest changes in m^{6}A content were enriched in pathways essential for successful virus replication including Notch signalling and mRNA biology.

Next, a prioritised group of cellular m^{6}A-modified transcripts were screened for changes in abundance, splicing, nuclear export, stability and translation. A group of 4 cellular transcripts emerged with large changes in abundance, in addition to increased stability or nuclear export, during lytic replication. Fascinatingly, the upregulation of these mRNAs could be diminished by m^{6}A-abrogation suggesting that the changes in their fate during lytic replication were m^{6}A-dependent.

Finally, two m^{6}A-modified cellular transcripts were further investigated for a role in KSHV lytic replication. Both encoded proteins were shown to be crucial for efficient viral gene expression and virion production. Furthermore, functional examination of these proteins demonstrates that changes in membrane dynamics and regulation of AU-rich mRNAs are of central importance to their involvement in KSHV lytic replication.

Chapter 2

~

Materials and Methods

2 Materials and Methods

2.1 Materials

2.1.1 Chemicals

Chemicals were purchased from Sigma Aldrich, Thermo Fisher Scientific or VWR International unless stated otherwise.

2.1.2 Cell culture reagents

All media, reagents and antibiotics used for cell culture and their suppliers are shown in the table below (Table 2.1).

Reagent	Supplier
Doxycycline hyclate	Sigma
Dulbecco's Modified Eagle's Medium (DMEM)	Gibco
Foetal bovine serum (FBS)	Gibco
Hygromycin B	ThermoFisher
Lipofectamine® 2000	ThermoFisher
Opti-MEM®	Gibco
Penicillin/streptomycin	Gibco
Phosphate buffered saline (PBS)	Lonza
Puromycin	ThermoFisher
RPMI1640	Gibco
Trypsin-EDTA	Gibco

Table 2.1. List of cell culture reagents and their suppliers.

2.1.3 Antibodies

Horseradish peroxidase (HRP)-conjugated anti-rabbit and anti-mouse secondary antibodies were obtained from Dako and used for western blotting at a dilution of 1:5000. Alexa Fluor 488- and 546-conjugated secondary antibodies were purchased from ThermoFisher and used for immunofluorescence microscopy at a dilution of 1:500. Primary antibodies including their working ratios for both western blot and immunofluorescence are detailed

in the table below (Table 2.2). Additionally, suppliers and origin species are shown are shown.

Antibody	Company	Identity	Origin species	Dilution (WB)	Dilution (IF)
Anti-Calnexin	Invitrogen	MA3-027	Mouse	-	1:100
Anti-C-myc	Sigma	M4439	Mouse	1:1000	-
Anti-CNOT2	Proteintech	10313-1-AP	Rabbit	1:1000	-
Anti-ENO2	Assay Biotech	C0280	Rabbit	1:1000	-
Anti-FLAG	Sigma	T7425	Rabbit	1:1000	-
Anti-FLOT1	CST	D2V7J	Rabbit	1:1000	1:50
Anti-FLOT2	CST	L294	Rabbit	1:1000	-
Anti-FOSB	CST	(5G4) #2251	Rabbit	1:1000	-
Anti-FTO	Abcam	ab126605	Rabbit	1:5000	-
Anti-GAPDH	Abcam	ab8247	Mouse	1:5000	-
Anti-GFP	Living Colours	632381	Mouse	1:1000	-
Anti-GPRC5A	Atlas	HPA007928	Rabbit	1:500	-
Anti-HSPA1A	Aviva systems Biotech	ARP33096	Rabbit	1:1000	-
Anti-ILF3	Bethyl	A303-120A-T	Rabbit	1:500	-
Anti-Lamin B	Abcam	ab16048	Rabbit	1:2500	-
Anti-m6A	Temecula	MABE1006	Mouse	-	-
Anti-METTL14	Atlas	ATLAS HPA038002	Rabbit	1:1000	-

Anti-METTL3	Bethyl	A301-567A	Rabbit	1:250	-
Anti-ORF57	Santa Cruz	Sc-135746	Mouse	1:1000	1:100
Anti-ORF59	University of California Berkeley	Gift from Britt Glaunsinger	Rabbit	1:1000	-
Anti-ORF65	Discovery antibodies	crb2005224	Rabbit	1:100	-
Anti-STC1	Proteintech	20621-1-AP	Rabbit	1:500	-
Anti-TIFA	Biorbyt	ORB 40285	Rabbit	1:2000	-
Anti-VDAC1	CST	D73D12	Rabbit	1:1000	1:50
Anti-WTAP	Abcam	ab195380	Rabbit	1:1000	-
Anti-ZFP36L1	Proteintech	12306-1-AP	Rabbit	-	1:100

Table 2.2. List of antibodies, their identifiers and dilutions used. WB stands for western blot and IF refers to immunofluorescence.

2.1.4 Plasmids

All plasmid constructs used in this study are detailed in the table below alongside their origin and Addgene identifiers (Table 2.3).

Plasmid	Origin	Addgene identifier
GFP-ORF50	James Boyne (Whitehouse laboratory)	
GFP-ORF57	James Boyne (Whitehouse laboratory)	
pLENTI-CMV-GFP	Bought from Addgene	#17448
pLENTI-CMV-GPRC5A	Cloned from pLENTI-CMV-GFP	
pLENTI-CMV-GPRC5A-FLAG	Cloned from pLENTI-CMV-GFP	
pLENTI-CMV-GPRC5A-GFP	Cloned from pLENTI-CMV-GFP	
pLENTI-CMV-ZFP36L1	Cloned from pLENTI-CMV-GFP	

pLENTI-CMV-ZFP36L1-FLAG	Cloned from pLENTI-CMV-GFP	
pLENTI-CMV-ZFP36L1-GFP	Cloned from pLENTI-CMV-GFP	
pLKO.1 TRC	Bought containing shRNAs from Sigma or Dharmacon. Originally designed by the RNAi consortium	#10878
psPAX2	Gift from Edwin Chen (University of Leeds)	#12260
pVSV.G	Gift from Edwin Chen (University of Leeds)	#138479

Table 2.3. List of plasmids used in the study. Origin and Addgene catalogue number are also listed.

2.1.5 shRNAs

All shRNA-expressing plasmids were purchased from Sigma or Dharmacon as stated in the table below. TRC numbers are shown as identifiers (Table 2.4).

shRNA	Company	TRC number
FTO	Sigma	TRCN0000246247
GPRC5A KD1	Dharmacon	TRCN0000005628
GPRC5A KD2	Dharmacon	TRCN0000005632
WTAP	Sigma	TRCN0000231423
YTHDF1	Sigma	TRCN0000286871
ZFP36L1 KD1	Dharmacon	TRCN0000013620
ZFP36L1 KD2	Dharmacon	TRCN0000013621

Table 2.4. List of shRNAs used in this study. The company the shRNAs were purchased from and TRC numbers associated with the shRNAs are also included.

2.1.6 Oligonucleotides

All oligonucleotides were purchased from Integrative DNA Technologies.

2.1.6.1 qPCR primers

Forward and reverse primers used for the qPCR of mRNA levels, transcript variants and m^6A sites are detailed separately in the tables below (Table 2.5, Table 2.6 and Table 2.7).

Primer	Forward (5'-3')	Reverse (5'-3')

18s rRNA	GATGGTAGTCGCCGTGCC	GCCTGCTGCCTTCCTTGG
ALKBH5	AGGGACCCTGCTCTGAAAC	TCCTTGTCCATCTCCAGGAT
CDK2	CCGAGCTCCTGAAATCCTCC	CCCAGAGTCCGAAAGATCCG
CNOT2	AGAAGCTCGCCAAGCATAAT	TCCTGTTCATTCCAAATCCAG
E2F1	CGGCGCATCTATGACATCAC	AGGGTCTGCAATGCTACGAA
ENO2	CCCGATACATCACTGGGGAC	TTCCACTGCCCGCTCAATAC
FLOT1	TCAGCCTTCTGATGATCCCAC	CAAAGTTGAAAACCTCCAGCCC
FLOT2	GCCGAGGGGGTAGCTTTAAC	GAAACTGCTCACAAGCCACG
FOSB	GAAATGCCCGGTTCCTTC	GAGGGTGGGTTGCACAAG
FOSB	TAGGAGACCCCGAGAGGAG	CCGACTCCAGCTCTGCTTT
FTO	TCTGACCCCCAAAGATGATG	CTCGGAGAATTAGTTTAGGATATTTCA
GAPDH	TGTCAGTGGTGGACCTGAC	GTGGTCGTTGAGGGCAATG
GPRC5A	CCTTTCCCTGTTGGTGATTCT	AGACATTGACGTTGGTCCTATTC
HAKAI	AGATGTGTCCAGGCTGTAGTG	TCAAGTGAAGCACGGGTAACA
HEY1	CTTTCCTGCCTCCTTCTCTTT	CAGTTCAGTGGAGGTCGTTT
HIF1A	TGATGACCAGCAACTTGAGG	CTGGGGCATGGTAAAAGAAA
HSPA1A	GGTGCTGGACAAGTGTCAA	TGATGGGGTTACACACCTGC
ILF3	ATGCCATTACGCCCATGA	GGCTCTGCCTTCTCCTCTTT
JUN	CGCCTGATAATCCAGTCCA	TTCTTGGGGCACAGGAACT
KIAA1429	TCGACGAACAGTAGACAGTATTCC	TGGAAATTTGTTCATAACCATCAT
METTL3	CAAGCTGCACTTCAGACGAA	GCTTGGCGTGTGGTCTTT
ORF47	CGCGGTCGTTCGAAGATTG	CGAGTCTGACTTCCGCTAA
ORF57	GCCATAATCAAGCGTACTGG	GCAGACAAATATTGCGGTGT
PLEKHA6	CCACCAGGCAAGAGGTAGAG	GCACAACGCCAACTTTGTT
PPIF	CCGCTTTCCTGACGAGAACT	GCCATCCAACCAGTCTGTCT
PTPRN2	GCCTTCACCTCTGGGAGATT	GAGGGTATGAATCCGTGCTC
RBM15	ATGCCTTCCCACCTTGTGAG	GGTCAGCGCCAAGTTTTCTC
RBM15B	CTTGCCTCTCCTGGAAGGTG	GAAGTGGGGTGTGTCCCTTT
STAT5B	TCAAAGAGGCGAACTGTGTG	GCTCCTCAGAGGCAGAGAGA
TIFA	GAGAGCTGGGCTACCTAAATAAA	TCCAATGACTCGCCATCTTC

TNN	CTTCCCTCTCACCTGCATTT	GCCGTTCCAGTACTGTCTTT
TNRC6A	CAGCCAGTCAGAAAGCAGTG	GGGATCCTGAAGTACTGTGGTT
VDAC1	TCCTCCCCTTCAAATGCTGTAA	GACAACAGAAGAAGGATGAGGTT
VDAC2	CTTGCAGTGGCGTGGAATTT	ATTTGGTCTCCAAGGTCCCAG
VDAC3	ACACACCAACGTACTGTGACC	ATTCCATCACTCCACTACAAGACT
VEGFA	GGCAAAAACGAAAGCGCAAG	GAGGCTCCAGGGCATTAGAC
WTAP	TTCCCAAGAAGGTTCGATTG	TGCAGACTCCTGCTGTTGTT
YTHDF1	ATAACCAGCTCCGGCACAT	GGGAGTTTGTGACCGGTTT
YTHDF2	TCCGTAAGTGCATACAGTTTTCTC	TTCTCCAAGTGCAAATGTCAA
YTHDF3	TGATGATGATTTTGAGCCATACTTA	GCTTCCCCAAGAGAATATGGA
ZC3H12A	TCTGTGGGAATTTGAGGACAG	GTGGATCTCCGTGGATGAATAG
ZC3H13	CTCGTCGTCGTCCTCCTG	TTTGACATTTTGTACTATTCCTCCC
ZFP36L1	GCGAAGTTTTATGCAAGGGTAA	GTGCCCACTGCCTTTCTG
ZNF12	AACAGTACCTTGTCTGGATGTG	GGTCTCAGGGTCTTTCAGTATTT

Table 2.5. List of qPCR primers used for amplification of viral and cellular transcripts.

Primer	Forward (5'-3')	Reverse (5'-3')
FOSB splice variant 1	AGAGGAAGAGGAGAAGCGAA	TGGAGTCGGTCGGTCAG
ZFP36L1 splice variants 1+2	TCTGTGCGTCCCAAATTTCTA	AAGTGTCTGCACAACTTACCT
ZNF12 splice variant 1	GATGTAGAAACGAACCCTGT	CTGAAACAGACGTTAAACACTT
ZNF12 splice variant 2	ATCTTCAGCAGACTTTCCATCTC	TCACAAAGTCCCACTTAAGTCAA

Table 2.6. List of qPCR primers used for detection of splice variants.

Primer	Forward (5'-3')	Reverse (5'-3')

FOSB Control	GGAGAGCTGGTGACTTTGGG	AGAGCCAACAGTCAGCTGGG
FOSB m^{6}A	CTCCCTCCTCGCTCTGTGAA	CAAGTCTCTCTCCCCCATGT
GPRC5A control	TTTGTGATAAGGCTGAAGCT	TTTTCGCCTGTTGGAGTCCT
GPRC5A m^{6}A	CCTAGAAACGGTGGCCACAG	CCAGGAGGAAGAGAAACTGA
JUN Ctrl	AGCGCCTGATAATCCAGTCC	ATCTGTCACGTTCTTGGGGC
JUN m^{6}A	ACCTTGAAAGCTCAGAACTCGG	TAAGCTGTGCCACCTGTTCC
SLC39A14 control	GCAGGATCTAATACATCGGTATGG	TGGTTGAGTAGGGCCTTCAG
SLC39A14 m^{6}A	GGACAGATCCAGATTGGGTAG	AGGGCCCGACTTCCAGT
ZFP36L1 control	GGCACACACACATTAAGATGAA	AGAGAAATAGAAAGCGACGGT
ZFP36L1 m^{6}A site 1	GGTTGCCTGCTGGACAGAAA	TTCTGGTGGAACTTGGAGCTG
ZFP36L1 m^{6}A site 2	CAGGATTCTCTCTCGGACCA	TCCAAGGTCGGGGAGTCT

Table 2.7. List of qPCR primers used to validate m^{6}A sites by m^{6}A-qPCR.

2.1.6.2 Cloning primers

Forward and reverse primers used for NEBuilder assembly of GPRC5A or ZFP36L1 containing constructs are shown in the table below (Table 2.8).

Primer	Forward (5'-3')	Reverse (5'-3')	Annealing temperature (°C)
GPRC5A	CGCCATCCACGCTGTTTG CCACCATGGCTACAACA GTCCCTG	AGAGGTTGATTGTCGACT TAGCTGCCCTCTTTCTTTA C	63
GPRC5A-FLAG	CGCCATCCACGCTGTTTG CCACCATGGCTACAACA GTCCCTG	AGAGGTTGATTGTCGACT TACTTGTCGTCATCGTCTT TGTAGTCGCTGCCCTCTT TCTTTAC	61
GPRC5A-GFP	CGCCATCCACGCTGTTTG CCACCATGGCTACAACA GTCCCTG	TCGCCCTTGCTCACCATG CTGCCCTCTTTCTTTAC	61

pLENTI-CMV-GFP	GTGAGCAAGGGCGAG	CAGCGTGGATGGCGTC	66
pLENTI-CMV-no GFP	GACAATCAACCTCTGGATTAC	CAGCGTGGATGGCGTC	66
ZFP36L1	CGCCATCCACGCTGTTTGCCACCATGACCACCACCCTCGTG	AGAGGTTGATTGTCGACTTAGTCATCTGAGATGGAAAGTCTG	64
ZFP36L1-FLAG	CGCCATCCACGCTGTTTGCCACCATGACCACCACCCTCGTG	AGAGGTTGATTGTCGACTTACTTGTCGTCATCGTCTTTGTAGTCGTCATCTGAGATGGAAAGTCTGC	66
ZFP36L1-GFP	CGCCATCCACGCTGTTTGCCACCATGACCACCACCCTCGTG	TCGCCCTTGCTCACCATGTCATCTGAGATGGAAAGTCTGC	66

Table 2.8. List of primers used for cloning of GPRC5A and ZFP36L1 into pLENTI-CMV-GFP.

2.2 Methods

2.2.1 Molecular cloning

2.2.1.1 Bacterial cell culture and cryopreservation

Any work with live bacterial cells was undertaken in the proximity of a sterile flame and with sterile tips to prevent contamination. Culture medium and agar were sterilised by autoclaving (121°C, 1 hour). Cells were frozen at -80°C for long term storage as a glycerol stock in 1ml lysogeny broth (LB) medium [1% (w/v) tryptone, 0.5% (w/v) yeast extract, 0.5% (w/v) NaCl] containing 25% glycerol.

2.2.1.2 Transformation of *E. coli* DH5α and NEB stable strains

50µl of competent cells were thawed on ice and mixed with 1ng of plasmid DNA or 2µl of NEBuilder assembly reaction (2.2.1.4) then incubated on ice for a further 30 mins. Cells were heat shocked at 42°C for 30 secs and immediately returned to ice for 5 mins. Next, 450µl SOC medium (NEB) or NEB stable outgrowth medium (NEB) was added to the cells followed by shaking of the culture at 37°C for 1 hour at 180rpm. After shaking, cells were spread onto agar plates [1.5% (w/v) in LB medium] containing 50 µg/ml ampicillin or kanamycin and incubated at 37°C overnight.

2.2.1.3 Plasmid purification

Bacterial glycerol stocks or transformed cells were spread onto 50µg/ml ampicillin or kanamycin 1.5% agar plates and incubated overnight at 37°C. Single colonies were used to inoculate 10ml Luria broth (Invitrogen) with 50µg/ml ampicillin and the culture grown overnight at 37°C with 180rpm shaking. The bacterial cells were collected by centrifugation at 4,500 x *g* for 5 mins at 4°C and removal of supernatant. Plasmid DNA was purified using a QIAprep Spin Miniprep Kit according to the manufacturer's instructions. Briefly, bacterial cell pellets were placed in 250µl buffer P1 followed by 250µl buffer P2 and 350µl buffer N3. On each addition of buffer, the solutions were inverted several times to allow mixing. The samples were centrifuged for 10 mins and supernatant transferred to a QIAprep spin column. After centrifugation, the columns were washed with 0.75ml of buffer PE and centrifuged twice to allow removal of residual buffer. Finally, 50µl of nuclease free water was added to columns, which were incubated for 1 minute, before centrifugation to elute the DNA. All centrifugation steps were carried out at 16,000 x *g* for 1 min unless otherwise stated. DNA concentrations in purified eluents were assessed using a NanoDrop ND-1000 spectrophotometer (NanoDrop Technologies). Purified plasmid DNA was stored at -20°C.

2.2.1.4 Cloning

Tagged and untagged version of GPRC5A and ZFP36L1 cDNA were cloned into the pLENTI-CMV-GFP vector using the NEBuilder HIFI DNA Assembly Kit (NEB). Primers were designed to amplify GPRC5A and ZFP36L1 coding sequences as well as the pLENTI-CMV-GFP backbone using the NEBuilder online assembly tool (https://nebuilder.neb.com). Primers were designed with overlaps between the genes and the pLENTI-CMV-GFP backbone to allow for blunt end cloning using the NEBuilder system. The entire coding sequences of GPRC5A and ZFP36L1 genes were amplified from cDNA using Q5 High-Fidelity 2X Master Mix (NEB). Reactions consisted of 1.25µl TREX cDNA, 1.25µl of 10uM forward and reverse primer mix, 10µl nuclease free water and 12.5µl Q5 High-Fidelity 2X Master Mix. Cycling conditions consisted of an initial denaturation step of 30 secs at 98°C, followed by 35 cycles of denaturation at 98°C for 10 secs, annealing at 60-72°C for 20 secs and finally extension at 72°C for 30secs/kb. A final extension step was carried out at 72°C for 2 mins after completion of cycling. Ligation reactions were set up containing 50ng pLENTI-CMV-GFP PCR product, 100ng GPRC5A or ZFP36L1 gene fragments, 10µl NEBuilder HiFi DNA Assembly Master Mix

and the reaction made up to 20µl with nuclease free water. The ligation reaction was incubated at 50°C for 15 minutes before 2µl of the mixture was transformed into NEB stable cells as in 2.2.1.2.

2.2.2 Mammalian cell culture

Cell culture was performed under sterile conditions in tissue culture hoods. TriGene disinfectant (Ceva) and 70% ethanol were regularly applied to maintain sterile working conditions and external reagents were filter sterilised before use in cell culture. Filter tips were used when handling lentivirus. Cells were submerged in antiviral Virkon disinfectant (Du Pont) for a minimum of 2 hours before disposal.

2.2.2.1 Cell lines

Human embryonic kidney (HEK) 293T cells (referred to as 293T cells) were purchased from the American Type Culture Collection (ATCC). TREX BCBL-1-Rta (TREX) cells were kindly provided by Dr Jae Jung, University of Southern California. TREX cells are a KSHV-infected, BCBL-1-derived primary effusion lymphoma B lymphocyte cell line. The cell line is engineered to express Myc-Rta under a tetracycline inducible promoter permitting robust lytic reactivation of the KSHV life cycle on the addition of doxycycline (Nakamura et al., 2003). The Myc-Rta vector also contains a hygromycin resistance gene which serves as a selectable marker to prevent loss of the cassette.

2.2.2.2 Cell maintenance

Cell lines were cultured using Corning tissue culture plastics with their respective media and maintained in humidified incubators at a temperature of 37˚C and a 5% CO_2 atmosphere. 293T cells were cultured in Dulbecco's modified eagle medium (DMEM) supplemented with 10% foetal bovine serum (FBS) and 1% penicillin and streptomycin (P/S). TREX cells were cultured in Roswell Park memorial institute 1640 (RPMI) medium supplemented with 10% FBS, 1% P/S and 100µg/ml hygromycin. TREX cells that had been transduced with lentiviral constructs were cultured in medium further supplemented with 3µg/ml puromycin.

Cells were passaged at 80% confluence to preclude the accumulation of toxic metabolites and exhaustion of nutrients. For adherent 293T cells, medium was removed and 2ml 0.05%

(v/v) trypsin in PBS was added to the cells until they had detached entirely. Trypsinised 293T cells were resuspended in 293T medium and split at the desired ratio. Supplementary medium was added to the flasks to ensure continued growth. For TREX suspension cells, the cells were collected in a 50ml falcon tube and centrifuged at 1200rpm for 3 minutes. Supernatant was removed and the TREX cells resuspended in TREX media and split at the desired ratio. Remaining cells were returned to their flask and supplemented with additional medium to allow further growth.

2.2.2.3 Cell counting

Cells suspensions were collected in falcon tubes and counted for seeding at required cell concentrations. A 7µl volume from a cell suspension was added to a sterile haemocytometer and the cells counted using a light microscope (Leica Microsystems) allowing the number of cells/ml to be calculated.

2.2.2.4 Cryopreservation

Cell suspensions at 50% confluency were collected, centrifuged at 1200rpm for 3 minutes and the supernatant removed. Pellets were resuspended in 3.6ml sterile FBS and incubated at 4°C for 10 minutes. After incubation, 1.2ml freezing medium [12% (w/v) glucose, 40% (v/v) DMSO and 60% (v/v) RPMI] was added to the cell suspension and the mixture aliquoted into CryoTubes (NUNC) in 1.6ml aliquots. The cells were immediately frozen at -80°C until further use. Cells to be stored for more than 6 months were transferred into liquid nitrogen after 24 hours. To raise cells from -80°C or liquid nitrogen storage, cells were incubated at 37°C until fully defrosted, then centrifuged at 500 *x g* for 3 minutes and the freeing mixture removed. Cells were resuspended in their respective culture medium and left to recover for a minimum of 3 days before experimental use.

2.2.2.5 Transfection

All transfections were carried out in 293T cells, 24 hours after seeding 4 x 10^5 cells per well in a 6-well plate. 1µg of plasmid DNA was combined with 100µl OPTI-MEM media. In addition, 4µl of Lipofectamine 2000 was added to 100µl OPTI-MEM. Both mixtures were incubated at room temperature for 5 minutes, then combined and incubated for a further

20 minutes at room temperature. After incubation, the lipofectamine/DNA solution was added dropwise to the 293T cells and at least 24 hours allowed before harvesting.

2.2.2.6 Transduction

293T cells were co-transfected with 1.2µg of lentiviral vector and 0.65µg of the packaging plasmids psPAX2 and VSV.G. The cells were incubated for 48 hours to allow efficient production of lentiviral particles. After incubation, the supernatant containing lentivirus was filter sterilised and mixed with 1 million TREX cells containing 8µg/ml polybrene. The cells were spin-inoculated at 800 *x g* for 1 hour and plated in 6-well plates. After 6 hours, the cells were placed in fresh TREX medium. At least 48 hours after transduction, transduced cells were selected with TREX medium containing 3µg/ml puromycin which was replaced every 2-3 days. If shRNA depletion was carried out, knockdown was assessed 7 days later through RNA isolation followed by RT-qPCR as in 2.2.5.1, 2.2.5.3 and 2.2.5.4.

2.2.2.7 Cell collection

Cells were collected and centrifuged at 500 *x g* (gravitational force) for 3 minutes. The supernatant was removed and cell pellets stored at -80°C until further use.

2.2.2.8 DAA cytotoxicity assay

Cytotoxicity of the drug DAA was assessed using the MTS-based CellTiter 96 AQ_{ueous} One Solution Cell Proliferation Assay (Promega). TREX cells were seeded at 80,000 cells per well into a 96-well plate and left for two hours to equilibrate. Cells were treated with varying DAA concentrations of 0-100µM or DMSO controls and incubated for 24 hours. Afterwards, growth medium was replaced with 20 µl of CellTiter 96 AQ_{ueous} One Solution Reagent for 1 h at 37°C. Finally, the absorbance was measured at 490 nm using an Infinite F50 Robotic microplate reader (Tecan).

2.2.3 Virus-based assays

2.2.3.1 TREX reactivation

Doxycycline hyclate (Sigma) was used at a working concentration of 2µg/ml to induce TREX cells into lytic replication.

2.2.3.2 Viral re-infection assays

TREX cells were seeded at 500,000 cells per well into 6-well plates and reactivated for 72 hours. KSHV virion-containing supernatant was collected by centrifugation at 500 x *g* for 5 min at room temperature. 2ml virus culture was added to 2ml 293T cells seeded at 400,000 cells per well in a 6-well plate. After incubation for a further 48 hours, cells were washed and pellets collected. RNA was isolated from the cells and used for RT-qPCR as described in 2.2.5.1, 2.2.5.3 and 2.2.5.4. mRNA levels of the viral transcript *ORF57* were measured by normalisation against the housekeeping gene *GAPDH.*

2.2.3.3 DAA virus inhibition assay

TREX cells were seeded at 1 million cells per well in a 6-well plate and treated with 25µM DAA for 24 hours. Cells were reactivated for a further 24 hours before cell collection and lysis. Viral protein levels were analysed by SDS-PAGE and immunoblotting of protein lysates with anti-ORF57 and anti-Myc-Rta antibodies using GAPDH protein levels as a negative control (2.2.4.2 and 2.2.4.3).

2.2.4 Protein analysis

2.2.4.1 Production of protein lysates

Depending on the cell number collected, between 50-200µl RIPA buffer [150 mM NaCl, 50 mM Tris-HCl pH 7.6, 1% (v/v) NP-40] was added to cell pellets followed by vortexing and lysis at 4°C for 30 minutes. Cell lysates were centrifuged at 12,000 x *g* for 10 minutes and the supernatants containing concentrated cellular protein collected. Finally, lysates were sonicated 3 times for 30 secs and stored at -80˚C until further use. If necessary, protein extracts were quantified using a Pierce BCA Protein Assay Kit (Thermo Scientific) according to the manufacturer's instructions. Briefly, a working reagent was prepared by mixing BCA reagents A and B at 50:1 reagent. 100ul of this reagent was mixed with 5µl of protein lysate into a microtiter plate in duplicate. After incubation for 30 minutes at 37°C, the absorbance was measured at 562nm using an Infinite® F50 Robotic microplate reader (Tecan).

2.2.4.2 SDS-polyacrylamide gel electrophoresis

Protein lysates were diluted 1:1 with 2x Laemmli sample buffer [100 mM Tris-HCl pH 6.8, 20% (v/v) glycerol, 4% (w/v) SDS, 10 mM DTT, 0.2% (w/v) bromophenol blue], boiled at 95°C for 10 mins, and loaded at equal volumes during protein separation. Lysates were separated according to their molecular weight by SDS-polyacrylamide gel electrophoresis (SDS-PAGE). Proteins were resolved through polyacrylamide gels composed of a 5% stacking gel [5% (v/v) acrylamide/bis-acrylamide 37.5:1 (Severn Biotech Ltd), 125 mM Tris-HCl pH 6.8, 0.1% (w/v) SDS, 0.08% (v/v) APS, 0.008% (v/v) TEMED] and 10-15% resolving gel [10-15% (v/v) acrylamide/bis-acrylamide 37.5:1, 375 mM Tris-HCl pH 8.8, 0.1% (w/v) SDS, 0.12% (v/v) APS, 0.012% (v/v) TEMED] at 180 volts for 1 hour. The running buffer used for SDS-PAGE consisted of 25mM Tris-HCl, 192mM Glycine and 0.1% (w/v) SDS.

2.2.4.3 Western Blot

After SDS-PAGE, protein samples were transferred onto Amersham Protran 0.45µm nitrocellulose blotting membrane (GE Healthcare) for 30 mins through transfer buffer [20% (v/v) methanol, 25 mM Tris, 192 mM glycine] at 25 volts by semi-dry transfer (Trans-Blot Turbo, BioRad) according to the manufacturer's instructions. Efficient protein transfer was confirmed by staining the membranes with Ponceau-S solution [5% (v/v) Acetic acid, 0.1% (w/v) Ponceau-S]. Membranes were blocked using 5% (w/v) non-fat milk (Marvel) in TBST [150 mM NaCl, 50 mM Tris-HCl pH 7.5, 1% (v/v) Tween-20] for 1 hour and incubated with primary antibody overnight at 4°C. Next, membranes were washed 3 times in TBST for 5 minutes, then incubated for 1 hour with the appropriate HRP-linked secondary antibodies (polyclonal goat anti-rabbit or anti-mouse, DAKO). Membranes were once again washed three additional times with TBST. Finally, the membranes were coated in Amersham ECL western blotting detection reagents (GE Healthcare) and chemiluminescence detected using a G:BOX Chemi XRQ (Syngene).

2.2.4.4 Protein immunoprecipitation

For all protein immunoprecipitations, 2.5 million cells were seeded into 25cm^2 tissue culture flasks and reactivated for 0 or 24 hours. After cell collection, pellets were lysed in 300µl immunoprecipitation buffer [150 mM NaCl, 2 mM EDTA, 0.5% Triton-X 100, 0.5 mM DTT, 10 mM Tris pH 7.4 and 1X protease and phosphatase inhibitors] and placed on ice for 30 mins.

Next, the lysates were centrifuged at 12,000 x *g* for 10 mins and the supernatant collected into new microcentrifuge tubes and placed on ice. A 5% input was taken at this stage and mixed with 15µl 2x Laemmli sample buffer for downstream applications

15µl Protein A or G Dynabeads (ThermoFisher) were pre-prepared by washing 3 times in immunoprecipitation buffer then resuspended in 200µl immunoprecipitation buffer and coated with 2µl capture antibody. The beads were then rotated for 1 hour at 4°C and then washed 3 times for 5 minutes with immunoprecipitation buffer. To allow antibody binding, the beads were incubated with lysates overnight at 4°C. The following day, beads were washed 3 times for 5 minutes in immunoprecipitation buffer. Immunoprecipitated proteins were eluted from the beads by resuspension in 30µl 2x Laemmli sample buffer and boiling the samples at 90°C for 10 minutes. Finally, the proteins were separated by SDS-PAGE and detected by western blotting as in 2.2.4.2 and 2.2.4.3.

2.2.4.5 Proteomics

TREX and GPRC5A-FLAG-expressing cells undergoing latent or lytic replication were processed as in 2.2.4.4; however, no elution step was carried out. Instead, the beads were sent to Dr. Kate Heesom at the University of Bristol Proteomics facility for tandem mass tagging (TMT) coupled with liquid chromatography and mass spectrometry analysis (LC-MS/MS). See 2.2.7.4 for quantitative proteomic analysis.

2.2.4.6 Immunofluorescence microscopy

TREX cells were seeded at 500,00 cells per well into 24-well plates containing 13mm sterile glass coverslips pre-treated with poly-L-lysine (Sigma) for 5 mins and washed with PBS before cell addition. After 3 hours, cells were reactivated for 24 hours. Cells were then washed in PBS before fixation with 4% (v/v) paraformaldehyde for 10 minutes at room temperature. After fixing, cells were washed 3 times in PBS and permeabilised with 1% (v/v) Trition-X-100 in PBS for 15 minutes at room temperature and washed 3 times once more. To prevent non-specific binding of proteins, the cells were blocked in 1% (w/v) bovine serum albumin (BSA) in PBS for 1 hour. Next, cells were incubated with primary antibody diluted in 1% BSA in PBS for 1 hour at 37°C in a humidity chamber. After 3 more PBS washes, Alexa Fluor-conjugated secondary antibodies (ThermoFisher) diluted in 1% BSA in PBS were added to the cells for 1 further hour at 37°C in a humidity chamber. Finally, after 3 more PBS

washes, the coverslips were mounted onto microscope slides using Hardset Antifade Mounting Medium with DAPI (VECTASHIELD) for detection of nuclei. After the mounting medium had set, the slides were stored in the dark at 4°C before visualisation on a LSM 880 Axio Observer Z1 confocal microscope (Zeiss).

2.2.5 RNA analysis

2.2.5.1 RNA extraction

Total RNA was isolated from cell pellets using a Monarch Total RNA Miniprep Kit (NEB) according to the manufacturer's instructions. Briefly, cell pellets were lysed in 400µl RNA Lysis Buffer and transferred to gDNA Removal Columns for removal of contaminating DNA. After centrifugation, the flow through was mixed with 400µl ethanol and transferred to an RNA Purification Column followed by another spin step. 500µl RNA Wash Buffer was added and the columns centrifuged once more before addition of 75µl DNAse I Reaction Buffer and 5µl of DNAse I. After a 15-minute incubation, 500µl RNA Priming Buffer was added to the columns followed by centrifugation. Next two wash steps were carried out, each involving the addition of 500µl RNA Wash Buffer to the columns, followed by centrifugation. In the second of these wash steps, the columns were centrifuged for 2 mins. Finally, the columns were transferred to fresh 1.5ml microcentrifuge tubes and 50µl of nuclease free water was added to centre of the columns followed by a final centrifugation step to elute the RNA. All centrifugation steps were carried out at 16,000 x *g* for 30 secs unless otherwise stated. The concentration and purity of RNA were measured using a NanoDrop ND-1000 spectrophotometer (NanoDrop Technologies). RNA eluents were used immediately for reverse transcription or stored at -80°C.

2.2.5.2 RNA extraction with TRIzol

After subcellular fractionation or m^6A immunoprecipitation, RNA was isolated by phenol-chloroform extraction using TRIzol LS reagent (Life Technologies) according to the manufacturer's protocol. Briefly, TRIzol solutions were incubated for 5 minutes at room temperature before addition of 200µl of chloroform and vigorous mixing. Samples were left at room temperature for another two minutes, then centrifuged at 12,000 x *g* for 15 mins at 4°C to separate the aqueous and organic phenol phases. 500µl of the upper, RNA-containing, aqueous phase was collected and mixed with 500µl of isopropanol. After

incubation for 10 mins at room temperature to allow precipitation, the samples were centrifuged at 12,000 x *g* for 10 minutes to pellet the RNA. The supernatant was discarded, and the RNA pellet washed with 70% ethanol and centrifuged once more at 7,500 x *g* for 5 mins. The wash was discarded and the pellet resuspended in 17µl nuclease free water.

When isolating RNA from subcellular fractions, contaminating DNA was removed using the DNA-free DNA removal kit (Ambion) following the manufacturer's protocol. Briefly, 2µl DNase I buffer and 1µl DNase I were added to the 17µl samples remaining after TRIzol RNA extraction for 30 mins at 37°C. Following digestion of DNA, 2µl of DNase inactivation reagent was added to each sample and gently mixed for 2 mins at room temperature. Next, the inactivation agent was separated from the samples by centrifugation at 10,000 x *g* for 2 minutes and the RNA-containing supernatant collect into new microcentrifuge tubes. As in 2.2.5.1, the RNA was used immediately for cDNA synthesis or stored at -80°C

2.2.5.3 cDNA synthesis

RNA was converted to cDNA for qPCR analysis using LunaScript RT SuperMix Kit (NEB). 1µg RNA was combined with 4µl 5X LunaScript RT SuperMix and the reaction made up to 20µl with nuclease free water. RT samples were placed in a thermocycler and incubated at 25°C for 2 mins to promote primer annealing, 55°C for 10 mins to allow cDNA synthesis and 95°C for 1 min to heat inactivate the enzyme mix. cDNA was used immediately for qPCR or stored at -20°C.

2.2.5.4 Quantitative PCR (qPCR)

qPCR reactions were set up in duplicate containing 1X GoTaq qPCR master mix (Promega), 5µl template cDNA (used at a 1:50 dilution in nuclease free water) and 0.5µM concentrations of each primer (all purchased from Integrative DNA Technologies). Thermocycling was carried out in a Rotor Gene 6000 real-time PCR machine (Eppendorf) involving a preliminary incubation of 10 minutes at 95°C followed by 40 cycles of denaturation at 95°C for 15 seconds, annealing at 60°C for 30 seconds and extension at 72°C for 20 seconds. Data was acquired in the elongation step in every cycle and analysed using the Rotor Gene 6000 series software. qPCR was immediately followed by a melting curve analysis between 65 and 95°C (with 0.2°C increments) to rule out the amplification of multiple products. For each primer set, template cDNA was quantified at six different

dilutions (1:50, 1:100, 1:200, 1;400, 1:800 and 1:1600) to generate a standard curve for which the gradient was used to determine the amplification efficiency (AE) using the equation AE =($10^{-1/gradient}$). A no template control was also used in primer efficiency tests to rule out primer dimerization. Relative expression levels of RNAs of interest were normalised to mRNA levels of the housekeeping gene *GAPDH* (unless stated otherwise) and quantified using the ΔCT method. Statistical significance was determined by Student's T-test across three biological replicates unless stated otherwise.

2.2.5.5 Splicing analysis

RT-qPCR analysis was carried out on total RNA extracted from TREX cells as in 2.2.5.1 and 2.2.5.4. Primers were designed spanning unique splice junctions to amplify specific transcript variants of a gene. Splice variant levels were compared to total mRNA levels for a particular gene.

2.2.5.6 Subcellular fractionation

Reactivated TREX cells were collected, washed in PBS, and lysed in 600µl 1% (V/V) triton-X-100 in PBS with 1µl/ml Murine RNase inhibitor (Invitrogen) at 4^{o}C for 10 minutes. A 250µl fraction of the extract was taken as a whole cell lysate, while the remaining 350µl were centrifuged at 720 *x g* for 5 minutes at 4°C. The supernatant was collected as the cytoplasmic fraction while the pelleted nuclei were washed in 1ml PBS and centrifuged once again at 720 *x g* for 5 minutes at 4°C. The pelleted nuclei were resuspended in 100µl 1% triton-X-100 in PBS with 1µl/ml Murine RNase inhibitor. The cellular fractions were then deposited in TRIzol LS reagent or 2x Laemmli sample buffer for assessment of RNA or protein levels respectively by RT-qPCR and western blotting (2.2.5.2,2.2.5.3 and 2.2.5.4 or 2.2.4.2 and 2.2.4.3).

2.2.5.7 RNA stability

TREX cells were reactivated for 24 hours before the addition of 2.5ug/ml actinomycin D (Thermo Scientific) for 0, 3 and 6 hour timepoints. Following actinomycin D treatment, cells were collected and total RNA isolated before reverse transcription and qPCR analysis of specific transcripts as in 2.2.5.1 and 2.2.5.4. RNA levels were normalised to *18s rRNA* rather than *GAPDH* as the rRNA is more stable.

2.2.6 m^{6}A based assays

2.2.6.1 m^{6}A-qPCR

100µg of total RNA was extracted from TREX cells as in 2.2.5.1 and divided into 18µl aliquots each containing ~50µg. RNA was fragmented into 100-200 nucleotide segments using an RNA fragmentation reagent (Ambion) according to the manufacturer's instructions. Briefly, 2µl of the 10x RNA fragmentation reagent were added to the samples and incubated at 70°C for 15 minutes to allow nucleotide shearing. 1µl of stop solution was then added to the samples before clean-up and concentration of the RNA by sodium acetate precipitation. 1ug of fragmented RNA was run on a 1% agarose gel against total RNA to confirm successful fragmentation to the desired length. To each sample, 79 µl of RNase free water, 10µl of 3M sodium acetate pH 5.2 and 300µl 100% ethanol were added. RNA was precipitated overnight at -80°C. The next day, samples were centrifuged at 16,000 x *g* for 15 mins at 4°C and the supernatant removed. The RNA pellet was washed in 1ml 70% ethanol and centrifuged at 7,500 x *g* for 5 mins at 4°C. Supernatant was removed and the RNA pellet resuspended in 10µl nuclease free water for m^{6}A immunoprecipitation.

For each m^{6}A immunoprecipitation, 25µl of Magna ChIP Protein A+G magnetic beads (Merck Millipore) were washed twice in m^{6}A wash buffer [20 mM Tris HCl pH 7.4, 150 mM NaCl, and 0.1% (v/v) NP-40 (v/v)]. Next, the beads were resuspended in 100µl of m^{6}A wash buffer, coated in 5µl of anti-m^{6}A antibody (Merck Millipore) and rotated for 45 mins at room temperature. After 3 washes with m^{6}A wash buffer, the beads were placed in m^{6}A immunoprecipitation buffer [900µl m^{6}A wash buffer, 35µl 0.5M EDTA pH 8.0, 4µl RNase inhibitor (ThermoFisher)] along with 9.5µl of fragmented RNA. The remaining 0.5µl of RNA was kept as a 5% input for later use. m^{6}A immunoprecipitations were incubated at 4°C overnight with rotation after which six washes in m^{6}A wash buffer were carried out. RNA from inputs and immunoprecipitations was eluted from the beads through incubation with proteinase K buffer [126µl m^{6}A wash buffer, 15µl 10% (v/v) SDS and 9µl 20mg/ml PCR-grade proteinase K (ThermoFisher)] at 55°C for 30 mins. After incubation, the supernatant containing m^{6}A immunoprecipitated RNA was removed and supplemented with 250µl m^{6}A wash buffer. 750µl Trizol LS was added to the samples and RNA isolated by phenol-chloroform extraction as in 2.2.5.2; however, 1µl RNA-grade glycogen (ThermoFisher) was added to the samples at the isopropanol stage to allow visualisation of the RNA pellet in

downstream steps. The entire RNA pellets for both immunoprecipitations and inputs were converted to cDNA using LunaScript RT SuperMix Kit (NEB) as in 2.2.5.3. qPCR cycling conditions were identical to those carried out in 2.2.5.4. However, m^{6}A-immunoprecipitated samples were normalised to their respective input samples and m^{6}A content at a particular region calculated relative to an unmodified control region within the same transcript.

2.2.6.2 m^{6}A-seq

m^{6}A-sequencing was carried out by Belinda Baquero, a former post-doctoral research assistant in the Whitehouse group. The protocol for m^{6}A-seq was carried out as in 2.2.6.1 with TREX cells reactivated for 0, 8 and 22 hours; however, the cDNA from 4-6 m^{6}A immunoprecipitations were pooled to gather enough material for cDNA library generation and NGS. Furthermore, a 1% input was used. Libraries were generated using the NEBNext ultra DNA Library Prep Kit (NEB) from the cDNA of input and m^{6}A immunoprecipitations. Sequencing was carried out on a HiSeq 3000 platform (Illumina) with a 151bp end lane. Two independent biological replicates were prepared for each timepoint analysed.

2.2.7 Bioinformatics and statistics

2.2.7.1 m^{6}A-seq analysis

Bioinformatic analysis of the m^{6}A-seq data was carried out by Agne Antanviciute, a former PhD student in St. James' Hospital. m^{6}A peaks were identified using the m^{6}A viewer peak calling software with default settings and exported in tab-delimited format to the statistical computing software R for further analyses including kernel density estimates and m^{6}A distribution (Antanaviciute et al., 2017). Significantly enriched m^{6}A peaks in both viral and cellular genomes were defined by a minimum 1.5-fold enrichment of m^{6}A-immunoprecipitation reads over input reads with a false discovery rate of 5% (FDR<5%) required in both biological replicates. Peak positions within 100nt were considered as overlapping.

Discovery of an m^{6}A peak motif was performed using the 100nt of sequence flanking viral m^{6}A peaks. Repetitive viral sequences were removed and the remaining sequence used for enriched sequence motif detection using the software MEME (Bailey et al., 2009).

2.2.7.2 Functional clustering of methylated mRNAs

Functional clustering was performed using STRING protein-protein interaction networks functional enrichment analysis.

2.2.7.3 CHIP-seq data processing

Raw CHIP-seq data was obtained from a previously published article and processed by Ivaylo Yonchev of the Wilson group at the University of Sheffield (Papp et al., 2019). Enriched peaks of RTA binding within cellular genes were called using the software MACS2.

2.2.7.4 Proteomic data analysis

Samples sent for quantitative proteomics were analysed by TMT labelling and LC-MS/MS analysis. Data was outputted as a Microsoft Excel spreadsheet containing the results of a Sequest search against the Uniprot Human Database. Data from two independent replicates were grouped before filtering of best interactors. Contaminating proteins from a common contaminants database were removed and data filtered to satisfy an FDR of less than 5%. Protein abundance ratios were calculated between GPRC5A-FLAG cells and TREX cells for both latently and lytically-infected cells. Proteins were filtered by a minimum abundance of 100 in GPRC5A-FLAG cells and a minimum net abundance of 50 after subtraction of background abundances in TREX cells. An abundance ratio of 2 was set for GPRC5A-FLAG cells relative to TREX cells in latency. However, a 1.4-fold enrichment was used for GPRC5A-FLAG cells relative to TREX cells in lytic replication as fewer proteins were detected due to the action of virus-mediated host-cell shutoff. Finally, proteins with enriched GPRC5A interaction in the lytic phase were identified using a minimum 1.5-fold interaction in lytic cells compared to those undergoing latent replication after subtraction of TREX cell background. The 51 proteins in latent, 51 proteins in lytic phase and 25 proteins enriched in the lytic phase which met these strict cut-offs were subjected to STRING protein-protein interaction networks functional enrichment analysis.

2.2.7.5 Statistical Analysis

For all quantified data, differences were considered to be statistically significant when $p<0.05$ with asterisks denoting the level of significance (*=$p<0.05$, **=$p<0.01$,

***=p<0.001). qPCR data was analysed for statistical significance using student's unpaired T test unless otherwise stated.

2.2.7.6 Image generation

All graphs and tables were drawn in Microsoft Excel unless otherwise stated and confocal images were generated using Zen blue software. Heat maps were constructed in Graphpad Prism 7. Scientific diagrams were generated using Biorender.

Chapter 3

~

The cellular m^6A landscape is altered upon KSHV reactivation

3 The cellular m^{6}A landscape is altered upon KSHV reactivation

3.1 Introduction

m^{6}A is a ubiquitous RNA modification, asymmetrically distributed across the transcriptome where it affects all stages of mRNA biology. The modification is installed on transcripts by the m^{6}A writer complex, in most cases in a cotranscriptional manner. The catalytic core of the m^{6}A writer complex consists of the methyltransferase METTL3 and adaptors METTL14 and WTAP. Additional subunits bind the complex through WTAP and regulate the efficiency and selectivity of deposition (Zaccara et al., 2019). m^{6}A erasers are able to convert a subset of m^{6}A residues back to adenosine, while m^{6}A readers decode the modification and dictate the methylated transcript towards a specific biological fate.

In recent years, the role of m^{6}A has been studied in a number of different viral life cycles where it plays diverse regulatory roles. Most of these studies have investigated the effects of m^{6}A sites on viral RNA, which vary from reduced stability to changes in reverse transcription and virion packaging (Finkel and Groner, 1983; Imam et al., 2018; Lu et al., 2018). However, few studies have described the changes in the host m^{6}A landscape upon infection. Crucially, evidence describing how such alterations in cellular m^{6}A distribution are achieved is lacking and needs further investigation. During KSHV infection, several studies have alluded to important regulatory roles for m^{6}A during reactivation. However, the global effects suggested by these groups are not entirely consistent (Ye, 2017; Tan et al., 2018; Hesser et al., 2018). One of these studies identified changes in the cellular m^{6}A landscape during reactivation, finding that differentially modified RNAs functionally cluster into various signalling pathways (Tan et al., 2018).

In this results chapter, m^{6}A-sequencing was used to identify changes in m^{6}A topology between KSHV latent and lytic replication programmes and differentially modified mRNAs were clustered by function. In addition, through inhibition of the m^{6}A addition, the modification was shown to be functionally important for KSHV reactivation. Finally, the expression of the m^{6}A machinery was monitored at both RNA and protein levels to account for changes in m^{6}A content and distribution.

3.2 m^{6}A distribution is altered in response to KSHV reactivation

In order to examine whether the m^{6}A landscape is altered by KSHV reactivation, m^{6}A-sequencing was performed by Dr Belinda Baquero-Perez (past Whitehouse lab member) to identify changes in m^{6}A distribution between TREX cells undergoing latent and lytic replication programmes. RNA was collected from latently-infected cells and those reactivated for 8 and 20 hours. The RNA was fragmented into 100-200 nt fractions and subjected to immunoprecipitation with an m^{6}A-specific antibody. Immunoprecipitated fragments were converted to cDNA and sent for next generation sequencing. Highly confident m^{6}A peaks were called by Dr Agne Antanaviciute using the newly developed bioinformatic software m^{6}A Viewer (Antanaviciute et al., 2017). Thus, for each mRNA, an m^{6}A profile could be generated showing number of reads for both input and immunoprecipitated samples. An example is shown in Figure 3.1 where the cellular transcript *ZNF12* undergoes a loss in methylation at a designated 5' m^{6}A peak during lytic replication.

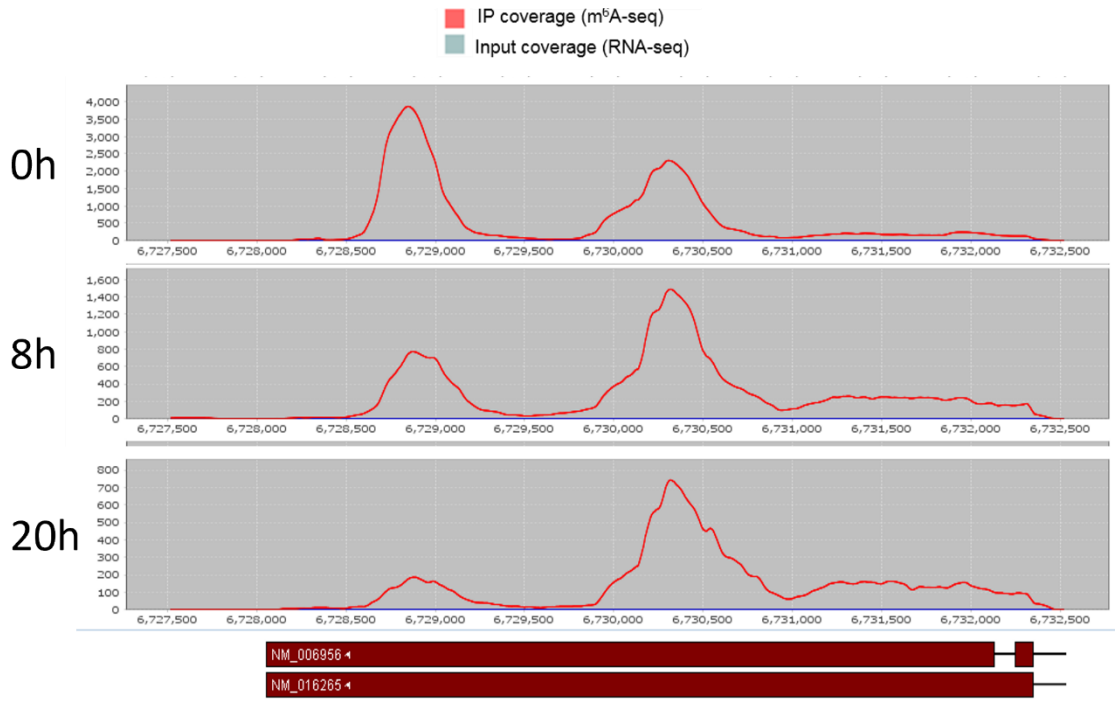

Figure 3.1. Differential modification of *ZNF12* mRNA. m^{6}A-seq data for the cellular transcript *ZNF12* which undergoes a progressive loss in methylation of a 5' peak at 8 and 20 hours post-induction of lytic reactivation (n=2). For each graph, the X-axis represents genomic position while the Y-axis describes the number of reads from deep sequencing for both input (blue) and IP samples (red).

Using the m^{6}A viewer system, the KSHV transcriptome was found to be extensively methylated with 85 m^{6}A peaks found in 42 of KSHV's 85 viral ORFs (Figure 3.2) (Baquero-Perez et al., 2019).

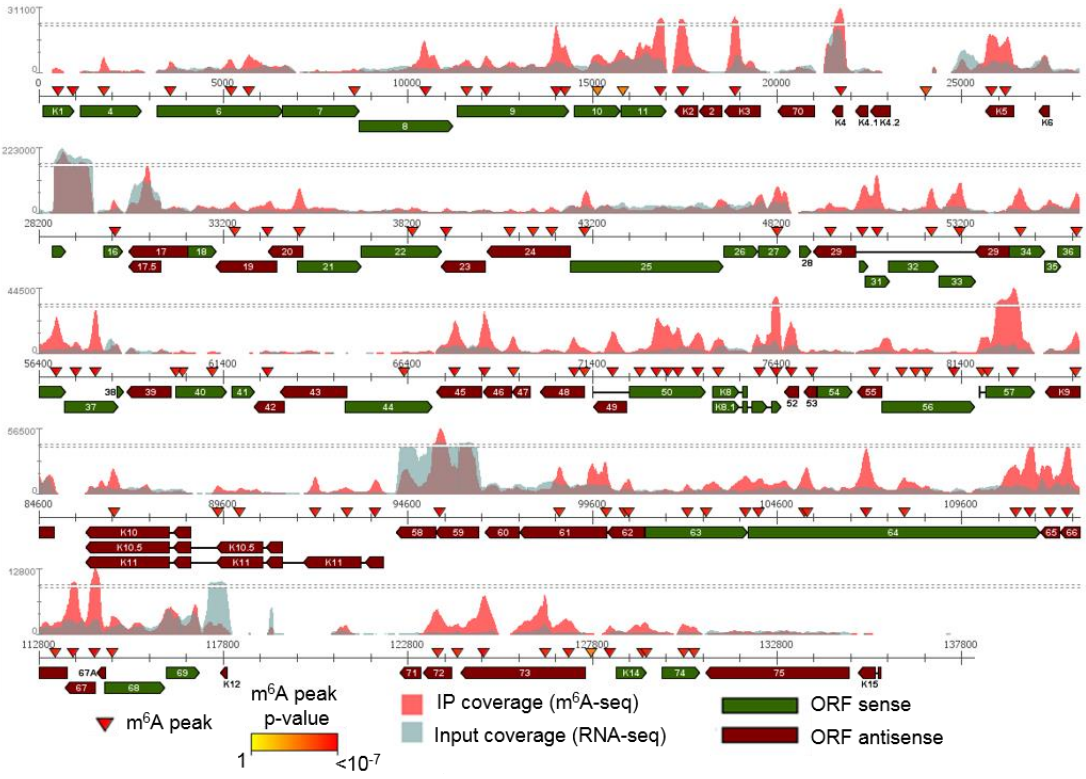

Figure 3.2. m^{6}A peaks in the KSHV transcriptome. Figure shows m^{6}A-seq data for the entire KSHV transcriptome at 20 hours post induction of lytic reactivation in TREX cells (n=2). m^{6}A peaks were called using m^{6}A Viewer software. Significantly enriched m^{6}A peaks were defined by a minimum fold change of ≥1.5 (m^{6}A-IP over input) and a false discovery rate (FDR) less than 5% was required across both biological replicates. Peaks were considered overlapping if less than 100nt were present between two enriched positions. Data collected by Dr Belinda Baquero and analysed by Agne Antanaviciute (published in eLife 2019;8:e47261)

Importantly, cellular m^{6}A peaks were also called consistently with 18,946 sites shared among latent cells between two biological replicates. Furthermore, at 8 hours post induction, reactivated cells shared 18,935 m^{6}A peaks, while at 20 hours, a reduction to 13,926 m^{6}A peaks was identified. m^{6}A sites were mostly maintained between latent cells and those induced for 8 hours with approximately 36% of total sites unique to either sample (Figure 3.3a). However, at 20 hours post induction, approximately 64% of m^{6}A peaks were unique to either latent or lytic cells. Furthermore, the majority of m^{6}A sites unique to cells undergoing lytic replication appeared within mRNAs whose expression increased during reactivation (Figure 3.3b). In contrast, m^{6}A peaks unique to latent infection transcriptomes tended towards downregulation during lytic replication. Taken together, these results

indicate that m^{6}A sites in latently infected cells generally reduce the abundance of modified mRNAs. Whereas, in lytic replication, m^{6}A tends towards an increase in the expression of methylated transcripts. Thus, these results suggest that the m^{6}A landscape undergoes radical remodelling during KSHV reactivation.

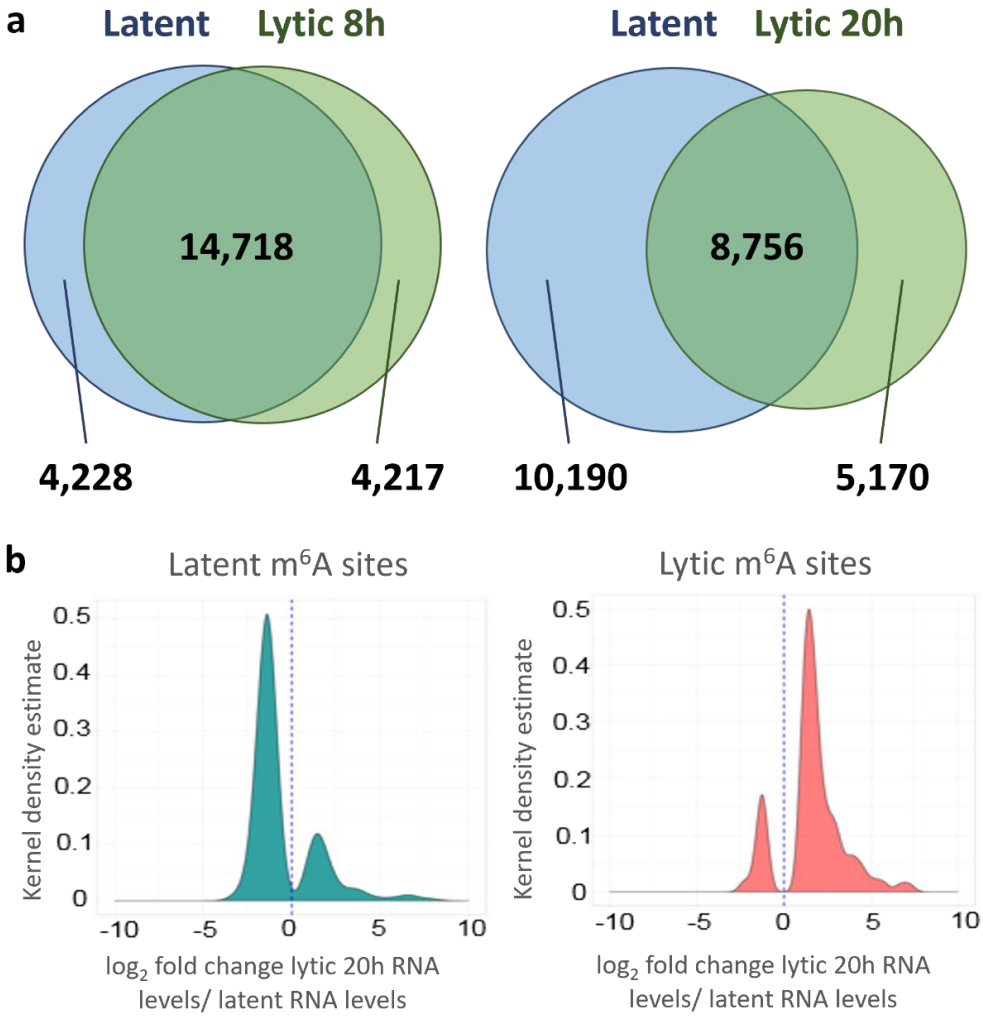

Figure 3.3. The cellular m^{6}A landscape is altered during KSHV reactivation. a) Venn diagram showing the number of cellular m^{6}A peaks consistently called by the m^{6}A Viewer software in two biological replicates throughout KSHV latent and lytic (8 and 20 hours) replication programmes. Significantly enriched m^{6}A peaks were defined by a minimum fold change of ≥1.5 (m^{6}A-IP over input) and FDR<5%. Once again, peaks were considered overlapping if less than 100nt were present between two enriched positions. (b) Kernel density estimate (KDE) for the RNAs encoding 10,190 m^{6}A peaks unique to latent cells (left graph) and the RNAs encoding the 5,170 m^{6}A peaks unique to cells reactivated for 20 hours (right graph).

3.3 m^{6}A immunoprecipitation confirms the modification of cellular mRNAs

To validate the m^{6}A-seq data indicating the modification of cellular transcripts, m^{6}A immunoprecipitation followed by RT-qPCR (m^{6}A-qPCR) was carried out to definitively prove the methylation of a selection of mRNAs at the specified sites. Given the low throughput

nature of this technique, only the mRNAs *GPRC5A, FOSB, ZFP36L1* and *JUN* were examined for m^{6}A. All of these mRNAs showed increased m^{6}A-content in lytic cells in the m^{6}A data set. 2 primer sets targeting putative methylated and non-methylated sites within the 4 mRNAs were generated. Furthermore, positive and negative controls were designed targeting the known methylated transcript *SLC39A14* and the mRNA *GAPDH* which contains no sites of m^{6}A. For each m^{6}A site tested, a negative control region was amplified within the same transcript, which was not enriched in the m^{6}A-seq data, to compare against the methylated region. This strategy successfully confirmed both the m^{6}A site within *SLC39A14* and the lack of methylation within *GAPDH* (Figure 3.4a). Excitingly, *GPRC5A, FOSB, ZFP36L1* and *JUN* mRNAs all showed enrichment for the methylated region over the non-methylated region in both latent and lytic TREX cells confirming m^{6}A-modification of these mRNAs at the expected site and validating the m^{6}A-seq data (Figure 3.4c). While no significant changes were detected in the m^{6}A modification of these transcripts between latent and lytic states, m^{6}A-qPCR neutralises the effect of increased expression of mRNAs. Thus, if the transcripts are also upregulated in the lytic phase this could mask an increase in m^{6}A content, but not stoichiometry. To account for this bias, the m^{6}A immunoprecipitated samples were reanalysed for increased expression of the mRNAs tested by m^{6}A-qPCR. Importantly, *GPRC5A, FOSB, ZFP36L1* and *JUN* were more abundant in lytic replication while the methylated transcript *SLC39A14* showed little change (Figure 3.4b). In conclusion, the m^{6}A levels of *GPRC5A, FOSB, ZFP36L1* and *JUN* are correlated with the mRNA levels of those transcripts. However, m^{6}A may play an important regulatory role in the increased abundance of these mRNAs in lytic replication.

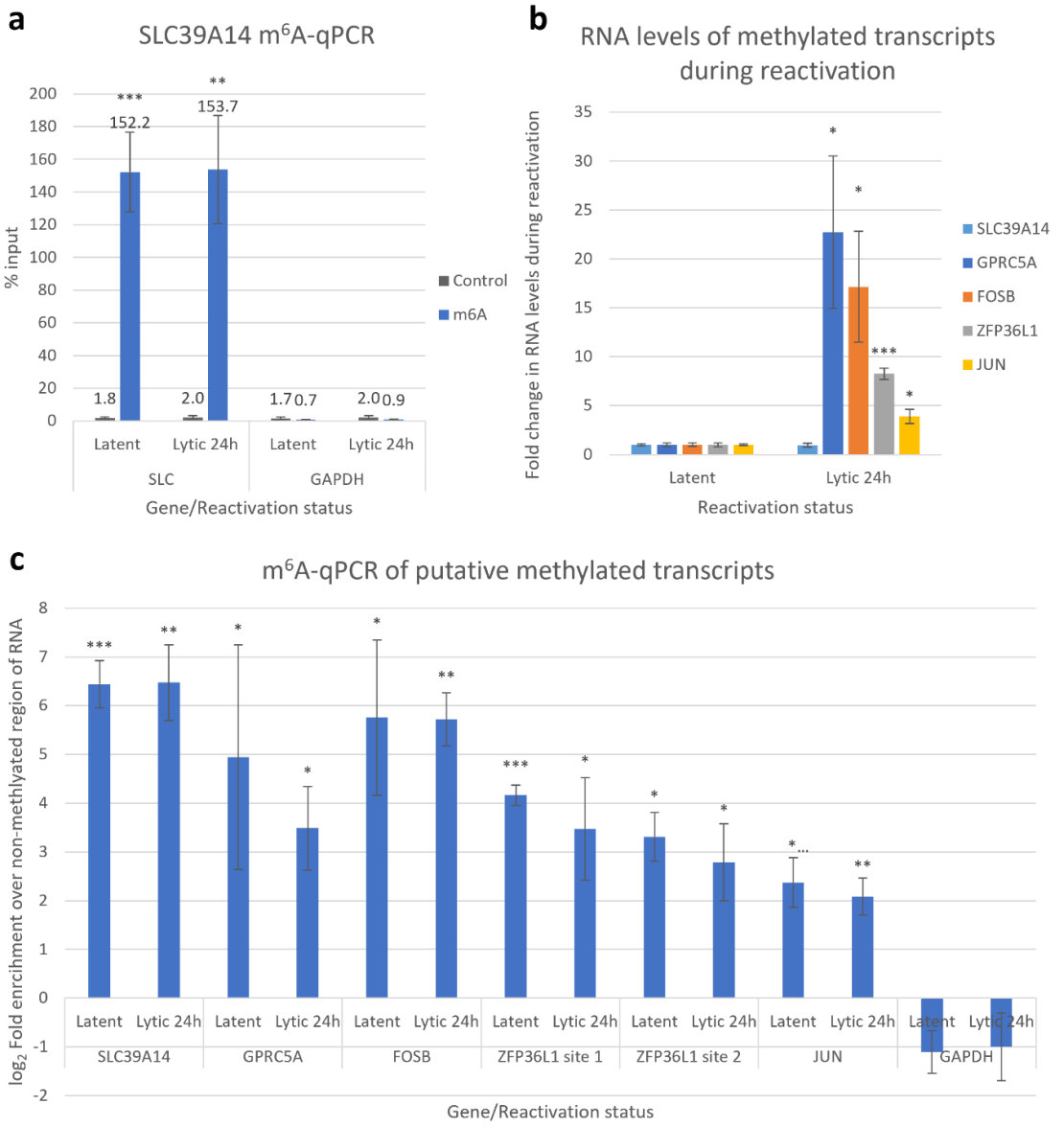

Figure 3.4. m^{6}A immunoprecipitations confirm the modification of *GPRC5A, FOSB, ZFP36L1* and *JUN* mRNAs. Total RNA was isolated from latent and lytic TREX cells, chemically fragmented into 100-200nts and precipitated with an m^{6}A-specific antibody. After precipitation, samples were analysed by RT-qPCR for enrichment at the putative m^{6}A site relative to a nonmethylated control region (all data presented as mean ±SD, n=3). a) Analysis of unmodified and m^{6}A-modified regions within positive *SLC39A14* and negative *GAPDH* control RNAs for m^{6}A enrichment. b) Fold change in RNA levels of m^{6}A-immunoprecipitated samples during reactivation normalised to *GAPDH*. c) m^{6}A-qPCR data showing the $\log_2$ fold enrichment of m^{6}A-modifed fragments over a non-methylated region within the same transcript. 2 regions were analysed within *ZFP36L1* as this mRNA contains a wide flat m^{6}A peak spanning several hundred bp.

3.4 m^{6}A redistribution does not favour a topological region of mRNA

In order to understand how the redistribution of m^{6}A under KSHV reactivation is coordinated, the distribution of m^{6}A peaks within cellular mRNAs in the m^{6}A data set was

compared between cells undergoing both latent and lytic replication. m^{6}A peaks were classified by five topological regions defined by Agne Antanaviciute. As with previous studies, m^{6}A was enriched in the coding sequence (CDS) and 3' UTR throughout the latent and lytic cell populations. Surprisingly, a proportion of m^{6}A peaks were identified in intergenic regions which may be represent m^{6}A sites in noncoding RNAs (Xiao et al., 2019). Interestingly, only subtle changes were detected in the proportions of m^{6}A within the different mRNA locations suggesting that large-scale relocalisation across different topological boundaries does not occur (Figure 3.5a). Finally, the preferred consensus sequence in each region of mRNA was analysed using MEME software for evidence that selective deposition of m^{6}A at certain sites takes place (Figure 3.5b). The expected DRACH consensus sequence was obtained with most sites deposited at a GGAC motif. However, this consensus sequence was maintained across all topological regions of mRNA indicating that selective deposition of m^{6}A in certain locations along a transcript is not mediated by alteration in consensus motif. As a result, these data do not explain how m^{6}A remodelling can be achieved mechanistically.

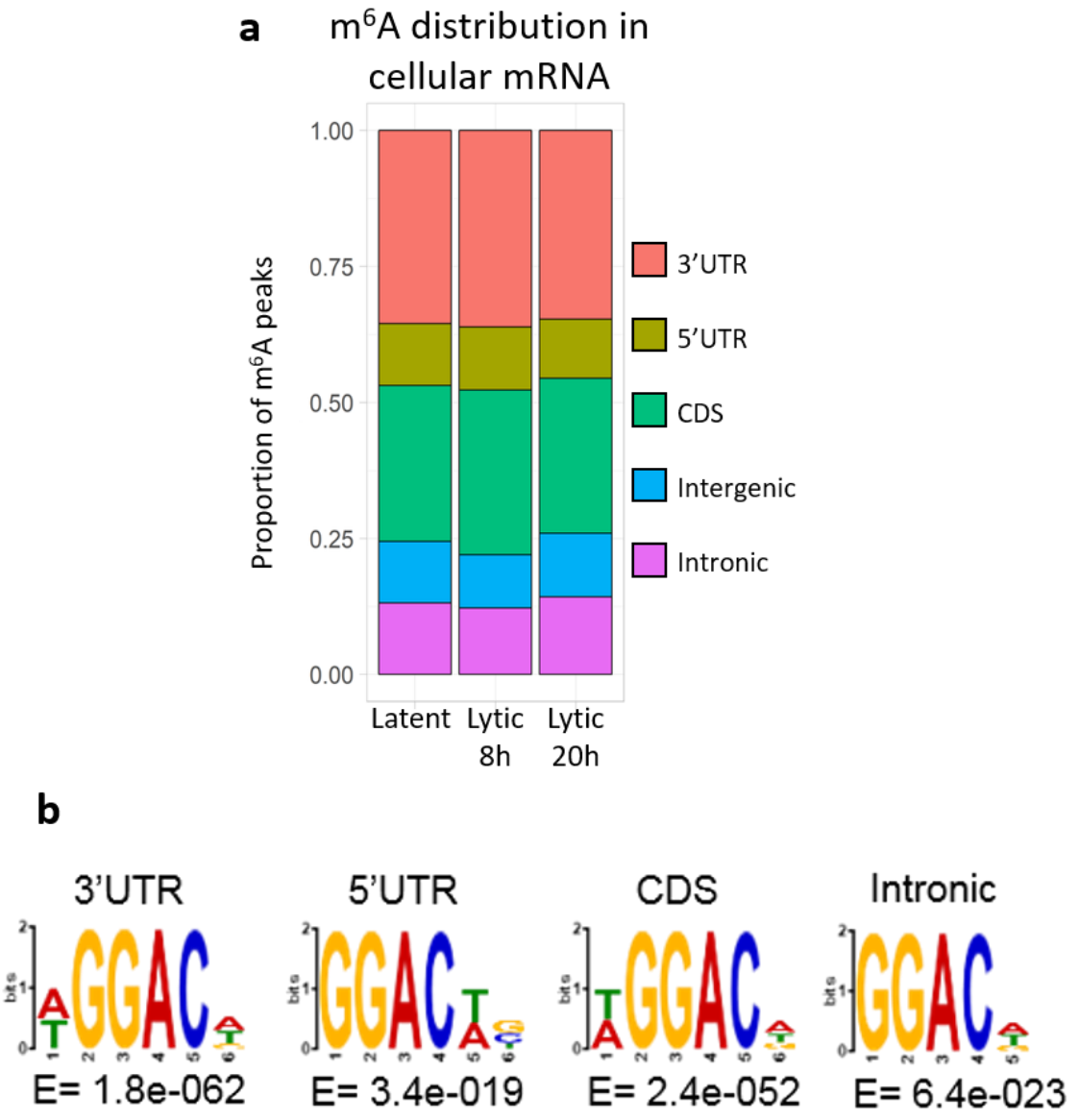

Figure 3.5. m^{6}A distribution is unchanged across topological regions of mRNA. a) Stacked column chart showing the proportions of m^{6}A peaks in five topological regions of cellular RNA during KSHV infection in TREX cells. Topological regions were defined by bioinformatics expert Agne Antanaviciute. b) Meme software analysis showing the most significantly enriched DRACH consensus motif among cellular m^{6}A peaks present in four topological regions of RNA (UTR, untranslated region. CDS, coding region).

3.5 The m^{6}A machinery is altered during KSHV reactivation

Since m^{6}A redistribution during KSHV reactivation is not caused by the preferential methylation of a particular topological region of mRNA, the m^{6}A machinery was analysed for changes that may affects m^{6}A localisation. Previous work carried out by Dr Belinda Baquero (Whitehouse lab alumni) showed the m^{6}A machinery components METTL3, METTL14 and DF1-3 do not show any change in cellular localisation during KSHV reactivation (unpublished data). As a result, it is unlikely that differential methylation occurs due to

relocalisation of the m^{6}A writer complex or demethylases to different subcellular compartments.

Subunits of the m^{6}A writer complex have been proposed to regulate the selectivity of m^{6}A deposition at specific sites. Therefore, a change in the expression of any of these components or demethylases could lead to large scale redistribution of the modification. Thus, the expression levels of m^{6}A machinery components were examined for changes during KSHV reactivation. RNA levels were measured by RT-qPCR and changes corroborated at the protein level by immunoblotting where antibodies were available. With the exception of *METTL3*, all other components of the m^{6}A machinery showed only subtle changes in expression consistent with no change or a slight reduction, indicating the start of KSHV initated host-cell shutoff (Figure 3.6a). However, *METTL3* had a marked reduction in both RNA and protein levels suggesting this gene may be targeted for downregulation by KSHV during the lytic cycle (Figure 3.6b). This observation may explain the reduction in m^{6}A peaks seen at 20 hours post reactivation in the m^{6}A-seq data.

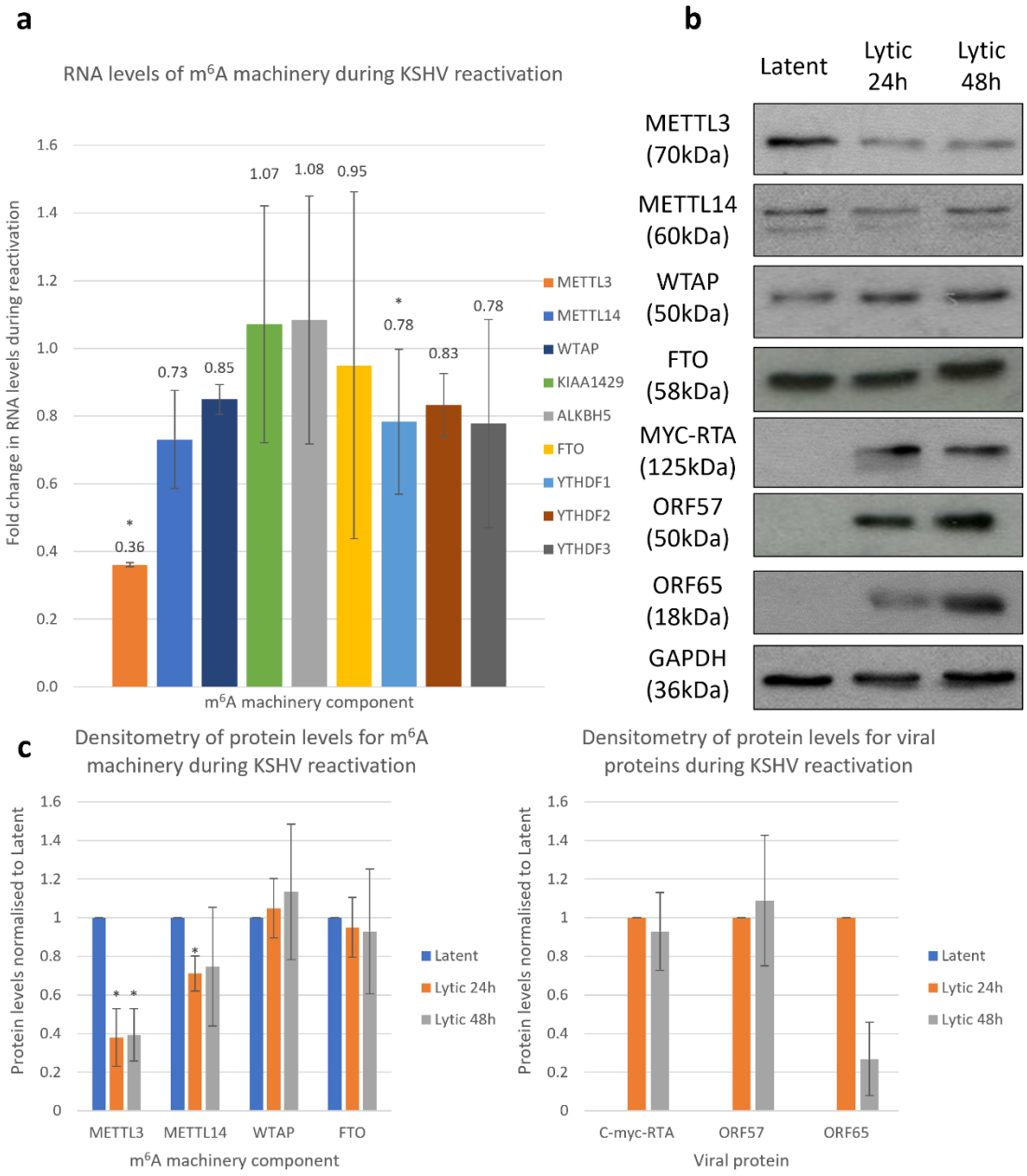

Figure 3.6. Changes in the expression of the m^{6}A machinery during KSHV lytic reactivation. a) RT-qPCR data showing the fold change in RNA levels of members of the m^{6}A machinery between latent and lytic TREX cells (lytic cells induced for 24 hours, data presented as mean ± SD, n=3). b) Western blots showing protein levels for members of the m^{6}A machinery during latent and lytic replication programmes (blots representative of 3 biological repeats). c) Densitometry of western blot in b).

In order to understand whether *METTL3* is targeted for downregulation during KSHV reactivation, two KSHV lytic genes, whose ability to reduce gene expression is well characterised, were transfected into uninfected 293T cells on GFP-tagged constructs (Figure 3.7a). Upon expression of the viral proteins RTA and ORF57, *METTL3* RNA levels were monitored to determine whether these two lytic proteins are responsible for downregulation (Figure 3.7b). Interestingly, no significant decline in *METTL3* upon the

ectopic expression of GFP-ORF50 was identified. However, a small but significant decline in *METTL3* levels upon expression of GFP-ORF57 was observed (Figure 3.7c). To confirm this finding, increasing doses of *GFP-ORF57* were transfected into 293T cells and *METTL3* mRNA levels monitored by RT-qPCR. While a significant reduction in *METTL3* mRNA was observed at 1,2 and 4 µg concentrations of *GFP-ORF57* relative to a GFP control, these transcript levels were not significantly different from untransfected cells (Figure 3.7d). Thus, it seems likely that ORF57 plays only a minor role, if any, in the reduction of *METTL3* mRNA seen during KSHV lytic reactivation. Instead, it is likely that other viral or cellular factors contribute to the downregulation of this methyltransferase.

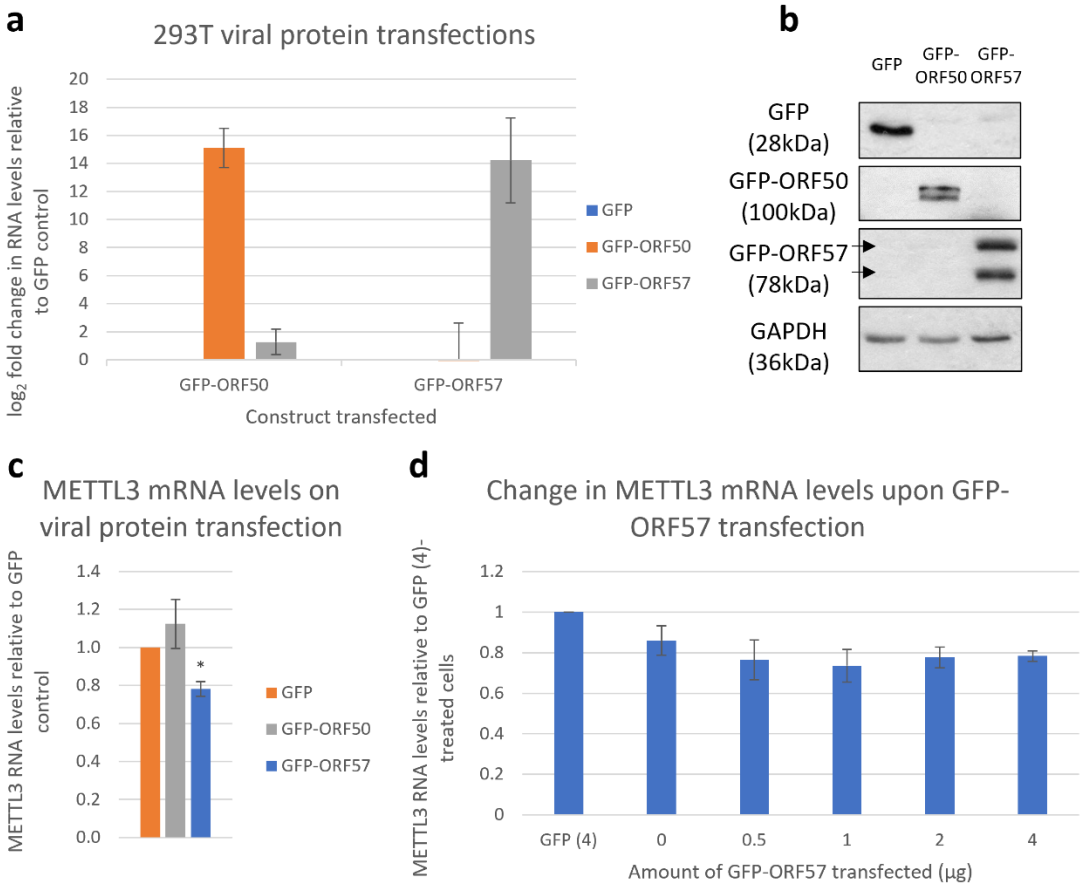

Figure 3.7. ORF50 and ORF57 are not responsible for *METTL3* downregulation. (a,b) *GFP-ORF50* and *GFP-ORF57* constructs were transfected into 293T cells and successful expression of fusion proteins confirmed by RT-qPCR and western blotting (data presented as mean ±SD, n=3; blots representative of 3 biological repeats). c) RT-qPCR data showing the mRNA levels of *METTL3* on expression of GFP tagged constructs in 293T cells (data presented as mean ±SD, n=3). d) RT-qPCR data displaying *METTL3* mRNA levels on transfection of increasing amounts of *GFP-ORF57* DNA (data presented as mean ±SD, n=3).

3.6 m^{6}A exerts a net proviral effect on KSHV lytic replication

Previous studies have found conflicting evidence on the overall effect of m^{6}A during KSHV reactivation, which may or may not be due to cell type specific effects of m^{6}A (Baquero-Perez et al., 2019). To investigate whether m^{6}A exerts an overall proviral or antiviral effect on the KSHV life cycle, the drug 3-deazaadenosine (DAA) was applied to TREX cells undergoing latent or lytic replication programmes. DAA inhibits the donation of a methyl group by the cofactor SAM during m^{6}A formation and thus blocks the modification of adenosines. However, SAM functions as a cofactor for other methyltransferase reactions within the cell which may result in some off-target effects. Firstly, the optimum concentration of 25μM DAA, determined as the highest usable concentration before a drop of more than 20% in cell viability, was obtained by MTS assay in TREX cells (Figure 3.8a). Next, the effect on KSHV reactivation was assayed by western blotting for viral proteins ORF57 and MYC-RTA (Figure 3.8b). Interestingly, DAA treatment resulted in a decrease in viral protein production in cells reactivated for 24 hours without any evidence of cytotoxicity. Overall, this suggests that loss of m^{6}A negatively affects reactivation and therefore m^{6}A exerts a net proviral effect on KSHV lytic replication programme in B cells.

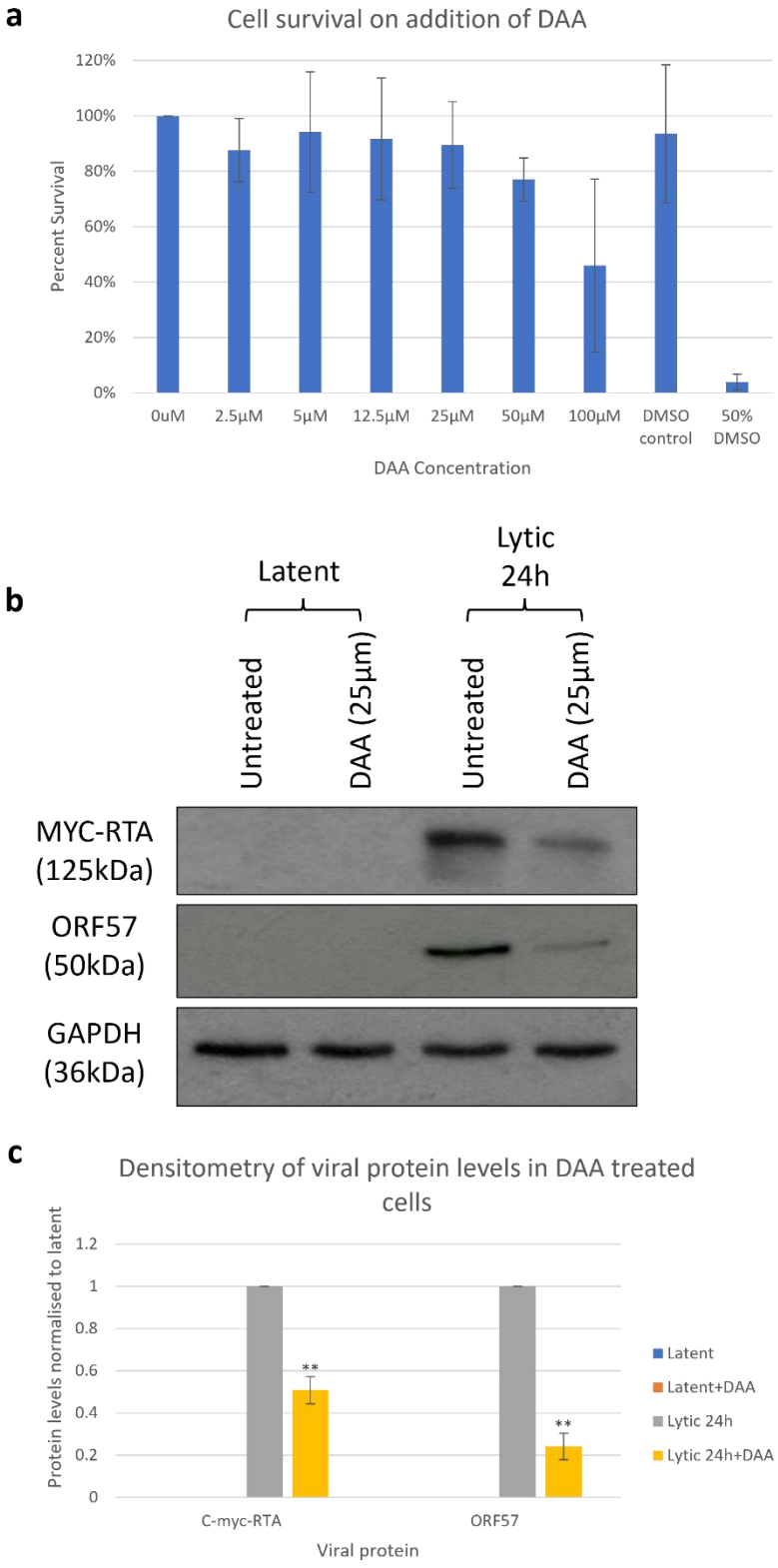

Figure 3.8. The m^{6}A inhibitor DAA reduces KSHV lytic protein production. a) MTS assay to determine optimal concentration of DAA to use in TREX cells (Data presented as mean ±SD, n=2). DMSO control has matched DMSO concentration to highest DAA concentration (100µM). b) Western blot showing RTA and ORF57 protein levels on addition of DAA in latent and lytic TREX cells (blots representative of 3 biological repeats). c) Densitometry of western blot in b). DAA was added to the cells 24 hours before induction of lytic replication.

3.7 Cellular mRNAs with altered m^{6}A levels between latent and lytic KSHV replication participate in common functional pathways

Although several groups have investigated the role of m^{6}A in viral transcripts, the understanding of how the cellular m^{6}A landscape is shaped under viral replication is relatively unknown (Manners et al., 2019; Gokhale et al., 2020). Among the cellular RNAs identified by m^{6}A-seq, whose modification is favoured in either latency or during lytic replication, 52 of those with the largest change in m^{6}A levels were selected for further investigation by Agne Antanaviciute who carried out the bioinformatics. To identify whether any specific cellular pathways are modulated in an m^{6}A-dependent manner, these 52 transcripts were subjected to functional clustering using String bioinformatic analysis. Many of the proteins encoded by these differentially modified mRNAs interacted directly (Figure 3.9a). Furthermore, gene ontology (GO) analysis identified the most enriched pathway as the negative regulation of translation followed by several additional mRNA regulatory pathways (Figure 3.9b). Other mRNAs of interest include the transcripts *JUN* and *FOSB* which encode the interacting partners of the AP-1 transcription factor complex. Finally, the genes *PCNX1*, *STC1*, *ZC3H12A*, *HEY1* and *PEAR1* are all members of the Notch signalling pathway. As both Notch and AP-1 signalling are critical for KSHV reactivation, the altered m^{6}A status of transcripts encoding key players in these pathways may regulate KSHV lytic replication. Moreover, the finding that regulation of mRNA biology is a common function among the differentially modified mRNAs indicates the process may be central to KSHV reactivation.

a

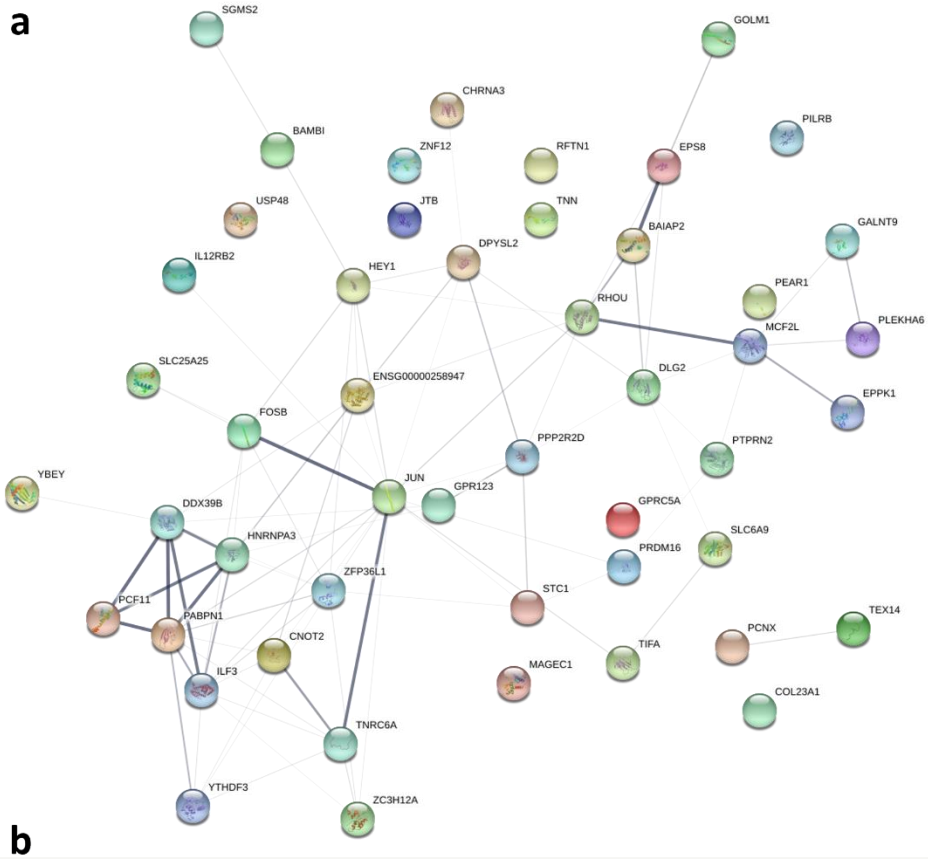

b

Biological Process (GO)

GO-term	*description*	*count in gene set*	*false discovery rate*
GO:0017148	negative regulation of translation	6 of 117	0.0010
GO:0006417	regulation of translation	7 of 327	0.0104
GO:0015931	nucleobase-containing compound transport	6 of 230	0.0111
GO:0061157	mRNA destabilization	3 of 23	0.0125
GO:0051591	response to cAMP	4 of 98	0.0249
GO:0050793	regulation of developmental process	16 of 2416	0.0249
GO:0050658	RNA transport	5 of 189	0.0249
GO:0045657	positive regulation of monocyte differentiation	2 of 10	0.0426
GO:2000113	negative regulation of cellular macromolecule biosynthetic ...	11 of 1348	0.0431
GO:0061158	3'-UTR-mediated mRNA destabilization	2 of 13	0.0446
GO:0051764	actin crosslink formation	2 of 12	0.0446
GO:0051028	mRNA transport	4 of 148	0.0446
GO:0045600	positive regulation of fat cell differentiation	3 of 59	0.0446
GO:0010458	exit from mitosis	2 of 12	0.0446
GO:0008360	regulation of cell shape	4 of 143	0.0446
GO:1903313	positive regulation of mRNA metabolic process	3 of 66	0.0448
GO:0007171	activation of transmembrane receptor protein tyrosine kina...	2 of 14	0.0448
GO:0045595	regulation of cell differentiation	12 of 1695	0.0472
GO:0022604	regulation of cell morphogenesis	6 of 442	0.0478
GO:0051239	regulation of multicellular organismal process	16 of 2788	0.0496
GO:0000278	mitotic cell cycle	7 of 628	0.0496

(less ...)

Cellular Component (GO)

GO-term	*description*	*count in gene set*	*false discovery rate*
GO:0000932	P-body	4 of 81	0.0146
GO:0035770	ribonucleoprotein granule	5 of 204	0.0208
GO:1990904	ribonucleoprotein complex	8 of 770	0.0417
GO:0044459	plasma membrane part	16 of 2651	0.0417

Figure 3.9. Functional clustering of transcripts differentially m^{6}A modified between KSHVs lytic and latent replication programmes. a) String protein interaction maps of differentially m^{6}A-modified transcripts. Weight of line indicates confidence of interaction. b) Gene ontology analysis showing the functional clustering of differentially m^{6}A-modified mRNAs according to biological process and cellular component. Transcripts are ranked with lowest FDR at the top.

3.8 Discussion

In this chapter, m^{6}A-sequencing was carried out to identify changes in m^{6}A topology during KSHV reactivation. A special focus was given to changes in the cellular m^{6}A landscape which have been studied in only a few viral contexts to date. Interestingly, fewer m^{6}A peaks were found in cells induced into the lytic cycle than those in latency. This is consistent with results from a previous study which compared m^{6}A-sequencing data between latent cells and those induced for 48 hours (Tan et al., 2018). It is likely this effect can partially be attributed to the activity of KSHV SOX protein encoded by ORF37. SOX mediates host cell shutoff by nicking cellular mRNAs and cooperating with the host exoribonuclease XRN1 in the exonucleolytic degradation of host transcripts (Lee et al., 2017). As a result, SOX leads to global degradation of cellular mRNAs allowing prioritisation of viral transcripts for translation. Therefore, the initiation of host cell shutoff at 20 hours post induction may explain, at least in part, why fewer m^{6}A sites were identified at this lytic timepoint.

To validate the m^{6}A-seq data, the precise location of m^{6}A sites within four cellular transcripts were validated by m^{6}A-qPCR. While m^{6}A-qPCR is only semi-quantitative and cannot precisely determine m^{6}A stoichiometry, it appears the m^{6}A content of GPRC5A, FOSB, ZFP36L1 and JUN is correlated with their abundance. Therefore, during reactivation, their m^{6}A content rises in line with their mRNA levels. From this data it is difficult to ascertain whether the modification is important for this increase or merely a modification which increases as mRNA levels rises. As a result, further research is required to clarify this observation.

Although many alterations in m^{6}A topology have been noted in virus-infected cells, it is not entirely clear how such remodelling is achieved. One study has suggested that reactivation leads to loss of m^{6}A at 5’ UTRs and a corresponding gain at 3’ UTRs (Tan et al., 2018). Conversely, in other cell lines, the opposite effect was observed. However, in this study, only very subtle changes were observed in the proportions of m^{6}A along each topological region of mRNA. Furthermore, in both studies, no change was found in m^{6}A consensus sequence usage between latently and lytically infected cells. Thus, it seems unlikely that changes in m^{6}A deposition are mediated by consensus sequence or preferential deposition at a particular topological position along an mRNA.

Conceivably, differential selectivity of m^{6}A deposition could be mediated by the composition of m^{6}A writer complex as any changes in the expression of certain subunits could lead to preferential binding of certain DRACH sites. Surprisingly, only small changes were observed within most members of the m^{6}A machinery with the striking exception of METTL3. METTL3 showed a marked downregulation above the level that could be attributed to host cell shutoff after 20 hours of lytic replication. It is unclear whether loss of METTL3 may cause changes in m^{6}A location; however, it almost certainly leads to loss of m^{6}A at certain sites. Thus, together with SOX, downregulation of METTL3 may also explain why fewer m^{6}A sites can be found in cellular mRNA during reactivation.

Previous studies to examine the global effect of m^{6}A on viral infection, especially those on KSHV reactivation, have not been entirely consistent (Tirumuru et al., 2016; Kennedy et al., 2016; Lichinchi, Gao, et al., 2016; Ye, 2017; Tan et al., 2018; Hesser et al., 2018). In this study, addition of the drug DAA to cells undergoing reactivation inhibited viral protein production suggesting that overall m^{6}A enhances lytic replication. Nevertheless, given its ubiquitous presence of viral and cellular transcripts, it is highly unlikely that m^{6}A exhibits solely proviral or antiviral effects towards viral replication. Instead, it is likely that in certain contexts, the modification acts in favour of the virus; while in others, it restricts infection. This is especially true for a herpesvirus such as KSHV which expresses over 80 mRNAs and causes mass remodelling of the host cell to undergo a highly complex life cycle. Thus, there are many opportunities for m^{6}A to modulate KSHV reactivation and the study of specific sites of methylation is vitally important in understanding KSHV biology and the wider field of viral epitranscriptomics.

Functional clustering of differentially m^{6}A-modified mRNAs during reactivation showed that several virus-associated pathways may be regulated by this epitranscriptomic modification. A previous study has suggested that differentially modified mRNAs belong to oncogenic signalling pathways including ERK/MAPK and PI3K/AKT signalling (Tan et al., 2018). Although in this study, such pathways were not identified by GO analysis, both members of the AP-1 signalling complex as well as various components of Notch signalling were found amongst differentially m^{6}A-modified mRNAs. AP-1 is indispensable for transcriptional activation of ORF50 and other IE genes in the early stages of reactivation (Wang et al., 2004). Similarly, the interaction of RTA with Notch component RBP-Jκ is also essential in the activation of IE gene promoters (DeCotiis and Lukac, 2017). Finally, the dysregulation of both AP-1 and

Notch signalling pathways are a common feature of cancer and both are well described factors in the tumourigenesis of KSHV-associated malignancies. Therefore, the results of this study and those conducted previously agree that changes in m^6A distribution on cellular mRNAs may be essential for KSHV reactivation and disease pathogenesis.

Aside from oncogenic signalling cascades, this study also identified mRNA biology pathways as most enriched among transcripts with altered m^6A profiles between KSHV latent and lytic replication programmes. During lytic replication, KSHV manipulates several host cell mRNA biology pathways to permit the efficient splicing, export and translation of viral transcripts (Boyne et al., 2010). Thus, m^6A could regulate the expression of many genes involved in the determination of viral mRNA fate and have major implications for KSHV reactivation. However, to identify whether m^6A exerts regulatory control over mRNA biology and signalling pathways during KSHV reactivation, the investigation of methylated mRNAs on an individual level is required.

Chapter 4

~

m^6A affects the abundance of differentially modified mRNAs during reactivation

4 m^{6}A affects the abundance of differentially modified mRNAs during reactivation

4.1 Introduction

m^{6}A is proposed to regulate all stages of mRNA biology leading to many downstream consequences for gene expression. This study and others have found that viral infection leads to large scale remodelling of the host m^{6}A landscape and thus likely serves as a critical factor for modulating both proviral and antiviral gene expression (Lichinchi, Gao, et al., 2016; Lichinchi, Zhao, et al., 2016; Tan et al., 2018). Furthermore, in agreement with previous studies, global depletion of m^{6}A leads to profound changes in KSHV replication. However, previous experiments have been unable to disentangle the relative contributions of cellular and viral m^{6}A to the viral life cycle. Therefore, despite the clear indications that cellular m^{6}A modulates viral life cycles, the extent of its influence is not well understood. As a result, the investigation of m^{6}A on individual cellular transcripts is required to support the hypothesis that cellular m^{6}A sites affect virus replication.

Aside from global changes in cellular m^{6}A during viral infection, there are several further clues that the host m^{6}A methylome regulates virus replication. The antiviral transcript *IFNB,* encoding a cytokine which drives the antiviral response, contains an m^{6}A site which regulates its stability (Rubio et al., 2018; Winkler et al., 2019). Thus, alterations in the m^{6}A content of this mRNA, which in turn affect its abundance, could serve as a broad mechanism for regulating diverse viral life cycles. Furthermore, a recent study has identified two transcripts with changes in their m^{6}A status between uninfected and flavivirus-infected cells. *RIOK3* and *CIRBP* mRNAs showed m^{6}A-dependent changes in translation and splicing that affected HCV, ZIKV and DENV infection (Gokhale et al., 2020). The study is currently unique in that it provides clear evidence that changes in m^{6}A content at a particular cellular location greatly influences virus replication.

In this chapter, differentially methylated cellular mRNAs were investigated for changes in fate and function which could be attributed to m^{6}A. Thus, these mRNAs were monitored during KSHV reactivation for alterations in splicing, nuclear export, stability and translation. After selection of suitable candidates for further exploration, four transcripts were identified with changes in mRNA abundance. These m^{6}A modified transcripts all fall within

enriched functional pathways identified in the previous chapter including mRNA biology and oncogenic signalling.

4.2 Differentially modified mRNAs display altered abundance during KSHV reactivation

In the previous chapter, 52 transcripts which undergo changes in their m^6A content between KSHV's latent and lytic replication programmes were further analysed. To investigate whether these differentially modified transcripts exhibit changes in abundance during reactivation, primers were designed to amplify 14 of these mRNAs with the largest changes in m^6A content and those which function in molecular pathways associated with herpesvirus infection. RT-qPCR was used to compare the levels of these 14 transcripts in latent and lytic TREX cells (Figure 4.1a). Six of these transcripts showed no change in expression or only minor downregulation consistent with the action of SOX-mediated host-cell shutoff during KSHV lytic replication (Figure 4.1b). However, *CNOT2* showed greater downregulation which suggests this transcript may be targeted for degradation or repressed at the transcriptional level (Figure 4.1b). Of particular interest were seven mRNAs which were upregulated during lytic replication compared to latency as these contrast from the expected trend of downregulation for most cellular genes (Figure 4.1c). The greatest change in RNA level was observed for *GPRC5A* and *FOSB* which both increased approximately 19-fold during virus reactivation.

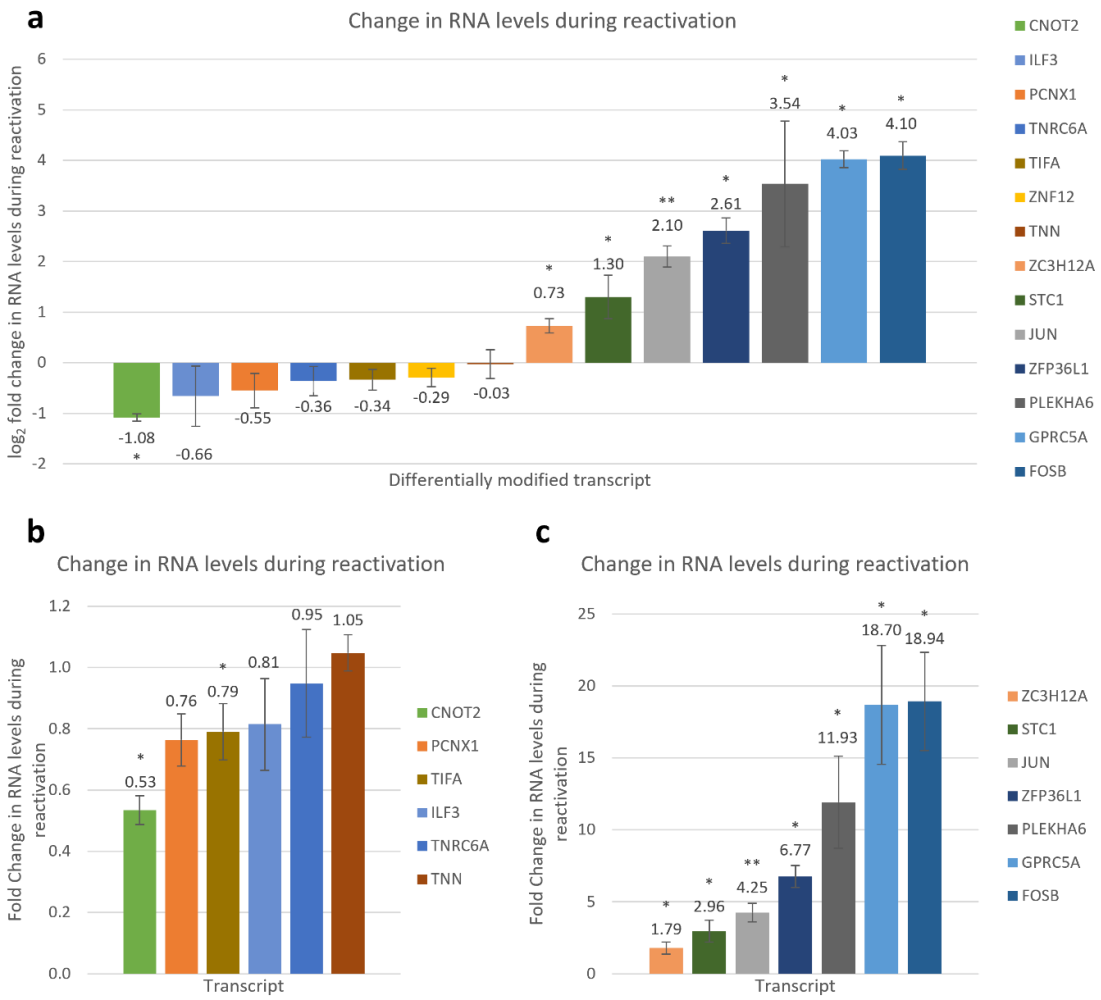

Figure 4.1. Changes in the RNA levels of differentially m^{6}A-modified transcripts during reactivation. All graphs show RT-qPCR data in which the expression of modified transcripts in TREX cells induced for 24 hours is compared to expression during latent infection (data presented as mean ±SD, n=4). a) $\log_2$ fold change in differentially methylated RNA levels during reactivation. b) Fold change among stable or downregulated transcripts. Order or transcripts different from a) as logs were applied to individual biological replicated before calculation of averages. c) Fold change among upregulated transcripts.

To identify whether the changes in abundance of methylated transcripts during reactivation has any significance regarding a functional change in gene expression, protein levels were analysed for six m^{6}A modified genes. Western blots were carried out on latent and lytically-infected TREX cell lysates using antibodies targeting several proteins encoded by the m^{6}A-modified cellular transcripts above (CNOT2, ILF3, FOSB, TIFA, GPRC5A and STC1). Importantly, this analysis also allows the identification of any discrepancies between mRNA and protein abundance which could indicate enhanced translation, perhaps in an m^{6}A-dependent manner. However, in correlation with mRNA levels, CNOT2 protein was less abundant in the lytic phase. Furthermore, ILF3 protein was mostly stable and TIFA protein levels were only slightly downregulated at the later time point of 48 hours post-reactivation

which is consistent with host-cell shutoff (Figure 4.2). In contrast, GPRC5A, FOSB and STC1 were upregulated at the protein level once again defying the trend of most cellular proteins and suggesting these genes may play a role in enhancing KSHV reactivation or serve as part of a host cell response (Figure 4.2). These results indicate that, at least in these contexts, changes in mRNA abundance bring about functional adjustments in gene expression through corresponding changes in protein levels. While these results do not preclude the fact that m^6A enhances translation, it seems that changes in mRNA abundance had the greatest impact on protein expression for the studied genes.

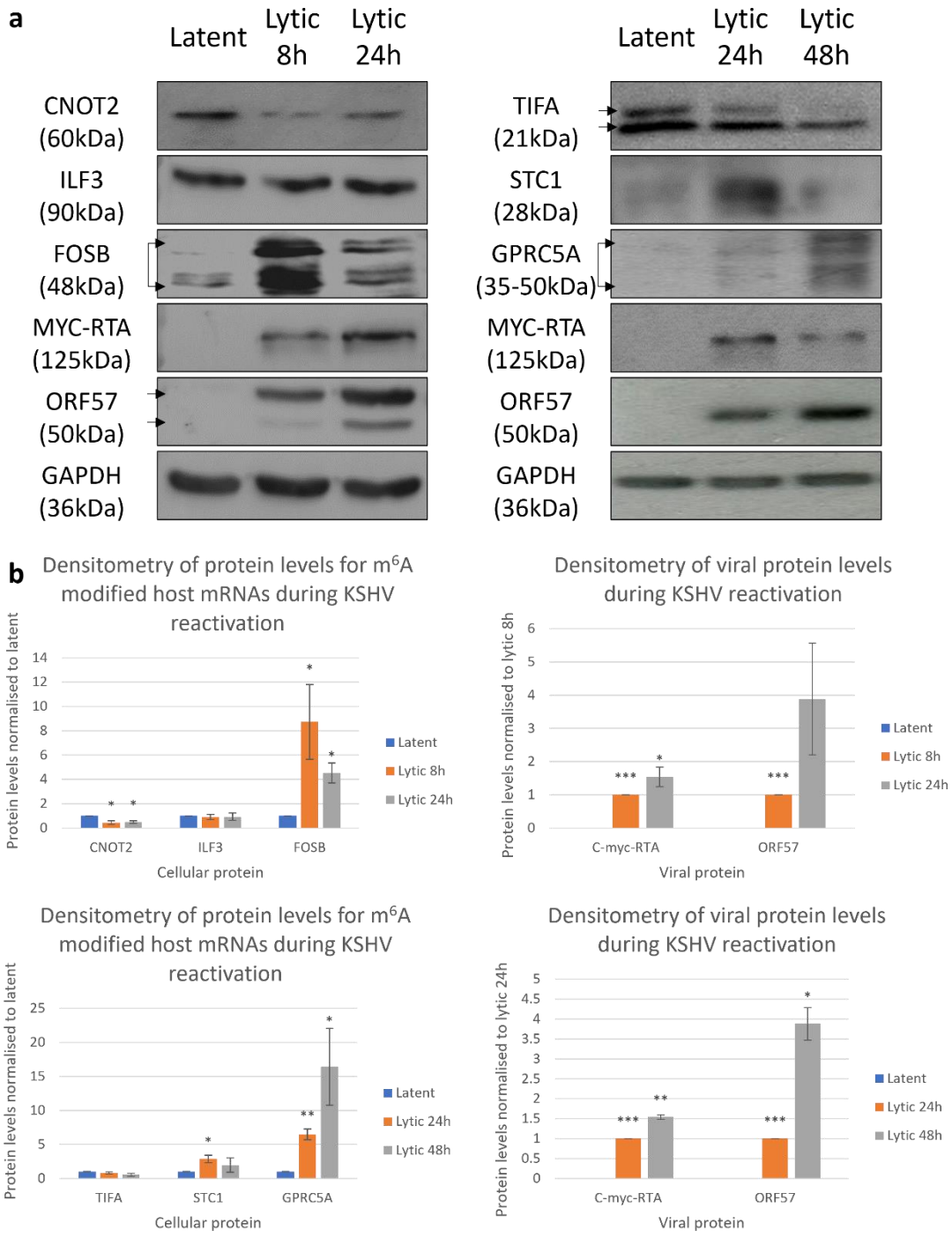

Figure 4.2. Changes in the protein levels of differentially m^{6}A-modified genes during reactivation. Western blots show protein levels for genes encoding differentially modified transcripts at different stages of the KSHV life cycle (blots are representative of 3 biological replicates). b) Densitometry of western blot in c).

4.3 Differentially modified mRNA levels are regulated by KSHV lytic proteins

Multiple m^{6}A modified mRNAs undergo changes in abundance during KSHV reactivation and cluster into pathways which are known to be modulated by KSHV infection. Thus, some of

these transcripts could be specifically targeted by the virus for up- or downregulation during lytic replication. To identify whether any of these methylated transcripts are modulated through the action of KSHV lytic proteins, 293T cells were transfected with GFP-tagged constructs containing viral immediate early proteins known to regulate cellular gene expression, namely RTA or ORF57. Changes in abundance among the methylated transcripts were examined upon ectopic expression of each viral protein relative to cells transfected with an empty GFP construct (Figure 4.3).

In GFP-ORF50-transfected-cells, a large and significant 230% upregulation in *GPRC5A* mRNA levels was observed in addition to a moderate but significant 30% increase in *ZFP36L1* levels. Given that these transcripts also increase in abundance during KSHV reactivation in TREX cells, these data suggests that RTA may induce this upregulation. A near significant 30% rise was also identified in *CNOT2* mRNA which is heavily downregulated in lytic replication. If RTA also controls the upregulation of this transcript, counteracting cellular or viral factors may act during reactivation to ensure an overall net decrease in *CNOT2* mRNA, perhaps to support or restrict lytic replication.

In *GFP-ORF57*-transfected cells a significant 25% decrease in *TIFA* and a near significant 20% decrease in *ZC3H12A* mRNA was identified. Additionally, *JUN* mRNA levels increased by a near significant 30% in GFP-ORF57 expressing cells suggesting ORF57 may regulate the levels of these 3 transcripts.

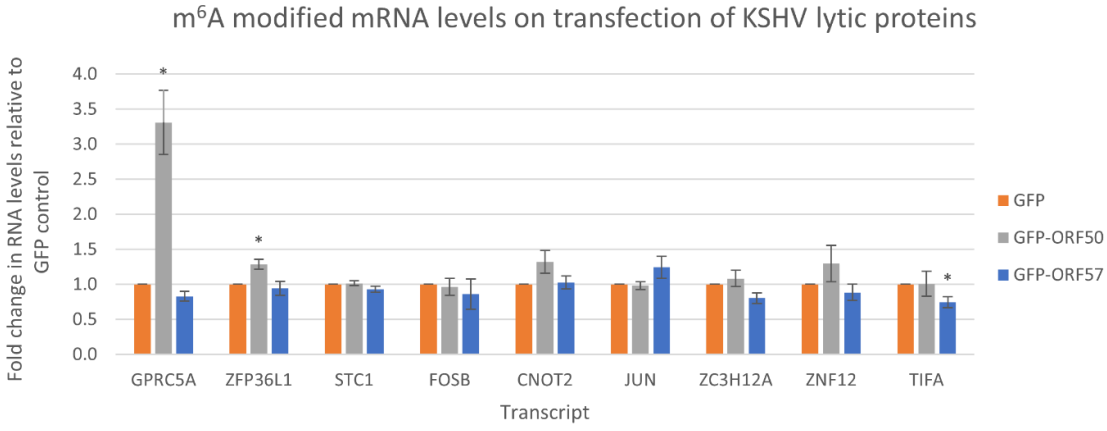

Figure 4.3. KSHV lytic proteins regulate the abundance of cellular m^{6}A modified mRNAs. 293T cells were transfected with constructs containing GFP-tagged viral genes *ORF50* and *ORF57*. The RT-qPCR data shows the relative RNA levels of methylated transcripts in *GFP-ORF50* and *GFP-ORF57* transfected cells compared to a GFP-control-expressing cell line (data presented as mean ± SD, n=3)

Except for *GPRC5A*, the m^6A modified mRNAs *ZFP36L1* and *TIFA* showed significant alterations in mRNA levels of less than 50%. Furthermore, the transcripts *CNOT2, ZC3H12A* and *JUN* showed small alterations, albeit at a non-significant level. As a result, further examination with higher concentrations of viral proteins was undertaken to magnify any effect on these transcripts and clarify whether the changes in mRNA were genuine. 293Ts were transfected with increasing concentrations of the *GFP-ORF50* and *GFP-ORF57* plasmids to determine whether changes in these mRNAs were viral protein dose-dependent (Figure 4.4a, e). Interestingly both *GPRC5A* and *ZFP36L1* levels increased in correlation with *GFP-ORF50* concentration suggesting that RTA regulates the abundance of these mRNAs (Figure 4.4b). In addition, western blotting confirmed that the elevation in *GPRC5A* transcripts effects a functional increase in the encoded protein (Figure 4.4c). However, while an increase was observed in *CNOT2* mRNA levels, this did not occur at a significant level for any of the *GFP-ORF50* concentrations; therefore, it is not entirely clear whether RTA increases the abundance of this transcript.

In *GFP-ORF57*-transfected cells, *JUN* mRNA increased up to 70% higher suggesting the viral protein upregulates this transcript (Figure 4.4f). Furthermore, *TIFA* mRNA levels were significantly lower than both untransfected and GFP control-transfected cells at two *GFP-ORF57* concentrations. Finally, *ZC3H12A* transcripts were significantly different from GFP-transfected but not untransfected 293T cells suggesting this mRNA may not be downregulated by ORF57. Taken together, these results demonstrate that the KSHV lytic proteins RTA and ORF57 regulate the mRNA levels of *GPRC5A, ZFP36L1, JUN* and *TIFA,* perhaps so that their encoded proteins may play an important role within KSHV lytic replication.

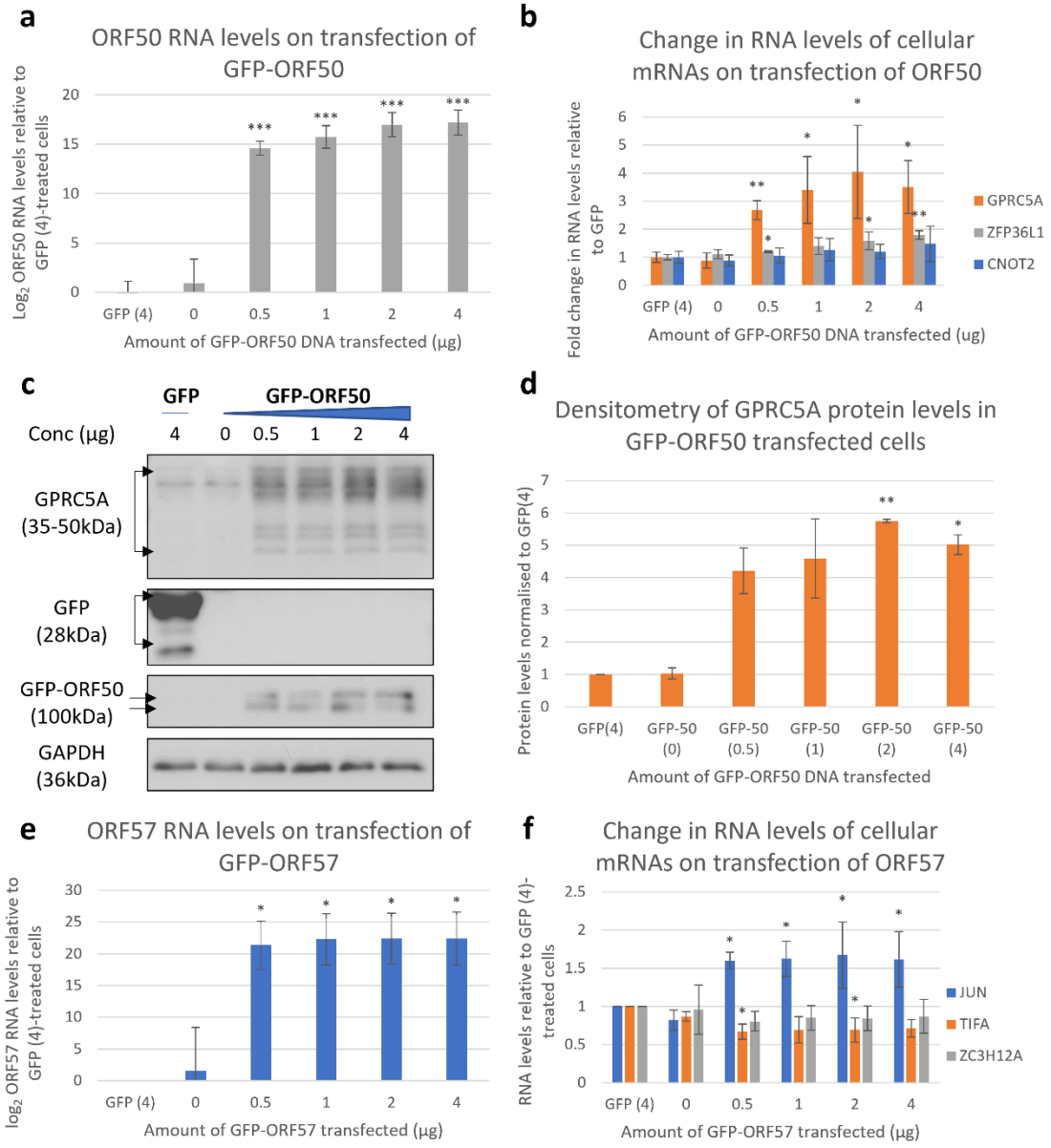

Figure 4.4. Ectopic expression of KSHV lytic proteins at varying concentrations confirms the elevation of *GPRC5A, ZFP36L1, JUN* and *TIFA* mRNA levels. a,e) Varying concentrations of *GFP-ORF50* and *GFP ORF57* were transfected into 293Ts and the ectopic expression of these lytic genes confirmed by RT-PCR (data presented as mean ± SD, n=3). b) The mRNA levels of *GPRC5A, ZFP36L1* and *CNOT2* were monitored by RT-qPCR at different concentrations of *GFP-ORF50* (data presented as mean ± SD, n=3). c) Western blot showing protein expression of GPRC5A at increasing concentrations of *GFP-ORF50* (blots are representative of 3 biological replicates). d) Densitometry of western blot in c). e) *JUN, TIFA* and *ZC3H12A* mRNA levels were examined by RT-qPCR at different concentrations of *GFP-ORF57* (data presented as mean ± SD, n=3).

4.4 RTA binds the promoters of *GPRC5A* and *ZFP36L1* to induce transcription

The KSHV viral gene *ORF50* encodes the lytic master regulator protein RTA which is able to activate transcription at many promoters within the viral and cellular genomes (Lukac et al., 2001; Bu et al., 2008). As *GPRC5A* and *ZFP36L1* mRNAs increased in abundance upon the

ectopic expression of RTA in uninfected 293T cells, this change could be explained by the RTA-mediated transactivation of *GPRC5A* and *ZFP36L1* promoters. To investigate this hypothesis, published RTA-CHIP-seq data in TREX cells was examined for RTA binding at the *GPRC5A* and *ZFP36L1* gene promoters (Papp et al., 2019). Raw data from the research paper was processed by Ivaylo Yonchev of the Wilson group at the University of Sheffield who used the peak calling software MACS2 to identify enriched areas of RTA binding within the cellular genome. As expected, CHIP peaks representing sites of RTA binding were present in known RTA-induced genes such as *NOTCH1* (Figure 4.5a). Interestingly, CHIP peaks were also present in several locations, including the promoter regions, of both *GPRC5A* and *ZFP36L1* gene loci across several replicates (Figure 4.5b, c). Therefore, combining the CHIP-seq data with the upregulation of *GPRC5A* and *ZFP36L1* mRNAs in *GFP-ORF50*-transfected cells, RTA likely binds to these genes and induces their transcription. Thus, it is possible that KSHV increases the expression of *GPRC5A* and *ZFP36L1* during reactivation to support an important role in the lytic replication of the virus.

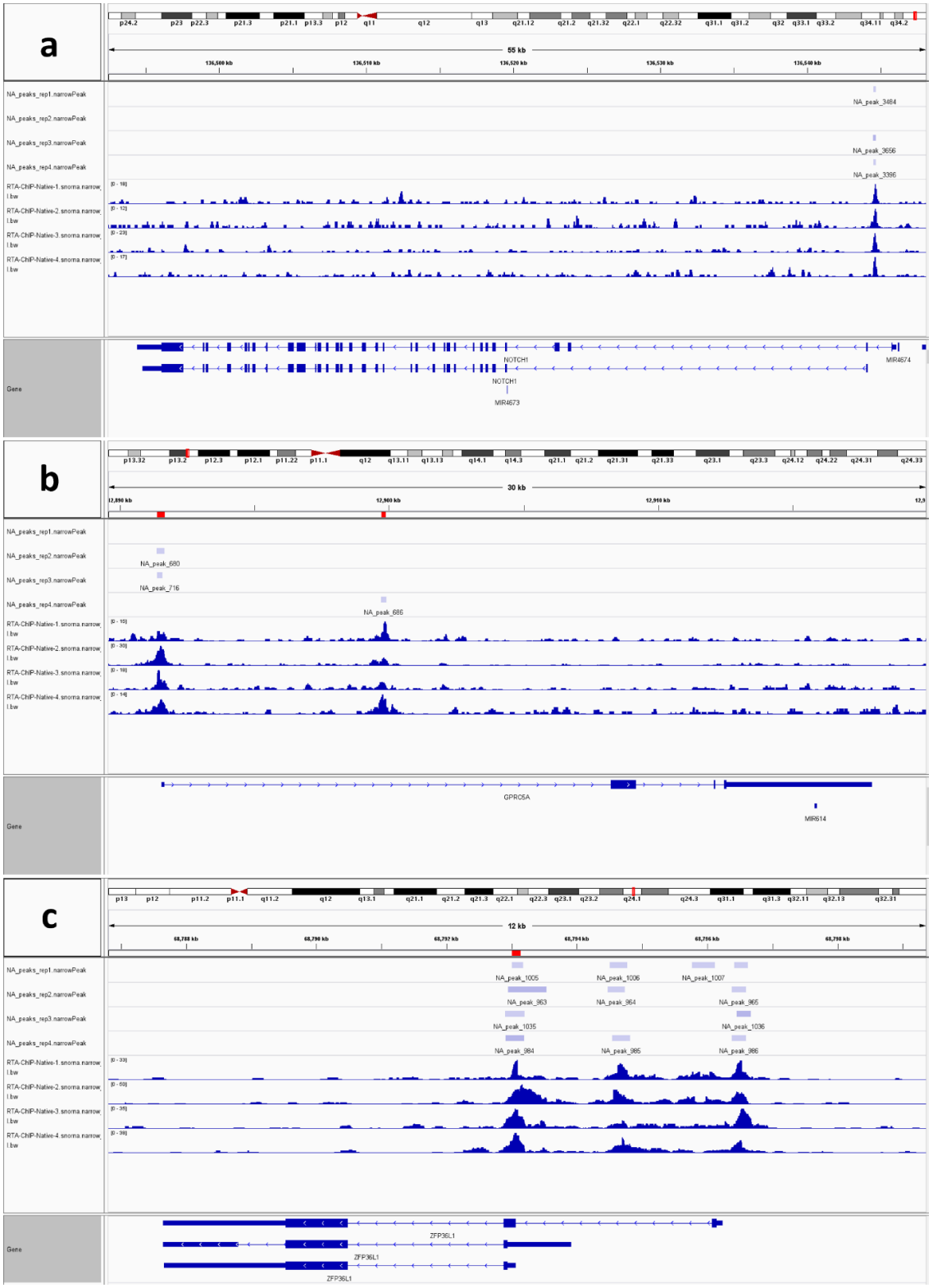

Figure 4.5. RTA binds to the *GPRC5A* and *ZFP36L1* gene promoters. Snapshots of RTA CHIP-seq data at (a) *NOTCH1*, (b) *GPRC5A* and (c) *ZFP36L1* gene loci visualised using the software integrative genome viewer. Peaks called by MACS2 are presented above raw enrichment data from 4 biological replicates. Genes including splice variants are presented below the raw data.

4.5 The KSHV lytic transactivator RTA interacts with WTAP of the m^{6}A methyltransferase complex

m^{6}A is suggested to be predominantly added in a co-transcriptional manner to a nascent RNA molecule. Interestingly, the recruitment of METTL14 to sites of histone H3 trimethylation at lysine-36 (H3K36me3) within DNA allows binding of the m^{6}A methyltransferase complex to RNAPII and the delivery of m^{6}A at adjacent sites within the synthesising RNA. Given that RTA binds numerous viral and cellular promoters including *GPRC5A* and *ZFP36L1* to activate their transcription, the viral protein may interact with proximally located members of the m^{6}A writer complex at sites of H3K36me3 and potentially affect their function. To identify any such interaction, c-Myc-RTA was immunoprecipitated from latent and lytic TREX cell lysates and members of the m^{6}A methyltransferase complex tested for coimmunoprecipitation (Figure 4.6). As expected, the RTA interactor ORF59 was clearly identified in C-myc lytic immunoprecipitates and absent from IgG immunoprecipitates indicating an association of the two proteins. However, no interaction with METTL14 was observed as the protein could not be identified in either latent or lytic immunoprecipitates. Furthermore, no METTL3 antibody was available which had the required sensitivity for this application. Curiously, a clear enrichment of WTAP protein was identified in c-Myc immunoprecipitates compared with non-specific igG immunoprecipitates during lytic replication. Thus, it appears RTA interacts with WTAP, but not METTL14, of the m^{6}A writer complex suggesting the viral protein may affect the function of the m^{6}A methyltransferase complex and regulate the deposition of m^{6}A.

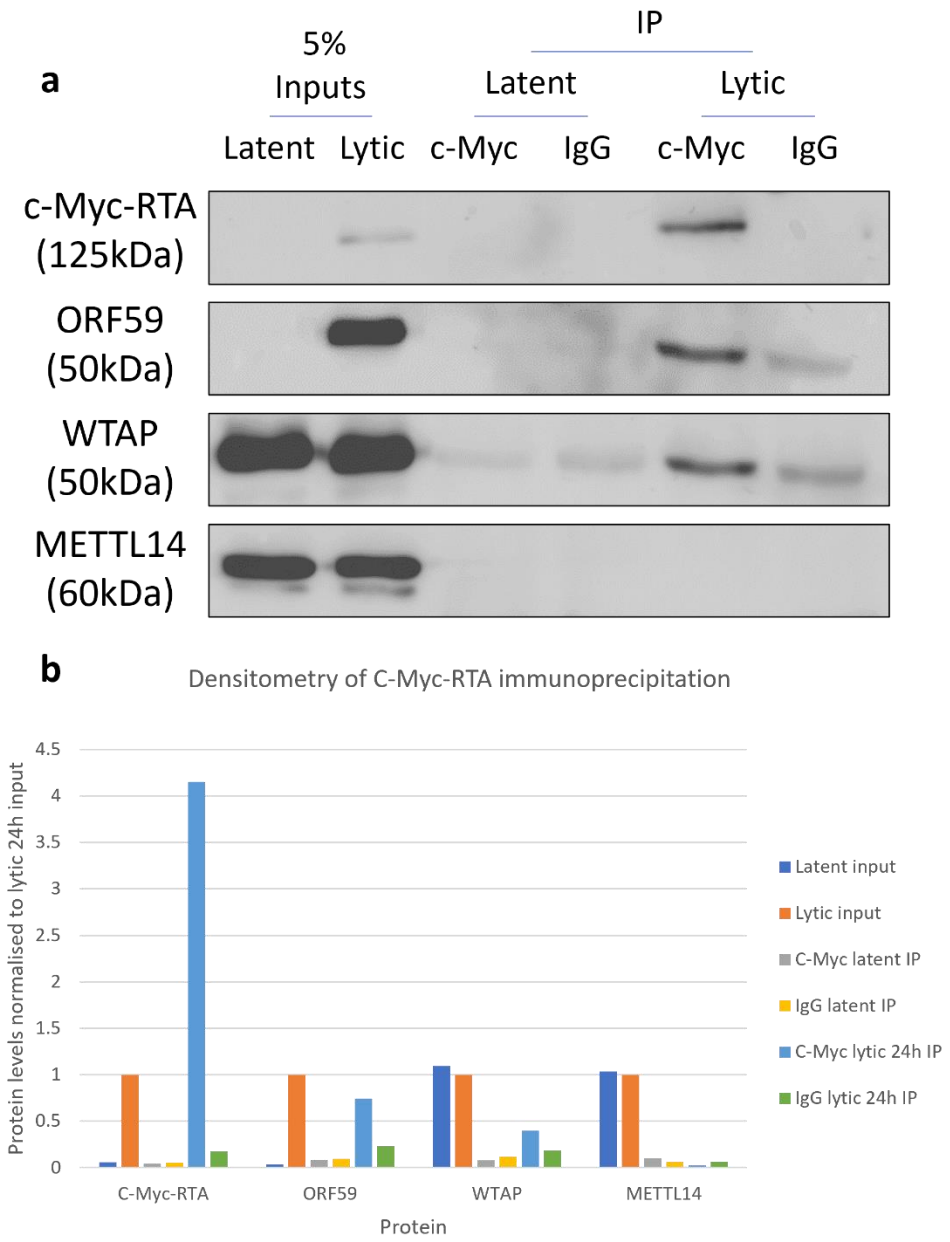

Figure 4.6. RTA interacts with WTAP. Immunoprecipitation was carried out on latent and lytic TREX cell lysates using IgG and c-Myc antibodies. Successful pulldown of c-Myc-RTA and coimmunoprecipitation of ORF59, WTAP and METTL14 were tested by western blotting using their respective antibodies (blots representative of 1 biological repeat). b) Densitometry of western blot in a).

4.6 Differentially modified mRNAs do not exhibit alternative splicing during KSHV reactivation

Multiple studies have functionally linked m^{6}A to the alternative splicing of cellular pre-mRNAs through recognition by the m^{6}A reader DC1 and other HNRNP family proteins (Alarcón et al., 2015; Xiao et al., 2016; N. Liu et al., 2017; Wu et al., 2018). To identify whether any of the differentially m^{6}A-modified mRNAs are subjected to changes in

alternative splicing during KSHV reactivation, several of these transcripts were examined for changes in their splicing patterns during KSHV reactivation. Primers were designed to amplify specific splice variants allowing determination of the splicing ratio in latent and reactivated cells by RT-qPCR (Figure 4.7d). *ZNF12, ZFP36L1* and *FOSB* were prioritised for study in this experiment as the m^6A-seq data identified m^6A peaks in these mRNAs located adjacent to splice junctions. However, no change in the splicing ratio for any of these transcripts was identified during KSHV reactivation, indicating that the differential methylation of these mRNAs does not affect their splicing pattern (Figure 4.7a-c).

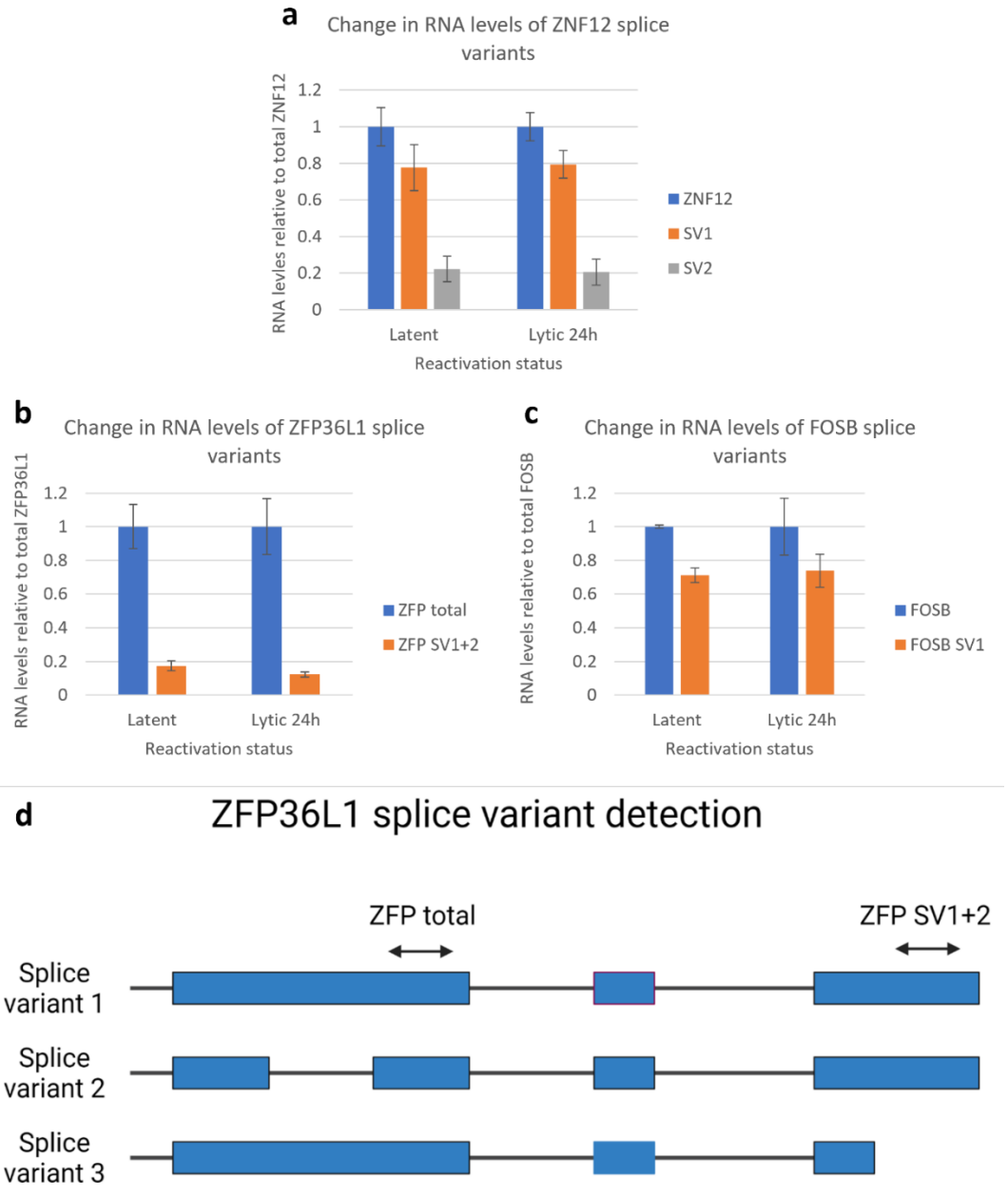

Figure 4.7. Alternative splicing of differentially m^{6}A-modified mRNAs during reactivation. (a-c) RT-qPCR data showing RNA levels of splice variants relative to total RNA levels for *ZNF12, ZFP36L1* and *FOSB* in latent TREX cells and 24 hours post-induction (data presented as mean ± SD, n=3). *ZNF12* and *FOSB* have two splice variants each while *ZFP36L1* has three. d) Example diagram showing the design of amplicons which detect different *ZFP36L1* splice variants.

4.7 Differentially modified mRNAs display changes in nuclear export efficiency during KSHV reactivation

In addition to alternative splicing, studies have shown that m^{6}A is also able to affect the nuclear export efficiency of an mRNA into the cytoplasm (Roundtree et al., 2017; Lesbirel et al., 2018). To identify whether m^{6}A regulates the nuclear export of differentially m^{6}A

modified transcripts, the nucleocytoplasmic (N/C) ratios of nine cellular mRNAs (*ZNF12, ZC3H12A, TIFA, STC1, GPRC5A, CNOT2, JUN*, *ZFP36L1* and *FOSB*) were compared between latent and reactivated TREX cells. Whole cell, nuclear and cytoplasmic fractions were obtained by subcellular fractionation and efficient fractionation demonstrated by western blotting for the proteins Lamin B and GAPDH which are restricted to their respective nuclear and cytoplasmic compartments (Figure 4.8a). RNA levels of differentially modified mRNAs were then analysed within each fraction by RT-qPCR (Figure 4.8b). Finally, N/C ratios were calculated and compared between latent and reactivated cells (Figure 4.8c). Surprisingly, *ORF57* showed a significant increase in N/C ratio suggesting it may be exported less efficiently during reactivation. However, it is also conceivable that the ~400-fold increase in *ORF57* mRNA seen during lytic replication leads to a bottleneck in its export. In contrast, a significant 40% decrease in N/C ratio was observed for *ZFP36L1* mRNA, while both *FOSB* and *JUN* also tended towards a decrease, suggesting their nuclear export is more efficient in lytically-reproducing cells. This may indicate that these transcripts are prioritised for export to affect viral replication, perhaps in an m^6A-dependent manner.

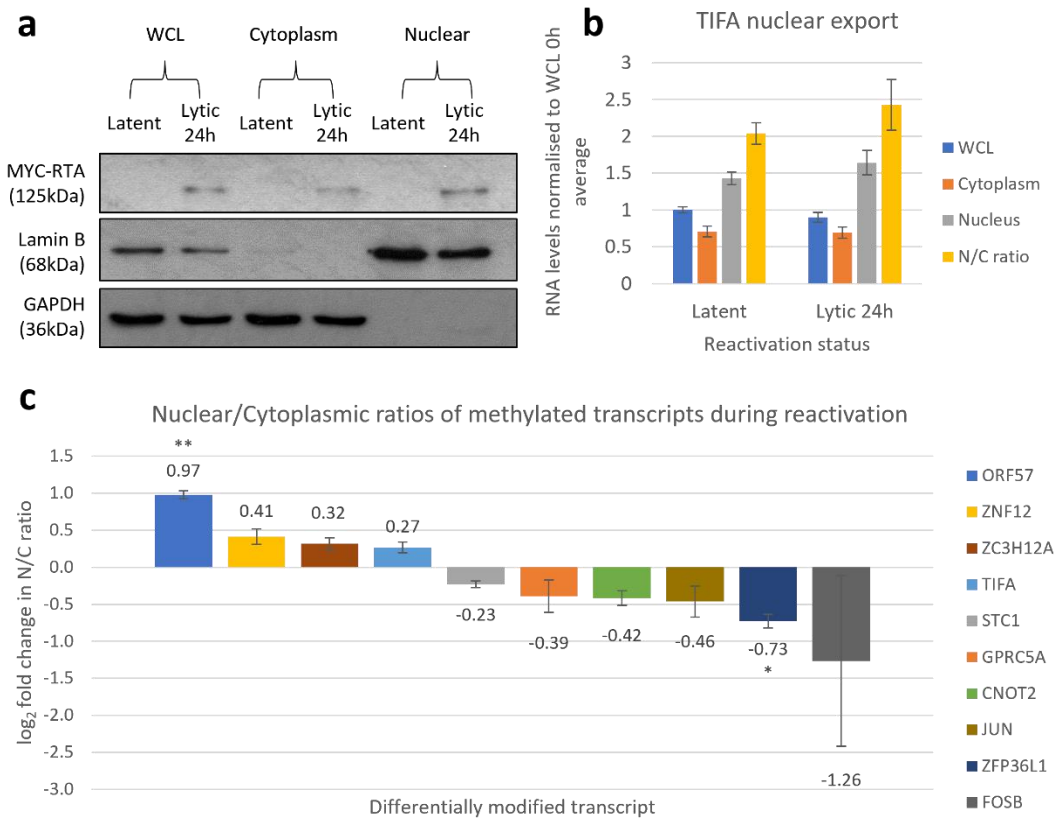

Figure 4.8. Subcellular fractionation of latent and lytic TREX cells shows altered nuclear export efficiency in differentially m^{6}A-modified mRNAs. Latent and lytic (24 hours) TREX cells were fractionated into whole cell (WCL), nuclear and cytoplasmic fractions (all RT-qPCR data presented as mean ± SD, n=3). a) Western blots showing the cytoplasmic and nuclear proteins GAPDH and Lamin B respectively to confirm efficient fractionation (blot representative of three biological repeats). b) RNA levels of the representative transcript *TIFA* in the WCL, cytoplasm and nucleus relative to *GAPDH*. N/C ratio calculated by dividing nuclear RNA levels by those in the cytoplasm. c) $\log_2$ fold change in N/C ratio of differentially methylated transcripts in reactivated compared to latent cells.

Intriguingly, one differentially modified transcript, ZNF12, displayed unusually high N/C ratios. Like all transcripts, qPCR primers were strictly designed within exonic sequences and nucleotide BLAST searches show no sequence identity between the ZNF12 primer set with other human RNAs. Thus, it seems unlikely that intronic amplification or non-specific amplification of ncRNAs could explain this finding. Nevertheless, subcellular fractionation showed the transcript to be 30-50-fold enriched in the nucleus compared to the cytoplasm suggesting this mRNA undergoes nuclear retention (Figure 4.9a). This effect was observed in both latent and reactivated TREX cells, with no significant change in N/C ratio, suggesting that the differential modification of this transcript does not contribute to its nuclear retention. As this effect was identified during both KSHV replication programmes it suggests that it has minimal functional relevance during lytic reactivation. Furthermore, subcellular fractionation in uninfected 293Ts showed that *ZNF12* mRNA was also retained in the nucleus

(Figure 4.9b). Thus, while *ZNF12* nuclear retention is an intriguing mechanism with potential cellular importance, it is unlikely to be functionally relevant in KSHV infection.

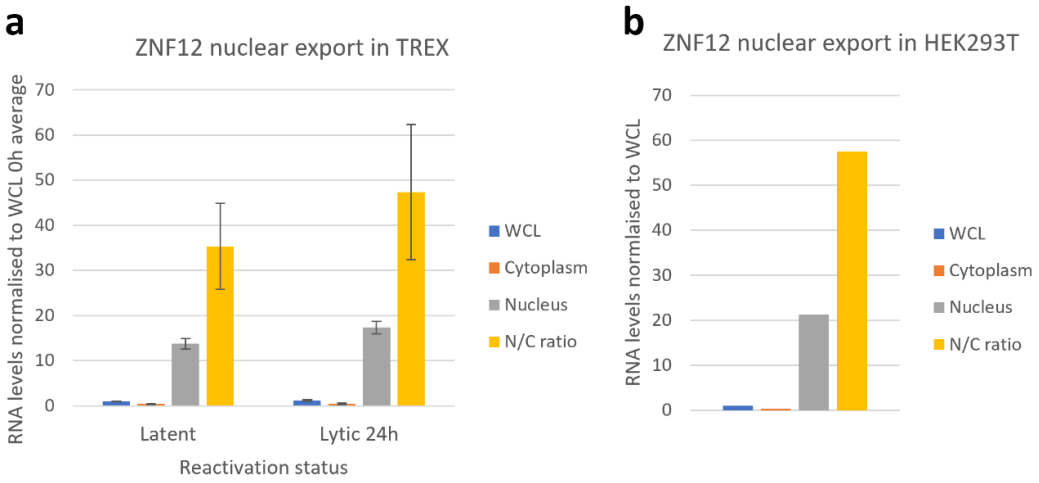

Figure 4.9. Nuclear retention of the differentially m^{6}A-modified mRNA *ZNF12*. RT-qPCR data showing *ZNF12* mRNA in both latent and lytic (24 hours) TREX cell fractions (data presented as mean ±SD, n=3). b) RT-qPCR data showing *ZNF12* mRNA in 293T cell fractions (n=1).

4.8 Differentially modified mRNAs may undergo changes in RNA stability during KSHV lytic reactivation

Many studies have linked m^{6}A to mRNA stability and recent evidence suggests this may be the principal function of the modification (Zaccara et al., 2019). Given that several methylated transcripts display alterations in their abundance during lytic reactivation, m^{6}A could play a key role in regulating the levels of these mRNAs through changes to their stability and thus cytoplasmic turnover. The drug actinomycin D binds transcription initiation complexes and inhibits elongation of nascent RNA chains preventing transcription. Thus, the drug stalls the synthesis of new RNA molecules and the stability of an existing pool of RNAs can be determined by measuring their declining levels over time. To study the stability of differentially modified mRNAs, actinomycin D was added to latent or lytic TREX cells and the levels of methylated transcripts (*ZNF12, ZC3H12A, TIFA, STC1, GPRC5A, CNOT2, JUN, ZFP36L1* and *FOSB)* monitored for 0, 3 and 6 hours after addition of the drug by RT-qPCR. For transcripts whose expression is not greatly changed during reactivation, a clear profile showing the decline in levels of the mRNA could be obtained (Figure 4.10a). Unfortunately however, it appears the shutoff of transcription by actinomycin D was either delayed or incomplete leading to leaky synthesis of some RNA molecules in the early hours

of drug treatment. Furthermore, actinomycin D led to cellular stress so that in latent cells, spontaneous reactivation occurred and certain transcripts that increase in lytic replication were upregulated. This effect was most apparent for *FOSB (*Figure 4.10b*)* and *JUN* mRNAs whose expression is rapidly increased very early during reactivation; however, the same effect could be identified for *ORF57, GPRC5A, STC1* and *ZFP36L1*. Fortunately, at 6 hours post actinomycin D treatment, this effect seemed to undergo correction for most mRNAs except *ZFP36L1, FOSB* and *JUN*. As a result, the 3 hour timepoint was excluded and the 0 and 6 hour actinomycin D-treated cells used to calculate the change in stability for methylated transcripts during reactivation (Figure 4.10c-d). Curiously, *STC1, ORF57* and *TIFA* underwent a significant increase in their stability in the lytic phase, while *GPRC5A* stability was also enhanced at a non-significant level (Figure 4.10e). It is unclear why *TIFA* protein levels are lower in lytic replication despite stable mRNA levels and an increase in the stability of the mRNA; however, the action of viral proteins or alternative cellular mechanisms may contribute to an overall loss in the protein levels of *TIFA.* Nevertheless, the change in stability associated with *ORF57, STC1* and *GPRC5A* could be a contributing factor towards the increased abundance of these transcripts in lytic replication. Importantly, the increased stability in these transcripts, which all undergo changes in their methylation status during reactivation, may be attributed to m^6A.

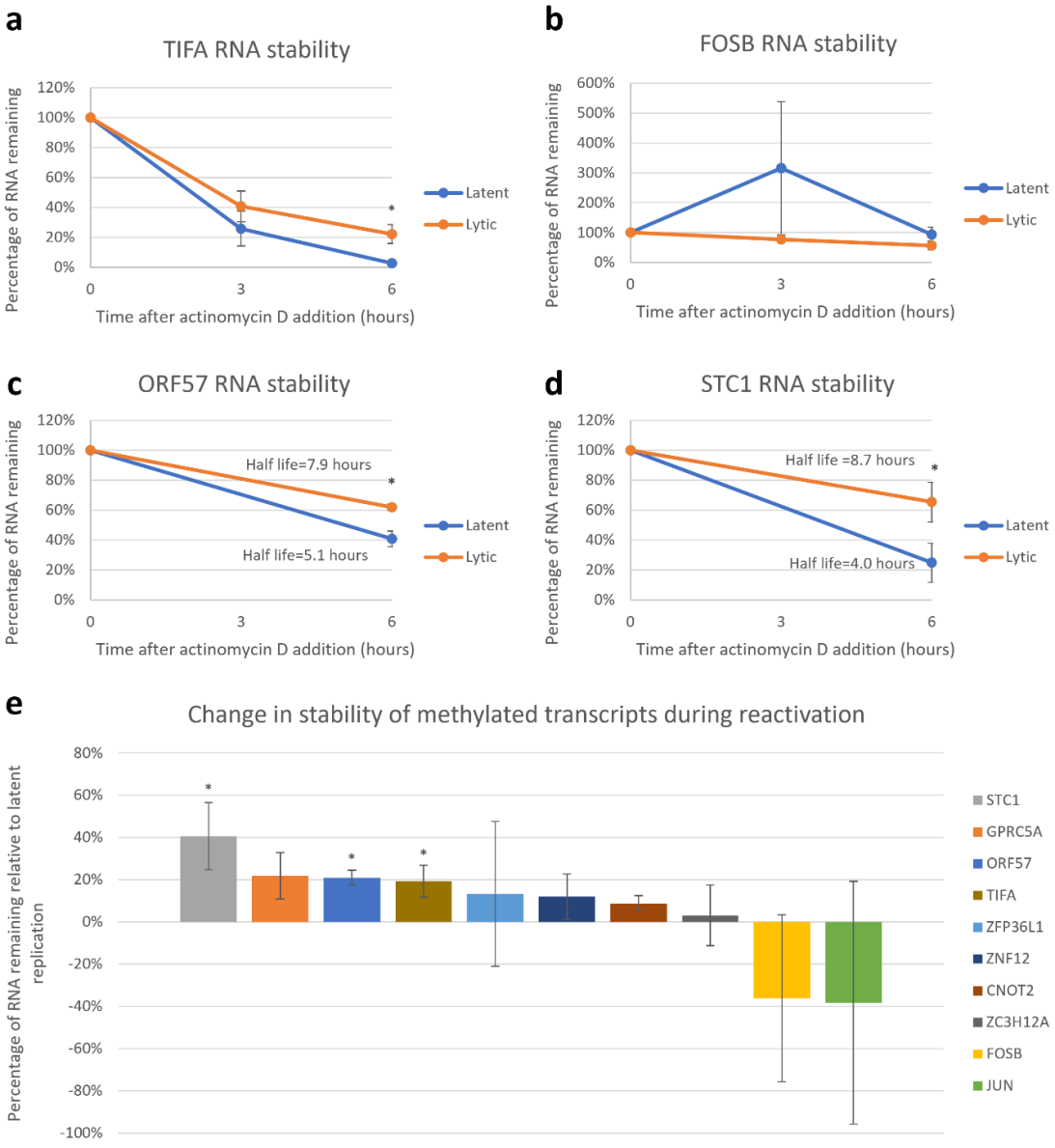

Figure 4.10. Changes in the stability of methylated transcripts during reactivation. Latent and reactivated TREX cells were incubated for 24 hours followed by addition of actinomycin D at 2.5µg/ml for 0, 3 or 6 hours. RNA levels of m^{6}A modified transcripts were measured by RT-qPCR compared with *18s rRNA* rather than *GAPDH* as it has a higher half-life (all data presented as mean ±SD, n=3). a, b) RNA levels of *TIFA* and *FOSB* mRNAs at 0, 3 and 6 hours after actinomycin D treatment in latent and lytic TREX cells. c, d) *ORF57* and *STC1* transcript levels at 0 and 6 hours only after actinomycin D treatment in both latent and lytic TREX cells (half-life calculated where the percentage of RNA remaining=50%). e) Change in stability of m^{6}A modified mRNAs during reactivation calculated from the difference in RNA remaining in latent and lytic TREX cells after 6 hours of actinomycin D treatment.

4.9 Depletion of the m^{6}A writer complex subunit WTAP affects the upregulation of differentially m^{6}A-modified mRNAs

Although changes have been shown in the abundance of a number of differentially m^{6}A-modiifed cellular mRNAs during KSHV reactivation, it is still unclear whether m^{6}A is

important for this process. As a result, the depletion of the m^{6}A machinery which install, erase and decode this modification was carried out to identify any associated changes in mRNA levels which could be due to the m^{6}A modification. Firstly, the m^{6}A methyltransferase subunit WTAP was depleted in TREX cells by stable transduction with shRNAs. After seven days of selecting transduced cells with puromycin, *WTAP* expression was assessed relative to a scrambled control shRNA by RT-qPCR and western blotting (Figure 4.11a-b). At both RNA and protein levels, a 75% depletion of WTAP was achieved suggesting an extensive global reduction in m^{6}A levels. Next, the abundance of differentially m^{6}A-modified transcripts was compared between scrambled-shRNA treated and WTAP-depleted TREX cells undergoing latent or lytic replication. Interestingly, RT-qPCR showed that WTAP depletion reduced the expression of four differentially modified transcripts in reactivated cells: *GPRC5A, FOSB, STC1* and *ZFP36L1* (Figure 4.11d). While these mRNAs are normally upregulated between three- and 20-fold in the lytic phase compared to latency, the loss of WTAP expression significantly diminished this increase from 30-50%. Therefore, these data suggest that m^{6}A is important for the elevated abundance of these transcripts during the lytic phase.

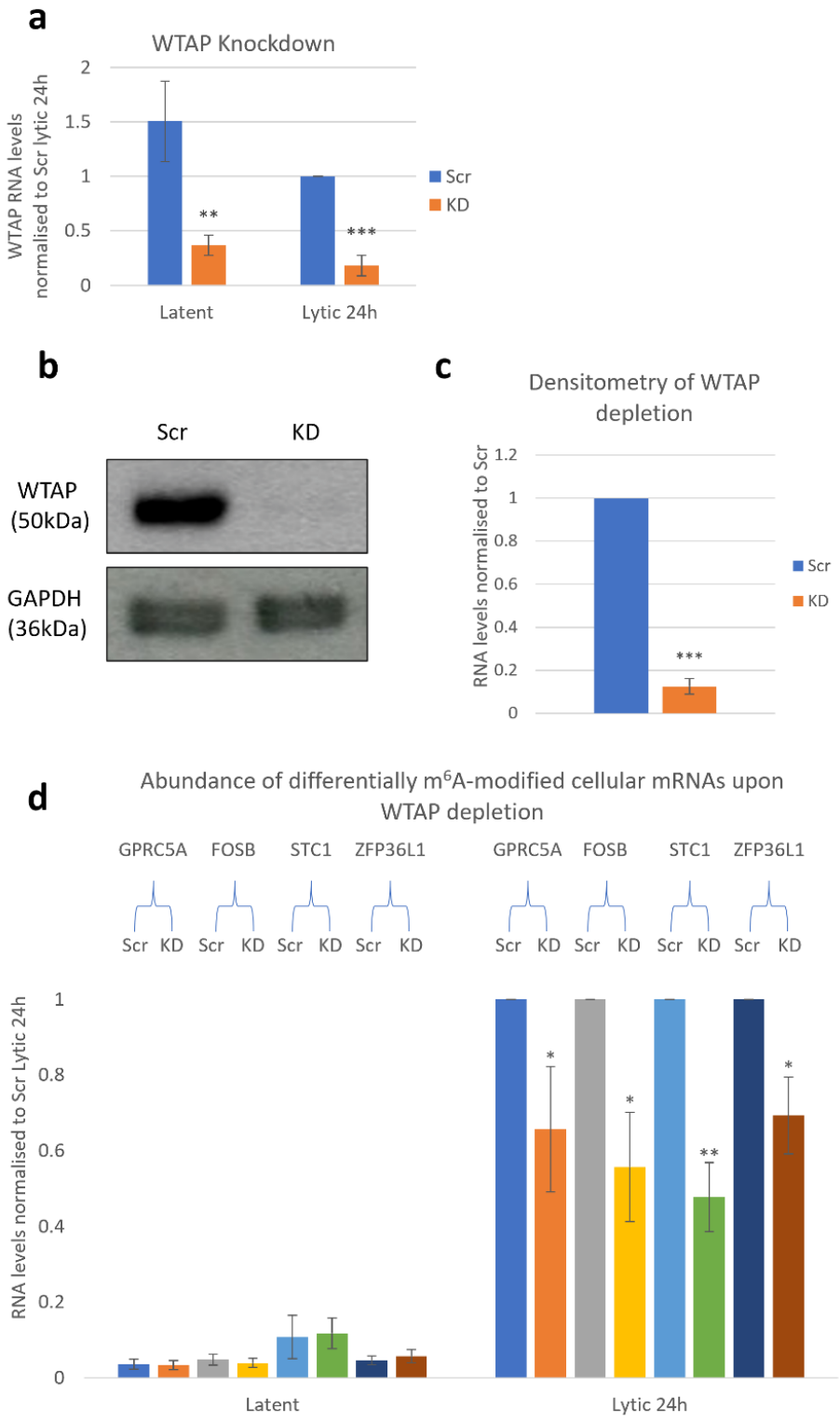

Figure 4.11. Depletion of WTAP inhibits the upregulation of m^{6}A modified cellular mRNAs during lytic reactivation. TREX cells were treated with scrambled control or *WTAP*-targeting shRNAs and placed under puromycin selection for 7 days. a) RT-qPCR showing confirmation of *WTAP* depletion at the RNA level (data presented as mean ± SD, n=3). b) Western blots confirming WTAP depletion at the protein level in latent TREX cells (blots representative of three biological repeats). c) Densitometry of western blot in b). d) RNA levels of *GPRC5A*, *STC1*, *FOSB* and *ZFP36L1* in response to WTAP-depletion in both latent and induced cells (data presented as mean ± SD, n=4).

4.10 Depletion of the putative m^{6}A eraser FTO enhances the upregulation of the m^{6}A modified *GPRC5A* transcript

As m^{6}A is a dynamic modification, the demethylation of modified transcripts by an m^{6}A eraser could also affect lytic reactivation. Although the true target of the demethylase FTO is controversial, studies have demonstrated that depletion of FTO reverses the effect on virus replication observed for depletion of an m^{6}A writer subunit (Gokhale et al., 2016; Lichinchi, Gao, et al., 2016; Lichinchi, Zhao, et al., 2016; Tan et al., 2018; Kevin Tsai et al., 2018). Therefore, to investigate whether FTO affects the abundance of the cellular m^{6}A-modified transcripts identified by m^{6}A-seq, the protein was depleted using shRNAs and a 75% reduction in FTO levels confirmed by RT-qPCR and western blot (Figure 4.12a-b). Interestingly, *GPRC5A* alone displayed 50% higher mRNA levels in the FTO-depleted cell line undergoing reactivation than those treated with scrambled shRNA (Figure 4.12d). This indicates that loss of FTO's demethylase activity leads to an increase in *GPRC5A* mRNA, perhaps through an increase in m^{6}A or m^{6}A$_m$ modifications upon this transcript. Importantly however, while the depletion of FTO did not increase *STC1, FOSB* or *ZFP36L1* mRNA levels, the knockdown of the m^{6}A eraser ALKBH5 may affect their expression.

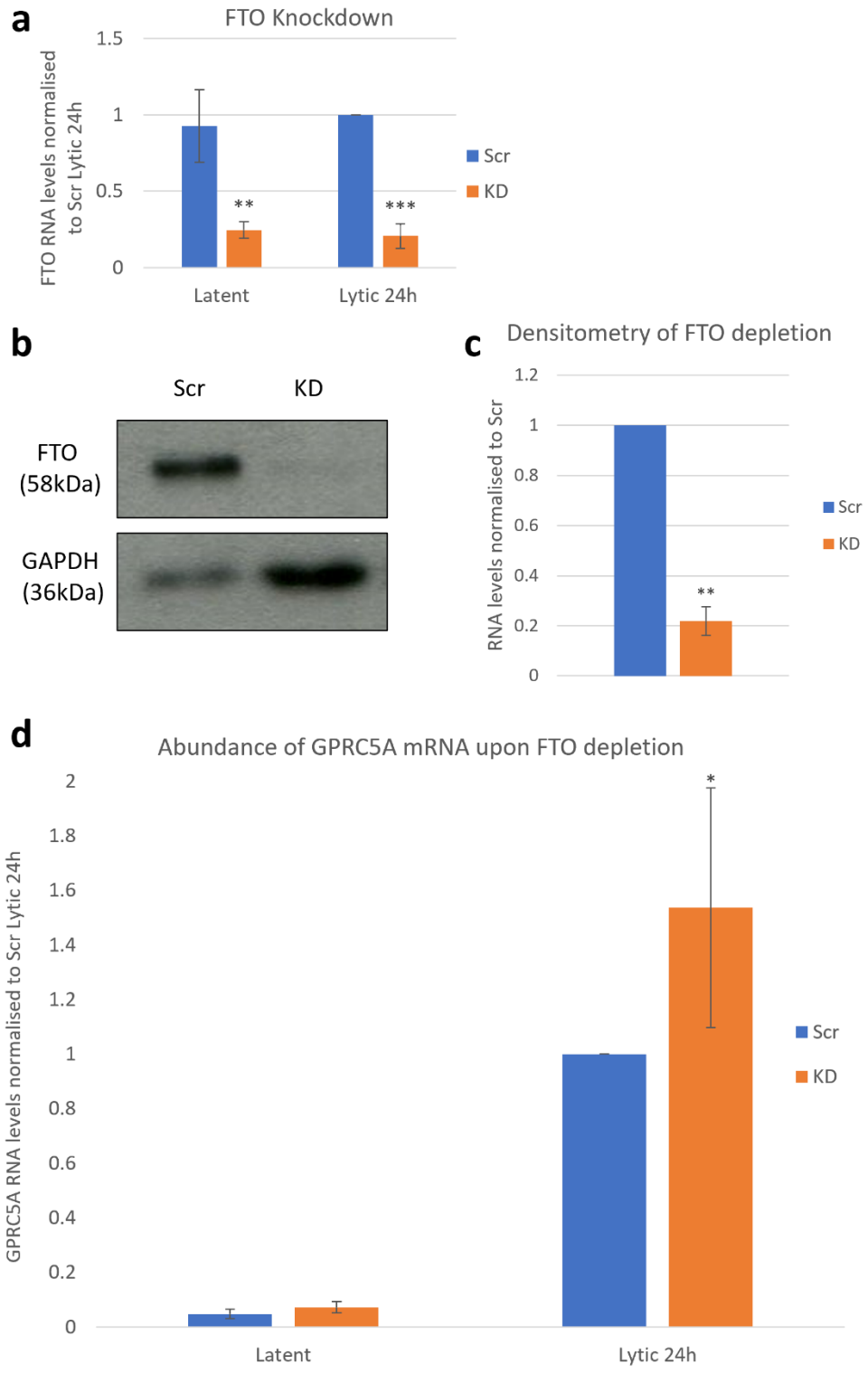

Figure 4.12. Depletion of FTO enhances the upregulation of *GPRC5A* mRNA during lytic reactivation. TREX cells were treated with scrambled control and FTO-targeting shRNAs and placed under puromycin selection for 7 days. a) RT-qPCR showing confirmation of *FTO* depletion at the RNA level (data presented as mean ± SD, n=3). b) Western blots confirming FTO depletion at the protein level in latent TREX cells (blots representative of three biological repeats). c) Densitometry of western blot in b). d) RNA levels of *GPRC5A* in response to FTO-depletion in both latent and reactivated cells (data presented as mean ± SD, n=4).

4.11 Depletion of the m^{6}A reader YTHDF1 affects the upregulation of differentially m^{6}A modified cellular mRNAs

Although m^{6}A deposition is carried out by the m^{6}A writer complex, in most cases the modification must be decoded by m^{6}A reader proteins to exert any physiological influence over the fate of a mRNA. As a result, several studies have shown that depletion of an m^{6}A reader recapitulates the effect of silencing of m^{6}A writer components during viral replication. The m^{6}A reader DF1 was silenced using shRNAs and depletion assessed by RT-qPCR (Figure 4.13a). After confirmation of an 80% reduction in *DF1* mRNA levels, the abundance of differentially m^{6}A-modified transcripts was again monitored for changes during reactivation. Like previous studies, DF1 depletion recapitulated the effect of WTAP silencing as *GPRC5A*, *STC1*, *FOSB* and *ZFP36L1* RNA levels showed diminished upregulation during lytic replication (Figure 4.13b). Although *GPRC5A* and *ZFP36L1* showed a modest decrease relative to *FOSB* and *STC1*, these two mRNAs could be targeted to a lesser extent by DF1 than its DF2 and DF3 homologues. As a result, the combined silencing of all three of these m^{6}A readers would likely produce a greater effect.

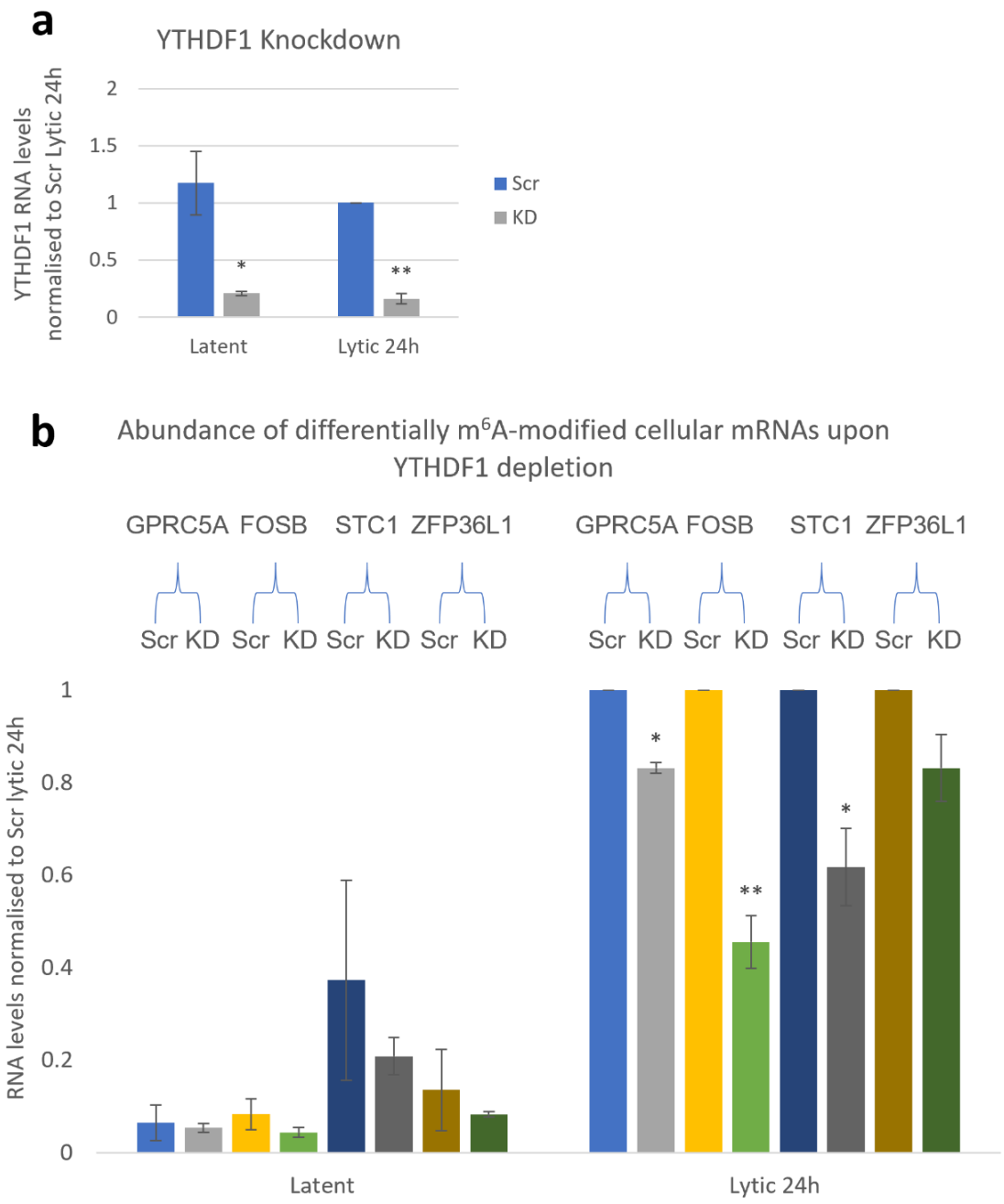

Figure 4.13. Depletion of YTHDF1 inhibits the upregulation of m^{6}A modified cellular mRNAs during lytic reactivation. TREX cells were treated with scrambled control and DF1-targeting shRNAs and placed under puromycin selection for 7 days. a) RT-qPCR showing confirmation of *YTHDF1* depletion at the RNA level in latent and lytic TREX cells (data presented as mean ± SD, n=3). b) RNA levels of *GPRC5A*, *STC1*, *FOSB* and *ZFP36L1* in response to DF1-depletion in both latent and induced cells (data presented as mean ± SD, n=4).

4.12 Discussion

In this chapter, the selected cellular transcripts identified by m^{6}A-seq as differentially methylated during reactivation were screened for changes in mRNA biology that might be attributable to m^{6}A. Interestingly, the largest changes in this set of transcripts were related

to their abundance, with many transcripts heavily upregulated during lytic replication. These cellular mRNAs with increased abundance defy the general downregulation associated with host transcripts as a result of KSHV-orchestrated host cell shutoff by the viral protein SOX. This observation suggests upregulation by the virus for the purposes of cell hijack or by the host in order to restrict infection; thus, these transcripts may be particularly important during KSHV lytic replication.

To test whether the virus has any influence in the changes in abundance among the modified cellular mRNAs during reactivation, their mRNA levels were monitored in 293T cells ectopically expressing the viral proteins RTA or ORF57. Both lytic proteins have well established roles in the modulation of cellular RNA abundance as RTA is able to transactivate cellular gene promoters inducing transcription while ORF57 can bind mRNAs to enhance their splicing, stability and export (Chiou et al., 2002; Boyne et al., 2010; Jackson et al., 2011; Vogt and Bohne, 2016). Recapitulating the effect of reactivation in TREX cells, *GPRC5A* was dramatically upregulated by RTA while Z*FP36L1* mRNAs levels also increased albeit to a lesser extent. Interestingly, a previously published ChIP-seq dataset demonstrates clear evidence of RTA binding in the promoters of these genes suggesting that KSHV induces *GPRC5A* and *ZFP36L1* to support an important function in lytic replication (Loh et al., 2020). Furthermore, an interaction between RTA and WTAP was identified providing exciting evidence that RTA interacts with the m^{6}A writer complex to modulate m^{6}A deposition. However, further study is required to support this finding. ORF57 upregulated the abundance of *JUN* mRNA suggesting this transcript may be bound and stabilised by the viral protein. However, a decrease in *TIFA* mRNA levels was also identified in ORF57-expressing cells. While the mechanisms underlying the regulation of *JUN* and *TIFA* levels by ORF57 remain unclear, these effects once again suggest the virus modulates the levels of several m^{6}A modified mRNAs to support lytic replication.

Although a large variation in the abundance of differentially m^{6}A-modified transcripts was observed during KSHV reactivation, when examined at the protein level these changes appeared entirely consistent with changes in mRNA. While this does not preclude the m^{6}A modification of these transcripts might affect their translation, it seems unlikely that the rate of protein synthesis is altered among these mRNAs during reactivation. Similarly, among the transcripts examined with m^{6}A sites located near splice junctions, almost no change in the ratios of their different splice variants could be observed. However, subtle

changes were observed in the N/C ratio of differentially modified transcripts which might indicate altered nuclear export. Interestingly, among the methylated cellular transcripts tested, those upregulated during reactivation including *GPRC5A, FOSB, STC1 and ZFP36L1* and *JUN* tended towards a lower N/C ratio. This might indicate that these transcripts are prioritised for export during lytic replication, perhaps in an m^6A dependent manner. In addition, though the study of RNA stability was skewed for several transcripts by actinomycin-D stress induced spontaneous reactivation, an increase in the stability of the mRNAs *STC1, GPRC5A* and *TIFA* was identified suggesting that these transcripts become more stable in lytic replication. Thus, these data may in part explain the large increase in abundance of *STC1* and *GPRC5A* in the lytic phase. Taken together, these data suggest that several differentially modified transcripts which are upregulated during lytic replication also display enhanced stability and nuclear export. Importantly, the m^6A modification of these residues may be important to enact these changes and support or restrict the lytic replication of the virus.

While searching for transcripts with altered nuclear export profiles during reactivation, the mRNA *ZNF12* was found to have an extremely high N/C ratio, consistent with nuclear retention. The phenomenon allows the storage of critically important mRNAs in the nucleus to be exported under stress, infection or differentiation to regulate these processes (Wegener and Müller-McNicoll, 2018). Unfortunately however, the nuclear retention of *ZNF12* was neither unique to lytic, latent, nor uninfected cells of a different cell type. Therefore, while the rapid efflux of *ZNF12* to the cytoplasm may nevertheless play an important role under certain cellular contexts it seems unlikely that this interesting mechanism is relevant to KSHV infection.

After screening differentially modified cellular transcripts for changes in mRNA biology, a subset became heavily upregulated in the lytic phase. Interestingly, the increase in abundance of *GPRC5A, FOSB, STC1* and *ZFP36L1* could be dampened or enhanced through the depletion of members of the m^6A machinery (Figure 4.14). Like previous studies, the knockdown of an m^6A writer complex component and an m^6A reader produced similar effects on this set of transcripts (Lichinchi, Zhao, et al., 2016; Courtney et al., 2017; K Tsai et al., 2018). Although the activity of FTO towards m^6A is disputed, the protein's depletion enhanced the upregulation of *GPRC5A* providing further evidence the transcript has an m^6A, or potentially m^6A_m residue important for its abundance. While in some cases the depletion

of WTAP, FTO or DF1 produced only modest effects on mRNA abundance, any greater effect may be partially recovered through the redundant action of other m^{6}A machinery components (Lesbirel et al., 2018). Thus, the combinatorial knockdown of different members of the m^{6}A machinery may produce a larger effect on the four methylated transcripts. Combining the results of these depletion experiments with those focusing of mRNA stability, the changes in abundance of *GPRC5A, FOSB, STC1,* and *ZFP36L1* seen between latent and lytic replication programmes may be greatly influenced by m^{6}A-dependent changes in stability. However, while these experiments allude to m^{6}A-mediated alterations in these four transcripts, it remains unknown whether these effects are achieved through direct or indirect means. Furthermore, all four transcripts have more than one m^{6}A site; therefore, it remains unclear if one or multiple m^{6}A sites are important for mRNA abundance. As a result, further work is required, on a site-specific basis, to determine whether m^{6}A acts *in cis* to regulate the stability of these transcripts. Nevertheless, if these transcripts are important for KSHV lytic replication, the targeting of their internal m^{6}A residues may hold therapeutic potential as an antiviral treatment method.

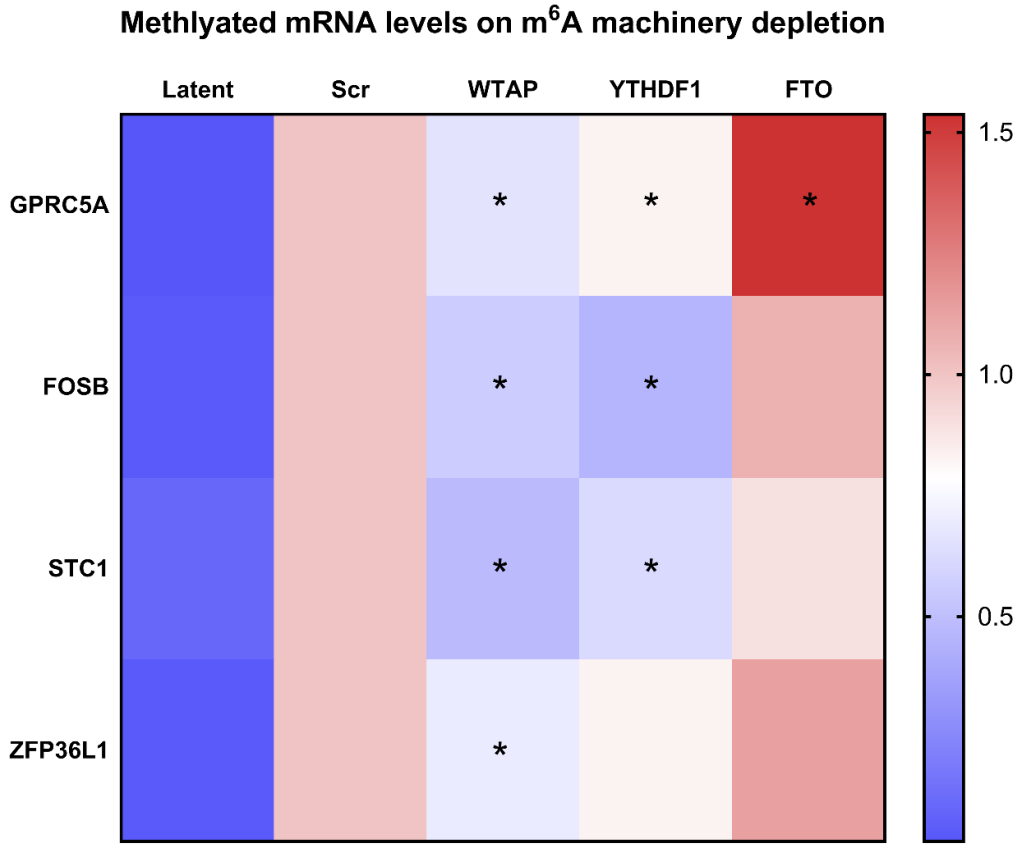

Figure 4.14. Summary of m^{6}A machinery depletion. Heat map summarises the data gathered in this chapter into depletion of the m^{6}A machinery and the effect on *GPRC5A, FOSB, STC1* and *ZFP36L1* mRNAs. Figure generated using the software GraphPad Prism 7. Data is relative to Scr lytic mRNA levels of each mRNA and asterisks denote statistical significance.

The experiments in this chapter have highlighted the mRNAs *GPRC5A, FOSB, STC1* and *ZFP36L1* as upregulated during KSHV reactivation, potentially post-transcriptionally regulated by m^{6}A and perhaps important for lytic replication. The four transcripts all encode proteins, with interesting cellular functions, which could conceivably be important in KSHV infection. GPRC5A is a membrane-bound G-protein coupled receptor implicated in a vast number of cancers and regulates oncogenic signalling pathways such as STAT-3 and EGFR (Yang et al., 2016; S. Liu et al., 2017). Additionally, STC1 is a secreted glycoprotein which activates several cellular signalling pathways including JNK and AP-1 and serves as a non-canonical Notch ligand that is dysregulated in a wide range of cancers (Chan et al., 2017; Leung and Wong, 2018; Li et al., 2018). Finally, FOSB is a member of the heterodimeric AP-1 transcription factor complex which binds to promoters of genes involved in cell differentiation, proliferation and apoptosis by modulating the expression of various cell cycle proteins (Cohen et al., 2006; Gazon et al., 2018). Importantly, many of the numerous

cellular signalling pathways influenced by these three proteins are implicated in KSHV-mediated tumorigenesis and cell hijack (Wen and Damania, 2010; Manners et al., 2018). As a result, in KSHV-infected individuals, ectopic expression of these oncoproteins beyond normal levels could transform cells into a state permissive to KSHV replication and drive tumourigenesis.

Unlike the other three transcripts whose increased abundance is m^6A dependent, *ZFP36L1* encodes an RNA binding protein which binds mRNAs with AU rich elements in their 3' UTRs (Adachi et al., 2014). Some studies have suggested ZFP36L1 is important the decay of these transcripts through recruitment of the CCR4-NOT deadenylase complex (Adachi et al., 2014; Zekavati et al., 2014). More recently however, one group has proposed that ZFP36L1 enriches AU-rich containing transcripts within a membraneless organelle interspersed within the endoplasmic reticulum (ER) (Ma and Mayr, 2018). As a result, these mRNAs undergo localised translation and proteins are synthesised exactly where they are required by the cell. Importantly, AU-rich mRNAs are spared from host cell shutoff by KSHV as they encode proto-oncogenes, cytokines and growth factors important for cell hijack and tumourigenesis. As a result, ZFP36L1 could play an important role in the regulation of KSHV replication through the processing of its target AU-rich mRNAs.

Chapter 5

~

The m^{6}A-modified cellular mRNAs *GPRC5A* and *ZFP36L1* encode proteins required for efficient KSHV lytic reactivation

5 The m^{6}A-modified cellular mRNAs *GPRC5A* and *ZFP36L1* encode proteins required for efficient KSHV lytic reactivation

5.1 Introduction

In the previous chapter, m^{6}A-modified cellular transcripts were screened for m^{6}A-dependent changes in mRNA transcription, splicing, export and decay during KSHV lytic reactivation. Four of these transcripts, *GPRC5A*, *FOSB*, *STC1* and *ZFP36L1* were heavily upregulated in the lytic phase; an effect which could be either diminished or enhanced through the depletion of various components of the m^{6}A machinery. Results suggested that the changes in expression levels might be due to a role for m^{6}A in the regulation of stability among these transcripts. However, all mRNAs were exported more efficiently during lytic replication which may also help to increase the functional levels of these transcripts in the lytic phase.

The mRNAs *GPRC5A*, *FOSB*, *STC1* and *ZFP36L1* all encode proteins which could conceivably play key roles in KSHV lytic replication and functionally cluster into pathways which are known to be modulated by KSHV infection. Previous studies have shown that GPRC5A, STC1 and FOSB influence many cellular signalling pathways, especially those associated with oncogenesis (Yang et al., 2016; S. Liu et al., 2017; Chan et al., 2017; Gazon et al., 2018; Leung and Wong, 2018). In addition, ZFP36L1 is an RNA binding protein whose AU-rich target mRNAs are critical for KSHV infection (Corcoran et al., 2012; Ma and Mayr, 2018). Interestingly, *GPRC5A* and *ZFP36L1* are directly upregulated by the KSHV lytic master regulator protein RTA through transcriptional induction. Therefore, we hypothesise these transcripts are likely to encode proteins which aid in KSHV lytic replication.

In this chapter, GPRC5A and ZFP36L1 proteins are given special focus to elucidate their function within the cell and determine whether they are important for KSHV lytic replication. The indications of previous experiments are confirmed as both proteins prove crucial for expression of viral genes and the production of infectious virus particles. Furthermore, GPRC5A is found to interact with members of the flotillin and voltage dependent anion channel families almost exclusively in lytic cells alluding to a potential mechanism through which the protein influences lytic replication. Finally, ZPF36L1 is shown

to localise to the endoplasmic reticulum where it regulates the stability and localisation of AU-rich mRNAs and their encoded protein products, perhaps to potentiate lytic replication.

5.2 GPRC5A is important for KSHV lytic replication

As *GPRC5A* expression is heavily upregulated during reactivation in an RTA-dependent manner, the protein could play an important role in lytic replication. To determine whether GPRC5A affects viral gene expression, the protein was depleted in TREX cells using targeted shRNAs (Figure 5.1a). Although in latent cells 40-60% of the prevailing low level of *GPRC5A* mRNA remained in the presence of a specific shRNA, the abundance of this transcript fell to just 20% of the substantially elevated level in reactivated scrambled shRNA-treated control cells. Next, GPRC5A-depleted cells were examined for alterations in the expression of lytic mRNA and protein levels (Figure 5.1b-d). Interestingly, the depletion of GPRC5A led to a drop in viral ORF57 mRNA (20-30%) and protein levels. This inhibition was even more dramatic in reducing late viral mRNA *ORF47* (30-40%) and ORF65 protein levels, suggesting a cumulative inhibition of the lytic cycle. Finally, a reinfection assay was undertaken to assess the ability of KSHV to produce infectious virus particles in GPRC5A-depleted cells. Notably, a 40-60% reduction in infectious virus produced was observed, measured by *ORF57* RNA levels in 293T cells following reinfection with virus produced in GPRC5A-deficient TREX cells (Figure 5.1f). Thus, these results strongly suggest that GPRC5A is important KSHV lytic replication.

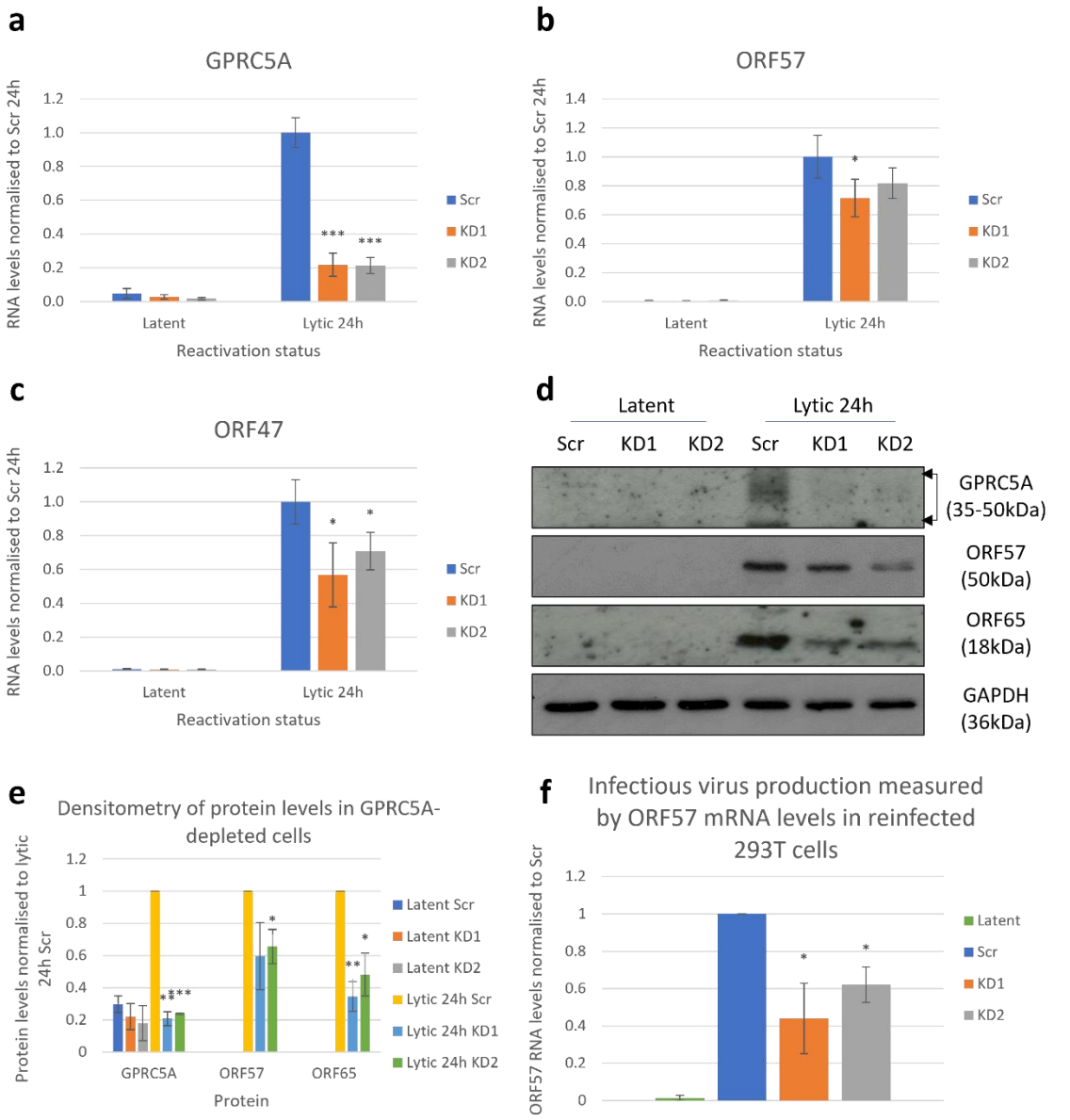

Figure 5.1. GPRC5A is required for KSHV lytic replication. GPRC5A was depleted using 2 shRNAs and the impact upon viral reactivation assessed by RT-qPCR, western blotting and a reinfection assay. (a-c) The RNA levels of *GPRC5A* (a), *ORF57* (b) and *ORF47* (c) were measured by RT-qPCR in latent and lytic GPRC5A-depleted TREX cells (data presented as mean ± SD, n=3). d) Protein levels of GPRC5A, ORF57 and ORF65 were measured by western blot in GPRC5A-deficient TREX cells undergoing latent or lytic replication (blots representative of 3 biological repeats). e) Densitometry of western blot in d). f) GPRC5A-depleted TREX cells were reactivated for 72 hours and viral supernatant harvested for reinfection of 293T cells. After 48 hours of reinfection, *ORF57* levels were assayed by RT-qPCR (data presented as mean ± SD, n=3).

5.3 GPRC5A localises to the cellular membrane

GPRC5A is a member of the G-protein coupled receptor family which become embedded into the cell membrane and respond to external stimuli by activating intracellular signalling (Zhou and Rigoutsos, 2014). Despite this, immunofluorescence data in the Human Protein

Atlas suggests that GPRC5A can also be detected in the cytoplasm by immunofluorescence indicating the protein may reside in other subcellular compartments (Thul et al., 2017). To precisely determine the subcellular localisation of GPRC5A in B-cells during KSHV reactivation, the cDNA was cloned into a pLENTI-CMV-GFP fusion vector. The construct, as well as its parental control vector, was then transduced into TREX cells and GFP or GPRC5A-GFP expression visualised in both latent and lytic cells using confocal microscopy (Figure 5.2a, b). While GFP alone was detected ubiquitously within the cell, most GPRC5A-GFP fluorescence was detected at the cell periphery, confirming the protein is mostly localised to the plasma membrane. However, in some cells, especially those expressing higher levels of the fusion protein, small deposits of peri-nuclear cytoplasmic fluorescence were identified. It is not entirely clear whether these cytoplasmic pools of GPRC5A-GFP are genuine areas to which the protein localises or artefacts of overexpression. Nevertheless, given that GPRC5A-GFP fluorescence was primarily located at the cell periphery, the protein mostly localises to the plasma membrane.

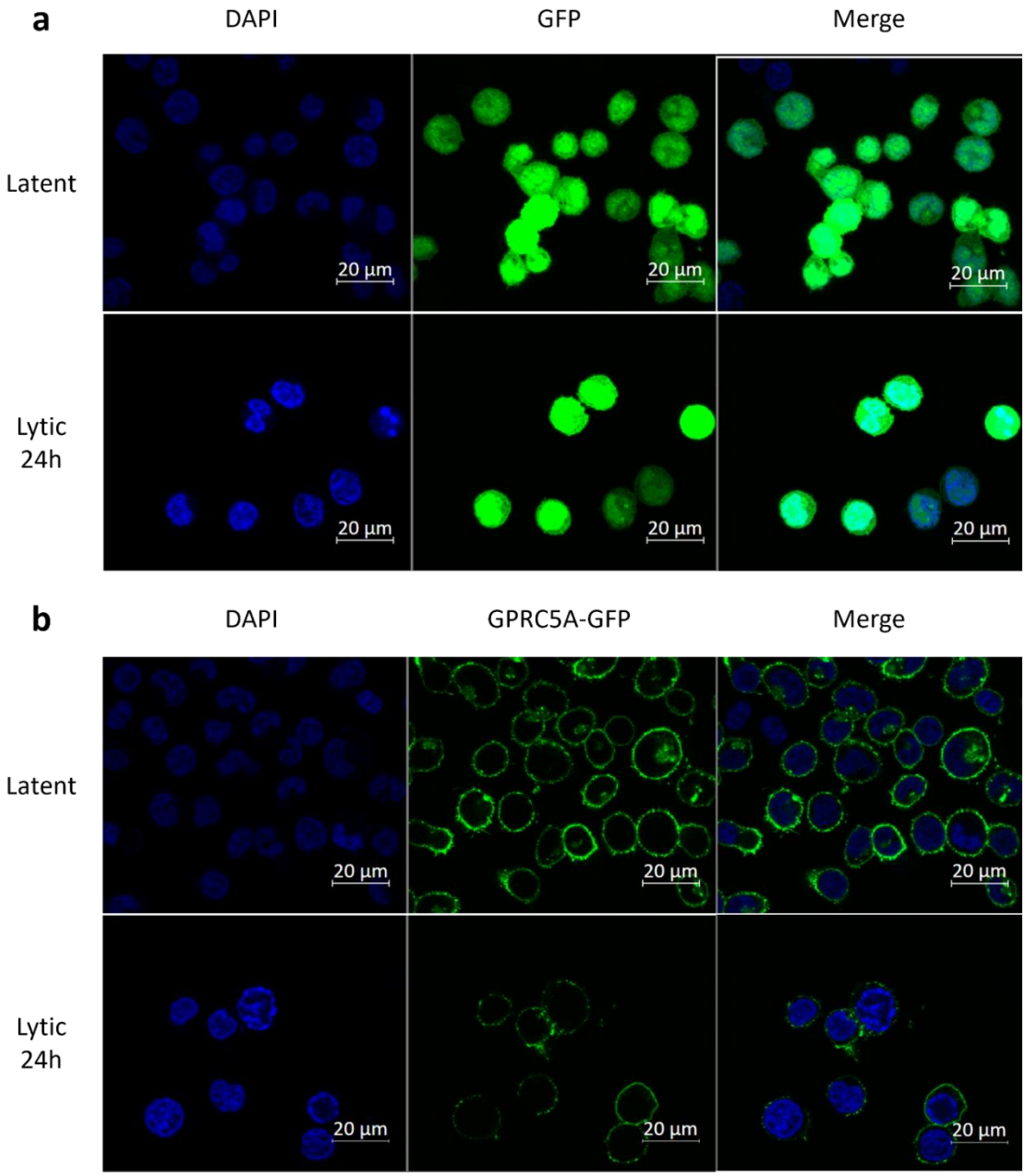

Figure 5.2. GPRC5A localises to the cell membrane. TREX cells were transduced with constructs containing (a) *GFP* or (b) *GPRC5A-GFP* genes under the control of a constitutive cytomegalovirus (CMV) promoter and fluorescence among latent and lytic cells visualised using a confocal microscope (images representative of 3 biological repeats).

5.4 GPRC5A interacts with members of the flotillin and voltage dependent anion channel families

Despite a multitude of reports attesting to the importance of GPRC5A dysregulation in cancer and other diseases, very little is known about the precise molecular function of this protein. To better understand the role of GPRC5A and its function within KSHV reactivation,

a global quantitative proteomic analysis was carried out to identify interactors with the protein in both latent and lytic cells. The coding sequence of *GPRC5A* was cloned into a modified pLENTI-CMV-GFP vector, with the internal GFP gene substituted for a 3' FLAG tag, to create a pLENTI-CMV-GPRC5A-FLAG construct. The plasmid was then transduced into TREX cells to create a stable cell line expressing FLAG-tagged GPRC5A. Immunoprecipitations with FLAG antibody were performed in latent and lytic TREX or GPRC5A-FLAG-TREX cells. Successful pulldown of GPRC5A-FLAG was confirmed by western blotting which showed an enrichment of GPRC5A-FLAG in TREX-GPRC5A-FLAG cell immunoprecipitations but not in parental TREX cell immunoprecipitations when a FLAG antibody was used for immunoprecipitation (Figure 5.3a). Furthermore much higher levels of GPRC5A-FLAG protein was immunoprecipitated when using a FLAG antibody rather than an IgG antibody for immunoprecipitation. To identify co-precipitated proteins in complex with GPRC5A-FLAG, two biological replicates were sent to the the University of Bristol proteomics facility for tandem mass tagging (TMT) coupled with liquid chromatography and mass spectrometry analysis (LC-MS/MS). The strongest interactors were identified based on enrichment relative to parental TREX cells not expressing FLAG-tagged GPRC5A (Figure 5.3c). Among both latent and lytic cells, a number of membrane proteins were identified supporting previous experiments which show that GPRC5A functions at the cell membrane (Figure 5.3d, e). Proteins which had an enriched interaction with GPRC5A in the lytic phase compared to latency were prioritised for investigation as these may be critical for the function of GPRC5A during KSHV lytic replication. Among the 25 proteins that fulfilled this criterion, both members of the flotillin family and all 3 members of the voltage-dependent anion (VDAC) family were present (Figure 5.3f). FLOT1 and FLOT2 were identified at 4-fold and 27-fold higher levels in the lytic phase respectively whereas VDAC1, VDAC2 and VDAC3 all showed no interaction with GPRC5A in latency despite a strong interaction during the lytic cycle. As a result, the interaction of GPRC5A with flotillin and VDAC proteins may be important for GPRC5A function within KSHV lytic replication.

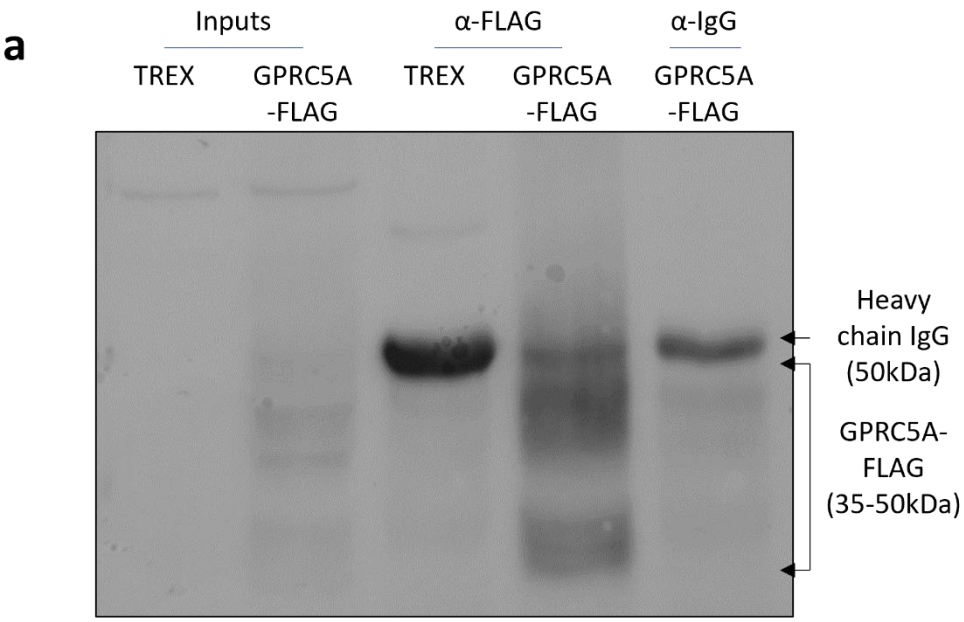
a
Inputs
α-FLAG
α-IgG
TREX
GPRC5A -FLAG
TREX
GPRC5A -FLAG
GPRC5A -FLAG
Heavy chain IgG (50kDa)
GPRC5A-FLAG (35-50kDa)

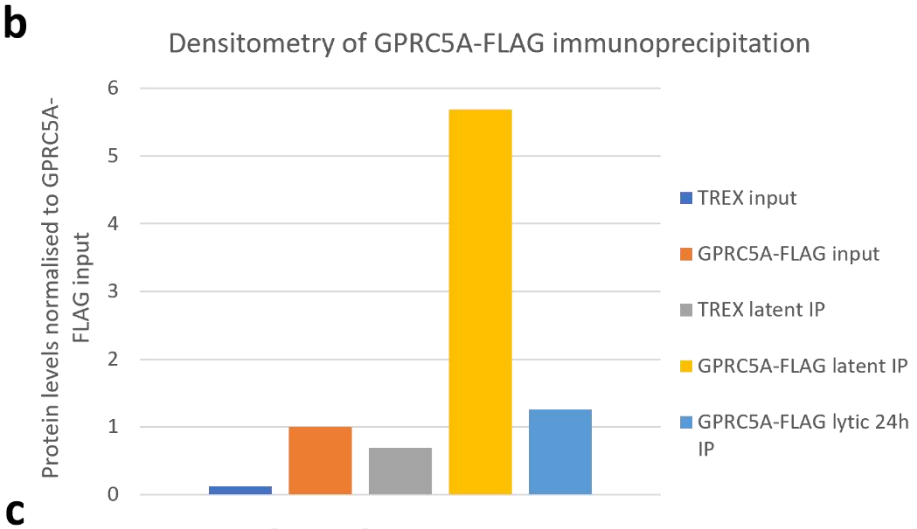
b
Densitometry of GPRC5A-FLAG immunoprecipitation
Protein levels normalised to GPRC5A-FLAG input
0
1
2
3
4
5
6
TREX input
GPRC5A-FLAG input
TREX latent IP
GPRC5A-FLAG latent IP
GPRC5A-FLAG lytic 24h IP

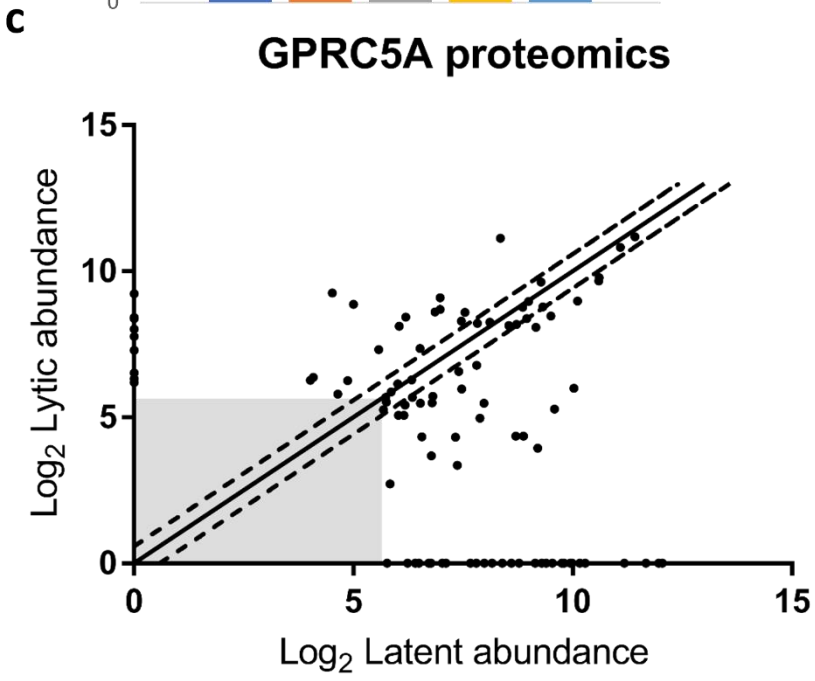
c
GPRC5A proteomics
Log2 Lytic abundance
Log2 Latent abundance
0
5
10
15

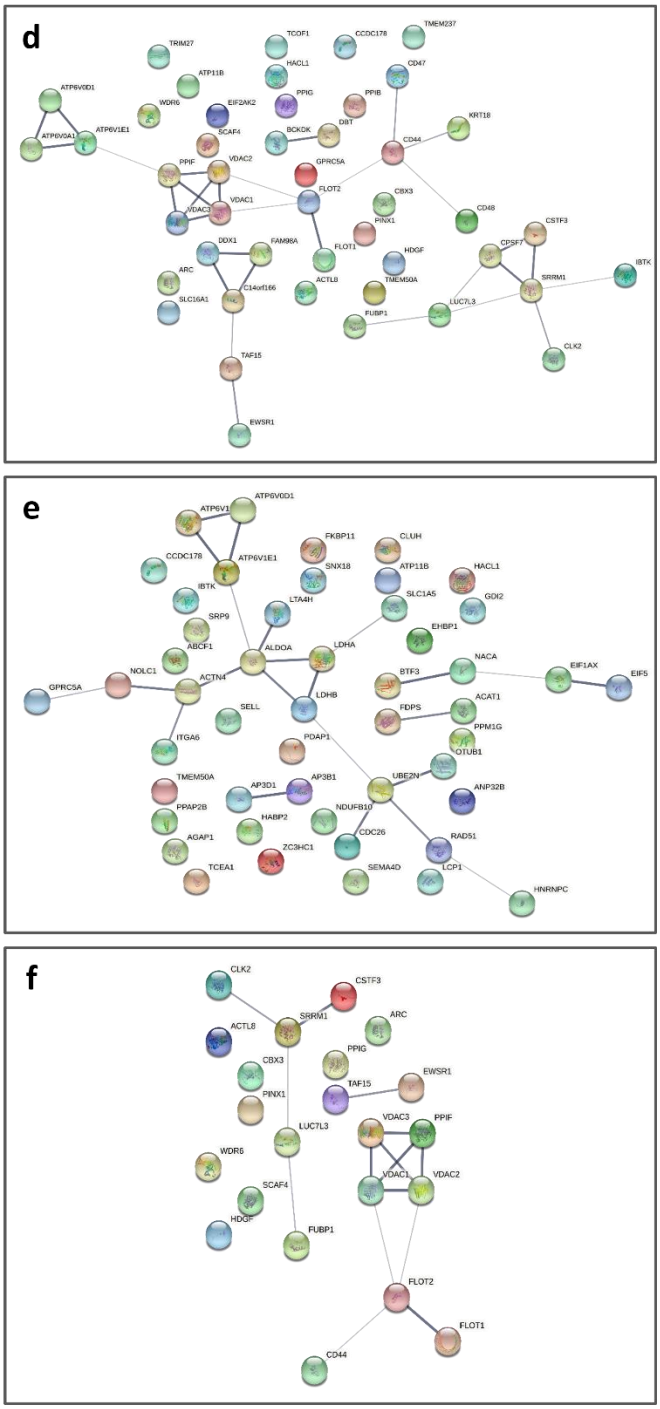

Figure 5.3. Characterisation of GPRC5A interactors in latent and lytic cells by quantitative proteomics. a) Western blot showing the successful immunoprecipitation of GPRC5A-FLAG using an anti-FLAG antibody (blot representative of 1 biological replicate. b) Densitometry of western blot in a). c) Top interactors with GPRC5A after the implementation of stringent cut-offs. Data points outside the dashed lines are enriched by more than 1.4-fold in latent or lytic replication, while those that lie on either axis exclusively interact with GPRC5A in either latent (x-axis) or lytic (y-axis) replication. Data inside the grey box does not meet the minimum required abundance threshold of 50. (d-f) String protein interaction maps displaying the most enriched GPRC5A-interactors in (d) latent or (e) lytic cells and those that associate with GPRC5A more (>1.4-fold) in the lytic phase (f). Weight of line indicates confidence of interaction.

5.5 Flotillin and VDAC proteins may colocalise with GPRC5A

As GPRC5A appears to interact with members of the Flotillin and VDAC families, the proteins should localise to the plasma membrane or similar subcellular compartments. To examine the localisation of these proteins, FLOT1 and VDAC1 were visualised by immunofluorescence in latent and lytic TREX cells. Interestingly, FLOT1 was primarily concentrated in the cytoplasm around the cell periphery indicating that the protein mostly localises to the plasma membrane (Figure 5.4a). However, this localisation did not appear to change between latent and lytic cells. Immunofluorescent staining of VDAC1 protein in TREX cells identified many discrete spots in both latent and lytic cells, some of which was present in the vicinity of the plasma membrane (Figure 5.4b). Thus, it appears both FLOT1 and VDAC1 are not plasma membrane-exclusive proteins but may localise transiently or partly to these regions under certain cellular contexts and perhaps interact with GPRC5A.

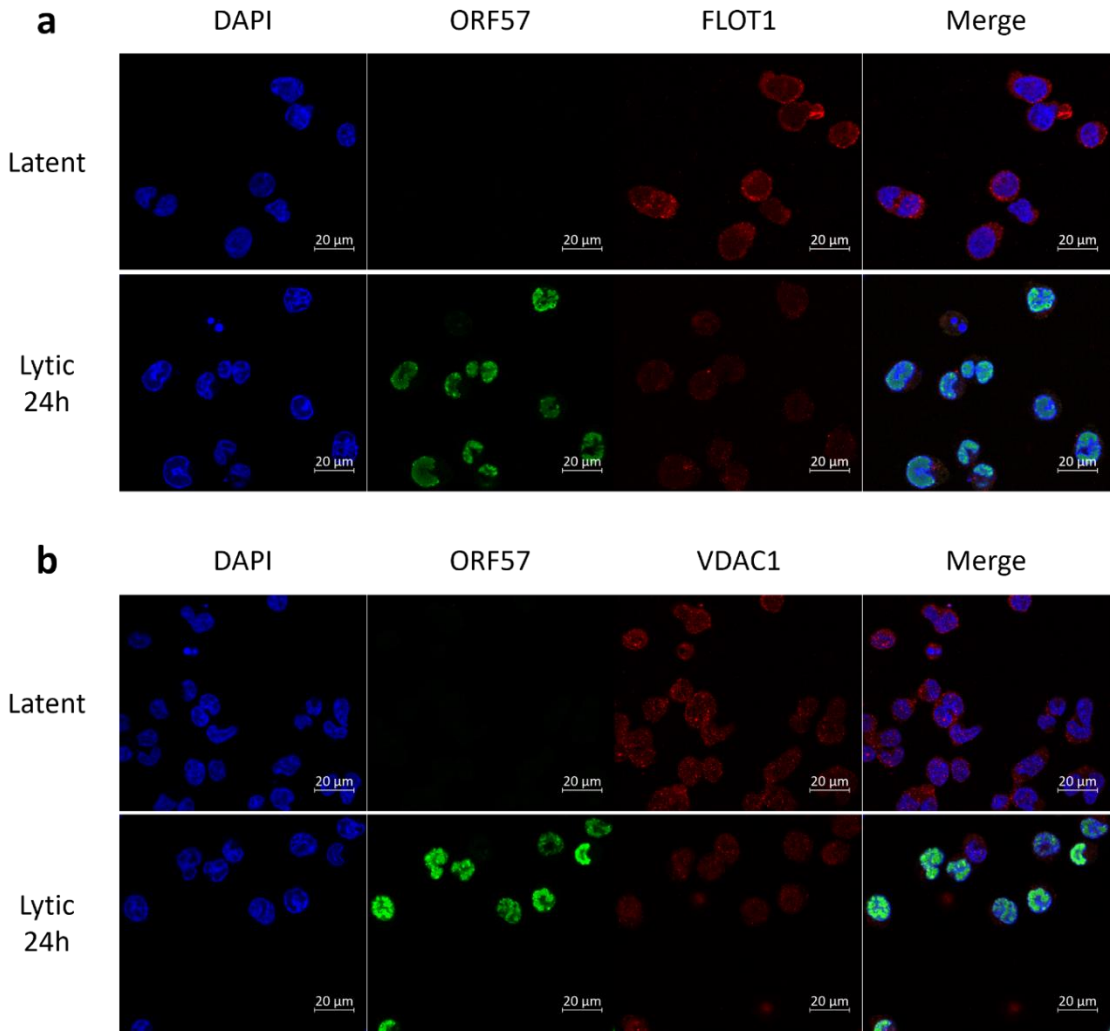

Figure 5.4. Immunofluorescence of FLOT1 and VDAC1 proteins. TREX cells undergoing latent or lytic replication were coimmunostained with ORF57 and FLOT1 (a) or VDAC1 (b) antibodies and viewed on a confocal microscope (Images representative of 1 biological repeat).

Since the subcellular localisation of FLOT1 and VDAC1 was not restricted to the cell membrane and thus the colocalization with GPRC5A not entirely clear, the localisation of these putative interactors was studied in GPRC5A-GFP-expressing cells. Once again, FLOT1 appeared to localise to the cell membrane and was detected in the vicinity of GPRC5A-GFP (Figure 5.5). However, VDAC1 immunostaining was more concentrated within cytoplasmic compartments and while the protein's localisation permits overlaps with GPRC5A, VDAC1 does not preferentially localise to areas of GPRC5A overexpression (Figure 5.6). Thus, these data suggests that FLOT1 is expressed in the vicinity of GPRC5A at the cell membrane whilst VDAC1 is located mostly elsewhere within the cytoplasm. Nevertheless, both VDAC1 and FLOT1 have the potential to interact with GPRC5A in lytic cells as suggested by proteomic analysis.

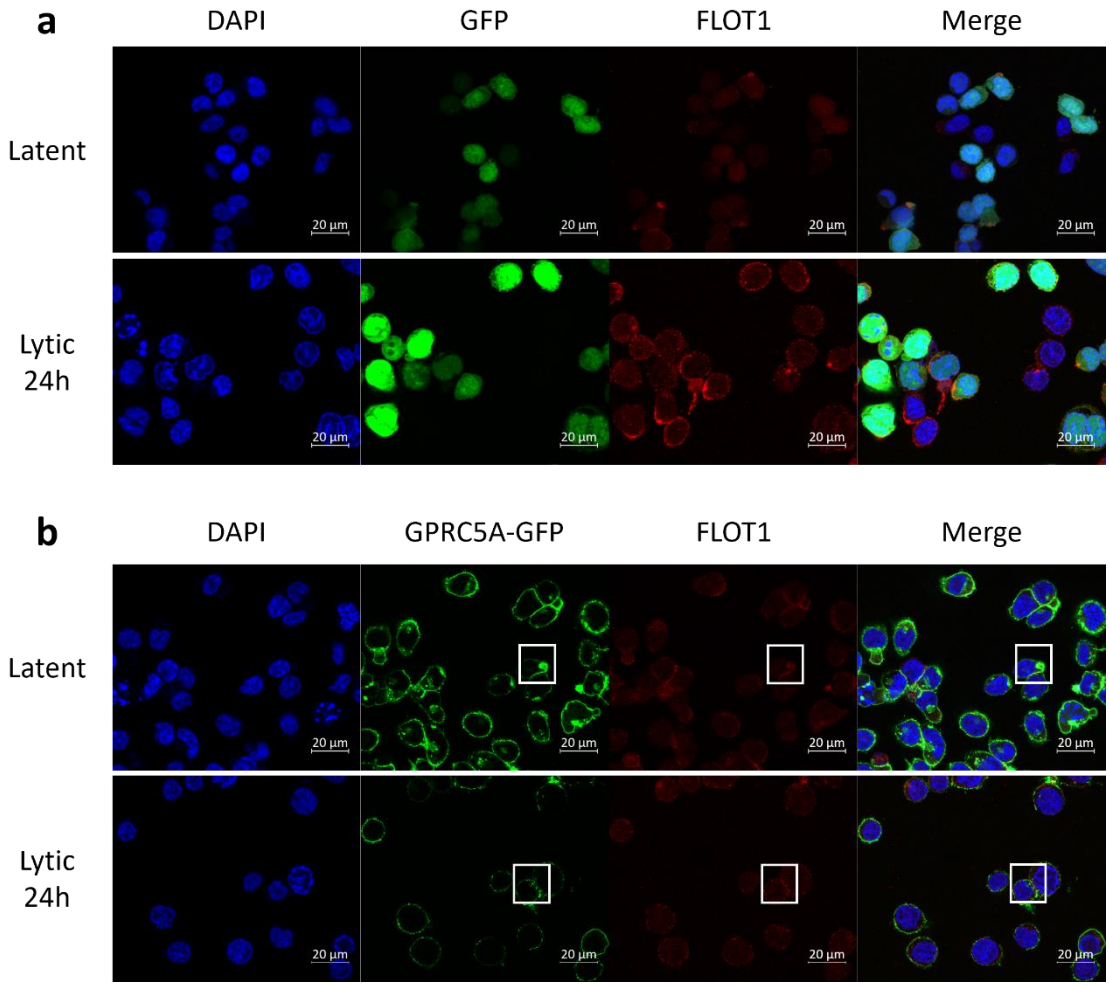

Figure 5.5. GPRC5A and FLOT1 colocalise at the cell membrane. Latent and lytic TREX cells were transduced with GFP or GPRC5A-GFP-expressing constructs and immunostained with FLOT1 antibody. Fluorescence was visualised and images collected on an LSM880 confocal microscope (Images representative of 1 biological repeat).

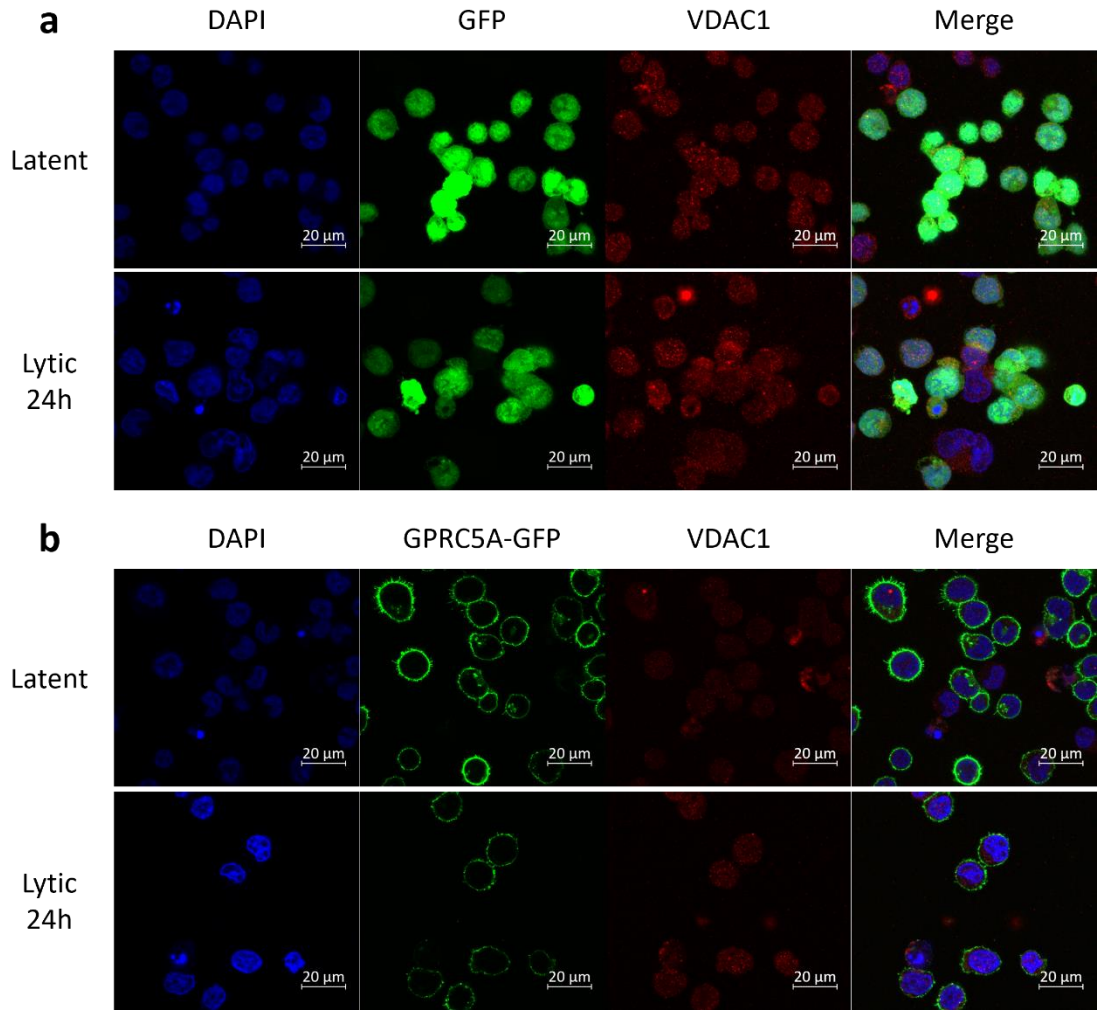

Figure 5.6. VDAC1 immunostaining is most concentrated in cytoplasmic compartments outside of GPRC5A expression. GFP or GPRC5A-GFP-expressing cells undergoing latent or lytic replication were immunostained with VDAC1 antibody and fluorescent images collected using an LSM880 confocal microscope (Images representative of 1 biological repeat).

5.6 Flotillin and VDAC family proteins are increased in expression during KSHV lytic replication

Given that *FLOT1, FLOT2* and *VDAC1-3* encode proteins which heavily favour interactions with GPRC5A in the lytic phase of the KSHV life cycle, their expression was monitored during KSHV reactivation for changes which might indicate a functional role. mRNA and protein levels were examined in latent and lytic TREX cells by RT-qPCR and western blotting respectively. Except for *FLOT1* and *VDAC1* which decreased in abundance, there were minimal changes in the mRNA levels of *FLOT2, VDAC2* and *VDAC3* (Figure 5.7a). In contrast however, an increase in FLOT1, FLOT2 and VDAC1 protein levels was observed in lytic

replication suggesting these proteins may be upregulated through a post-transcriptional or post-translational mechanism during reactivation (Figure 5.7b).

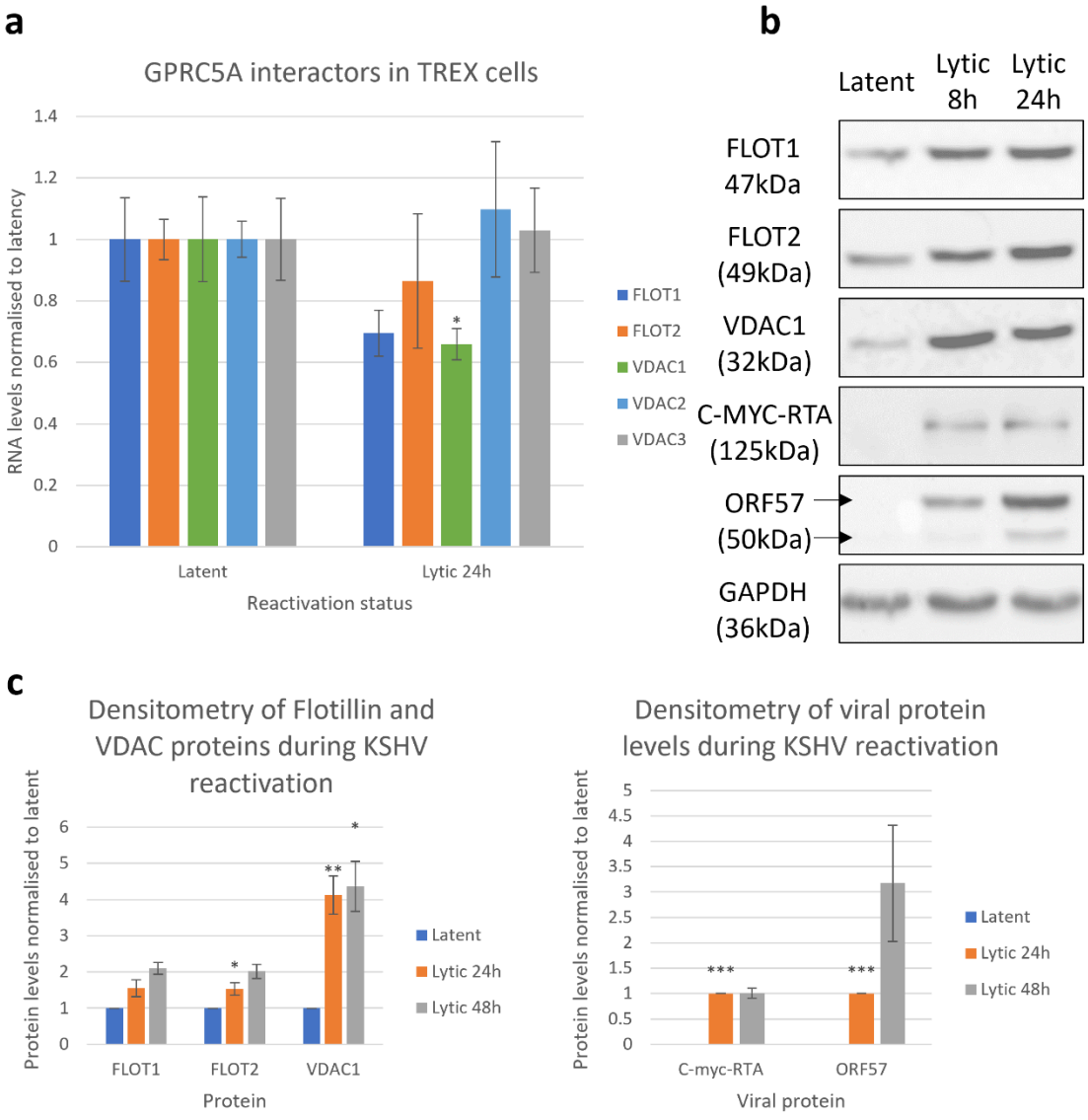

Figure 5.7. Flotillin and VDAC genes are upregulated at protein, but not mRNA, levels. a) RT-qPCR data showing the fold change in levels of flotillin and VDAC mRNAs during reactivation (data presented as mean ± SD, n=3). b) Western blot data showing FLOT1, FLOT2 and VDAC1 protein levels in latent TREX cells and at 8 and 24 hours following the induction of lytic replication (blots representative of 3 biological repeats). c) Densitometry of western blot in b).

5.7 ZFP36L1 is important for KSHV replication

Given the RTA-mediated upregulation of ZFP36L1 during KSHV lytic replication and its previously described targeting of AU-rich elements, which are fundamentally important for reactivation, ZFP36L1 could potentially play an essential role in the KSHV life cycle. To test

this hypothesis, ZFP36L1 was depleted using lentivirus-mediated shRNA delivery and knockdown assessed by comparison with a scrambled shRNA-treated cell line. After confirmation of a 50-65% reduction in *ZFP36L1* levels in two different shRNA-treated cell lines, the expression of lytic mRNAs was assessed during reactivation by RT-qPCR. A consistent 20-35% decrease in the expression of *ORF57* and *ORF47* was identified suggesting that ZFP36L1 is important for lytic replication. Supporting this hypothesis, a ~50% reduction in infectious virion production was observed, as measured by *ORF57* RNA levels after reinfection of 293T cells, in ZFP36L1-deficient TREX cells. Therefore, the results suggest that ZPF36L1 contributes to the efficient production of lytic mRNAs and infectious virus particles during KSHV lytic replication.

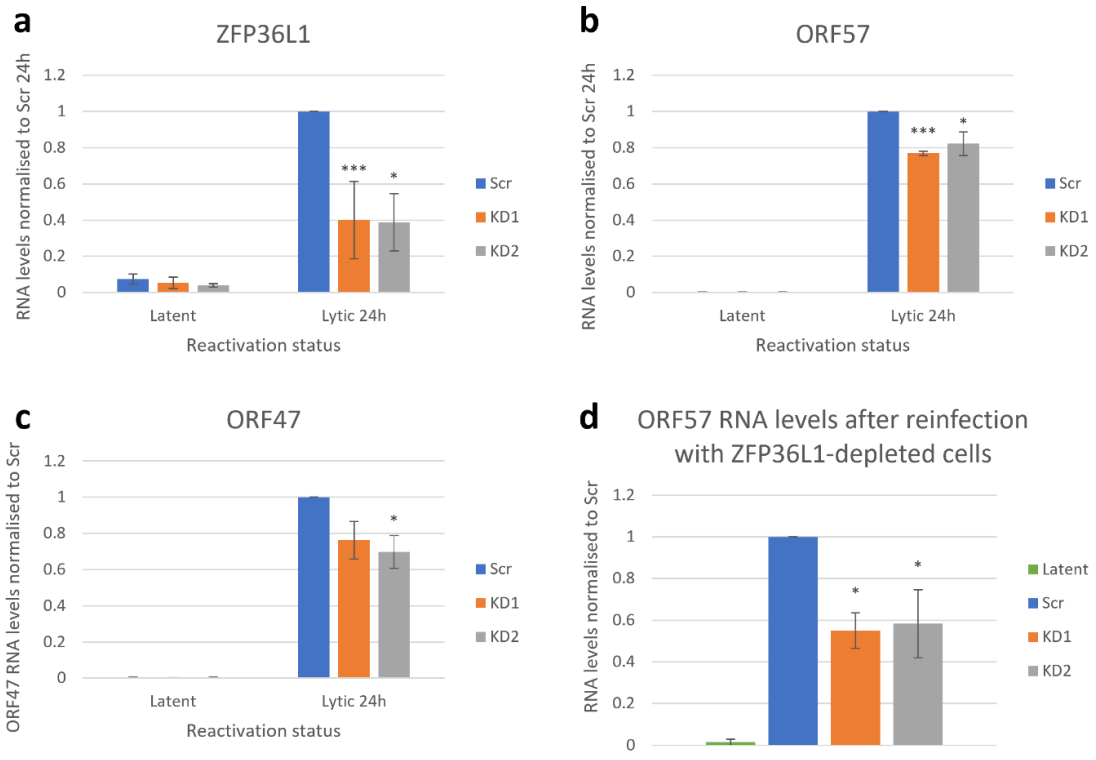

Figure 5.8. ZFP36L1 depletion affects the abundance of KSHV lytic mRNAs. ZFP36L1 was depleted using 2 shRNAs and the RNA levels of *ZFP36L1* (a), *ORF57* (b) and *ORF47* (c) measured by RT-qPCR in latent and lytic TREX cells (data presented as mean ± SD, n=3). d) RT-qPCR analysis of *ORF57* levels in 293T cells reinfected with virus produced in ZFP36L1-deficient TREX (data presented as mean ± SD, n=3).

5.8 ZFP36L1 forms ER-associated granules

Previous reports have suggested various functions of ZFP36L1, with some studies suggesting the protein is involved in mRNA decay; however, more recently, a report has suggested that ZFP36L1 forms ER-associated granule structures which enrich specific AU-rich mRNAs and RNA binding proteins to allow for localised translation (Adachi et al., 2014; Ma and Mayr, 2018). To identify whether ZFP36L1 forms ER-associated granules, cells were immunostained with a ZFP36L1-specific antibody and visualised using confocal microscopy (Figure 5.9a). Supporting our previous immunoblotting evidence that ZFP36L1 expression is upregulated during lytic replication, immunofluorescence staining also shows a clear increase in ZFP36L1 protein levels in cells undergoing lytic replication (indicated by ORF57 protein expression). Furthermore, while some diffusely cytoplasmic ZFP36L1 was detected, most of the protein formed perinuclear assemblies as would be expected for an ER-associated protein. Nevertheless, to confirm the localisation, cells were once again visualised after coimmunostaining with ZFP36L1 and Calnexin antibodies (Figure 5.9b). Interestingly, a line profile analysis shows colocalization of ZFP36L1 with the ER marker protein confirming the association of ZFP36L1 with this subcellular structure (Figure 5.9c).

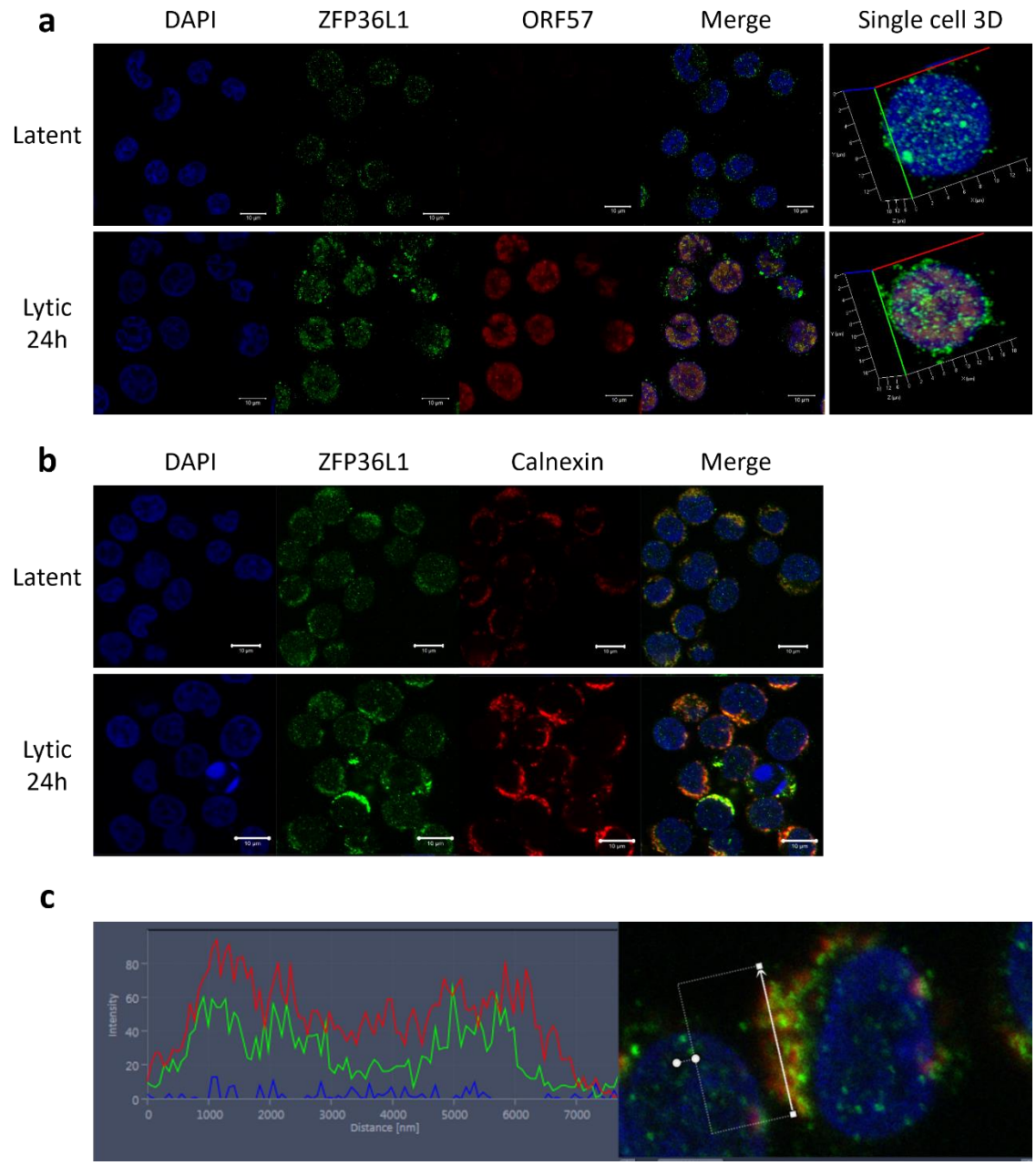

Figure 5.9. ZFP36L1 forms granule structures at the endoplasmic reticulum. a, b) Latent and lytic TREX cells were coimmunostained with ZFP36L1 and ORF57 (a) or Calnexin (b) antibodies and viewed on a confocal microscope. c) Line profile analysis showing correlation between ZFP36L1 (green), Calnexin (red) and DAPI (blue) using Zen confocal software.

5.9 AU-rich mRNAs undergo changes in abundance during KSHV lytic replication

ZFP36L1 is an RNA-binding protein which targets AU-rich transcripts to alter their decay or localisation (Adachi et al., 2014; Ma and Mayr, 2018). We therefore hypothesised that the importance of ZFP36L1 in KSHV lytic replication is most likely due to its interaction with these AU-rich mRNAs. To determine the effect of ZFP36L1 on its target transcripts, five AU-rich mRNAs were selected which were bound by wild type, but not mutant, GST-tagged

ZFP36L1 in recently published RNA immunoprecipitation-sequencing data (Loh et al., 2020). Furthermore, a further two mRNAs which are reported as ZFP36L1 targets in other published literature were also examined (Ma and Mayr, 2018; Son et al., 2019). The transcripts were chosen to represent a broad range of downstream cellular pathways comprising inflammation, proliferation, angiogenesis and metabolism.

First, the expression of the seven AU-rich mRNAs, *E2F1, VEGFA, HIF1A, ELAV1, CDK2, HSPA1A* and *ENO2* was examined in TREX cells during KSHV reactivation as changes may indicate an important role in the viral life cycle (Figure 5.10a). RT-qPCR analysis of the transcripts in latent and lytic TREX cells identified the downregulation of two transcripts *E2F1* and *VEGFA* by approximately 30% and 50% respectively indicating these mRNAs are degraded by the viral endonuclease SOX or diminished by other host or viral mechanisms. *HIF1A, ELAV1* and *CDK2* showed little change in abundance whereas *HSPA1A* and *ENO2* mRNA levels in the lytic phase were 3-fold and 12-fold higher than in latency suggesting their encoded proteins may influence reactivation. While western blotting demonstrated that HSPA1A protein rose in accordance with mRNA in lytic replication, the striking change in *ENO2* mRNA was not correlated with a substantial change in ENO2 protein (Figure 5.10b). Therefore, it is unlikely that increased *ENO2* abundance effects any functional change in the activity of the gene and thus lytic replication.

Given the rise in *HSPA1A* and *ENO2* mRNA levels during lytic replication, these increases could be initiated by the viral proteins RTA or ORF57. To study this hypothesis, 293T cells were once again transfected with constructs expressing *GFP-ORF50* and *GFP-ORF57* and both *HSPA1A* and *ENO2* RNA levels compared with a GFP-transfected control by RT-qPCR (Figure 5.10d). *ENO2* mRNA was unchanged upon the ectopic expression of RTA or ORF57; however, *HSPA1A* levels declined when either viral protein was present. Therefore, this transcript appears to be upregulated in lytic TREX cells despite the inhibitory action of the two KSHV lytic proteins.

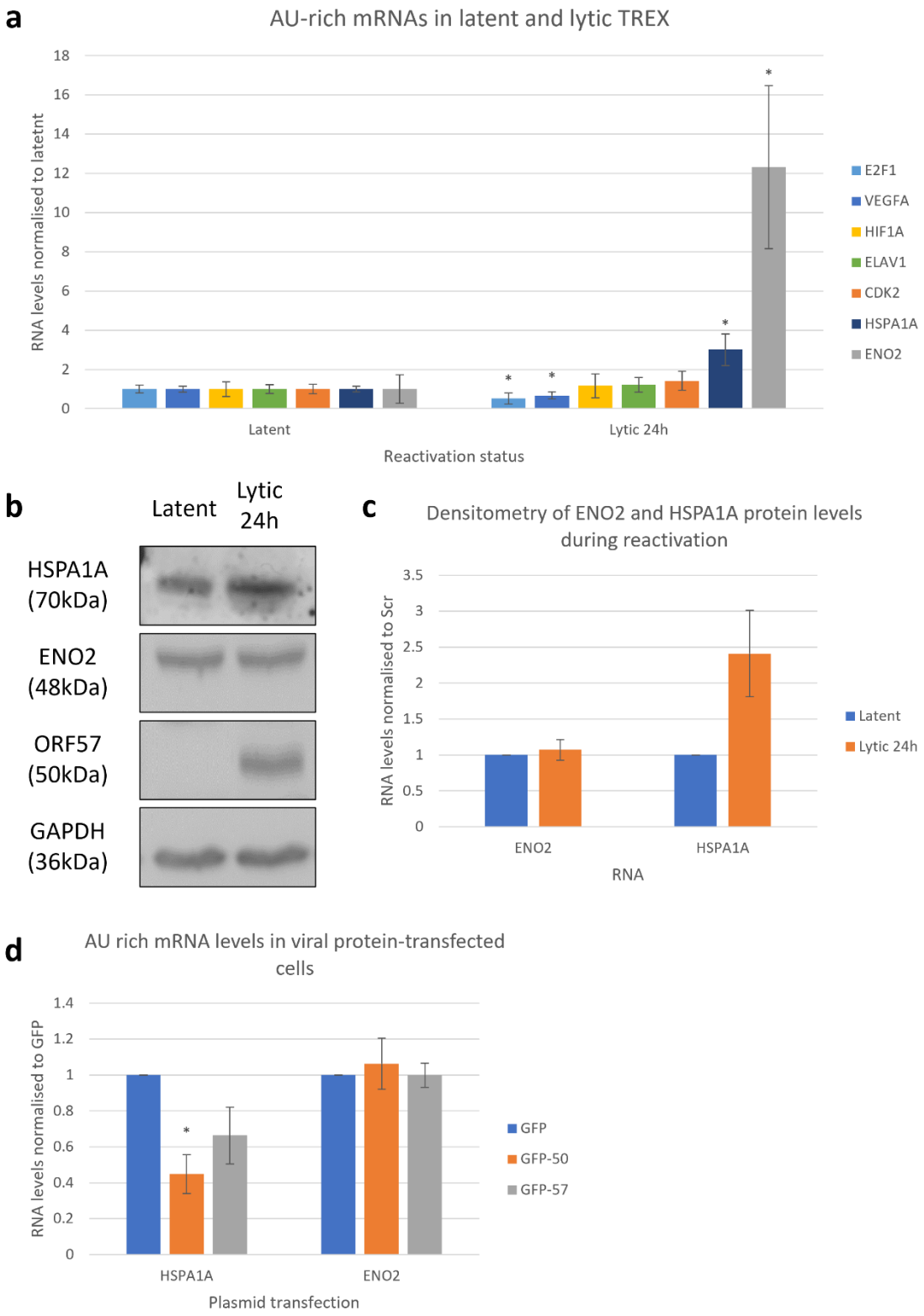

Figure 5.10. AU rich mRNAs are changed in expression during KSHV lytic replication. a) RT-qPCR showing the fold change in abundance of AU-rich transcripts between latency and lytic replication (data presented as mean ±SD, n=4). b) Western blots highlighting the levels of HSPA1A and ENO2 protein in latent and lytic TREX cells (blots representative of 2 biological repeats). c) Densitometry of western blot in b). d) RT-qPCR data demonstrating the RNA levels of the *HSPA1A* and *ENO2* transcripts in cells transfected with *GFP, GFP-ORF50* and *GFP-ORF57*-expressing constructs (data presented as mean ±SD, n=3).

5.10 ZFP36L1 regulates the levels of AU-rich mRNAs

Multiple reports attest to the role of ZFP36L1 in the targeting of AU-rich mRNAs towards decay pathways. Thus, if the activity of the RNA-binding protein is altered by overexpression or depletion, its downstream targets should become dysregulated. Firstly, to overexpress ZFP36L1, several plasmids expressing both tagged and unmodified ZFP36L1 were generated by cloning of the gene's coding sequence into a pLENTI-CMV-GFP construct. The plasmids expressing GFP-tagged, FLAG-tagged or unmodified ZFP36L1 were transfected into 293T cells alongside the parental GFP construct. ZFP36L1 overexpression was confirmed relative to GFP-control and untransfected cells by RT-qPCR analysis of *ZFP36L1* mRNA levels (Figure 5.11a). Next, AU-rich mRNA levels were monitored for changes following the transfection of the constructs (Figure 5.11b). While *VEGFA, ENO2* and *E2F1* all showed some evidence of diminished abundance in ZFP36L1-overexpressing cells, only *VEGFA* was exclusively downregulated by 25-40% in all 3 ZFP36L1-transfected cell populations and not in the 2 control cell populations. While the downregulation of *VEGFA* was only significant in the *ZFP36L1-GFP*-transfected cells, the protein may bind the transcript and reduced its stability. Curiously, a very large and unusual 4-fold increase in the levels of *HSPA1A* was observed exclusively in cells transfected with *ZFP36L1-GFP*. It is unclear why this dramatic change is unique to GFP-tagged ZFP36L1 overexpression cells and not other cell populations overexpressing the protein. However, it is likely the ectopic, GFP-tagging of ZFP36L1 alters its activity or interaction with other cellular factors to bring about this effect. Nevertheless, the increase in *HSPA1A* mRNA in ZFP36L1-GFP expressing cells may suggest the RNA-binding protein modulates this cellular transcript at some level.

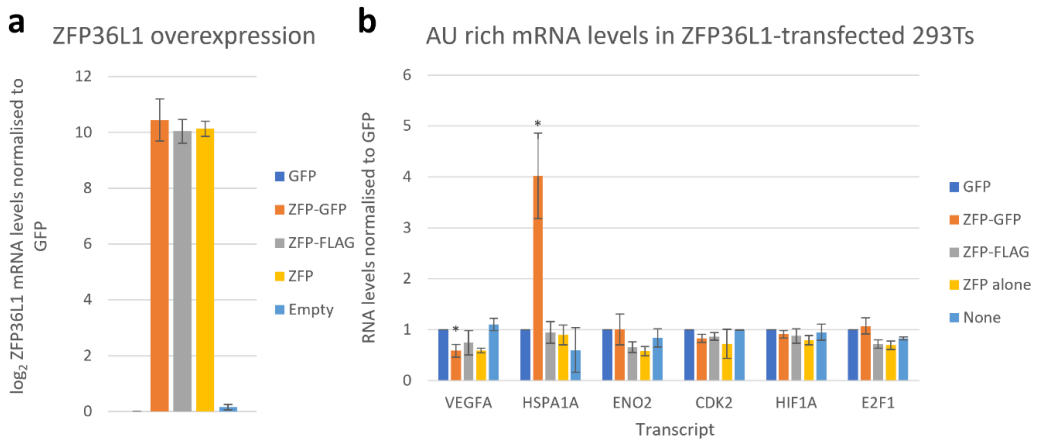

Figure 5.11. Overexpression of ZFP36L1 affects *VEGFA* and *HSPA1A* mRNA levels. 293T cells were transfected with constructs expressing GFP or tagged and untagged forms of ZFP36L1. RNA levels of (a) *ZFP36L1* and (b) AU-rich transcripts were analysed by RT-qPCR (data presented as mean ±SD, n=3).

To further examine whether ZFP36L1 affects the levels of AU-rich mRNAs, the previously generated ZFP36L1-knockdown cell lines used to study the effect of the protein on viral transcripts were examined for changes in the abundance of AU-rich transcripts. The levels of AU-rich mRNAs were monitored in both latent and lytic ZFP36L1-depleted or scrambled shRNA-treated TREX cells by RT-qPCR (Figure 5.12). For several mRNAs including *CDK2, HSPA1A* and *ENO2*, a decrease in their abundance was identified in ZFP36L1-depleted lytic cells (Figure 5.12d-f). However, given that these transcripts are all upregulated in the lytic phase, their mRNA levels likely rise in correlation with lytic transcripts. Thus, the reduction in viral mRNA levels and likely protein in ZFP36L1-depleted cells could account for a similar decrease in the abundance of cellular mRNAs such as *CDK2*, *HSPA1A* and *ENO2*. Therefore, it is difficult to ascertain whether the effect of ZFP36L1 depletion directly affects these transcripts or is an indirect consequence of impaired lytic replication. Despite this, *ENO2* mRNA levels were lower in ZFP36L1-depleted cells among both latent and lytic cells. In latency, although some basal expression of lytic transcripts exists due to spontaneous reactivation, ORF57 and ORF47 levels were not lower in ZFP36L1-depleted cells as they were for *ENO2*. Thus, the reduction in *ENO2* mRNA levels is more likely to be caused by the direct action of ZFP36L1 suggesting the AU-rich transcript may be a genuine target of the RNA-binding protein. Interestingly, a reduction in the mRNA levels of *VEGFA* was also identified in ZFP36L1-depleted cells undergoing lytic replication, even though this transcript is downregulated in the lytic phase (Figure 5.12b). Thus, ZFP36L1 may directly increase the abundance of both *ENO2* and *VEGFA*; however, the mechanism underlying this change is not yet clear.

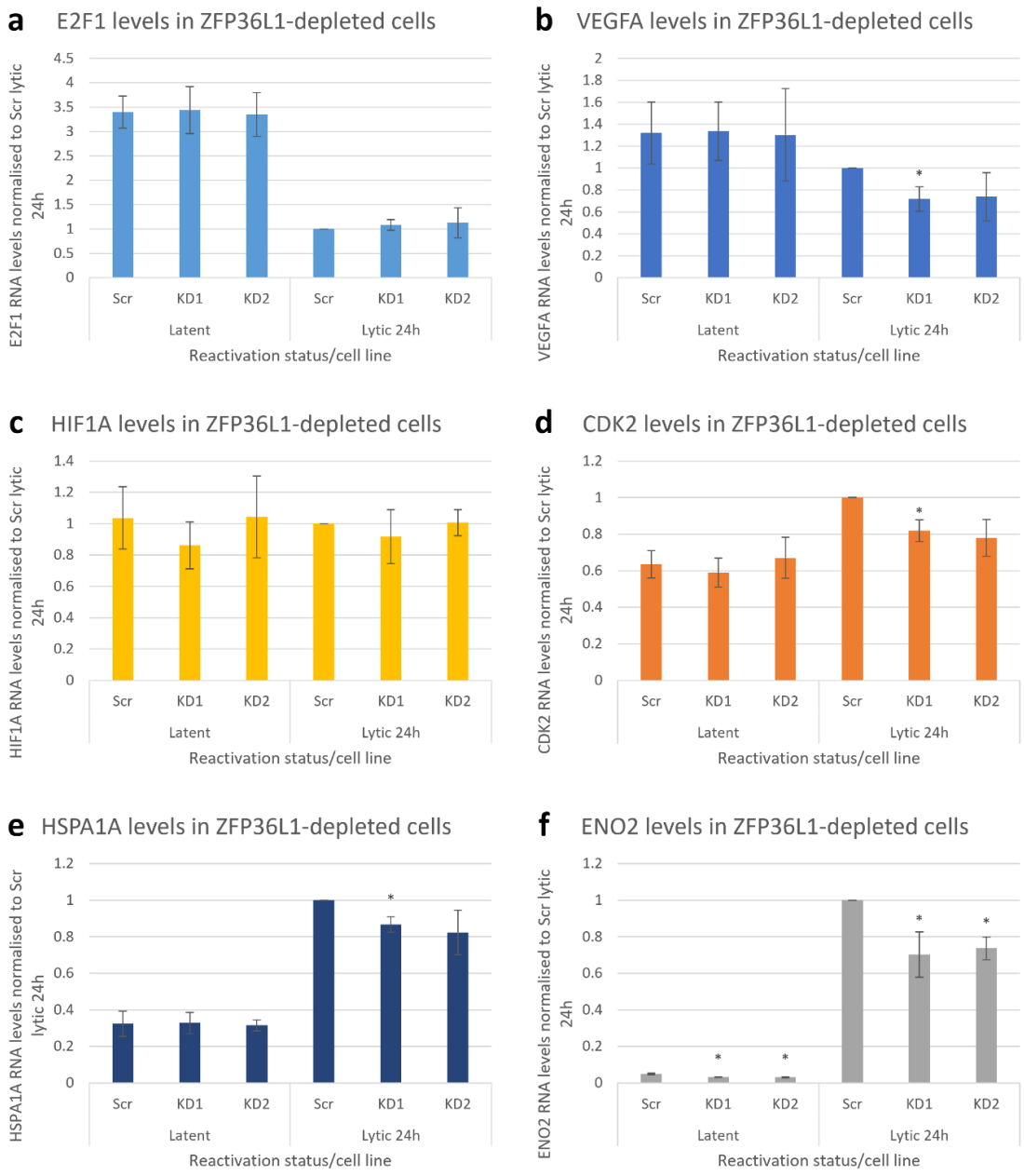

Figure 5.12. ZFP36L1 depletion affects AU-rich mRNA levels. Two ZFP36L1-depleted cell lines were generated using shRNAs and the RNA levels of putative AU-rich mRNA targets measured by RT-qPCR in latent and lytic TREX cells (data presented as mean ± SD, n=3).

5.11 Discussion

In this chapter, the proteins GPRC5A and ZFP36L1, encoded by m^{6}A-modified transcripts, were investigated for a role in KSHV lytic replication. Supporting this hypothesis, both proteins are upregulated during reactivation and transcriptionally activated by the viral

protein RTA. Tantalisingly, the depletion of either protein produced a concomitant drop in KSHV lytic mRNA and protein as well as infectious virion production. As a result, it is clear these proteins are important for the lytic replication of the virus.

GPRC5A is a membrane protein which functions as both a tumour suppressor and oncogene in various cancers. (Zhou and Rigoutsos, 2014) The hypothesised role for GPRC5A is within signalling cascades which contribute to the promotion or suppression of tumourigenesis. However, few interactors of GPRC5A have been suggested and these mainly include nuclear general transcription factors whose association with a plasma membrane protein is enigmatic (Havugimana et al., 2012). For these reasons, a proteomic screen was undertaken to identify proteins which associate with GPRC5A preferentially in lytic replication. If identified, these may allude to a previously unknown cellular mechanism governing the lytic cycle. Interestingly, the analysis highlighted members of the Flotillin and VDAC families as interactors with GPRC5A in cells undergoing lytic replication.

The flotillin proteins FLOT1 and FLOT2 interact to form a heterooligomeric complex which serves as the scaffold for lipid rafts at the plasma membrane (Otto and Nichols, 2011). These microdomains in turn act as a platform for protein-protein interactions. Through this role, the flotillin proteins regulate many cellular processes including endocytosis, proliferation, adhesion, invasion and apoptosis (X. xu Liu et al., 2018). In contrast, VDACs are the most abundant protein in the outer mitochondrial membrane (OMM) where they perform a scaffolding role as well as regulating the entry and exit of metabolites between the cytoplasm and mitochondria (Camara et al., 2017). However, a body of evidence now exists highlighting the presence of VDACs in the plasma membrane, especially in disease states (De Pinto et al., 2010). Although, the function of plasma membrane VDAC proteins is not well established, multiple reports speculate that its role is related to that of VDAC within the OMM. Interestingly, plasma membrane VDAC is present in caveolae microdomains where specific proteins and lipids are subcompartmentalised and the protein may participate in unique protein-protein interactions (Lisanti et al., 1994). Like GPRC5A, flotillin and VDAC proteins are frequently dysregulated in cancer and implicated in a wide range of diseases. Thus, these proteins may play an important role in the transformation of endothelial cells to increase their permissiveness to KSHV lytic replication.

Immunofluorescent analysis of FLOT1 and VDAC1 proteins showed that FLOT1 is primarily expressed at the plasma membrane whereas VDAC1 is mostly localised to cytoplasmic structures which may be mitochondria. The localisation of FLOT1 to a similar subcellular compartment as GPRC5A-GFP may suggest that the two proteins can interact; however, this requires further validation to identify any colocalization. Furthermore, no change in the localisation of FLOT1 could be detected between cells undergoing latent or lytic replication suggesting that additional factors within the lytic phase may bring this protein into contact with GPRC5A. The finding that VDAC1 is primarily cytoplasmic supports the theory that the protein is mostly expressed at the OMM. However, some punctate VDAC1 immunostaining was identified at the cell periphery suggesting that small proportions of plasma membrane VDAC1 could exist which are able to interact with GPRC5A during lytic reactivation. Importantly, further study and coimmunoprecipitation of flotillin and VDAC proteins with GPRC5A are required to validate the interactions identified by proteomic analysis.

FLOT1, FLOT2 and VDAC1 proteins were upregulated during KSHV lytic replication, despite a reduction in mRNA levels. This is an interesting observation as it alludes to post transcriptional regulation of these genes in parallel with the m^6A-dependent changes in GPRC5A expression. As a result, these data suggest that KSHV may modulate several post-transcriptional regulatory pathways to ensure successful lytic replication. Regardless, in contrast to the general trend of host cell shutoff during reactivation, the increased levels of FLOT1, FLOT2 and VDAC1 indicates a role for these proteins in lytic replication and perhaps in collaboration with GPRC5A.

ZFP36L1 is an RNA binding protein which exclusively binds transcripts with AU-rich elements in their 3’ UTR through its tandem zinc finger domains (Adachi et al., 2014). Numerous studies attest to the ability of ZFP36L1 to bind its target mRNAs and destabilise them through interactions with members of the RNA degradation machinery (Loh et al., 2020). However, recent research suggests that assembled ZFP36L1 enriches AU-rich mRNAs encoding membrane proteins within a novel RNA granule at the endoplasmic reticulum termed the TIGER domain (Ma and Mayr, 2018). The assembly of ZFP36L1 into a biophysical compartment distinct from the cytoplasm allows the protein to gain novel functions including the increased expression of membrane proteins at the cell periphery. Importantly, in TREX cells, the subcellular location of ZFP36L1 overlapped almost completely with the endoplasmic reticulum. Thus, this distribution suggests the primary function of the ZFP36L1

within B cells is to form the scaffold of the TIGER domain and enrich AU-rich mRNAs rather than destabilise them. Supporting this hypothesis, no increase in the levels of AU-rich mRNAs could be detected following the depletion of ZFP36L1.

AU-rich elements are adenine and uridine enriched sequences present within the 3' UTRs of ~8% of the transcriptome (Bakheet et al., 2001). These genetic elements are targeted by a number of RNA -binding proteins, including ZFP36L1, which are hypothesised to stabilise or destabilise the transcripts *in cis* (Otsuka et al., 2019). As a result, AU-rich elements are enriched in mRNAs which undergo rapid changes in gene expression and rare among the transcripts of housekeeping genes. Like other viruses, KSHV modulates AU-rich mRNA levels by expressing proteins which activate the p38/MK2 pathway leading to increased accumulation of the AU-rich mRNA binding protein HuR (Corcoran et al., 2012). As a result, AU-rich transcripts encoding cytokines are stabilised and proangiogenic signalling is stimulated. Thus, it is highly conceivable that KSHV could also dysregulate ZFP36L1 expression to further influence AU-rich mRNA levels.

To study the influence of ZFP36L1 on AU-rich mRNAs during KSHV lytic reactivation, six putative AU-rich transcripts targeted by the RNA binding protein were selected from published data (Loh et al., 2020). These transcripts representing multiple cellular processes were subject to diverse changes in abundance during KSHV reactivation suggesting that no single effect is shared among all AU-rich mRNAs. Interestingly, despite a 12-fold increase in the expression of *ENO2* mRNA, the levels of the encoded protein remained constant between latent and lytic states suggesting additional post-transcriptional mechanisms control the expression of this gene. However, HSPA1A protein increased in correlation with mRNA abundance in lytic replication suggesting this protein could influence KSHV reactivation.

Given the changes in AU-rich mRNA levels during reactivation, ZFP36L1 expression was altered in latent and lytic TREX cells to monitor any concomitant changes in the putative AU-rich targets. Surprisingly, a dramatic 3-fold increase in the levels of *HSPA1A* mRNA was observed upon overexpression of ZFP36L1-GFP, but not ZFP36L1-FLAG or ZFP36L1 alone in uninfected cells. This may suggest that GFP-tagging of ZFP36L1 alters its activity towards certain target transcripts such as *HSPA1A* and thus the AU-rich mRNA may be a genuine target of the RNA binding protein. However, the depletion of ZFP36L1 in cells undergoing

latent or lytic replication did not produce a convincing effect on *HSPA1A* abundance. Therefore, an interaction between ZFP36L1 and the AU-rich mRNA *HSPA1A* may affect the fate of the transcript without altering its abundance or may not be relevant for KSHV infection. Interestingly, a significant decrease in the levels of the AU-rich mRNAs *VEGFA* and *ENO2* was identified in ZFP36L1-depleted vs scrambled-treated cells. However, given that *ENO2* mRNA levels did not correlate with ENO2 protein in the previous experiment, it is unlikely that a ZFP36L1-*ENO2* interaction is physiologically relevant for KSHV infection. Furthermore, *VEGFA* levels were lower in both cells overexpressing and depleted of ZFP36L1. Thus, the nature of ZFP36L1's interaction with *VEGFA* is not entirely clear. Importantly, these data do not preclude the fact that ZFP36L1 interacts with the six AU-rich mRNAs examined in a way that is meaningful for KSHV reactivation as the RNA binding protein may relocalise the transcripts into the TIGER domain. Furthermore, ZFP36L1 may interact with other AU-rich mRNAs to fulfil its important role within KSHV lytic replication. As a result, further study involving the identification of ZFP36L1 targets in latent and lytic cells as well as the monitoring of their subcellular localisation in relation to the TIGER domain will be crucial in the understanding of ZFP36L1's contribution towards KSHV lytic replication.

Chapter 6

~

Discussion

6 Discussion

KSHV is an oncogenic herpesvirus which replicates in the nucleus of infected cells by hijacking multiple aspects of the cellular machinery. One way the virus achieves this is by modulating the host gene expression profile into a favourable state for lytic replication. In addition to alterations in the transcription of cellular genes, KSHV influences various post-transcriptional stages of cellular gene expression. Well described mechanisms include degradation of host transcripts by the viral endonuclease SOX and engaging virus-encoded miRNAs in mRNA silencing (Majerciak and Zheng, 2015; Yan et al., 2019). However, KSHV may utilise other mechanisms to control the fate and function of cellular mRNAs in order to subvert the host and support lytic replication.

m^6A and the wider study of RNA modifications is an emerging field of interest within virus life cycles. Studies to date have shown that the modification has widespread impact in the replication of numerous viruses including KSHV (Manners et al., 2019). Many of these have highlighted the effect of the modification on viral transcripts. Furthermore, examination of changes in m^6A distribution among cellular transcripts during infection have alluded to a fundamental role in host cell subversion. Nevertheless, a limited number of studies have linked the modification of individual transcripts to an important role within virus life cycles. Thus, the aim of this study was to gain a deeper understanding of the role of m^6A upon cellular mRNAs in virus-infected cells.

6.1 KSHV lytic replication alters the m^6A profile of transcripts within RNA dynamics and oncogenic signalling pathways

In chapter 3, the topology of m^6A was examined across the transcriptome to identify host cell mRNAs with altered methylation during KSHV lytic replication. Interestingly, the experiment highlighted transcripts of the AP-1 and Notch signalling pathways, in addition to those involved in mRNA dynamics, as those most altered in their m^6A status between latent and lytic replication. Other studies to investigate changes in m^6A distribution upon viral infection have identified similar but distinct pathways including immune signalling and viral gene expression. However, in KSHV infection, a similar study also found ‘molecular mechanisms of cancer’ among enriched pathways of differentially modified transcripts during reactivation (Tan et al., 2018). Given that tumourigenesis is critical for successful

replication of KSHV in endothelial cells, m^{6}A may be important in driving cell transformation and long-term persistence of the virus. Supporting this hypothesis, a large body of evidence now attests to the relevance of m^{6}A dysregulation in cancer development (Dai et al., 2018; Wang et al., 2020). As a result, m^{6}A may play a specialised role in oncovirus infections and further study is required to elucidate whether the alterations in the pattern or extent of the modification are a common mechanism of virus-mediated tumourigenesis.

While other studies have not found that mRNA dynamics are a common pathway among differentially m^{6}A-modified transcripts in viral infection, the data collected in this study suggests that m^{6}A topology is most likely altered in a virus-specific manner. As herpesviruses induces global dysregulation of the host machinery, harnessing multiple post-transcriptional mechanisms to achieve this, interference with mRNA dynamics may be especially relevant for this virus family. In contrast, other viruses often utilise a more subtle approach in the subversion of their host which does not require large scale host-cell shutoff. Supporting this hypothesis, the functional sub-cluster most enriched in methylated transcripts was 'negative regulation of translation.' Therefore, m^{6}A may participate in the host-cell shutoff initiated by KSHV during lytic replication. Taken together, the finding that differentially methylated transcripts are enriched in pathways including oncogenic signalling and mRNA dynamics suggests that m^{6}A may play virus-specific roles in infection rather than conserved functions shared across viruses.

6.2 Cellular transcripts undergo m^{6}A-dependent changes in abundance, stability and nuclear export during KSHV reactivation

In chapter 4, m^{6}A-modified cellular transcripts were monitored for changes in mRNA splicing, stability, nuclear export and translation. Given that many of these methylated transcripts also underwent large changes in their abundance during KSHV reactivation, this effect was monitored in cells where members of the m^{6}A machinery had been depleted. Interestingly, the four transcripts *GPRC5A, STC1, FOSB* and *ZFP36L1* emerged as interesting targets for further investigation with a potential role in KSHV infection. All four of these transcripts underwent increases in mRNA levels during lytic replication which were dampened in WTAP- or YTHDF1-depleted cells. Furthermore, the nuclear export of the four transcripts was more efficient in cells undergoing lytic replication. While the stability of *FOSB* and *ZFP36L1* could not be accurately determined, *GPRC5A* and *STC1* were more stable in

lytic cells. Taken together, these 4 transcripts appear to undergo m^{6}A-dependent changes which correlate with the increased expression of their encoded proteins during reactivation.

Although FOSB and STC1 were not examined further in this study, both serve as promising candidates for the investigation of m^{6}A dynamics in KSHV lytic replication. FOSB is a member of the dimeric AP-1 signalling complex whose interaction partner, JUN, was also identified as a differentially modified transcript in this study. The AP-1 transcription factor plays a well-established role in infection by KSHV and many other viruses, especially those with oncogenic properties such as HBV, HCV, human papillomaviruses, EBV, HSV, HIV-1 and human T-cell lymphotropic virus (Mirzaei et al., 2020). In KSHV infection, AP-1 is activated by multiple MAPK signalling pathways which in turn activates transcription of the viral genes *ORF50*, *ORF57* and *ORFK8.1* (Wang et al., 2004). Furthermore, AP-1 activates the transcription of the key angiogenesis factor Ang-2 which is critical for transformation of infected cells into KS lesions (Ye et al., 2007). Together these insights highlight the crucial role of AP-1 signalling in oncovirus infection and demonstrate a novel post-transcriptional mechanism for modulating AP-1 gene expression during KSHV lytic replication.

STC1 is a potent oncogene which encodes a secreted glycoprotein involved in the pathogenesis of many cancers (Chan et al., 2017; Leung and Wong, 2018). While research into the function of this protein is still lacking, a recent study has suggested the protein serves as a non-canonical Notch ligand (Li et al., 2018). Like AP-1 signalling, Notch signalling plays a well-defined role in KSHV infection. As previously discussed, RTA co-opts the Notch transcription factor RBP-Jκ in the transactivation of cellular and viral promoters during lytic replication (Yang et al., 2008). In addition, the viral factors vGPCR and vFLIP activate the canonical notch ligands DLL4 and JAG1 respectively (Emuss et al., 2009). This exciting mechanism is thought to alter the plasticity of adjacent cells and perhaps increase their susceptibility to infection. If STC1 operates via a similar mechanism, the extracellular secretion of the protein from a B-cell may render surrounding endothelial cells within blood vessels more permissive to KSHV replication and permit KS tumourigenesis (Figure 6.1).

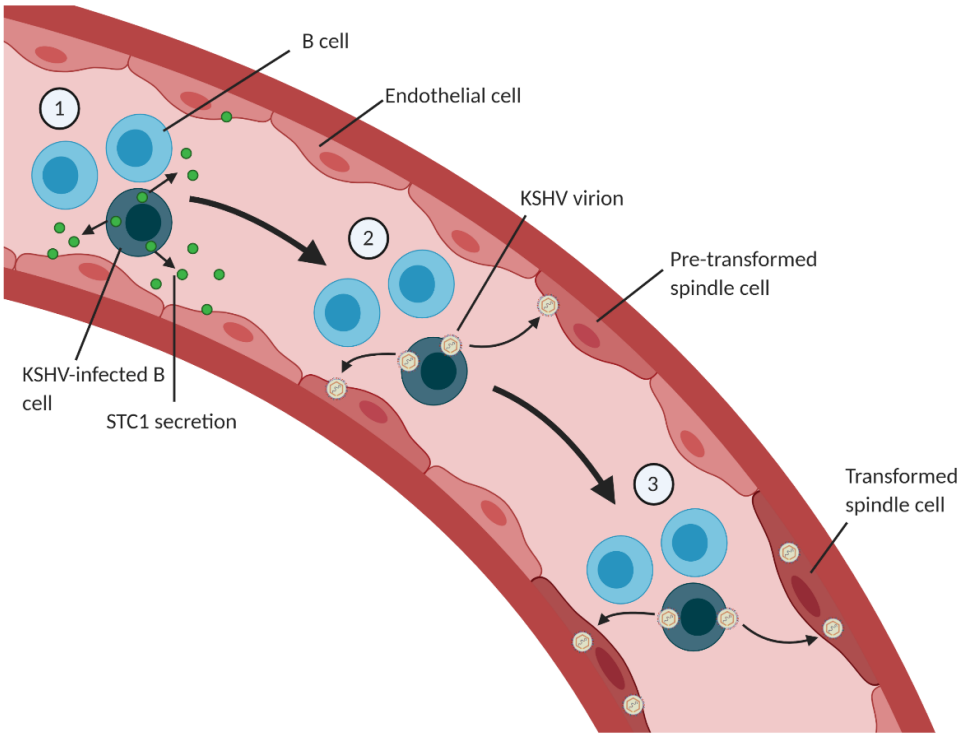

Figure 6.1. Hypothesised STC1 mechanism of action within KSHV infection. STC1 is a secreted glycoprotein which may function in the priming of endothelial cells to make them more permissible to KSHV replication. 1) B-cells undergoing KSHV lytic reactivation upregulate the expression of STC1 leading to elevated secretion of the peptide. Acting as a non-canonical notch ligand, the protein binds membrane bound notch receptors upon endothelial cells and activates intracellular notch signalling. 2) These oncogenic signalling events cause endothelial cells to enter a pre-transformed state which is more permissive to infection with KSHV virions and subsequent replication. 3) Infection of endothelial cells with KSHV viral particles and multiple round of lytic replication drive further transformative events which lead to the formation of malignant KS lesions.

6.3 GPRC5A and ZFP36L1 enhance the lytic replication of KSHV through the regulation of membrane dynamics and AU-rich mRNAs

In chapter 5, the proteins GPRC5A and ZFP36L1 were investigated for a role in the lytic replication of KSHV. These proteins were prioritised based on their transactivation by RTA, the extent of their upregulation during lytic replication and their enigmatic molecular function. The depletion of each proteins decreased the production of lytic transcripts and inhibited the production of infectious virions suggesting a cumulative inhibition of lytic life cycle. Further experiments were carried out to elucidate the molecular function of these proteins.

6.4 GPRC5A is a membrane bound protein which interacts with members of the Flotillin and VDAC families

In the present study, comparison of GPRC5A's interactors between latent and lytic cells highlighted members of the flotillin and VDAC families as factors which preferentially associate with GPRC5A during lytic replication. Interestingly, like GPRC5A, FLOT1, FLOT2 and VDAC1 were upregulated in lytic cells despite the global trend of downregulation initiated by host cell shutoff. Currently published literature indicates that flotillins are structural components of plasma membrane microdomains (Otto and Nichols, 2011). The proteins have been shown to interact with many ion channels and regulate various cellular functions. While the primary location of VDAC proteins appears to be in the OMM, a body of evidence now suggests that these proteins may also localise within the plasma membrane (De Pinto et al., 2010). Given the differing potential between the OMM and plasma membrane, some studies have speculated that under normal cellular conditions, plasma membrane VDACs are closed. However, given the increased presence of plasma membrane VDACs in various disease states these proteins may open in response to certain signals. Furthermore, in the OMM, VDACs play an important structural role which may also be physiologically relevant in the plasma membrane.

It is not entirely clear how the interaction between the members of the flotillin and VDAC families with GPRC5A influences lytic replication. Flotillins are implicated in a wide range of processes including cell adhesion, actin cytoskeleton reorganisation, endocytosis and signal transduction. Furthermore, the function of plasma membrane VDAC is controversial as these channels likely remain closed under normal physiological conditions. As a result, speculation on the role of flotillins and plasma membrane VDAC in KSHV infection is difficult. Nevertheless, given that both these protein families localise to lipid rafts and participate in structural roles, they may be involved in the restructuring of these microdomains to make the host cell more permissive towards KSHV lytic replication. As these microdomains are crucial for egress of KSHV, these insights may indicate that GPRC5A is important in this process (Xin Wang et al., 2015). However, lipid rafts also influence multiple intracellular signalling cascades which could be equally important for reactivation. Therefore, further research is required to elucidate the function of GPRC5A in KSHV lytic replication (Figure 6.2).

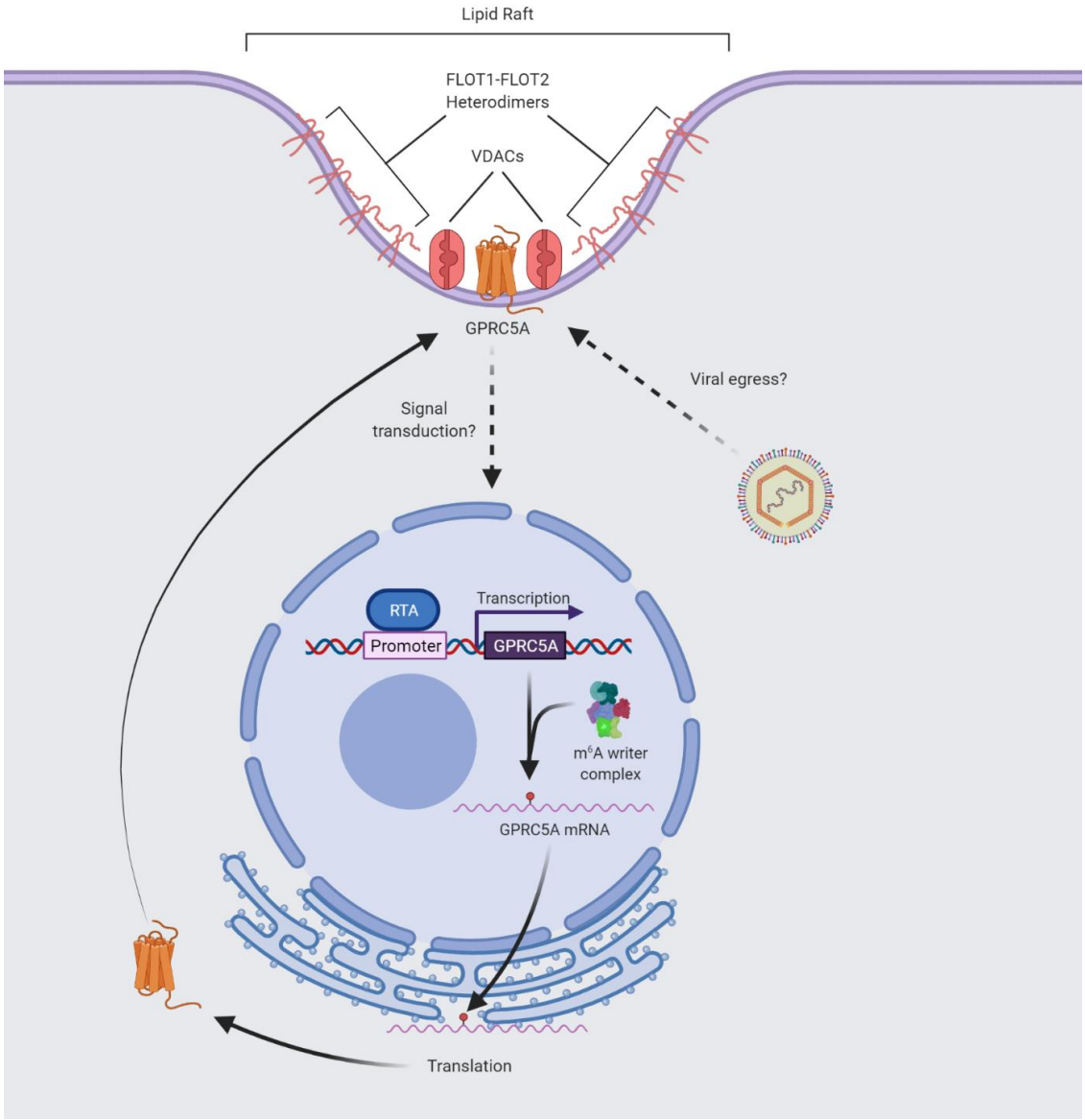

Figure 6.2. Hypothesised GPRC5A function in KSHV lytic replication. *GPRC5A* transcription is strongly induced by the viral protein RTA in KSHV lytic replication. Once transcribed, the abundance of the mRNA is regulated by internal m^{6}A sites. After translation of GPRC5A, the protein localises to the plasma membrane where it is thought to interact with flotillin and VDAC family proteins within lipid rafts. If GPRC5A localises to these microdomains, this might indicate a role for GPRC5A in signal transduction or viral egress. Importantly, this function is crucial for efficient KSHV lytic replication.

6.5 ZFP36L1 is an AU-rich mRNA binding protein which assembles into ER-associated granules

While several studies have alluded to a role for ZFP36L1 in the decay of AU-rich mRNAs, strong evidence to implicate the protein in the decay of AU-rich mRNAs during KSHV infection could not be obtained (Newman et al., 2017). Interestingly however, a recent paper has suggested that soluble and assembled forms of ZFP36L1 have divergent functions (Ma and Mayr, 2018). While the authors suggest that soluble ZFP36L1 is thought to destabilise mRNA, the assembled form of the protein creates a membraneless organelle which enriches AU-rich mRNAs and allows unique protein-protein interactions to occur which cannot take place in the cytosol. Intriguingly, within this 'TIGER' domain, proteins may bind AU-rich mRNAs and become transferred to their newly synthesised protein products. This was demonstrated for the protein SET which first interacts with the AU-rich mRNA CD47 and later associates with newly translated CD47 protein in a molecular handover event (Ma and Mayr, 2018). SET then relocalises CD47 to the plasma membrane where it fulfils its molecular function. As a result, the TIGER domain was shown to improve the surface expression of CD47 at the plasma membrane. However, the authors conclude that many additional proteins may interact with AU-rich mRNAs in ZFP36L1 assemblies to aid in the relocalisation of newly translated proteins to sites where they are needed within the cell. As a result, the TIGER domain may serve as a nexus for the distribution of novel peptides to subcellular compartments that require them.

Interestingly, in this study, the localisation of ZFP36L1 in KSHV-infected cells overlapped almost entirely with the endoplasmic reticulum and the protein showed clear evidence of assembly into granule structures. Furthermore, these granules were more frequent and greater in size among cells undergoing lytic replication suggesting ZFP36L1 favours assembly rather than its soluble form for enhancement of KSHV lytic replication. As a result, in the context of KSHV lytic replication, an enlarged TIGER domain may serve as the critical distribution centre for the sorting of viral and cellular proteins to specific locations within the cell (Figure 6.3).

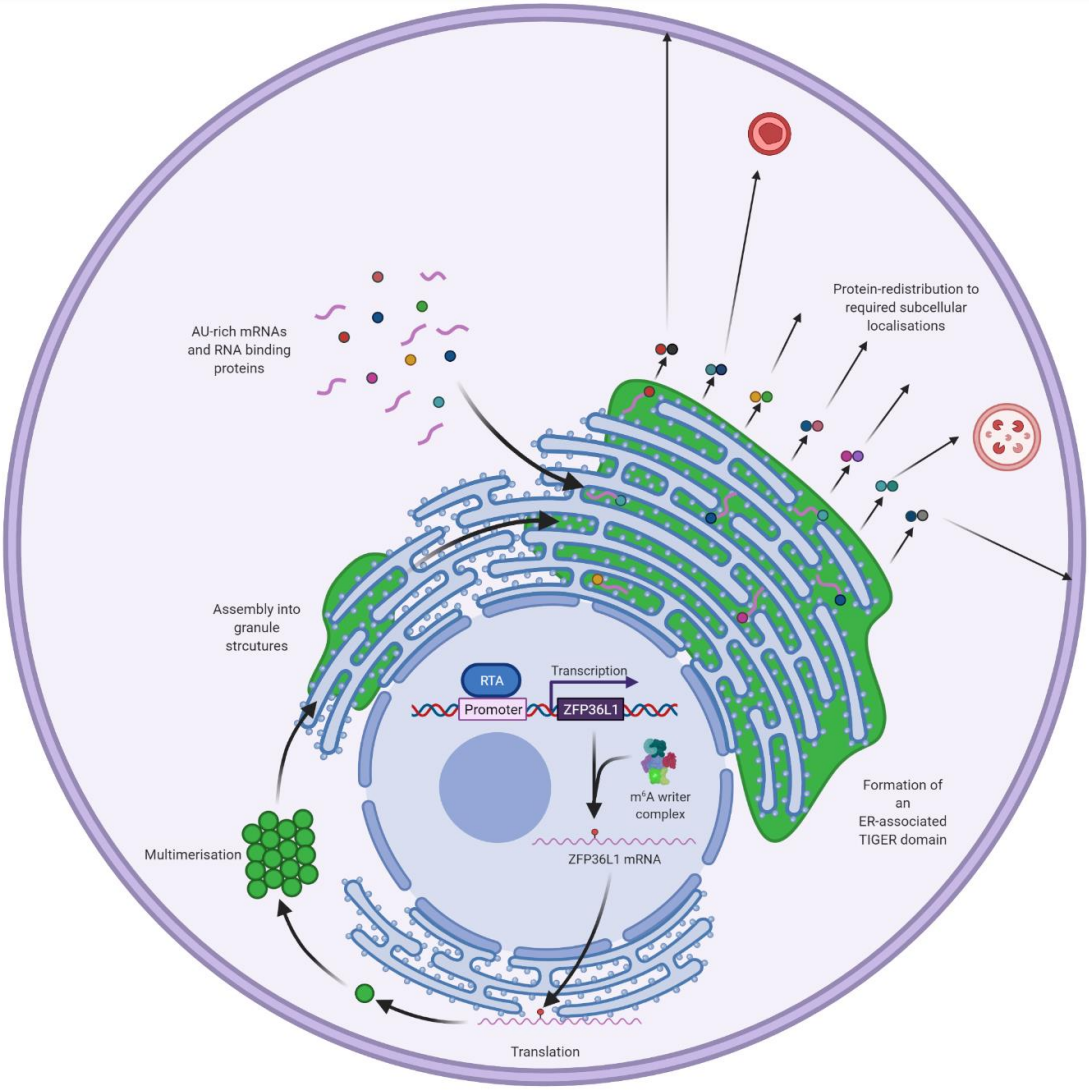

Figure 6.3. Hypothesised function of ZFP36L1 in KSHV lytic replication. Data presented in this study shows that *ZFP36L1* transcription is induced by the viral protein RTA and the abundance of the mRNA is regulated by internal m^{6}A sites. Once translated, the protein assembles into a membraneless organelle within the endoplasmic reticulum known as the TIGER domain. This domain enriches various AU-rich elements and RNA-binding proteins allowing unique protein-protein interactions to occur. The handover of trafficking proteins from mRNAs to their encoded proteins allows the relocalisation of the newly synthesised peptides to the sites where they are needed within the cell. In this way, ZFP36L1 granules act as a distribution centre to newly translated proteins. Given the upregulation of this protein in reactivated cells, the resultant enlarged TIGER domain may be an essential sorting platform for the virus in the subversion of the host.

6.6 Final conclusions and further study

The present study has identified several m^{6}A modified transcripts which undergo m^{6}A-dependent changes in their abundance during KSHV lytic reactivation. To conclusively prove that individual m^{6}A residues upon these transcripts are important for their stability, site specific examination is required. As a result, the pLENTI-CMV-GPRC5A construct generated

in this study has been subjected to site directed mutagenesis so that m^{6}A deficient forms of GPRC5A mRNA can be studied in future experiments within the Whitehouse laboratory. Furthermore, the ongoing improvements in CRISPR-Cas technology now allow for site specific abrogation of m^{6}A which permits the study of endogenous m^{6}A mutants. Therefore, the study of individual m^{6}A sites within methylated transcripts is likely to become a key focus of future research into the epitranscriptomic modification.

The protein GPRC5A is encoded by an m^{6}A-modified transcript which is heavily upregulated in KSHV lytic replication. Furthermore, the protein was found to interact preferentially with all members of the flotillin and VDAC families in reactivated cells. While the functional nature of this interaction is not entirely clear, these factors may colocalise within lipid rafts at the plasma membrane which are integral for KSHV lytic replication. Given the indication that GPRC5A is functionally relevant within lipid rafts, future experiments should explore viral egress and intracellular signalling as potential roles for the protein in lytic replication. As a result, the activity of key signalling cascades and the ability of virions to egress from the cell should be examined in GPRC5A-depleted cells. Together, these experiments may highlight a novel mechanism of GPRC5A-dependent plasma membrane restructuring by KSHV to support lytic replication.

ZFP36L1 was identified as a promising m^{6}A-modified transcript for further investigation during KSHV lytic replication. Despite a body of evidence suggesting that ZFP36L1 encourages the decay of AU-rich mRNAs, those that were examined did not display any increase in abundance upon ZFP36L1 depletion. Future research into ZFP36L1 should utilise RNA-binding protein immunoprecipitation assays coupled with sequencing (RIP-seq) to identify AU-rich mRNA targets, especially those that increase in their association with ZFP36L1 during lytic replication. Furthermore, as with GPRC5A, proteomic analysis of ZFP36L1 interactors in reactivated cells will provide clues as to the function of ZFP36L1 in lytic replication. Should the protein interact with members of the RNA decay machinery, it suggests that ZFP36L1 acts as an RNA decay regulator. However, if ZFP36L1 interacts with proteins involved in folding or transport, this would indicate a scaffolding function in the formation of the TIGER domain. Finally, the subcellular localisation of both protein and mRNA interactors should be monitored during reactivation by immunofluorescence and RNA-FISH to assess whether these factors are recruited to the TIGER domain. Together,

these experiments should highlight a role for ZFP36L1 in lytic replication and identify important cofactors in this process.

In conclusion, the present study has identified two highly interesting m^6A-modified transcripts which encode proteins crucial for KSHV lytic replication through their roles in the regulation of AU-rich mRNA and plasma membrane dynamics. With further research, the proteins may become valuable therapeutic targets in the treatment of KSHV and perhaps other herpesvirus infections. Given that 34% of FDA approved drugs currently target G-protein couple receptors, the protein GPRC5A may be an especially promising candidate for drug targeting (Hauser et al., 2018).

This work also highlights the vast regulatory potential of m^6A-modification on cellular transcripts within viral infections. Given the current renaissance of study into epitranscriptomics, this work contributes further support to the hypothesis that RNA modifications may serve as valuable therapeutic targets for antiviral drugs in the future. Therefore, the use of METTL3 inhibitors currently being developed as antivirals could emerge as an exciting treatment for the malignancies associated with KSHV infection (Yankova et al., 2021).

References

Abere, B., Li, J., Zhou, H., Toptan, T., Moore, P.S. and Chang, Y. 2020. Kaposi's sarcoma-associated herpesvirus-encoded circrnas are expressed in infected tumor tissues and are incorporated into virions. *mBio*. **11**(1), pp.1–16.

Ackermann, M. 2006. Pathogenesis of gammaherpesvirus infections. *Veterinary Microbiology*. **113**(3–4), pp.211–222.

Adachi, S., Homoto, M., Tanaka, R., Hioki, Y., Murakami, H., Suga, H., Matsumoto, M., Nakayama, K.I., Hatta, T., Iemura, S.I. and Natsume, T. 2014. ZFP36L1 and ZFP36L2 control LDLR mRNA stability via the ERK-RSK pathway. *Nucleic Acids Research*. **42**(15), pp.10037–10049.

Agarwala, S.D., Blitzblau, H.G., Hochwagen, A. and Fink, G.R. 2012. RNA Methylation by the MIS Complex Regulates a Cell Fate Decision in Yeast M. Lichten, ed. *PLoS Genetics*. **8**(6), p.e1002732.

Akula, S.M., Naranatt, P.P., Walia, N.-S., Wang, F.-Z., Fegley, B. and Chandran, B. 2003. Kaposi's Sarcoma-Associated Herpesvirus (Human Herpesvirus 8) Infection of Human Fibroblast Cells Occurs through Endocytosis. *Journal of Virology*. **77**(14), pp.7978–7990.

Alarcón, C.R., Goodarzi, H., Lee, H., Liu, X., Tavazoie, S.S.F. and Tavazoie, S.S.F. 2015. HNRNPA2B1 is a mediator of m 6 A-dependent nuclear RNA processing events. *Cell*. **162**(6), pp.1299–1308.

Amon, W. and Farrell, P.J. 2005. Reactivation of Epstein-Barr virus from latency. *Reviews in Medical Virology*. **15**(3), pp.149–156.

Aneja, K.K. and Yuan, Y. 2017. Reactivation and Lytic Replication of Kaposi's Sarcoma-Associated Herpesvirus: An Update. *Frontiers in microbiology*. **8**(APR), p.613.

Antanaviciute, A., Baquero-Perez, B., Watson, C.M., Harrison, S.M., Lascelles, C., Crinnion, L., Markham, A.F., Bonthron, D.T., Whitehouse, A. and Carr, I.M. 2017. M6aViewer: Software for the detection, analysis, and visualization of N6-methyladenosine peaks from m6A-seq/ME-RIP sequencing data. *RNA*. **23**(10), pp.1493–1501.

Arias, C., Weisburd, B., Stern-Ginossar, N., Mercier, A., Madrid, A.S., Bellare, P., Holdorf, M., Weissman, J.S. and Ganem, D. 2014. KSHV 2.0: a comprehensive annotation of the Kaposi's sarcoma-associated herpesvirus genome using next-generation sequencing reveals novel genomic and functional features. *PLoS pathogens*. **10**(1), p.e1003847.

Arvin, A., Campadelli-Fiume, G., Mocarski, E., Moore, P.S., Roizman, B., Whitley, R. and Yamanishi, K. 2007. *Introduction: definition and classification of the human herpesviruses - comparative analysis of the genomes, in Human Herpesviruses - Biology, Therapy and immunoprophylaxis*. Cambridge: Cambridge University Press.

Ashworth, W., Stoney, P.N. and Yamamoto, T. 2019. States of decay: The systems biology of mRNA stability. *Current Opinion in Systems Biology*. **15**, pp.48–57.

Aswad, A. and Katzourakis, A. 2018. Cell-Derived Viral Genes Evolve under Stronger Purifying Selection in Rhadinoviruses. *Journal of Virology*. **92**(19), pp.1–20.

Bailey, T.L., Boden, M., Buske, F.A., Frith, M., Grant, C.E., Clementi, L., Ren, J., Li, W.W. and Noble, W.S. 2009. MEME Suite: Tools for motif discovery and searching. *Nucleic Acids Research*. **37**(SUPPL. 2), pp.202–208.

Bakheet, T., Frevel, M., Williams, B.R.G., Greer, W. and Khabar, K.S.A. 2001. ARED: Human AU-rich element-containing mRNA database reveals an unexpectedly diverse functional repertoire of encoded proteins. *Nucleic Acids Research*. **29**(1), pp.246–254.

Baquero-Perez, B., Antanaviciute, A., Yonchev, I.D., Carr, I.M., Wilson, S.A. and Whitehouse, A. 2019. The Tudor SND1 protein is an m6A RNA reader essential for replication of Kaposi's sarcoma-associated herpesvirus. *eLife*. **8**.

Biryahwaho, B., Dollard, S.C., Pfeiffer, R.M., Shebl, F.M., Munuo, S., Amin, M.M., Hladik, W., Parsons, R. and Mbulaiteye, S.M. 2010. Sex and Geographic Patterns of Human Herpesvirus 8 Infection in a Nationally Representative Population-Based Sample in Uganda. *The Journal of Infectious Diseases*. **202**(9), pp.1347–1353.

Blissenbach, M., Grewe, B., Hoffmann, B., Brandt, S. and Überla, K. 2010. Nuclear RNA Export and Packaging Functions of HIV-1 Rev Revisited. *Journal of Virology*. **84**(13), pp.6598–6604.

Bokar, J.A., Shambaugh, M.E., Polayes, D., Matera, A.G. and Rottman, F.M. 1997. Purification and cDNA cloning of the AdoMet-binding subunit of the human mRNA (N6-adenosine)-methyltransferase. *RNA*. **3**(11), pp.1233–1247.

Boshoff, C., Endo, Y., Collins, P.D., Takeuchi, Y., Reeves, J.D., Schweickart, V.L., Siani, M.A., Sasaki, T., Williams, T.J., Gray, P.W., Moore, P.S., Chang, Y. and Weiss, R.A. 1997. Angiogenic and HIV-inhibitory functions of KSHV-encoded chemokines. *Science (New York, N.Y.)*. **278**(5336), pp.290–294.

Boulias, K., Toczydłowska-Socha, D., Hawley, B.R., Liberman, N., Takashima, K., Zaccara, S., Guez, T., Vasseur, J.J., Debart, F., Aravind, L., Jaffrey, S.R. and Greer, E.L. 2019. Identification of the m6Am Methyltransferase PCIF1 Reveals the Location and Functions of m6Am in the Transcriptome. *Molecular Cell*. **75**(3), pp.631-643.e8.

Bowman, B.R., Baker, M.L., Rixon, F.J., Chiu, W. and Quiocho, F.A. 2003. Structure of the herpesvirus major capsid protein. *The EMBO journal*. **22**(4), pp.757–765.

Boyne, J.R., Jackson, B.R., Taylor, A., MacNab, S.A. and Whitehouse, A. 2010. Kaposi's sarcoma-associated herpesvirus ORF57 protein interacts with PYM to enhance translation of viral intronless mRNAs. *EMBO Journal*. **29**(11), pp.1851–1864.

Brasey, A., Lopez-Lastra, M., Ohlmann, T., Beerens, N., Berkhout, B., Darlix, J.-L. and Sonenberg, N. 2003. The Leader of Human Immunodeficiency Virus Type 1 Genomic RNA Harbors an Internal Ribosome Entry Segment That Is Active during the G2/M Phase of the Cell Cycle. *Journal of Virology*. **77**(7), pp.3939–3949.

Bu, W., Palmeri, D., Krishnan, R., Marin, R., Aris, V.M., Soteropoulos, P. and Lukac, D.M. 2008. Identification of Direct Transcriptional Targets of the Kaposi's Sarcoma-Associated Herpesvirus Rta Lytic Switch Protein by Conditional Nuclear Localization. *Journal of Virology*. **82**(21), pp.10709–10723.

Butler, L.M., Were, W.A., Balinandi, S., Downing, R., Dollard, S., Neilands, T.B., Gupta, S., Rutherford, G.W. and Mermin, J. 2011. Human herpesvirus 8 infection in children and adults in a population-based study in rural Uganda. *Journal of Infectious Diseases*. **203**(5), pp.625–634.

Cai, Q., Verma, S.C., Lu, J. and Robertson, E.S. 2010. *Molecular Biology of Kaposi's Sarcoma-associated Herpesvirus and Related Oncogenesis*.

Camara, A.K.S., Zhou, Y.F., Wen, P.C., Tajkhorshid, E. and Kwok, W.M. 2017. Mitochondrial VDAC1: A key gatekeeper as potential therapeutic target. *Frontiers in Physiology*. **8**(JUN), pp.1–18.

Canaani, D., Kahana, C., Lavi, S. and Groner, Y. 1979. Identification and mapping of N6-methyladenosine containing sequences in simian virus 40 RNA. *Nucleic Acids Research*. **6**(8), pp.2879–2899.

Carlile, T.M., Rojas-Duran, M.F., Zinshteyn, B., Shin, H., Bartoli, K.M. and Gilbert, W. V. 2014. Pseudouridine profiling reveals regulated mRNA pseudouridylation in yeast and human cells. *Nature*. **515**(7525), pp.143–146.

Carmody, S.R. and Wente, S.R. 2009. mRNA nuclear export at a glance. *Journal of Cell Science*. **122**(12), pp.1933–1937.

Chan, K.K.S., Leung, C.O.N., Wong, C.C.L., Ho, D.W.H., Chok, K.S.H., Lai, C.L., Ng, I.O.L. and Lo, R.C.L. 2017. Secretory Stanniocalcin 1 promotes metastasis of hepatocellular carcinoma through activation of JNK signaling pathway. *Cancer Letters*. **403**, pp.330–338.

Chang, Y., Cesarman, E., Pessin, M.S., Lee, F., Culpepper, J., Knowles, D.M. and Moore, P.S. 1994. Identification of herpesvirus-like DNA sequences in AIDS-associated Kaposi's sarcoma. *Science*. **266**(5192), pp.1865–1869.

Chiou, C.-J., Poole, L.J., Kim, P.S., Ciufo, D.M., Cannon, J.S., ap Rhys, C.M., Alcendor, D.J., Zong, J.-C., Ambinder, R.F. and Hayward, G.S. 2002. Patterns of gene expression and a transactivation function exhibited by the vGCR (ORF74) chemokine receptor protein of Kaposi's sarcoma-associated herpesvirus. *Journal of virology*. **76**(7), pp.3421–39.

Chu, C.C., Liu, B., Plangger, R., Kreutz, C. and Al-Hashimi, H.M. 2019. M6A minimally impacts the structure, dynamics, and Rev ARM binding properties of HIV-1 RRE stem IIB. *PLoS ONE*. **14**(12), p.e0224850.

Cohen, A., Brodie, C. and Sarid, R. 2006. An essential role of ERK signalling in TPA-induced reactivation of Kaposi's sarcoma-associated herpesvirus. *Journal of General Virology*. **87**(4), pp.795–802.

Cohn, W.E. 1960. Pseudouridine, a carbon-carbon linked ribonucleoside in ribonucleic

acids: isolation, structure, and chemical characteristics. *The Journal of biological chemistry*. **235**, pp.1488–1498.

Coppin, L., Leclerc, J., Vincent, A., Porchet, N. and Pigny, P. 2018. Messenger RNA Life-Cycle in Cancer Cells: Emerging Role of Conventional and Non-Conventional RNA-Binding Proteins? *International Journal of Molecular Sciences*. **19**(3), p.650.

Corcoran, J.A., Khaperskyy, D.A., Johnston, B.P., King, C.A., Cyr, D.P., Olsthoorn, A. V. and McCormick, C. 2012. Kaposi's Sarcoma-Associated Herpesvirus G-Protein-Coupled Receptor Prevents AU-Rich-Element-Mediated mRNA Decay. *Journal of Virology*. **86**(16), pp.8859–8871.

Costanzo, F., Campadelli-Fiume, G., Foa-Tomasi, L. and Cassai, E. 1977. Evidence that herpes simplex virus DNA is transcribed by cellular RNA polymerase B. *Journal of Virology*. **21**(3), pp.996–1001.

Courtney, D.G., Kennedy, E.M., Dumm, R.E., Bogerd, H.P., Tsai, K., Heaton, N.S. and Cullen, B.R. 2017. Epitranscriptomic Enhancement of Influenza A Virus Gene Expression and Replication. *Cell Host & Microbe*. **22**(3), pp.377-386.e5.

Dai, D., Wang, H., Zhu, L., Jin, H. and Wang, X. 2018. N6-methyladenosine links RNA metabolism to cancer progression. *Cell death & disease*. **9**(2), p.124.

Dai, Q., Moshitch-Moshkovitz, S., Han, D., Kol, N., Amariglio, N., Rechavi, G., Dominissini, D. and He, C. 2017. Nm-seq maps 2'-O-methylation sites in human mRNA with base precision. *Nature Methods*. **14**(7), pp.695–698.

Darnell, R.R., Shengdong, K.E. and Darnell, J.E. 2018. Pre-mRNA processing includes N6 methylation of adenosine residues that are retained in mRNA exons and the fallacy of "RNA epigenetics". *RNA*. **24**(3), pp.262–267.

Davis, D.A., Rinderknecht, A.S., Zoeteweij, J.P., Aoki, Y., Read-connole, E.L., Tosato, G., Blauvelt, A. and Yarchoan, R. 2011. Hypoxia induces lytic replication of Kaposi sarcoma − associated herpesvirus Hypoxia induces lytic replication of Kaposi sarcoma – associated herpesvirus. *Vascular*. **97**(10), pp.3244–3250.

Davis, D.R. 1995. Stabilization of RNA stacking by pseudouridine. *Nucleic Acids Research*. **23**(24), pp.5020–5026.

DAVIS, F.F. and ALLEN, F.W. 1957. Ribonucleic acids from yeast which contain a fifth nucleotide. *The Journal of biological chemistry*. **227**(2), pp.907–915.

Davison, A.J., Eberle, R., Ehlers, B., Hayward, G.S., McGeoch, D.J., Minson, A.C., Pellett, P.E., Roizman, B., Studdert, M.J. and Thiry, E. 2009. The order Herpesvirales. *Archives of virology*. **154**(1), pp.171–177.

Decker, C.J. and Parker, R. 2012. P-Bodies and Stress Granules: Possible Roles in the Control of Translation and mRNA Degradation. *Cold Spring Harbor Perspectives in Biology*. **4**(9), pp.a012286–a012286.

Decker, L.L., Shankar, P., Khan, G., Freeman, R.B., Dezube, B.J., Lieberman, J. and Thorley-Lawson, D.A. 1996. The Kaposi sarcoma-associated herpesvirus (KSHV) is present as an intact latent genome in KS tissue but replicates in the peripheral blood mononuclear cells of KS patients. *The Journal of experimental medicine*. **184**(1), pp.283–288.

DeCotiis, J. and Lukac, D. 2017. KSHV and the Role of Notch Receptor Dysregulation in Disease Progression. *Pathogens*. **6**(3), p.34.

Delatte, B., Wang, F., Ngoc, L.V., Collignon, E., Bonvin, E., Deplus, R., Calonne, E., Hassabi, B., Putmans, P., Awe, S., Wetzel, C., Kreher, J., Soin, R., Creppe, C., Limbach, P.A., Gueydan, C., Kruys, V., Brehm, A., Minakhina, S., Defrance, M., Steward, R. and Fuks, F. 2016. Transcriptome-wide distribution and function of RNA hydroxymethylcytosine. *Science*. **351**(6270), pp.282–285.

Deng, X., Chen, K., Luo, G.Z., Weng, X., Ji, Q., Zhou, T. and He, C. 2015. Widespread occurrence of N6-methyladenosine in bacterial mRNA. *Nucleic Acids Research*. **43**(13), pp.6557–6567.

Deshmane, S.L. and Fraser, N.W. 1989. During latency, herpes simplex virus type 1 DNA is associated with nucleosomes in a chromatin structure. *Journal of Virology*. **63**(2), pp.943–947.

Desrosiers, R., Friderici, K. and Rottman, F. 1974. Identification of methylated nucleosides in messenger RNA from Novikoff hepatoma cells. *Proceedings of the National Academy of Sciences of the United States of America*. **71**(10), pp.3971–3975.

Dever, T.E. and Green, R. 2012. The elongation, termination, and recycling phases of translation in eukaryotes. *Cold Spring Harbor Perspectives in Biology*. **4**(7), pp.1–16.

Dierks, D., Garcia-Campos, M.A., Uzonyi, A., Safra, M., Edelheit, S., Rossi, A., Sideri, T., Varier, R.A., Brandis, A., Stelzer, Y., van Werven, F., Scherz-Shouval, R. and Schwartz, S. 2021. Multiplexed profiling facilitates robust m6A quantification at site, gene and sample resolution. *Nature Methods*. **18**(9), pp.1060–1067.

Dimock, K. and Stoltzfus, C.M. 1977. Sequence specificity of internal methylation in B77 avian sarcoma virus RNA subunits. *Biochemistry*. **16**(3), pp.471–478.

Döhner, K., Wolfstein, A., Prank, U., Echeverri, C., Dujardin, D., Vallee, R. and Sodeik, B. 2002. Function of dynein and dynactin in herpes simplex virus capsid transport. *Molecular biology of the cell*. **13**(8), pp.2795–2809.

Dominissini, D., Moshitch-Moshkovitz, S., Schwartz, S., Salmon-Divon, M., Ungar, L., Osenberg, S., Cesarkas, K., Jacob-Hirsch, J., Amariglio, N. and Kupiec, M. 2012. Topology of the human and mouse m6A RNA methylomes revealed by m6A-seq. *Nature*. **485**(7397), pp.201–206.

Dominissini, D., Nachtergaele, S., Moshitch-Moshkovitz, S., Peer, E., Kol, N., Ben-Haim, M.S., Dai, Q., Di Segni, A., Salmon-Divon, M., Clark, W.C., Zheng, G., Pan, T., Solomon, O., Eyal, E., Hershkovitz, V., Han, D., Doré, L.C., Amariglio, N., Rechavi, G. and He, C. 2016. The dynamic N1 -methyladenosine methylome in eukaryotic messenger RNA. *Nature*. **530**(7591), pp.441–446.

Du, H., Zhao, Y., He, J., Zhang, Y., Xi, H., Liu, M., Ma, J. and Wu, L. 2016. YTHDF2 destabilizes m6A-containing RNA through direct recruitment of the CCR4–NOT deadenylase complex. *Nature Communications*. **7**, p.12626.

Edelheit, S., Schwartz, S., Mumbach, M.R., Wurtzel, O. and Sorek, R. 2013. Transcriptome-Wide Mapping of 5-methylcytidine RNA Modifications in Bacteria, Archaea, and Yeast Reveals m5C within Archaeal mRNAs V. de Crécy-Lagard, ed. *PLoS Genetics*. **9**(6), p.e1003602.

Edupuganti, R.R., Geiger, S., Lindeboom, R.G.H., Shi, H., Hsu, P.J., Lu, Z., Wang, S.Y., Baltissen, M.P.A., Jansen, P.W.T.C., Rossa, M., Müller, M., Stunnenberg, H.G., He, C., Carell, T. and Vermeulen, M. 2017. N6-methyladenosine (m6A) recruits and

repels proteins to regulate mRNA homeostasis. *Nature Structural and Molecular Biology*. **24**(10), pp.870–878.

Eisenberg, R.J., Atanasiu, D., Cairns, T.M., Gallagher, J.R., Krummenacher, C. and Cohen, G.H. 2012. Herpes virus fusion and entry: a story with many characters. *Viruses*. **4**(5), pp.800–832.

Elliott, B.A., Ho, H.-T., Ranganathan, S. V., Vangaveti, S., Ilkayeva, O., Abou Assi, H., Choi, A.K., Agris, P.F. and Holley, C.L. 2019. Modification of messenger RNA by 2'-O-methylation regulates gene expression in vivo. *Nature Communications*. **10**(1), p.3401.

Emuss, V., Lagos, D., Pizzey, A., Gratrix, F., Henderson, S.R. and Boshoff, C. 2009. KSHV Manipulates Notch Signaling by DLL4 and JAG1 to Alter Cell Cycle Genes in Lymphatic Endothelia S. H. Speck, ed. *PLoS Pathogens*. **5**(10), p.e1000616.

Engels, E.A., Atkinson, J.O., Graubard, B.I., McQuillan, G.M., Gamache, C., Mbisa, G., Cohn, S., Whitby, D. and Goedert, J.J. 2007. Risk Factors for Human Herpesvirus 8 Infection among Adults in the United States and Evidence for Sexual Transmission. *The Journal of Infectious Diseases*. **196**(2), pp.199–207.

Esteve-Puig, R., Bueno-Costa, A. and Esteller, M. 2020. Writers, readers and erasers of RNA modifications in cancer. *Cancer Letters*. **474**(November 2019), pp.127–137.

Finkel, D. and Groner, Y. 1983. Methylations of adenosine residues (m6A) in pre-mRNA are important for formation of late simian virus 40 mRNAs. *Virology*. **131**(2), pp.409–425.

Fiorelli, V., Gendelman, R., Caterina Sirianni, M., Chang, H.-K., Colombini, S., Markham, P.D., Monini, P., Sonnabend, J., Pintus, A. and Gallo, R.C. 1998. γ-Interferon produced by CD8+ T cells infiltrating Kaposi's sarcoma induces spindle cells with angiogenic phenotype and synergy with human immunodeficiency virus-1 Tat protein: an immune response to human herpesvirus-8 infection? *Blood, The Journal of the American Society of Hematology*. **91**(3), pp.956–967.

Furlong, D., Swift, H. and Roizman, B. 1972. Arrangement of herpesvirus deoxyribonucleic acid in the core. *Journal of virology*. **10**(5), pp.1071–1074.

Ganem, D. 1997. KSHV and Kaposi's sarcoma: the end of the beginning? *Cell*. **91**(2),

pp.157–160.

Gao, S.J., Kingsley, L., Li, M., Zheng, W., Parravicini, C., Ziegler, J., Newton, R., Rinaldo, C.R., Saah, A., Phair, J., Detels, R., Chang, Y. and Moore, P.S. 1996. KSHV antibodies among Americans, Italians and Ugandans with and without Kaposi's sarcoma. *Nature medicine*. **2**(8), pp.925–928.

Garneau, N.L., Wilusz, J. and Wilusz, C.J. 2007. The highways and byways of mRNA decay. *Nature Reviews Molecular Cell Biology*. **8**(2), pp.113–126.

Gazon, H., Barbeau, B., Mesnard, J.M. and Peloponese, J.M. 2018. Hijacking of the AP-1 signaling pathway during development of ATL. *Frontiers in Microbiology*. **8**(JAN), pp.1–13.

Geula, S., Moshitch-Moshkovitz, S., Dominissini, D., Mansour, A.A.F., Kol, N., Salmon-Divon, M., Hershkovitz, V., Peer, E., Mor, N., Manor, Y.S., Ben-Haim, M.S., Eyal, E., Yunger, S., Pinto, Y., Jaitin, D.A., Viukov, S., Rais, Y., Krupalnik, V., Chomsky, E., Zerbib, M., Maza, I., Rechavi, Y., Massarwa, R., Hanna, S., Amit, I., Levanon, E.Y., Amariglio, N., Stern-Ginossar, N., Novershtern, N., Rechavi, G. and Hanna, J.H. 2015. m6A mRNA methylation facilitates resolution of naïve pluripotency toward differentiation. *Science*. **347**(6225), pp.1002–1006.

Ghildiyal, M. and Zamore, P.D. 2009. Small silencing RNAs: An expanding universe. *Nature Reviews Genetics*. **10**(2), pp.94–108.

Gil, L., Martínez, G., González, I., Tarinas, A., Álvarez, A., Giuliani, A., Molina, R., Tápanes, R., Pérez, J. and León, O.S. 2003. Contribution to characterization of oxidative stress in HIV/AIDS patients. *Pharmacological Research*. **47**(3), pp.217–224.

Glick, J.M. and Leboy, P.S. 1977. Purification and properties of tRNA (adenine 1) methyltransferase from rat liver. *Journal of Biological Chemistry*. **252**(14), pp.4790–4795.

Gokhale, N.S., McIntyre, A.B.R., Mattocks, M.D., Holley, C.L., Lazear, H.M., Mason, C.E. and Horner, S.M. 2020. Altered m6A Modification of Specific Cellular Transcripts Affects Flaviviridae Infection. *Molecular cell*. **77**(3), pp.542-555.e8.

Gokhale, N.S., McIntyre, A.B.R., McFadden, M.J., Roder, A.E., Kennedy, E.M., Gandara, J.A., Hopcraft, S.E., Quicke, K.M., Vazquez, C., Willer, J., Ilkayeva, O.R., Law, B.A.,

Holley, C.L., Garcia-Blanco, M.A., Evans, M.J., Suthar, M.S., Bradrick, S.S., Mason, C.E. and Horner, S.M. 2016. N6-Methyladenosine in Flaviviridae Viral RNA Genomes Regulates Infection. *Cell Host and Microbe*. **20**(5), pp.654–665.

Goodrum, F. 2016. Human Cytomegalovirus Latency: Approaching the Gordian Knot. *Annual review of virology*. **3**(1), pp.333–357.

Gould, F., Harrison, S.M., Hewitt, E.W. and Whitehouse, A. 2009. Kaposi's Sarcoma-Associated Herpesvirus RTA Promotes Degradation of the Hey1 Repressor Protein through the Ubiquitin Proteasome Pathway. *Journal of Virology*. **83**(13), pp.6727–6738.

Gruffat, H., Marchione, R. and Manet, E. 2016. Herpesvirus late gene expression: A viral-specific pre-initiation complex is key. *Frontiers in Microbiology*. **7**(JUN), pp.1–15.

Grundhoff, A. and Ganem, D. 2004. Inefficient establishment of KSHV latency suggests an additional role for continued lytic replication in Kaposi sarcoma pathogenesis. *Journal of Clinical Investigation*. **113**(1), pp.124–136.

Guo, H., Wang, L., Peng, L., Zhou, Z.H. and Deng, H. 2009. Open Reading Frame 33 of a Gammaherpesvirus Encodes a Tegument Protein Essential for Virion Morphogenesis and Egress. *Journal of Virology*. **83**(20), pp.10582–10595.

Guo, J., Tang, H.-W., Li, J., Perrimon, N. and Yan, D. 2018. Xio is a component of the Drosophila sex determination pathway and RNA N6-methyladenosine methyltransferase complex. *Proceedings of the National Academy of Sciences of the United States of America*. **115**(14), pp.3674–3679.

Hamma, T. and Ferré-D'Amaré, A.R. 2006. Pseudouridine synthases. *Chemistry & biology*. **13**(11), pp.1125–35.

Hanson, D.J., Hill, J.A. and Koelle, D.M. 2018. Advances in the characterization of the T-cell response to human herpesvirus-6. *Frontiers in Immunology*. **9**(JUN), pp.4–11.

Hao, H., Hao, S., Chen, H., Chen, Z., Zhang, Y., Wang, J., Wang, H., Zhang, B., Qiu, J., Deng, F. and Guan, W. 2019. N6-methyladenosine modification and METTL3 modulate enterovirus 71 replication. *Nucleic acids research*. **47**(1), pp.362–374.

Hauser, A.S., Chavali, S., Masuho, I., Jahn, L.J., Martemyanov, K.A., Gloriam, D.E. and

Babu, M.M. 2018. Pharmacogenomics of GPCR Drug Targets. *Cell*. **172**(1–2), pp.41-54.e19.

Haussmann, I.U., Bodi, Z., Sanchez-Moran, E., Mongan, N.P., Archer, N., Fray, R.G. and Soller, M. 2016. M6A potentiates Sxl alternative pre-mRNA splicing for robust Drosophila sex determination. *Nature*. **540**(7632), pp.301–304.

Havugimana, P.C., Hart, G.T., Nepusz, T., Yang, H., Turinsky, A.L., Li, Z., Wang, P.I., Boutz, D.R., Fong, V., Phanse, S., Babu, M., Craig, S.A., Hu, P., Wan, C., Vlasblom, J., Dar, V.U.N., Bezginov, A., Clark, G.W., Wu, G.C., Wodak, S.J., Tillier, E.R.M., Paccanaro, A., Marcotte, E.M. and Emili, A. 2012. A census of human soluble protein complexes. *Cell*. **150**(5), pp.1068–1081.

Heming, J.D., Conway, J.F. and Homa, F.L. 2017. Herpesvirus Capsid Assembly and DNA Packaging *In*: *Advances in Anatomy Embryology and Cell Biology*., pp.119–142.

Hesser, C.R., Karijolich, J., Dominissini, D., He, C. and Glaunsinger, B.A. 2018. N6-methyladenosine modification and the YTHDF2 reader protein play cell type specific roles in lytic viral gene expression during Kaposi's sarcoma-associated herpesvirus infection D. P. Dittmer, ed. *PLOS Pathogens*. **14**(4), p.e1006995.

Holzerlandt, R., Orengo, C., Kellam, P. and Albà, M.M. 2002. Identification of new herpesvirus gene homologs in the human genome. *Genome research*. **12**(11), pp.1739–1748.

Horiuchi, K., Kawamura, T., Iwanari, H., Ohashi, R., Naito, M., Kodama, T. and Hamakubo, T. 2013. Identification of Wilms' tumor 1-associating protein complex and its role in alternative splicing and the cell cycle. *Journal of Biological Chemistry*. **288**(46), pp.33292–33302.

Huang, H., Weng, H., Sun, W., Qin, X., Shi, H., Wu, H., Zhao, B.S., Mesquita, A., Liu, C., Yuan, C.L., Hu, Y.-C., Hüttelmaier, S., Skibbe, J.R., Su, R., Deng, X., Dong, L., Sun, M., Li, C., Nachtergaele, S., Wang, Y., Hu, C., Ferchen, K., Greis, K.D., Jiang, X., Wei, M., Qu, L., Guan, J.-L., He, C., Yang, J. and Chen, J. 2018. Author Correction: Recognition of RNA N6-methyladenosine by IGF2BP proteins enhances mRNA stability and translation. *Nature cell biology*. **20**(9), p.1098.

Imam, H., Khan, M., Gokhale, N.S., McIntyre, A.B.R., Kim, G.W., Jang, J.Y., Kim, S.J.,

Mason, C.E., Horner, S.M. and Siddiqui, A. 2018. N6-methyladenosine modification of hepatitis b virus RNA differentially regulates the viral life cycle. *Proceedings of the National Academy of Sciences of the United States of America*. **115**(35), pp.8829–8834.

Inoue, N., Winter, J., Lal, R.B., Offermann, M.K. and Koyano, S. 2003. Characterization of Entry Mechanisms of Human Herpesvirus 8 by Using an Rta-Dependent Reporter Cell Line. *Journal of Virology*. **77**(18), pp.10177–10177.

Jackson, B.R., Boyne, J.R., Noerenberg, M., Taylor, A., Hautbergue, G.M., Walsh, M.J., Wheat, R., Blackbourn, D.J., Wilson, S.A. and Whitehouse, A. 2011. An Interaction between KSHV ORF57 and UIF Provides mRNA-Adaptor Redundancy in Herpesvirus Intronless mRNA Export B. A. Glaunsinger, ed. *PLoS Pathogens*. **7**(7), p.e1002138.

Jacob, R.J., Morse, L.S. and Roizman, B. 1979. Anatomy of Herpes Simplex Virus DNA XII. Accumulation of Head-to-Tail Concatemers in Nuclei of Infected Cells and Their Role in the Generation of the Four Isomeric Arrangements of Viral DNA. *Journal of Virology*. **29**(2), pp.448–457.

Jeffery-Smith, A. and Riddell, A. 2021. Herpesviruses S. Baron, ed. *Medicine*. **49**(12), pp.780–784.

Jha, H., Banerjee, S. and Robertson, E. 2016. The Role of Gammaherpesviruses in Cancer Pathogenesis. *Pathogens*. **5**(1), p.18.

Jia, G., Fu, Y., Zhao, X., Dai, Q., Zheng, G., Yang, Y.Y.-G.G., Yi, C., Lindahl, T., Pan, T., Yang, Y.Y.-G.G. and He, C. 2011. N6-methyladenosine in nuclear RNA is a major substrate of the obesity-associated FTO. *Nature chemical biology*. **7**(12), pp.885–887.

Johnson, D.C. and Baines, J.D. 2011. Herpesviruses remodel host membranes for virus egress. *Nature Reviews Microbiology*. **9**(5), pp.382–394.

Kan, L., Grozhik, A. V., Vedanayagam, J., Patil, D.P., Pang, N., Lim, K.S., Huang, Y.C., Joseph, B., Lin, C.J., Despic, V., Guo, J., Yan, D., Kondo, S., Deng, W.M., Dedon, P.C., Jaffrey, S.R. and Lai, E.C. 2017. The m 6 A pathway facilitates sex determination in Drosophila. *Nature Communications*. **8**, pp.1–16.

Kane, S.E. and Beemon, K. 1985. Precise localization of m6A in Rous sarcoma virus RNA reveals clustering of methylation sites: implications for RNA processing. *Molecular*

and cellular biology. **5**(9), pp.2298–2306.

Kaplan, L.D. 2013. Human herpesvirus-8: Kaposi sarcoma, multicentric Castleman disease, and primary effusion lymphoma. *Hematology / the Education Program of the American Society of Hematology. American Society of Hematology. Education Program*. **2013**, pp.103–108.

Karijolich, J. and Yu, Y.T. 2011. Converting nonsense codons into sense codons by targeted pseudouridylation. *Nature*. **474**(7351), pp.395–399.

Katahira, J. 2015. Nuclear export of messenger RNA. *Genes*. **6**(2), pp.163–184.

Ke, S., Pandya-Jones, A., Saito, Y., Fak, J.J., Vågbø, C.B., Geula, S., Hanna, J.H., Black, D.L., Darnell, J.E. and Darnell, R.B. 2017. m6A mRNA modifications are deposited in nascent pre-mRNA and are not required for splicing but do specify cytoplasmic turnover. *Genes and Development*. **31**(10), pp.990–1006.

Kelly, B.J., Fraefel, C., Cunningham, A.L. and Diefenbach, R.J. 2009. Functional roles of the tegument proteins of herpes simplex virus type 1. *Virus Research*. **145**(2), pp.173–186.

Kennedy, E.M., Bogerd, H.P., Kornepati, A.V.R., Kang, D., Ghoshal, D., Marshall, J.B., Poling, B.C., Tsai, K., Gokhale, N.S., Horner, S.M. and Cullen, B.R. 2016. Posttranscriptional m 6 A editing of HIV-1 mRNAs enhances viral gene expression. *Cell host & microbe*. **19**(5), pp.675–685.

Knuckles, P., Lence, T., Haussmann, I.U., Jacob, D., Kreim, N., Carl, S.H., Masiello, I., Hares, T., Villaseñor, R., Hess, D., Andrade-navarro, M.A., Biggiogera, M., Helm, M., Soller, M. and Bühler, M. 2018. Zc3h13 / Flacc is required for adenosine methylation by bridging the mRNA- binding factor Rbm15 / Spenito to the m 6 A machinery component Wtap / Fl (2) d. *Genes and Development*. **32**(2), pp.415–429.

Koelle, D.M., Huang, M.L., Chandran, B., Vieira, J., Piepkorn, M. and Corey, L. 1997. Frequent detection of Kaposi's sarcoma-associated herpesvirus (human herpesvirus 8) DNA in saliva of human immunodeficiency virus-infected men: clinical and immunologic correlates. *The Journal of infectious diseases*. **176**(1), pp.94–102.

Kowalak, J.A., Dalluge, J.J., McCloskey, J.A. and Stetter, K.O. 1994. The Role of Posttranscriptional Modification in Stabilization of Transfer RNA from Hyperthermophiles. *Biochemistry*. **33**(25), pp.7869–7876.

Krug, R.M., Morgan, M.A. and Shatkin, A.J. 1976. Influenza viral mRNA contains internal N6 methyladenosine and 5' terminal 7 methylguanosine in cap structures. *Journal of Virology*. **20**(1), pp.45–53.

Kumar, B. and Chandran, B. 2016. KSHV entry and trafficking in target cells—Hijacking of cell signal pathways,actin and membrane dynamics. *Viruses*. **8**(11).

Lan, K., Kuppers, D.A., Verma, S.C. and Robertson, E.S. 2004. Kaposi's Sarcoma-Associated Herpesvirus-Encoded Latency-Associated Nuclear Antigen Inhibits Lytic Replication by Targeting Rta: a Potential Mechanism for Virus-Mediated Control of Latency. *Journal of Virology*. **78**(12), pp.6585–6594.

Lang, F., Singh, R.K., Pei, Y., Zhang, S., Sun, K. and Robertson, E.S. 2019. EBV epitranscriptome reprogramming by METTL14 is critical for viral-associated tumorigenesis B. E. Gewurz, ed. *PLOS Pathogens*. **15**(6), p.e1007796.

Lanternier, F., Lebbe, C., Schartz, N., Farhi, D., Marcelin, A.-G., Kerob, D., Agbalika, F., Verola, O., Gorin, I., Janier, M., Avril, M.-F. and Dupin, N. 2008. Kaposi's sarcoma in HIV-negative men having sex with men. *AIDS (London, England)*. **22**(10), pp.1163–1168.

Lee, H., Patschull, A.O.M., Bagnéris, C., Ryan, H., Sanderson, C.M., Ebrahimi, B., Nobeli, I. and Barrett, T.E. 2017. KSHV SOX mediated host shutoff: The molecular mechanism underlying mRNA transcript processing. *Nucleic Acids Research*. **45**(8), pp.4756–4767.

Lee, Y.J. and Glaunsinger, B.A. 2009. Aberrant herpesvirus-induced polyadenylation correlates with cellular messenger RNA destruction. *PLoS biology*. **7**(5), p.e1000107.

Legrand, C., Tuorto, F., Hartmann, M., Liebers, R., Jacob, D., Helm, M. and Lyko, F. 2017. Statistically robust methylation calling for wholetranscriptome bisulfite sequencing reveals distinct methylation patterns for mouse RNAs. *Genome Research*. **27**(9), pp.1589–1596.

Lence, T., Akhtar, J., Bayer, M., Schmid, K., Spindler, L., Ho, C.H., Kreim, N., Andrade-Navarro, M.A., Poeck, B., Helm, M. and Roignant, J.Y. 2016. M6A modulates neuronal functions and sex determination in Drosophila. *Nature*. **540**(7632), pp.242–247.

Lenstra, T.L., Rodriguez, J., Chen, H. and Larson, D.R. 2016. Transcription Dynamics in Living Cells. *Annual Review of Biophysics*. **45**(1), pp.25–47.

Lesbirel, S., Viphakone, N., Parker, M., Parker, J., Heath, C., Sudbery, I. and Wilson, S.A. 2018. The m6A-methylase complex recruits TREX and regulates mRNA export. *Scientific Reports*. **8**(1), p.13827.

Leung, C.C. and Wong, C.K. 2018. Effects of STC1 overexpression on tumorigenicity and metabolism of hepatocellular carcinoma. *Oncotarget*. **9**(6), pp.6852–6861.

Li, X., Xiong, X., Wang, K., Wang, L., Shu, X., Ma, S. and Yi, C. 2016. Transcriptome-wide mapping reveals reversible and dynamic N1-methyladenosine methylome. *Nature Chemical Biology*. **12**(5), pp.311–316.

Li, X., Zhu, P., Ma, S., Song, J., Bai, J., Sun, F. and Yi, C. 2015. Chemical pulldown reveals dynamic pseudouridylation of the mammalian transcriptome. *Nature Chemical Biology*. **11**(8), pp.592–597.

Li, Y., He, Z.C., Zhang, X.N., Liu, Q., Chen, C., Zhu, Z., Chen, Q., Shi, Y., Yao, X.H., Cui, Y.H., Zhang, X., Wang, Y., Kung, H.F., Ping, Y.F. and Bian, X.W. 2018. Stanniocalcin-1 augments stem-like traits of glioblastoma cells through binding and activating NOTCH1. *Cancer Letters*. **416**, pp.66–74.

Li, Z., Weng, H., Su, R., Weng, X., Zuo, Z., Li, C., Huang, Huilin, Nachtergaele, S., Dong, L., Hu, C., Qin, X., Tang, L., Wang, Y., Hong, G.M., Huang, Hao, Wang, X., Chen, P., Gurbuxani, S., Arnovitz, S., Li, Y., Li, S., Strong, J., Neilly, M.B., Larson, R.A., Jiang, X., Zhang, P., Jin, J., He, C. and Chen, J. 2017. FTO Plays an Oncogenic Role in Acute Myeloid Leukemia as a N6-Methyladenosine RNA Demethylase. *Cancer Cell*. **31**(1), pp.127–141.

Liang, Y., Chang, J., Lynch, S.J., Lukac, D.M. and Ganem, D. 2002. The lytic switch protein of KSHV activates gene expression via functional interaction with RBP-Jκ (CSL), the target of the Notch signaling pathway. *Genes and Development*. **16**(15), pp.1977–

1989.

Lichinchi, G., Gao, S., Saletore, Y., Gonzalez, G.M., Bansal, V., Wang, Y., Mason, C.E. and Rana, T.M. 2016. Dynamics of the human and viral m(6)A RNA methylomes during HIV-1 infection of T cells. *Nature microbiology*. **1**(4), p.16011.

Lichinchi, G., Zhao, B.S., Wu, Y., Lu, Z., Qin, Y., He, C. and Rana, T.M. 2016. Dynamics of Human and Viral RNA Methylation during Zika Virus Infection. *Cell Host and Microbe*. **20**(5), pp.666–673.

Lin, Y., Protter, D.S.W., Rosen, M.K. and Parker, R. 2015. Formation and Maturation of Phase-Separated Liquid Droplets by RNA-Binding Proteins. *Molecular Cell*. **60**(2), pp.208–219.

Linder, B., Grozhik, A. V, Olarerin-George, A.O., Meydan, C., Mason, C.E. and Jaffrey, S.R. 2015. Single-nucleotide-resolution mapping of m6A and m6Am throughout the transcriptome. *Nature methods*. **12**(8), pp.767–772.

Lisanti, M.P., Scherer, P.E., Vidugiriene, J., Tang, Z.L., Hermanowski-Vosatka, A., Tu, Y.H., Cook, R.F. and Sargiacomo, M. 1994. Characterization of caveolin-rich membrane domains isolated from an endothelial-rich source: Implications for human disease. *Journal of Cell Biology*. **126**(1), pp.111–126.

Liu, B., Merriman, D.K., Choi, S.H., Schumacher, M.A., Plangger, R., Kreutz, C., Horner, S.M., Meyer, K.D. and Al-Hashimi, H.M. 2018. A potentially abundant junctional RNA motif stabilized by m6A and Mg2+. *Nature Communications*. **9**(1), pp.1–10.

Liu, F., Clark, W., Luo, G., Wang, Xiaoyun, Fu, Y., Wei, J., Wang, Xiao, Hao, Z., Dai, Q., Zheng, G., Ma, H., Han, D., Evans, M., Klungland, A., Pan, T. and He, C. 2016. ALKBH1-Mediated tRNA Demethylation Regulates Translation. *Cell*. **167**(3), pp.816-828.e16.

Liu, J., Li, K., Cai, J., Zhang, M., Zhang, X., Xiong, X., Meng, H., Xu, X., Huang, Z., Peng, J., Fan, J. and Yi, C. 2020. Landscape and Regulation of m6A and m6Am Methylome across Human and Mouse Tissues. *Molecular Cell*. **77**(2), pp.426-440.e6.

Liu, J., Yue, Y., Han, D., Wang, X., Fu, Y., Zhang, L., Jia, G., Yu, M., Lu, Z. and Deng, X. 2014. A METTL3-METTL14 complex mediates mammalian nuclear RNA N6-adenosine methylation. *Nature chemical biology*. **10**(2), pp.93–95.

Liu, N., Dai, Q., Zheng, G., He, C., Parisien, M. and Pan, T. 2015. N6-methyladenosine-dependent RNA structural switches regulate RNA-protein interactions. *Nature*. **518**(7540), pp.560–564.

Liu, N., Zhou, K.I., Parisien, M., Dai, Q., Diatchenko, L. and Pan, T. 2017. N6-methyladenosine alters RNA structure to regulate binding of a low-complexity protein. *Nucleic Acids Research*. **45**(10), pp.6051–6063.

Liu, S., Ye, D., Wang, T., Guo, W., Song, H., Liao, Y., Xu, D., Zhu, H., Zhang, Z. and Deng, J. 2017. Repression of GPRC5A is associated with activated STAT3, which contributes to tumor progression of head and neck squamous cell carcinoma. *Cancer Cell International*. **17**(1), pp.1–11.

Liu, X. xu, Liu, W. dong, Wang, L., Zhu, B., Shi, X., Peng, Z. xuan, Zhu, H. cheng, Liu, Xing dong, Zhong, M. zuo, Xie, D., Zeng, M. sheng and Ren, C. ping 2018. Roles of flotillins in tumors. *Journal of Zhejiang University: Science B*. **19**(3), pp.171–182.

Loh, X.Y., Sun, Q.Y., Ding, L.W., Mayakonda, A., Venkatachalam, N., Yeo, M.S., Silva, T.C., Xiao, J.F., Doan, N.B., Said, J.W., Ran, X. Bin, Zhou, S.Q., Dakle, P., Shyamsunder, P., Koh, A.P.F., Huang, R.Y.J., Berman, B.P., Tan, S.Y., Yang, H., Lin, D.C. and Phillip Koeffler, H. 2020. RNA-binding protein ZFP36L1 suppresses hypoxia and cell-cycle signaling. *Cancer Research*. **80**(2), pp.219–233.

Loret, S., Guay, G. and Lippe, R. 2008. Comprehensive Characterization of Extracellular Herpes Simplex Virus Type 1 Virions. *Journal of Virology*. **82**(17), pp.8605–8618.

Louloupi, A., Ntini, E., Conrad, T. and Ørom, U.A.V. 2018. Transient N-6-Methyladenosine Transcriptome Sequencing Reveals a Regulatory Role of m6A in Splicing Efficiency. *Cell Reports*. **23**(12), pp.3429–3437.

Lu, W., Tirumuru, N., St. Gelais, C., Koneru, P.C., Liu, C., Kvaratskhelia, M., He, C. and Wu, L. 2018. N6-Methyladenosine–binding proteins suppress HIV-1 infectivity and viral production. *Journal of Biological Chemistry* . **293**(34), pp.12992–13005.

Lukac, D.M., Garibyan, L., Kirshner, J.R., Palmeri, D. and Ganem, D. 2001. DNA Binding by Kaposi's Sarcoma-Associated Herpesvirus Lytic Switch Protein Is Necessary for Transcriptional Activation of Two Viral Delayed Early Promoters. *Journal of Virology*. **75**(15), pp.6786–6799.

Lukac, D.M., Kirshner, J.R. and Ganem, D. 1999. Transcriptional Activation by the Product of Open Reading Frame 50 of Kaposi's Sarcoma-Associated Herpesvirus Is Required for Lytic Viral Reactivation in B Cells. *Journal of Virology*. **73**(11), pp.9348–9361.

Lv, Y., Zhou, S., Gao, S. and Deng, H. 2019. Remodeling of host membranes during herpesvirus assembly and egress. *Protein and Cell*. **10**(5), pp.315–326.

Ma, W. and Mayr, C. 2018. A Membraneless Organelle Associated with the Endoplasmic Reticulum Enables 3'UTR-Mediated Protein-Protein Interactions. *Cell*. **175**(6), pp.1492-1506.e19.

Machnicka, M.A., Milanowska, K., Oglou, O.O., Purta, E., Kurkowska, M., Olchowik, A., Januszewski, W., Kalinowski, S., Dunin-Horkawicz, S., Rother, K.M., Helm, M., Bujnicki, J.M. and Grosjean, H. 2013. MODOMICS: A database of RNA modification pathways - 2013 update. *Nucleic Acids Research*. **41**(D1), pp.262–267.

Majerciak, V. and Zheng, Z.M. 2015. KSHV ORF57, a protein of many faces. *Viruses*. **7**(2), pp.604–633.

Manners, O., Baquero-Perez, B. and Whitehouse, A. 2019. m 6 A: Widespread regulatory control in virus replication. *Biochimica et Biophysica Acta - Gene Regulatory Mechanisms*. **1862**(3), pp.370–381.

Manners, O., Murphy, J.C., Coleman, A., Hughes, D.J. and Whitehouse, A. 2018. Contribution of the KSHV and EBV lytic cycles to tumourigenesis. *Current Opinion in Virology*. **32**, pp.60–70.

Martin, J.N., Ganem, D.E., Osmond, D.H., Page-Shafer, K.A., Macrae, D. and Kedes, D.H. 1998. Sexual transmission and the natural history of human herpesvirus 8 infection. *The New England journal of medicine*. **338**(14), pp.948–954.

Martin, J.N. and Osmond, D.H. 2000. Invited commentary: determining specific sexual practices associated with human herpesvirus 8 transmission. *American journal of epidemiology*. **151**(3), pp.225–9; discussion 230.

Martin, J.N. and Osmond, D.H. 1999. Kaposi's sarcoma-associated herpesvirus and sexual transmission of cancer risk. *Current Opinion in Oncology*. **11**(6), pp.508–515.

Martin, K.C. and Ephrussi, A. 2009. mRNA Localization: Gene Expression in the Spatial

Dimension. *Cell*. **136**(4), pp.719–730.

Matthews, R.E. 1979. Third report of the International Committee on Taxonomy of Viruses. Classification and nomenclature of viruses. *Intervirology*. **12**(3–5), pp.129–296.

Mauer, J., Luo, X., Blanjoie, A., Jiao, X., Grozhik, A. V., Patil, D.P., Linder, B., Pickering, B.F., Vasseur, J.J., Chen, Q., Gross, S.S., Elemento, O., Debart, F., Kiledjian, M. and Jaffrey, S.R. 2017. Reversible methylation of m6 Am in the 5′ cap controls mRNA stability. *Nature*. **541**(7637), pp.371–375.

Mauer, J., Luo, X., Blanjoie, A., Jiao, X., Grozhik, A. V, Patil, D.P., Linder, B., Pickering, B.F., Vasseur, J.J., Chen, Q., Gross, S.S., Elemento, O., Debart, F., Kiledjian, M. and Jaffrey, S.R. 2017. Reversible methylation of m6 Am in the 5′ cap controls mRNA stability. *Nature*. **541**(7637), pp.371–375.

Mauer, J., Sindelar, M., Despic, V., Guez, T., Hawley, B.R., Vasseur, J.J., Rentmeister, A., Gross, S.S., Pellizzoni, L., Debart, F., Goodarzi, H. and Jaffrey, S.R. 2019. FTO controls reversible m 6 Am RNA methylation during snRNA biogenesis. *Nature Chemical Biology*. **15**(4), pp.340–347.

Meyer, K.D., Patil, D.P., Zhou, J., Zinoviev, A., Skabkin, M.A., Elemento, O., Pestova, T. V, Qian, S.-B. and Jaffrey, S.R. 2015. 5′ UTR m(6)A Promotes Cap-Independent Translation. *Cell*. **163**(4), pp.999–1010.

Meyer, K.D., Saletore, Y., Zumbo, P., Elemento, O., Mason, C.E. and Jaffrey, S.R. 2012. Comprehensive analysis of mRNA methylation reveals enrichment in 3′ UTRs and near stop codons. *Cell*. **149**(7), pp.1635–1646.

Miller, G., Heston, L., Grogan, E., Gradoville, L., Rigsby, M., Sun, R., Shedd, D., Kushnaryov, V.M., Grossberg, S. and Chang, Y. 1997. Selective switch between latency and lytic replication of Kaposi's sarcoma herpesvirus and Epstein-Barr virus in dually infected body cavity lymphoma cells. *Journal of Virology*. **71**(1), pp.314–324.

Mirzaei, H., Khodadad, N., Karami, C., Pirmoradi, R. and Khanizadeh, S. 2020. The AP-1 pathway; A key regulator of cellular transformation modulated by oncogenic viruses. *Reviews in Medical Virology*. **30**(1), pp.1–13.

Mohl, B.S., Chen, J. and Longnecker, R. 2019. Gammaherpesvirus entry and fusion: A tale how two human pathogenic viruses enter their host cells. *Advances in virus research*. **104**, pp.313–343.

Moore, K.S. and von Lindern, M. 2018. RNA binding proteins and regulation of mRNA translation in erythropoiesis. *Frontiers in Physiology*. **9**(JUL), pp.1–17.

Moss, B., Gershowitz, A., Stringer, J.R., Holland, L.E. and Wagner, E.K. 1977. 5' Terminal and internal methylated nucleosides in herpes and simplex virus type 1 mRNA. *Journal of Virology*. **23**(2), pp.234–239.

Murdoch, D.M., Venter, W.D.F., Feldman, C. and Van Rie, A. 2008. Incidence and risk factors for the immune reconstitution inflammatory syndrome in HIV patients in South Africa: A prospective study. *AIDS*. **22**(5), pp.601–610.

Nador, R.G., Cesarman, E., Chadburn, A., Dawson, D.B., Ansari, M.Q., Said, J. and Knowles, D.M. 1996. Primary effusion lymphoma: A distinct clinicopathologic entity associated with the Kaposi's sarcoma-associated herpes virus. *Blood*. **88**(2), pp.645–656.

Nakamura, H., Lu, M., Gwack, Y., Souvlis, J., Zeichner, S.L. and Jung, J.U. 2003. Global changes in Kaposi's sarcoma-associated virus gene expression patterns following expression of a tetracycline-inducible Rta transactivator. *Journal of virology*. **77**(7), pp.4205–20.

Nance, D.J., Satterwhite, E.R., Bhaskar, B., Misra, S., Carraway, K.R. and Mansfield, K.D. 2020. Characterization of METTL16 as a cytoplasmic RNA binding protein A. F. Palazzo, ed. *PLOS ONE*. **15**(1), p.e0227647.

Narayan, P., Ayers, D.F., Rottman, F.M., Maroney, P.A. and Nilsen, T.W. 1987. Unequal distribution of N6-methyladenosine in influenza virus mRNAs. *Molecular and Cellular Biology*. **7**(4), pp.1572–1575.

Narkhede, M., Arora, S. and Ujjani, C. 2018. Primary effusion lymphoma: Current perspectives. *OncoTargets and Therapy*. **11**, pp.3747–3754.

Newman, R., Ahlfors, H., Saveliev, A., Galloway, A., Hodson, D.J., Williams, R., Besra, G.S., Cook, C.N., Cunningham, A.F., Bell, S.E. and Turner, M. 2017. Maintenance of the marginal-zone B cell compartment specifically requires the RNA-binding protein

ZFP36L1. *Nature Immunology*. **18**(6), pp.683–693.

Nicola, A. V., McEvoy, A.M. and Straus, S.E. 2003. Roles for Endocytosis and Low pH in Herpes Simplex Virus Entry into HeLa and Chinese Hamster Ovary Cells. *Journal of Virology*. **77**(9), pp.5324–5332.

Nicola, A. V. and Straus, S.E. 2004. Cellular and Viral Requirements for Rapid Endocytic Entry of Herpes Simplex Virus. *Journal of Virology*. **78**(14), pp.7508–7517.

Otsuka, H., Fukao, A., Funakami, Y., Duncan, K.E. and Fujiwara, T. 2019. Emerging evidence of translational control by AU-rich element-binding proteins. *Frontiers in Genetics*. **10**(MAY), pp.1–10.

Otto, G.P. and Nichols, B.J. 2011. The roles of flotillin microdomains-endocytosis and beyond. *Journal of Cell Science*. **124**(23), pp.3933–3940.

Owen, D.J., Crump, C.M. and Graham, S.C. 2015. Tegument Assembly and Secondary Envelopment of Alphaherpesviruses. *Viruses*. **7**(9), pp.5084–5114.

Pageau, G.J., Hall, L.L., Ganesan, S., Livingston, D.M. and Lawrence, J.B. 2007. The disappearing Barr body in breast and ovarian cancers. *Nature Reviews Cancer*. **7**(8), pp.628–633.

Papp, B., Motlagh, N., Smindak, R.J., Jin Jang, S., Sharma, A., Alonso, J.D. and Toth, Z. 2019. Genome-Wide Identification of Direct RTA Targets Reveals Key Host Factors for Kaposi's Sarcoma-Associated Herpesvirus Lytic Reactivation. *Journal of Virology*. **93**(5), pp.e01978-18.

Pasdeloup, D., Blondel, D., Isidro, A.L. and Rixon, F.J. 2009. Herpesvirus Capsid Association with the Nuclear Pore Complex and Viral DNA Release Involve the Nucleoporin CAN/Nup214 and the Capsid Protein pUL25. *Journal of Virology*. **83**(13), pp.6610–6623.

Patil, D.P., Chen, C.-K., Pickering, B.F., Chow, A., Jackson, C., Guttman, M. and Jaffrey, S.R. 2016. m6A RNA methylation promotes XIST-mediated transcriptional repression. *Nature*. **537**(7620), pp.369–373.

Patrick, J.T., McBride, W.J. and Felten, D.L. 1983. Brief communication. *Brain Research Bulletin*. **10**(3), pp.415–418.

Ping, X.-L., Sun, B.-F., Wang, L., Xiao, W., Yang, X., Wang, W.-J., Adhikari, S., Shi, Y., Lv, Y. and Chen, Y.-S. 2014. Mammalian WTAP is a regulatory subunit of the RNA N6-methyladenosine methyltransferase. *Cell research*. **24**(2), pp.177–189.

De Pinto, V., Messina, A., Lane, D.J.R. and Lawen, A. 2010. Voltage-dependent anion-selective channel (VDAC) in the plasma membrane. *FEBS Letters*. **584**(9), pp.1793–1799.

Polizzotto, M.N., Uldrick, T.S., Hu, D. and Yarchoan, R. 2012. Clinical manifestations of Kaposi sarcoma herpesvirus lytic activation: Multicentric Castleman disease (KSHV-MCD) and the KSHV inflammatory cytokine syndrome. *Frontiers in Microbiology*. **3**(MAR), pp.1–9.

Purcell, D.F. and Martin, M.A. 1993. Alternative splicing of human immunodeficiency virus type 1 mRNA modulates viral protein expression, replication, and infectivity. *Journal of Virology*. **67**(11), pp.6365–6378.

Purushothaman, P., Uppal, T. and Verma, S.C. 2015. Molecular biology of KSHV lytic reactivation. *Viruses*. **7**(1), pp.116–153.

Raghu, H., Sharma-Walia, N., Veettil, M. V., Sadagopan, S. and Chandran, B. 2009. Kaposi's Sarcoma-Associated Herpesvirus Utilizes an Actin Polymerization-Dependent Macropinocytic Pathway To Enter Human Dermal Microvascular Endothelial and Human Umbilical Vein Endothelial Cells. *Journal of Virology*. **83**(10), pp.4895–4911.

Regamey, N., Cathomas, G., Schwager, M., Wernli, M., Harr, T. and Erb, P. 1998. High human herpesvirus 8 seroprevalence in the homosexual population in switzerland. *Journal of Clinical Microbiology*. **36**(6), pp.1784–1786.

Regamey, N, Tamm, M., Wernli, M., Witschi, A., Thiel, G., Cathomas, G. and Erb, P. 1998. Transmission of human herpesvirus 8 infection from renal-transplant donors to recipients. *The New England journal of medicine*. **339**(19), pp.1358–1363.

Ries, R.J., Zaccara, S., Klein, P., Olarerin-George, A., Namkoong, S., Pickering, B.F., Patil, D.P., Kwak, H., Lee, J.H. and Jaffrey, S.R. 2019. m6A enhances the phase separation potential of mRNA. *Nature*. **571**(7765), pp.424–428.

Roizmann, B., Desrosiers, R.C., Fleckenstein, B., Lopez, C., Minson, A.C. and Studdert,

M.J. 1992. The family Herpesviridae: an update. The Herpesvirus Study Group of the International Committee on Taxonomy of Viruses. *Archives of virology*. **123**(3–4), pp.425–449.

Roost, C., Lynch, S.R., Batista, P.J., Qu, K., Chang, H.Y. and Kool, E.T. 2015. Structure and thermodynamics of N6-methyladenosine in RNA: A spring-loaded base modification. *Journal of the American Chemical Society*. **137**(5), pp.2107–2115.

Roundtree, I.A., Luo, G.-Z., Zhang, Z., Wang, X., Zhou, T., Cui, Y., Sha, J., Huang, X., Guerrero, L., Xie, P., He, E., Shen, B. and He, C. 2017. YTHDC1 mediates nuclear export of N(6)-methyladenosine methylated mRNAs. *eLife*. **6**, p.e31311.

Rubio, R.M., Depledge, D.P., Bianco, C., Thompson, L. and Mohr, I. 2018. RNA m 6 A modification enzymes shape innate responses to DNA by regulating interferon β. *Genes and Development*. **32**(23–24), pp.1472–1484.

Russo, J.J., Bohenzky, R.A., Chien, M.C., Chen, J., Yan, M., Maddalena, D., Parry, J.P., Peruzzi, D., Edelman, I.S., Chang, Y. and Moore, P.S. 1996. Nucleotide sequence of the Kaposi sarcoma-associated herpesvirus (HHV8). *Proceedings of the National Academy of Sciences of the United States of America*. **93**(25), pp.14862–14867.

Růžička, K., Zhang, M., Campilho, A., Bodi, Z., Kashif, M., Saleh, M., Eeckhout, D., El-Showk, S., Li, H., Zhong, S., Jaeger, G. De, Mongan, N.P., Hejátko, J., Helariutta, Y. and Fray, R.G. 2017. Identification of factors required for m6A mRNA methylation in Arabidopsis reveals a role for the conserved E3 ubiquitin ligase HAKAI. *New Phytologist*. **215**(1), pp.157–172.

Sakakibara, S. and Tosato, G. 2014. Contribution of viral mimics of cellular genes to KSHV infection and disease. *Viruses*. **6**(9), pp.3472–3486.

Schiffer, J.T. and Corey, L. 2009. New concepts in understanding genital herpes. *Current Infectious Disease Reports*. **11**(6), pp.457–464.

Schrag, J.D. 1988. Three-Dimensional Nucleocapsid Structure of the HSVI. . **56**, pp.651–660.

Schuller, A.P. and Green, R. 2018. Roadblocks and resolutions in eukaryotic translation. *Nature Reviews Molecular Cell Biology*. **19**(8), pp.526–541.

Schumann, S., Jackson, B.R., Yule, I., Whitehead, S.K., Revill, C., Foster, R. and Whitehouse, A. 2016. Targeting the ATP-dependent formation of herpesvirus ribonucleoprotein particle assembly as an antiviral approach. *Nature Microbiology*. **2**, p.16201.

Schwartz, S., Bernstein, D.A., Mumbach, M.R., Jovanovic, M., Herbst, R.H., León-Ricardo, B.X., Engreitz, J.M., Guttman, M., Satija, R., Lander, E.S., Fink, G. and Regev, A. 2014. Transcriptome-wide mapping reveals widespread dynamic-regulated pseudouridylation of ncRNA and mRNA. *Cell*. **159**(1), pp.148–162.

Schwartz, S., Mumbach, M.R., Jovanovic, M., Wang, T., Maciag, K., Bushkin, G.G., Mertins, P., Ter-Ovanesyan, D., Habib, N. and Cacchiarelli, D. 2014. Perturbation of m6A writers reveals two distinct classes of mRNA methylation at internal and 5′ sites. *Cell reports*. **8**(1), pp.284–296.

Sehrawat, S., Kumar, D. and Rouse, B.T. 2018. Herpesviruses: Harmonious pathogens but relevant cofactors in other diseases? *Frontiers in Cellular and Infection Microbiology*. **8**(MAY), pp.1–15.

Shi, H., Wang, X., Lu, Z., Zhao, B.S., Ma, H., Hsu, P.J., Liu, C. and He, C. 2017. YTHDF3 facilitates translation and decay of N6-methyladenosine-modified RNA. *Cell Research*. **27**, p.315.

Shi, Y. 2017. Mechanistic insights into precursor messenger RNA splicing by the spliceosome. *Nature Reviews Molecular Cell Biology*. **18**(11), pp.655–670.

Śledź, P. and Jinek, M. 2016. Structural insights into the molecular mechanism of the m(6)A writer complex. *eLife*. **5**, p.e18434.

Sodeik, B., Ebersold, M.W. and Helenius, A. 1997. Microtubule-mediated transport of incoming herpes simplex virus 1 capsids to the nucleus. *Journal of Cell Biology*. **136**(5), pp.1007–1021.

Sommer, S., Salditt-Georgieff, M., Bachenheimer, S., Darnell, J.E., Furuichi, Y., Morgan, M. and Shatkin, A.J. 1976. The methylation of adenovirus-specific nuclear and cytoplasmic RNA. *Nucleic acids research*. **3**(3), pp.749–766.

Son, Y.-O., Kim, H.-E., Choi, W.-S., Chun, C.-H. and Chun, J.-S. 2019. RNA-binding protein ZFP36L1 regulates osteoarthritis by modulating members of the heat shock protein

70 family. *Nature Communications*. **10**(1), p.77.

Soulier, J., Grollet, L., Oksenhendler, E., Cacoub, P., Cazals-Hatem, D., Babinet, P., d'Agay, M.F., Clauvel, J.P., Raphael, M. and Degos, L. 1995. Kaposi's sarcoma-associated herpesvirus-like DNA sequences in multicentric Castleman's disease. *Blood*. **86**(4), pp.1276–80.

Squires, J.E., Patel, H.R., Nousch, M., Sibbritt, T., Humphreys, D.T., Parker, B.J., Suter, C.M. and Preiss, T. 2012. Widespread occurrence of 5-methylcytosine in human coding and non-coding RNA. *Nucleic Acids Research*. **40**(11), pp.5023–5033.

Stewart, J.P., Usherwood, E.J., Ross, A., Dyson, H. and Nash, T. 1998. Lung epithelial cells are a major site of murine gammaherpesvirus persistence. *The Journal of experimental medicine*. **187**(12), pp.1941–1951.

Sträßer, K., Masuda, S., Mason, P., Pfannstiel, J., Oppizzi, M., Rodriguez-Navarro, S., Rondón, A.G., Aguilera, A., Struhl, K., Reed, R. and Hurt, E. 2002. TREX is a conserved complex coupling transcription with messenger RNA export. *Nature*. **417**(6886), pp.304–308.

Tan, B., Liu, H., Zhang, S.S.-W., da Silva, S.R., Zhang, L., Meng, J., Cui, X., Yuan, H., Sorel, O., Zhang, S.S.-W., Huang, Y. and Gao, S.-J. 2018. Viral and cellular N6-methyladenosine and N6,2'-O-dimethyladenosine epitranscriptomes in the KSHV life cycle. *Nature Microbiology*. **3**(1), pp.108–120.

Tang, Q., Qin, D., Lv, Z., Zhu, X., Ma, X., Yan, Q., Zeng, Y., Guo, Y., Feng, N. and Lu, C. 2012. Herpes simplex virus type 2 triggers reactivation of Kaposi's sarcoma-associated herpesvirus from latency and collaborates with HIV-1 tat. *PLoS ONE*. **7**(2).

Theler, D., Dominguez, C., Blatter, M., Boudet, J. and Allain, F.H.T. 2014. Solution structure of the YTH domain in complex with N6-methyladenosine RNA: a reader of methylated RNA. *Nucleic Acids Research*. **42**(22), pp.13911–13919.

Thul, P.J., Åkesson, L., Wiking, M., Mahdessian, D., Geladaki, A., Ait Blal, H., Alm, T., Asplund, A., Björk, L., Breckels, L.M., Bäckström, A., Danielsson, F., Fagerberg, L., Fall, J., Gatto, L., Gnann, C., Hober, S., Hjelmare, M., Johansson, F., Lee, S., Lindskog, C., Mulder, J., Mulvey, C.M., Nilsson, P., Oksvold, P., Rockberg, J., Schutten, R.,

Schwenk, J.M., Sivertsson, Å., Sjöstedt, E., Skogs, M., Stadler, C., Sullivan, D.P., Tegel, H., Winsnes, C., Zhang, C., Zwahlen, M., Mardinoglu, A., Pontén, F., von Feilitzen, K., Lilley, K.S., Uhlén, M. and Lundberg, E. 2017. A subcellular map of the human proteome. *Science*. **356**(6340).

Tirumuru, N., Zhao, B.S., Lu, W., Lu, Z., He, C. and Wu, L. 2016. N(6)-methyladenosine of HIV-1 RNA regulates viral infection and HIV-1 Gag protein expression. *eLife*. **5**, p.e15528.

Tsai, K, Courtney, D.G. and Cullen, B.R. 2018. Addition of m6A to SV40 late mRNAs enhances viral structural gene expression and replication. *PLoS Pathog*. **14**(2), p.e1006919.

Tsai, Kevin, Courtney, D.G. and Cullen, B.R. 2018. Addition of m6A to SV40 late mRNAs enhances viral structural gene expression and replication. *PLoS Pathog*. **14**(2), p.e1006919.

Uldrick, T.S., Wang, V., O'Mahony, D., Aleman, K., Wyvill, K.M., Marshall, V., Steinberg, S.M., Pittaluga, S., Maric, I., Whitby, D., Tosato, G., Little, R.F. and Yarchoan, R. 2010. An interleukin-6-related systemic inflammatory syndrome in patients co-infected with kaposi sarcoma-associated herpesvirus and HIV but without multicentric castleman disease. *Clinical Infectious Diseases*. **51**(3), pp.350–358.

Uppal, T., Banerjee, S., Sun, Z., Verma, S.C. and Robertson, E.S. 2014. KSHV LANA—The Master Regulator of KSHV Latency. *Viruses*. **6**(12), pp.4691–4998.

Vieira, J., O'Hearn, P., Kimball, L., Chandran, B. and Corey, L. 2001. Activation of Kaposi's Sarcoma-Associated Herpesvirus (Human Herpesvirus 8) Lytic Replication by Human Cytomegalovirus. *Journal of Virology*. **75**(3), pp.1378–1386.

Viphakone, N., Hautbergue, G.M., Walsh, M., Chang, C.-T., Holland, A., Folco, E.G., Reed, R. and Wilson, S.A. 2012. TREX exposes the RNA-binding domain of Nxf1 to enable mRNA export. *Nature Communications*. **3**(1), p.1006.

Vogt, C. and Bohne, J. 2016. The KSHV RNA regulator ORF57: Target specificity and its role in the viral life cycle. *Wiley Interdisciplinary Reviews: RNA*. **7**(2), pp.173–185.

Wabinga, H.R., Parkin, D.M., Wabwire-Mangen, F. and Mugerwa, J.W. 1993. Cancer in Kampala, Uganda, in 1989-91: changes in incidence in the era of AIDS. *International*

journal of cancer. **54**(1), pp.26–36.

Wang, P., Doxtader, K.A. and Nam, Y. 2016. Structural Basis for Cooperative Function of Mettl3 and Mettl14 Methyltransferases. *Molecular Cell*. **63**(2), pp.306–317.

Wang, S.E., Wu, F.Y., Chen, H., Shamay, M., Zheng, Q. and Hayward, G.S. 2004. Early Activation of the Kaposi's Sarcoma-Associated Herpesvirus RTA, RAP, and MTA Promoters by the Tetradecanoyl Phorbol Acetate-Induced AP1 Pathway. *Journal of Virology*. **78**(8), pp.4248–4267.

Wang, T., Kong, S., Tao, M. and Ju, S. 2020. The potential role of RNA N6-methyladenosine in Cancer progression. *Molecular Cancer*. **19**(1), pp.1–18.

Wang, X., Feng, J., Xue, Y., Guan, Z., Zhang, D., Liu, Z., Gong, Z., Wang, Q., Huang, J., Tang, C., Zou, T. and Yin, P. 2016. Structural basis of N6-adenosine methylation by the METTL3–METTL14 complex. *Nature*. **534**, p.575.

Wang, X., Lu, Z., Gomez, A., Hon, G.C., Yue, Y., Han, D., Fu, Y., Parisien, M., Dai, Q., Jia, G., Ren, B., Pan, T. and He, C. 2014. m(6)A-dependent regulation of messenger RNA stability. *Nature*. **505**(7481), pp.117–120.

Wang, Xiao, Zhao, B.S.S., Roundtree, I.A.A., Lu, Z., Han, D., Ma, H., Weng, X., Chen, K., Shi, H. and He, C. 2015. N6-methyladenosine Modulates Messenger RNA Translation Efficiency. *Cell*. **161**(6), pp.1388–1399.

Wang, Xin, Zhu, N., Li, W., Zhu, F., Wang, Y. and Yuan, Y. 2015. Mono-ubiquitylated ORF45 Mediates Association of KSHV Particles with Internal Lipid Rafts for Viral Assembly and Egress. *PLoS Pathogens*. **11**(12), pp.1–26.

Wegener, M. and Müller-McNicoll, M. 2018. Nuclear retention of mRNAs – quality control, gene regulation and human disease. *Seminars in Cell and Developmental Biology*. **79**, pp.131–142.

Wei, C.M., Gershowitz, A. and Moss, B. 1975. Methylated nucleotides block 5' terminus of HeLa cell messenger RNA. *Cell*. **4**(4), pp.379–386.

Wen, J., Lv, R., Ma, H., Shen, H., He, C., Wang, J., Jiao, F., Liu, H., Yang, P., Tan, L., Lan, F., Shi, Y.G., Shi, Y.G. and Diao, J. 2018. Zc3h13 Regulates Nuclear RNA m(6)A Methylation and Mouse Embryonic Stem Cell Self-Renewal. *Mol Cell*. **69**(6),

pp.1028-1038.e6.

Wen, K.W. and Damania, B. 2010. Kaposi Sarcoma-associated Herpesvirus (KSHV): Molecular Biology and Oncogenesis. *Cancer letters*. **289**(2), pp.140–150.

Winkler, R., Gillis, E., Lasman, L., Safra, M., Geula, S., Soyris, C., Nachshon, A., Tai-Schmiedel, J., Friedman, N., Le-Trilling, V.T.K., Trilling, M., Mandelboim, M., Hanna, J.H., Schwartz, S. and Stern-Ginossar, N. 2019. m6A modification controls the innate immune response to infection by targeting type I interferons. *Nature Immunology*. **20**(2), pp.173–182.

Winther, J.F., Møller, H., Tryggvadottir, L. and Kler, S.K. 1997. Biological agents. *APMIS, Supplement*. **105**(76), pp.120–131.

Wojtas, M.N., Pandey, R.R., Mendel, M., Homolka, D., Sachidanandam, R. and Pillai, R.S. 2017. Regulation of m6A Transcripts by the 3′→5′ RNA Helicase YTHDC2 Is Essential for a Successful Meiotic Program in the Mammalian Germline. *Molecular Cell*. **68**(2), pp.374-387.e12.

Woo, H.H. and Chambers, S.K. 2019. Human ALKBH3-induced m1A demethylation increases the CSF-1 mRNA stability in breast and ovarian cancer cells. *Biochimica et Biophysica Acta - Gene Regulatory Mechanisms*. **1862**(1), pp.35–46.

Wu, B., Su, S., Patil, D.P., Liu, H., Gan, J., Jaffrey, S.R. and Ma, J. 2018. Molecular basis for the specific and multivariant recognitions of RNA substrates by human hnRNP A2/B1. *Nature Communications*. **9**(1), p.420.

Xiao, S., Cao, S., Huang, Q., Xia, Linjian, Deng, M., Yang, M., Jia, G., Liu, X., Shi, J., Wang, W., Li, Y., Liu, S., Zhu, H., Tan, K., Luo, Q., Zhong, M., He, C. and Xia, Laixin 2019. The RNA N6-methyladenosine modification landscape of human fetal tissues. *Nature cell biology*. **21**(5), pp.651–661.

Xiao, W., Adhikari, S., Dahal, U., Chen, Y.-S., Hao, Y.-J., Sun, B.-F., Sun, H.-Y., Li, A., Ping, X.-L. and Lai, W.-Y. 2016. Nuclear m 6 A reader YTHDC1 regulates mRNA splicing. *Molecular cell*. **61**(4), pp.507–519.

Xu, C., Wang, X., Liu, K., Roundtree, I.A., Tempel, W., Li, Y., Lu, Z., He, C. and Min, J. 2014. Structural basis for selective binding of m6A RNA by the YTHDC1 YTH domain. *Nature Chemical Biology*. **10**, p.927.

Yan, L., Majerciak, V., Zheng, Z.M. and Lan, K. 2019. Towards Better Understanding of KSHV Life Cycle: from Transcription and Posttranscriptional Regulations to Pathogenesis. *Virologica Sinica*. **34**(2), pp.135–161.

Yang, L., Ma, T. and Zhang, J. 2016. GPRC5A exerts its tumor-suppressive effects in breast cancer cells by inhibiting EGFR and its downstream pathway. *Oncology Reports*. **36**(5), pp.2983–2990.

Yang, X., Yang, Y., Sun, B.-F., Chen, Y.-S., Xu, J.-W., Lai, W.-Y., Li, A., Wang, X., Bhattarai, D.P., Xiao, W., Sun, H.-Y., Zhu, Q., Ma, H.-L., Adhikari, S., Sun, M., Hao, Y.-J., Zhang, B., Huang, C.-M., Huang, N., Jiang, G.-B., Zhao, Y.-L., Wang, H.-L., Sun, Y.-P. and Yang, Y.-G. 2017. 5-methylcytosine promotes mRNA export - NSUN2 as the methyltransferase and ALYREF as an m5C reader. *Cell research*. **27**(5), pp.606–625.

Yang, Z., Yan, Z. and Wood, C. 2008. Kaposi's Sarcoma-Associated Herpesvirus Transactivator RTA Promotes Degradation of the Repressors To Regulate Viral Lytic Replication. *Journal of Virology*. **82**(7), pp.3590–3603.

Yankova, E., Blackaby, W., Albertella, M., Rak, J., De Braekeleer, E., Tsagkogeorga, G., Pilka, E.S., Aspris, D., Leggate, D., Hendrick, A.G., Webster, N.A., Andrews, B., Fosbeary, R., Guest, P., Irigoyen, N., Eleftheriou, M., Gozdecka, M., Dias, J.M.L., Bannister, A.J., Vick, B., Jeremias, I., Vassiliou, G.S., Rausch, O., Tzelepis, K. and Kouzarides, T. 2021. Small-molecule inhibition of METTL3 as a strategy against myeloid leukaemia. *Nature*. **593**(7860), pp.597–601.

Ye, F.-C., Blackbourn, D.J., Mengel, M., Xie, J.-P., Qian, L.-W., Greene, W., Yeh, I.-T., Graham, D. and Gao, S.-J. 2007. Kaposi's Sarcoma-Associated Herpesvirus Promotes Angiogenesis by Inducing Angiopoietin-2 Expression via AP-1 and Ets1. *Journal of Virology*. **81**(8), pp.3980–3991.

Ye, F. 2017. RNA N6-adenosine methylation (m6A) steers epitranscriptomic control of herpesvirus replication. *Inflammation and cell signaling*. **4**(3).

Ye, F., Chen, E.R. and Nilsen, T.W. 2017. Kaposi's Sarcoma-Associated Herpesvirus Utilizes and Manipulates RNA N6-Adenosine Methylation To Promote Lytic Replication. *Journal of virology*. **91**(16), JVI-00466.

Yoshikawa, T. 2018. Betaherpesvirus Complications and Management During

Hematopoietic Stem Cell Transplantation *In*: Y. Kawaguchi, Y. Mori and H. Kimura, eds. *Advances in Experimental Medicine and Biology*. Singapore: Springer Singapore, pp.251–270.

Yuan, S., Wang, Jialing, Zhu, D., Wang, N., Gao, Q., Chen, W., Tang, H., Wang, Junzhi, Zhang, X., Liu, H., Rao, Z. and Wang, X. 2018. Cryo-EM structure of a herpesvirus capsid at 3.1 Å. *Science*. **360**(6384).

Yue, Y., Liu, J.J., Cui, X., Cao, J., Luo, G., Zhang, Z., Cheng, T., Gao, M., Shu, X., Ma, H., Wang, F., Wang, X., Shen, B., Wang, Y., Feng, X., He, C. and Liu, J.J. 2018. VIRMA mediates preferential m(6)A mRNA methylation in 3'UTR and near stop codon and associates with alternative polyadenylation. *Cell Discovery*. **4**, p.10.

Zaccara, S., Ries, R.J. and Jaffrey, S.R. 2019. Reading, writing and erasing mRNA methylation. *Nature Reviews Molecular Cell Biology*. **20**(10), pp.608–624.

Zekavati, A., Nasir, A., Alcaraz, A., Aldrovandi, M., Marsh, P., Norton, J.D. and Murphy, J.J. 2014. Post-Transcriptional Regulation of BCL2 mRNA by the RNA-Binding Protein ZFP36L1 in Malignant B Cells P. Fei, ed. *PLoS ONE*. **9**(7), p.e102625.

Zhang, C. and Jia, G. 2018. Reversible RNA Modification N 1 -methyladenosine (m 1 A) in mRNA and tRNA. *Genomics, Proteomics & Bioinformatics*. **16**(3), pp.155–161.

Zhang, Z., Theler, D., Kaminska, K.H., Hiller, M., de la Grange, P., Pudimat, R., Rafalska, I., Heinrich, B., Bujnicki, J.M., Allain, F.H. and Stamm, S. 2010. The YTH domain is a novel RNA binding domain. *J Biol Chem*. **285**(19), pp.14701–14710.

Zhao, B.S. and He, C. 2015. Pseudouridine in a new era of RNA modifications. *Cell Research*. **25**(2), pp.153–154.

Zheng, G., Dahl, J.A., Niu, Y., Fedorcsak, P., Huang, C.-M., Li, C.J., Vågbø, C.B., Shi, Y., Wang, W.-L. and Song, S.-H. 2013. ALKBH5 is a mammalian RNA demethylase that impacts RNA metabolism and mouse fertility. *Molecular cell*. **49**(1), pp.18–29.

Zhong, W., Wang, H., Herndier, B. and Ganem, D. 1996. Restricted expression of Kaposi sarcoma-associated herpesvirus (human herpesvirus 8) genes in Kaposi sarcoma. *Proceedings of the National Academy of Sciences of the United States of America*. **93**(13), pp.6641–6646.

Zhou, H. and Rigoutsos, I. 2014. The emerging roles of GPRC5A in diseases. *Oncoscience*. **1**(12), pp.765–776.

Zhou, J., Wan, J., Gao, X., Zhang, X., Jaffrey, S.R. and Qian, S.-B. 2015. Dynamic m6A mRNA methylation directs translational control of heat shock response. *Nature*. **526**, p.591.